Proximity Effects and Josephson Currents in Ferromagnet - Spin-Triplet Superconductors Junctions

Von der Fakultät Mathematik und Physik der Universität Stuttgart
zur Erlangung der Würde eines Doktors der Naturwissenschaften
(Dr. rer. nat.) genehmigte Abhandlung

Vorgelegt von

Damien Terrade

aus Marseille (Frankreich)

Vorsitz: Prof. Dr. Peter Michler
Hauptberichter: Prof. Dr. Walter Metzner
Mitberichter: Prof. Dr. Maria Daghofer
Prof. Dr. Dirk Manske

Tag der mündlichen Prüfung: 12. Februar 2015

Max-Planck-Institut für Festkörperforschung
Stuttgart 2015

Abstract

Spin-triplet superconductivity, first attached to the description of ^{3}He, is now generally considered to also occur in heavy-fermions compounds and in perovskite ruthenium oxide Sr_2RuO_4. The latter material is especially interesting since many experiments show strong evidences for a unitary chiral spin-triplet state. Moreover, the recent fabrication of thin heterostructures made of ferromagnetic $SrRuO_3$ on the top of Sr_2RuO_4 strongly encourages new theoretical studies on the interplay between spin-triplet superconductor and ferromagnet in similar fashion to spin-singlet superconductors. Using an extended tight-binding Hamiltonian to model the superconductor, we discuss in this thesis the specific proximity effects of such interface by solving self-consistently the Bogoliubov-De Gennes equations on two- and three-dimensional lattices in the ballistic limit. We obtain the spatial profile of the superconducting order parameters at the interface as well as the spin-polarisation and the current across the Josephson junctions. In contrast to heterostructures made of spin-singlet superconductor, the physical properties at the interface are not only controlled by the strength of the magnetization inside the ferromagnet but also by its orientation due to the existence of a finite pair spin projection of the spin-triplet Cooper pairs.

The spin-polarisation and the Gibbs free energy at the three-dimensional ferromagnet-spin-triplet superconductor interface are analysed in the first part of the thesis. More specifically we show that, close to the interface, the spin-polarisation is modified in the ferromagnet and induced in the superconductor such that the total magnetization can be reduced, but also enhanced, depending on the magnetic orientation. On the other hand, the inspection of the total energy shows that the superconductor always favours the magnetization to be parallel to the spin-projection of the spin-triplet Cooper pairs, and so perpendicular to the $\vec{d}$-vector. In addition, we find that, depending on the strength of the ferromagnetic exchange field, a spin-active interface can be spontaneously induced. In other words, a misalignment between the magnetic moments in the bulk and at the interface can be energetically more favourable than a constant profile. Therefore, the experimental observation of the magnetic profile at the interface could give crucial information on the nature of the Cooper pairs present in the superconductor.

The second part of the thesis is dedicated to the study of the Josephson junctions with a ferromagnetic barrier. We first observe the existence of 0-π state transitions in two-dimensional junctions with respect to the strength and the orientation of the magnetization, in good agreement with the results obtained recently with quasiclassical formalism. We show that both methods qualitatively predict similar phase diagrams and maximal critical angles, which can be understood by inspecting the spatial variations of the induced correlation functions inside the barrier. On the other hand, the critical angle is found to be over estimated compare to the three-dimensional junctions although the general phase diagrams are qualitatively identical. Our main results concern the drastic influence of spin-active interfaces on the state of the junctions, configuration which can be experimentally relevant since the spin-triplet superconductor tends to spontaneously misalign

the magnetization. We show that this generally leads to the reduction of the π-state domains, which are in particular destroyed for a strong ferromagnet, while the critical angle remains unchanged. We predict such effect to be directly observable by analysing the critical current for various length of the barrier.
In the last part, we study the proximity effects at the interface of helical spin-triplet superconductors. It differs from the chiral one by the direction of the pair spin polarisation of the Cooper pairs and by the properties of the edge states, present at the boundaries, which sustain dissipationless spin-current. We analyse the modifications of the spin-current as well as the induced charge-current at the interface controlled by the strength of the magnetization. Depending on the number of gapless helical edge states, the capacity of carrying spin and charge currents is shown to be directly related to the amplitude and orientation of the ferromagnetic magnetization with respect to the superconducting $\vec{d}$-vector. We show that the modifications of the current are due to the degree of hybridization between the edge states and the ferromagnetic Fermi surface. Differently from the one-helical mode spin-triplet superconductor, the presence of a finite amount of electronic hybridization with the two pairs of Majorana helical modes induces a nonvanishing charge current independent of the strength of the magnetization. We finally provide a general overview of the modifications of the spin-current for the several directions of the magnetization.

Deutsche Zusammenfassung

Spin-Triplett Supraleitung, welche zuerst in flüssigem He_3 beobachtet wurde, wird inzwischen auch den Schwere-Fermionen-Systemen und dem Perowskit Rutheniumoxid Sr_2RuO_4 zugeschrieben. Rutheniumoxid ist dabei von besonderem Interesse, da viele Experimente auf einen unitären, chiralen Spin-Triplett Zustand hinweisen. Zudem ist es seit kurzer Zeit möglich, dünne Heterostrukturen mit ferromagnetischem $SrRuO_3$ auf einem Substrat von Sr_2RuO_4 herzustellen. Damit wird eine Untersuchung der Grenzflächeneffekte zwischen Spin-Triplett Supraleiter und Ferromagnet möglich, ganz ähnlich wie für den bekannten Fall der Spin-Singlett Supraleiter. In dieser Dissertation diskutieren wir theoretisch den spezifischen Nahfeldeffekt an einer solchen Grenzfläche. Dabei verwenden wir einen erweiterten tight-binding Hamiltonian für den Supraleiter und lösen die Bogoliubov-De Gennes Gleichungen in zwei oder drei dimensionalen Kristallgittern in dem ballistischen Grenzfall. Auf diesem Wege erhalten wir sowohl das räumliche Profil des supraleitenden Ordnungsparameters nahe der Grenzfläche als auch die Spin-polarisation und den Strom durch den Josephson-Kontakt. Insbesondere sind die physikalischen Eigenschaften an der Grenzfläche nicht allein vom Betrag der Magnetisierung des Ferromagnets abhängig, sondern auch von der Orientierung der Magnetisierung, da die Projektion des Paarspins der Spin-Triplett Cooper-Paare endlich ist.

Im ersten Teil der Dissertation wird die Spinpolarisation und die gesamte freie Energie an der Grenzfläche von Ferromagnet und Spin-Triplett Supraleiter in drei Dimensionen untersucht. Wir zeigen, dass nahe der Grenzfläche im Supraleiter eine Spinpolarisation induziert wird, während sie im Ferromagnet so modifiziert wird, dass die Magnetisierung insgesamt sowohl reduziert als auch verstärkt werden kann, je nach Richtung des Magnetfeldvektors. Andererseits zeigt eine Untersuchung der Gesamtenergie, dass der Supraleiter immer einen Zustand bevorzugt, bei dem die Magnetisierung parallel zur Spinprojektion der Spin-Triplett Cooper-Paare ausgerichtet ist, und damit senkrecht zum $\vec{d}$-Vektor. Des Weiteren kann abhängig von der Stärke des ferromagnetischen Austauschfelds eine spinaktive Grenzfläche spontan induziert werden. In diesem Fall ist eine nicht kollineare Ausrichtung zwischen den magnetischen Momenten im Ferromagneten und an der Grenzfläche energetisch günstiger als ein konstantes Profil. Eine experimentelle Untersuchung des magnetischen Profils an der Grenzfläche könnte darum wertvolle Informationen über die Natur der Cooperpaare im Supraleiter geben.

Der zweite Teil der Dissertation beschäftigt sich mit Josephson-Kontakten mit einer ferromagnetischen Barriere. Wir führen eine Analyse des 0-π-Zustandsübergangs in zweidimensionalen Kontakten in Abhängigkeit von Stärke und Richtung der Magnetisierung durch, um sie mit früheren Resultaten aus quasiklassischen Rechnungen zu vergleichen. Beide Methoden stimmen qualitativ überein, was anhand der räumlichen Variationen der induzierten Korrelationsfunktionen innerhalb der Barriere erklärt werden kann. Unsere Hauptergebnisse betreffen den drastischen Einfluss, den spinaktive Grenzflächen auf das Phasendiagram des Josephson-Kontaktes haben. Diese Konfiguration ist von experimentellem Interesse, da Spin-Triplett Supraleiter dazu neigen, spontan eine nichtparallele Magnetisierung einzunehmen. Wir demonstrieren, dass dies im Allgemeinen zu einer Verkleinerung des Phasenraums des π-Zustands führt, welcher insbesondere von einem

starken Ferromagneten vollständig zerstört wird, während der kritische Winkel sich nicht ändert. Wir zeigen, dass solch ein Effekt direkt beobachtbar ist, wenn der kritische Strom für verschiedene Längen der Barriere analysiert wird.
Im letzten Teil der Dissertation betrachten wir den Nahfeldeffekt an der Grenzfläche von helikalen Spin-Triplett Supraleitern. Dieser unterscheidet sich von dem chiralen Supraleiter durch die Richtung der Paarspinpolarisation der Cooper-Paare und durch die Eigenschaften der Randzustände an der Oberfläche, welche einen dissipationslosen Spinstrom führen. Wir untersuchen die Veränderungen des Spinstroms und des induzierten Ladungsstroms an der Grenzfläche als Funktion der Magnetisierungsstärke. Abhängig von der Anzahl der helikalen Randzustände ohne Bandlücke steht die Kapazität der Spin- und Ladungsströme in direktem Zusammenhang mit der Amplitude und Richtung der ferromagnetischen Magnetisierung in Bezug auf den supraleitenden $\vec{d}$-Vektor. Es zeigt sich, dass die Veränderungen des Stroms direkt vom Grad der Hybridisierung zwischen Randzustand und ferromagnetischer Fermifläche abhängen. Im Unterschied zu einem Spin-Triplett Supraleiter mit einer helikalen Mode führt die Anwesenheit einer endlichen elektronischen Hybridisierung mit zwei Paaren von helikalen Majorana-Moden zu einem nichtverschwindenden Ladungsstrom, welcher unabhängig von der Magnetisierungsstärke ist. Abschließend präsentieren wir einen allgemeinen Überblick über die Modifikationen des Spinstromes für verschiedene Magnetisierungsrichtungen.

Acknowledgement

The adventure of the last four years would not have been possible without the presence and the support of many people who contributed in various manners to this accomplishment. First and foremost, I would like to thank Prof. Dr. Walter Metzner, for having welcomed me in his group and by giving me the great opportunity to work in a brilliant institution, and the Max-Planck-Institute for Solid Matter Physics of Stuttgart, for having provided me financial and technical support for my studies. I am very grateful to Prof. Dr. Dirk Manske who trusted me, despite my poor English, and accepted to be my supervisor. He always gave me a full support, always kept his door open for me and I highly beneficed of his valued discussions, knowledge and advices during the last past years. I also thank Dr. Giniyat Khaliullin for his assistance and his useful comments on my work all along these years, as well as Prof. Dr. Maria Daghofer and Prof. Dr. Peter Michler for having accepted to be members of my PhD committee.

I am greatly indebted to Dr. Mario Cuoco without whom this work would not have been possible. With the help of Prof. Dr. Dirk Manske, this project started from our collaboration and I have been enjoying many useful and interesting discussions on this subject as on others. I am also very grateful to him, not only for having invited me, but also for having taken care of me during my several long journeys at the University of Fisciano. Thanks to him, each time has been a great opportunity to improve my work and increase my motivation. I also thank Dr. Paola Gentile for her collaboration and her support during my journeys in Italy.

I also had a great pleasure to collaborate for a short period with Dr. Yuan Li and Dr. Mathieu Le Tacon on experimental project, which has been very stimulating for me. I thank also Prof. Dr. Bernard Keimer for having conducted this project.

I greatly appreciated many discussions with people in the Prof. Metzner's research group during these years. In particular Wei and Gaetano, who always took time to share their knowledge and to discuss about old and new projects. I am especially grateful to Tobias for very stimulating exchanges on many subjects the last two years, notably in physics, and for having helped me greatly with my thesis. I also have to thank the people from the IT service for always having taken great care of our working tools.

I believe the life during my PhD studies would have been much bitter without the presence of friends and great friends who have been around me during these last years, be them far or very close. My deeply thanks goes to my old friends Florent and Michael with whom I derived my first differential equations. To Salome, Madeleine and Hilton for having shared much more than a flat with me. To Ricardo, Laura, Miguel, Tsvety, Josh, Anna, Petr, Karsten, Adam, Amélie, Jan, Manon, Pierre-Yves, Jovana, Matthias, Jyh-Lih, and forgotten people, for their support and their friendship.

I am finally grateful to my family for their unlimited support all these years, and much before, and in particular to my parents, and grandparents, who always provided the best for me. I would not have wrote this thesis without them.

Last but not least, my lovely thanks go to Izabela for being so strong by my side.

Contents

Introduction

Since the discovery of the expulsion of magnetic field by superconductors by Meissner and Ochsenfeld in 1933, the interplay between superconductivity and magnetization has fascinated several generations of condensed matter physicists. It led to the first macroscopic theory of superconductivity by the Londons brothers before the development of the theory of phase transition for superconductors by Ginzburg and Landau. The first microscopic theory of superconductivity by Bardeen, Cooper and Schieffer (BCS) in late 1950s has been a milestone in that field, not only to provide a clear understanding of the physical scenario responsible for the condensate state, made of pairs of electrons referred today as the Cooper pairs, but also to understand its response to electric or magnetic external perturbations. Also, it became clear that a finite magnetization destroys the Cooper pairs and that ferromagnetism, in contrast to antiferromagnetism, could not coexist with superconductivity in conventional BCS superconductors. On the other hand, it has been soon imagined to induce artificially such coexistence at the interface of a ferromagnet and a superconductor. Due to the nature of the Cooper pairs made of fermions, it has been then predicted that such interplay should lead to various and specific modifications of the physical properties of the interface, which are still under close investigation nowadays.

The study of the ferromagnet-superconductor interfaces first requires a clear understanding of the proximity effects, that means of the modifications of properties of the superconducting state, at the interface of a metal and a superconductor. Such analyses have be done soon after the formulation of the BCS theory, which gave a very good framework to understand the physical mechanisms occurring at the interface. It has been shown that, through the so-called Andreev reflections, the superconducting order parameter is induced in the metallic region while it is suppressed in the superconducting one and leads to the decrease of the critical temperature of structure made of thin superconductors. They are also responsible for the existence of a supercurrent in junctions made of superconductors as demonstrated by Josephson and which is used in SQUID devices. Concerning the simple proximity effects with ferromagnets, the exchange field, being pair breaking for the Cooper pairs, produces additional oscillations of the superconducting order parameter induced in the ferromagnetic region, similarly than for the FFLO states. The consequences of the presence of the magnetization at the interface of the superconductor go far beyond the simple modification of the order parameters or the critical temperature. We can for instance mention that the Josephson effect is modified and can exhibit two different states, generally denoted 0 or π, depending on the length of the ferromagnetic barrier and on the strength of the exchange field. Interest in such effect has been growing since it has been shown it could be use to design coherent quantum states suitable for quantum computing. However, it is only in the last decade that the improvement of the experimental techniques

permitted to study such interfaces. Then, the observation of Josephson effects in junctions made of half-metallic barriers has been another key discovery, which is admitted to be the proof for the existence of unconventional long range spin-triplet state induced in ferromagnet-superconductor junctions in presence of spin-active interfaces. These results were obtained in junctions made of conventional superconductors, i.e. with spin-singlet Cooper pairs and for which the order parameters are independent of the momentum, but also extended to spin-singlet unconventional superconductors having a non-uniform gap parameters. In this case the conductance can be modified but not the Josephson effects. In both cases, however, the proximity effects are independent from the magnetization's orientation in the ferromagnetic region.

Ferromagnet-spin-triplet superconductors (TSC) interfaces are expected to exhibit even more exotic behaviours. Indeed, in contrast to the spin-singlet cases, the Cooper pairs forming the spin-triplet superconducting states carry a non-zero spin projection in one direction. Although the proximity effects are due to the Andreev reflections and depend on the spin of each electrons, the relative orientation between the magnetization in the ferromagnet and the direction of the spin-projection of the spin-triplet Cooper pairs is the main parameter driving the proximity effects, additionally of the strength of the exchange field. The consequences of this effect has been particularly studied in the case of Josephson junctions for which it has been shown that their state could be switched by changing the orientation of the magnetization. Moreover, in spintronic fashion, spin-currents have been be predicted to be also induced in the junction, still depending on the magnetization orientation.

The aim of the following work is to get a deeper understanding of the proximity effects at such interfaces but also to predict novel kind of proximity effects due to the peculiar interplay between the magnetization and the chiral spin-triplet state. The consideration of this interface became especially relevant since the recent experimental achievements of junctions made of Sr_2RuO_4 thin films, which is believed to exhibit such a spin-triplet pairing. For this purpose, we solve the Bogoliubov-De Gennes equations using an effective quasi one-dimensional lattice model in ballistic limit decoupled within the Hartree-Fock approximation. The superconducting order parameters are computing self-consistently at the interface and allow the study of the proximity effects on the atomic scale. As we shall see, this is especially important in the research of the magnetic profile occurring close to the interface. Indeed, due to the spin nature of the Cooper pairs, we find that the superconductor not only tends to favour one direction of the magnetization, but also that a spin-active interface, due to a misalignment of the magnetization at the interface, can be spontaneously induced due to the influence of the spin-triplet state. Additionally, we analyse the spin-polarisation which is also modified site by site close to the interface. We show that the latter is modified in the ferromagnet and induced in the superconductor such that the total magnetization can be reduced, but also enhanced, by rotation of the magnetization.

The consequences of a non-constant magnetic profile can especially be seen in the analysis of the Josephson effects in TSC-FM-TSC junctions. Before all, we discuss the state of the Josephson junction for various magnetic configurations. After having shown that the results predicted by our theoretical model are in good agreement with the previous quasiclassical studies for two-dimensional systems, we extend our analysis to self-consistent

derivation of the problem and to three-dimensional systems. Although some quantitative differences arise, we show that the main features, that means the state transitions according to the strength and the orientation of the magnetization as well as the barrier's length, are preserved. We finally predict that the presence of a spin-active interface should lead to an overall modification of the critical current characteristic of the junction and that non-periodic oscillations with respect of the barrier's length should be observed.
The last part of the thesis is dedicated to the study of proximity effects at the interface of helical p-wave spin-triplet superconductors. Due to its topological character, it exhibits gapless edge states at this boundaries, which carry dissipationless spin-current along the interface in a similar fashion than in quantum spin hall effect. Depending on the number of gapless helical edge states, the capacity of carrying spin-currents as well as inducing charge-currents is shown to be directly related to the amplitude and orientation of the ferromagnetic magnetization with respect to the superconducting $\vec{d}$-vector. We show that the modifications of the currents are directly related of the degree of hybridization between the edge states and the ferromagnetic Fermi surface. It leads that, differently from the one-helical mode spin-triplet superconductor, the presence of a finite amount of electronic hybridization with the two pairs of Majorana helical modes induces a nonvanishing charge current independently of the strength of the magnetization. We finally study the tuning of the spin-current for several direction of the magnetization. We show that a magnetization coplanar to the $\vec{d}$-vector generally tends to decrease the spin-current.
Hence, in contrast to ferromagnetic heterostructures made of spin-singlet superconductors, we show that the orientation of the magnetization in the ferromagnet is a key feature which leads to various novel proximity effects. Interestingly, most of the results presented in the thesis show that these effects could be used experimentally not only as key evidences of the spin-triplet pairing in superconducting materials, which is still nowadays under intense investigation, but also to identify more precisely the nature of the spin-triplet states.

Chapter 1

Spin-Triplet Superconductors and Extended Tight-Binding Model

Transfer mechanisms and proximity effects at the interfaces between superconductors and metals or insulators have been intensively studied since the 1960s [26, 38, 87]. At that time, quasiclassical approximations of the Gor'kov equations for ballistic [48] and diffusive limits [130] have been developed for the normal and anomalous Green's functions of the microscopic theory of superconductivity. They describe the spatial variations of the energy- and spatial-integrated Green's functions using the fact that much of the superconducting effects, for instance Josephson currents and Andreev reflections, can be described on the scales of the superconducting coherence length and the thermal diffusion length which are larger that the Fermi wavelength. Since then, they have been employed to investigate many problems involving electronic transport in superconducting heterostructures, be it at equilibrium or out-of equilibrium. We can mention, for instance, the predictions of the variations of the critical current and the critical temperature in ferromagnetic Josephson junctions [40, 41, 108], the density of states at the interface of superconductors [30, 91] or the creation of spin-triplet component at the interface of a ferromagnet [24, 26, 51], which have been observed [77, 78]. Additionally, conclusive results have also been obtained by means of the Bogoliubov-De Gennes equations which describe the transmissions and reflections of the electrons through barriers between metals or insulator and superconductors. This have been remarkably used to study the conductance using the so-called Blonder-Tinkham-Klapwijk (BTK) formalism [28, 45, 103]. Both methods have been intensively used to characterise heterostructures with spin-singlet s-wave and d-wave superconductors [7, 88] and have been then extended to spin-triplet superconductors [88] and junctions made of noncentrosymmetric superconductors [8, 9, 109].

The tight-binding lattice model with an attractive pairing between electrons on the same site or on two nearest-neighbours sites is another formalism by mean the proximity effects at such interfaces can be studied. Indeed, within the Hartree-Fock approximation, it has been shown that the phase diagrams of the model can exhibit s-, d- or p-wave superconducting states depending on the value of the attractive pairing and on the electronic filling, i.e. on the value of the chemical potential [84]. The bulk values of the order parameters can be obtained by solving self-consistently the lattice model or the gap equations while spatial variations can be computed at the edge of the system or at the interface with insulator, metallic or ferromagnetic regions. In contrast to the quasiclassical

analysis, such self-consistent evaluation of the Bogoliubov-De Gennes equations provides spatial variations on the scale of the lattice site instead of the superconducting coherence length. Moreover, it has the advantage to not require the derivation of the boundary conditions at the various interfaces. Last decade, this lattice model has been used for in various spin-singlet (SC) as well as spin-triplet superconductors (TSC) heterostructures. In particular, density of states and Josephson currents have be computed at the interfaces of normal (N) [13, 120, 131], ferromagnetic (FM) [31, 44, 60, 88, 142] or antiferromagnetic (AFM) [2, 3, 83] metals with superconductors. Spin- and charge-currents and spin-polarisation at the interface between ferromagnet and chiral superconductors have also been investigated [85].
Hence, the model is appropriate to evaluate site by site the order parameters, the currents and the spin-polarisation around the interface and hence to obtain the proximity effects between two different regions. New results about proximity and inverse proximity effects concerning the chiral and helical superconductors will be presented in the next Chapters. In the following introducing Chapter, we present the derivation of the superconducting order parameters within the attractive tight-binding framework by solving the Bogoliubov-De Gennes equations. Focusing on the chiral TSC, we discuss in details the bulk state obtained after self-consistent computation as well as the spatial variations of the order parameters at the interface with the vacuum and with normal metal. We then discuss the case of the two-dimensional FM-TSC interface for which we reproduced results. Indeed, that first example is useful to introduce the various mechanisms at the FM-TSC interface such as the Andreev reflections and the oscillations of the induced order parameters in the ferromagnetic region. As we shall see, these are important mechanism present at such interface and which will be discussed all along the manuscript.

The Chapter is organised as follows. The section 1.1 is devoted to the introduction of the spin-triplet superconductors defined within the BCS formalism. We introduce in section 1.2 the extended-tight-binding model on the lattice with attractive coupling between electrons and we define the superconducting order parameters in the section 1.3. The remaining sections are used to discuss few properties of the bulk and interface of the chiral superconductors by mean of the lattice model in section 1.4 and 1.5, respectively. Finally, the last section gives an overview on the proximity effects treated in the rest of this manuscript.

1.1 Spin-Triplet Superconductors

We introduce in this section the basic components of the general BCS theory of superconductivity and describe both spin-singlet and spin-triplet order parameters within this framework. We also introduce and briefly discuss the electronic properties of the two spin-triplet superconducting states, the chiral p_x+ip_y-wave and the helical superconductor, that we shall examine in the next Chapters of this thesis.

BCS Hamiltonian and Superconducting Order Parameters The first microscopic theory of superconductivity was published in 1957 by Bardeen, Cooper and Schrieffer(BCS). It shown that a Fermi liquid can exhibit a superconducting ground state at

low temperature and was based on three important results [6, 21]. Firstly, the total effective force between two conducting electrons in a metal are not only repulsive but can be attractive due to the electron-phonon coupling. Secondly, it is energetically favourable that two attracted electrons, with opposite spin and momentum and whose energies are greater than the Fermi energy, form a bound pair independently on the strength of this effective interaction. The two electrons form hence the so-called Cooper pair. Finally, depending on the maximal energy of the phonons in the metal and on the temperature, it was shown that the complete Fermi surface is unstable and that electrons close to the Fermi energy tend to form such Cooper pairs. It is then possible to construct a quantum coherent wave function made of Cooper pairs and describing the ground state of the superconducting state. The model was successfully able to explain the isotope effect and to predict the existence of a gap of $2 \cdot \Delta_0$ in the energy spectrum. Moreover, Gor'kov showed two years later that, close to the superconducting transition temperature T_c, the BCS model is equivalent to the Ginzburg-Landau theory. Hence, the superconducting order parameter of the latter theory is equivalent to the gap Δ_0 in the superconducting spectrum, i.e. to the correlations functions of Cooper pairs. As we mentioned in the introduction of this chapter, this theory was not only a breakthrough to understand the microscopic mechanism of superconductivity, but also lead to the understanding of the proximity effects as well as the conduction in metallic - superconducting junctions.

Within the BCS model of superconductivity, the creation of the the Cooper pairs in a Fermi liquid are justified from the existence of an effective attractive pairing $V(k, \omega)$ between two electrons, with opposite spin and momentum, mediated by phonons. While it depends generally on the wavevector k and the energy ω of the electrons, it was assumed to be constant, i.e. $V(k, \omega) \sim V_{\text{eff}}$, and non zero only for frequencies inferior to the Debye frequency ω_D. Since the described system is invariant by translation, it is convenient to work in momentum space. It leads to the basic BCS Hamiltonian

$$H_{BCS} = \sum_{k,\sigma} \epsilon_k c^\dagger_{k\sigma} c_{k\sigma} - V_{\text{eff}} \sum_{k,k'} c^\dagger_{k\uparrow} c^\dagger_{-k\downarrow} c_{-k'\downarrow} c_{k'\uparrow} \tag{1.1}$$

where ϵ_k is the energy spectrum of the electrons of the Fermi liquid and for which we should restrict the interaction to the momentum k such that ϵ_k is within $\pm\omega_D$. This general many-body quantum system is not exactly solvable but can be studied in some limit in case. As we mentioned, the BCS theory assumes that all electrons close to the Fermi energy form Cooper pairs which are used to construct the quantum BCS ground state of the system. In other words, that means that, under T_c, the correlations functions for the ground states $\langle c_{k,\sigma} c_{-k,-\sigma} \rangle$ and its conjugate are finite and that the fluctuations around this average value are small. In this case, the Hamiltonian Eq. 1.1 can be exactly solved using the mean-field approximation and corresponds to the limit of weak-coupling $V_{\text{eff}} \ll E_F$, E_F being the Fermi energy. The justification of this equivalence as well as the results presented in the following require more detailed derivations that we do not aim to reproduce here. The readers can refer to several books for a more exhaustive development of the BCS theory [6, 128] as well as for the studies of intermediate- and strong-coupling limits [1]. Using the mean-field approximation and the Wick's theorem, the four-particles interaction in Eq. 1.1 is split in two-particles interactions and the mean-field Hamiltonian

becomes

$$H_{BCS}^{MF} = \sum_{k,\sigma}(\epsilon_k - \mu)c_{k\sigma}^{\dagger}c_{k\sigma} - V_{\text{eff}}\sum_{k,k'}\langle c_{k\uparrow}^{\dagger}c_{-k\downarrow}^{\dagger}\rangle c_{-k'\downarrow}c_{k'\uparrow} + h.c.\ . \tag{1.2}$$

The mean-field BCS Hamiltonian is solvable by using the Bogoliubov-Valatin transformations and can be written as an Hamiltonian of free quasiparticles

$$H_{BCS}^{MF} = \sum E_k(\gamma_{k\uparrow}^{\dagger}\gamma_{k\uparrow} + \gamma_{k\downarrow}^{\dagger}\gamma_{k\downarrow}) \tag{1.3}$$

$$\text{with}\quad E_k = \sqrt{(\epsilon_k - \mu)^2 + |\Delta_0|^2}\ , \tag{1.4}$$

where the superconducting gap is defined as

$$\Delta_0 = V_{\text{eff}}\sum_k \langle c_{-k\downarrow}c_{k\uparrow}\rangle. \tag{1.5}$$

The new creation and annihilation operators for the quasiparticle excitations are linear combinations of the previous operators such that

$$\gamma_{k\uparrow} = u_k^* c_{k\uparrow} - v_k^* c_{-k\downarrow}^{\dagger}\ , \tag{1.6}$$

$$\gamma_{-k\downarrow}^{\dagger} = v_k c_{k\uparrow} + u_k c_{-k\downarrow}^{\dagger}\ , \tag{1.7}$$

where the coherence factors u_k and v_k satisfy $|u_k|^2 = 1-|v_k|^2 = (1-\epsilon_k/E_k)/2$. The excited states of the superconductors are hence quasiparticles which are not electrons or holes but a linear combination of both particles. Moreover, we can notice that the energy spectrum exhibits a gap Δ_0 independent on the quasiparticles momentum. Taking into account a finite temperature T by using the Fermi-Dirac distribution, the gap $\Delta_0(T)$ verifies the so-called gap equation

$$\Delta_0 = V_{\text{eff}}\sum_k \frac{\Delta_0}{2E_k}\tanh\left(\frac{E_k}{2k_BT}\right), \tag{1.8}$$

where k_b the Boltzmann constant. Therefore, the BCS theory provides a way to determine self-consistently the evolution of the gap with the temperature $\Delta_0(T)$, which is found to be maximal at T=0K, monotonously decreasing when the temperature increases and cancelling at T_c. As shown by Gor'kov, the expectation value of the Cooper pairs Δ_0 is not only a gap in the energy spectrum but also correspond to the order parameter of the superconducting phase. The success of the BCS theory was definitely guaranteed after that the gap Δ_0 as well as the ratio $\Delta_0(T=0)/k_bT_c = 1.76$ was experimentally observed for various, but not all, metals in the 1960s [6].

Let us now comment on the symmetry of the superconducting order parameter. Indeed, within the BCS approximation, a simple permutation of the fermion operators in Eq. 1.5 shows us that $\Delta_{\uparrow\downarrow} = -\Delta_{\downarrow\uparrow}$. It is then important to have in mind that the quantum many-body problem described by Eq. 1.2 follows the mean field approximation or, more exactly, the Hartree-Fock approximation. Hence, the total wave function of the system is approximate by a set of single-electron wave functions, each one being a product of

dissociated spatial orbital function and a spin state. It is worth to mention that this approximation is reasonable in our system but should be treated with much care in the case of the existence of an additional spin-orbit coupling. Coming back to the superconducting order parameter, the wave function of the zero-momentum Cooper pairs made of two electrons of opposite spin can be thus dissociated into a product of spin and orbital functions. Since Δ_0 is independent of the momentum, the spin part of the total wave function must be antisymmetric with respect to exchange of spins and the electrons are hence paired in a spin-singlet state. Finally, it is worth mentioning that the gap equation and the non-dependence in momentum of the order parameters are due to the local character of the coupling V_{eff}.

The experimental observation in early 1970s of the superfluid phases of the ^{3}He at very low temperature, i.e. of the existence of a condensate state in a system made of fermions, has been another key discovery in the understanding of the superconductivity although it does not involve electrons in a metal. Indeed, the fact that the ^{3}He gas is made of fermion atoms suggested that the superfluid states were analogue to the BCS superconductivity. On the other hand, it exists no equivalent of phonons in this system and the coupling between Helium atoms should be of different nature. The key idea in this system is that the effective coupling V_{eff} is not local, or in other words, that the superconducting order parameters Δ_0 is momentum-dependent. This can be physically understood by the fact that two atoms of helium are strongly repulsive when they are very close to each other, as in the model of two hard balls and, thus, it becomes unlikely for two atoms of a pair to be located at the same place. The correlation functions of a pair of Helium atoms should hence be suppressed in such case.
In order to describe such condensate states with a more general pairing between electrons or helium atoms, we must derive a more general Hamiltonian. In a general way, we use now a pairing between fermions which can exist not only for two electrons with opposite spin but also with the same spin. However, we must still limit the scattering from (k,-k) to (k',-k'), which corresponds to Cooper pairs with zero momentum. In this case, Eq. 1.1 is only one approximation of the more general Hamiltonian

$$H = \sum_{k,\sigma} (\epsilon_k - \mu) c^\dagger_{k\sigma} c_{k\sigma} + \sum_{kk'} V_{\alpha\beta\gamma\delta}(k,k') c^\dagger_{k'\alpha} c^\dagger_{-k'\beta} c_{-k\gamma} c_{k\delta} \tag{1.9}$$

which allows at this point all possible spin and momentum dependence of the interaction V between the four particles of spin $\alpha, \beta, \gamma, \delta$. Following the usual mean-field arguments for the BCS theory, we can decouple the four-particles interactions and we obtain the mean-field Hamiltonian

$$H^{MF}_{int} = \sum_{kk'} V_{\alpha\beta\gamma\delta}(k,k') \langle c^\dagger_{k'\alpha} c^\dagger_{-k'\beta} \rangle c_{-k\gamma} c_{k\delta} + h.c. \tag{1.10}$$

where the BCS gap parameters are

$$\Delta_{\alpha\beta} = \sum_{k'\gamma\delta} V_{\alpha\beta\gamma\delta} \langle c_{-k'\gamma} c_{k'\delta} \rangle. \tag{1.11}$$

Hence, within the generalised BCS theory, the superconducting order parameters can be formed by four different expectation values which depend on the spin of the electrons

forming the Cooper pairs. It is usually convenient to express them in a matrix form which can be decoupled as the sum of a scalar Δ_0 and a three-dimensional vector, the so-called $\vec{d}$-vector, such that

$$\hat{\Delta}(k) = \begin{pmatrix} \Delta_{\uparrow\uparrow}(k) & \Delta_{\uparrow\downarrow}(k) \\ \Delta_{\downarrow\uparrow}(k) & \Delta_{\downarrow\downarrow}(k) \end{pmatrix} = \begin{pmatrix} -d_x(k) + id_y(k) & d_z(k) + \Delta_0(k) \\ d_z(k) - \Delta_0(k) & d_x(k) + id_y(k) \end{pmatrix},$$

where the $\vec{d}$-vector components are related to the pair correlations for the various Cooper pair configurations such that

$$d_x = \frac{1}{2}(-\Delta_{\uparrow\uparrow}(k) + \Delta_{\downarrow\downarrow}(k)), \tag{1.12}$$

$$d_y = \frac{1}{2i}(\Delta_{\uparrow\uparrow}(k) + \Delta_{\downarrow\downarrow}(k)), \tag{1.13}$$

$$d_z = \Delta_{\uparrow\downarrow}(k) - \Delta_0(k). \tag{1.14}$$

As we have done previously, let us now analyse the symmetry of the order parameters. By exchanging momentum and spin between the operators of the correlation functions, we find that

$$\Delta_k = \Delta_{-k}\ , \tag{1.15}$$

$$d_k = -d_{-k}\ . \tag{1.16}$$

The scalar order parameters is even under the parity operation $k \to -k$, while the $\vec{d}$-vector is odd. It follows that the electrons bounded in Cooper pairs represented by the scalar order parameter form therefore a spin-singlet state, while the electron pairs described with the $\vec{d}$-vector are forming a spin-triplet state.
From the definitions of the spin-triplet order parameters, we can see that the electrons can formed three different quantum states $|\uparrow\uparrow\rangle$, $|\downarrow\downarrow\rangle$ and $(|\uparrow\downarrow\rangle + |\downarrow\uparrow\rangle)/\sqrt{2}$ with three different pair spin projections along the z-direction $S_z = 1, -1$ and 0, respectively. Thus, the $\vec{d}$-vector has a direct physical meaning since it is defined such that the its direction $\vec{u}$ is associated to the quantum axis for which the pair spin projection is zero, i.e. $S_{\vec{u}} = 0$. For unitary states, with $\vec{d} \times \vec{d} = 0$, the electrons of the Cooper pairs associated to this state can be seen as having spins lying in the plane perpendicular to the $\vec{d}$-vector . The pair spin projection is especially important in the analysis of the system in interaction with a magnetic field or, as in our case, at the interface with a ferromagnet, since the magnetization interacts directly with the spin of the electrons and, as a consequence, leads to various observable effects which are directly related to the orientation of the $\vec{d}$-vector .
In contrast to the BCS theory with local pairing for which the superconducting gap is independent of the momentum, the generalised BCS Hamiltonian allows various dependence in momentum of the orbital part of the order parameters, for spin-triplet as well as spin-singlet pairings. Materials with such dependence are generally referred as the unconventional superconductors but the experimental identification of the exact symmetry remains one challenging task, in particular in the case of spin-triplet superconductors. The theoretical arguments to justify the possible kinds of pairing achieved in the various superconducting materials are based on the point group symmetries of the crystals as

well as the strength of the pairing coupling between electrons. The discussion about all possible superconducting states as well as the exact nature of the pairing in the various materials goes far beyond our analysis and readers can find detailed overviews in few references [101, 121]. It is especially not necessary to know the proper form of the electrons pairing in problems dealing with proximity effects since generally only the spin states of the order parameters as well as the orbital symmetry are important. In the following, we shall focus on the spin-triplet superconductors with specific p-wave orbital symmetries which are our main interest in this manuscript.

Helical and Chiral p-wave Superconductors The results on proximity effects analysed in this thesis are obtained at the interface of two different p-wave superconductors with specific spin-triplet superconducting states that we described in the following paragraph. First of all, it is important to mention that both of them have in common to occur in two-dimensional planes although the system can be three-dimensional. In other words, the attractive pairing is assuming to form Cooper pairs with electrons belonging to the same two-dimensional planes, as it is believed for instance to occur generally in superconducting cuprates. If we define this plane to be represented by the x- and y-directions, the orbital function of the $\vec{d}$-vector, i.e. of the superconducting order parameters, depends hence on the k_x and k_y in-plane momenta.
The first spin-triplet state upon interest are the spinful chiral (p_x+ip_y)-wave or (p_x−ip_y)-wave states, both cases being equivalent. The symmetry order parameter is characterised by

$$\vec{d} = (0, 0, \sin(k_x) \pm i\sin(k_y)). \tag{1.17}$$

By definition, the chiral superconducting state represented by the above $\vec{d}$-vector respects the odd symmetry under the parity operation $(k_x,k_y)\rightarrow(-k_x,-k_y)$. Moreover, the $\vec{d}$-vector is pointing in the z-direction, i.e. perpendicular to the (xy)-plane, and therefore the pair spin projection of the Cooper pairs is $S_z = 0$. The Cooper pairs can be represented as an equal superposition of pairs of electrons having same spins, in any direction in the (xy)-plane [96]. Finally, this spin-triplet state has the particularity to break the particle-hole symmetry as well as the time-reversal symmetry.
The second spin-triplet state that we shall consider in the last Chapter is the helical state characterised by the order parameter

$$\vec{d} = (\sin(k_y), \sin(k_x), 0). \tag{1.18}$$

In this case, the $\vec{d}$-vector lies in plane and both components d_x and d_y depend on the momentum of the electrons forming the Cooper pairs. In this case, the spin-triplet state is made of Cooper pairs with equal-spin electrons parallel or antiparallel to the z-direction. The first kind of Cooper pairs carry a spin pair projection $S_z = +1$ while the second have $S_z = -1$ [96]. In contrast to the chiral states, the helical state respects both the time-reversal symmetry as well as the particle-hole symmetry. The presence or not of the time-reversal and particle-holes symmetries in the framework of the BCS theory became one of the major way to characterise and analyse the superconducting states. Indeed, according to those symmetries, it was shown that the BCS superconductors could be sorted in few universal classes, in a similar fashion than the topological insulators [106,115]. Each

class of topological superconductors exhibits different electronic properties in the bulk and at the edge of the materials, which depend strongly on the dimension of the system. The two-dimensional chiral and helical spin-triplet states do not have the same symmetries and do not belong to the same class of topological superconductors. Both kinds have a fully gapped energy spectrum in the bulk, as for conventional superconductors, and have gapless edge states at theirs boundaries. However, the dispersion of the edge states are different and depend on the symmetry of the superconducting state. For chiral spin-triplet state, the spin up and spin down have the same dispersions and, therefore, charge current can be carried along the edges. On the other hand, spin up and spin down electrons at the edge of helical spin-triplet superconductor have opposite dispersions and are propagating in opposite direction, leading to the existence of a dissipationless spin-current. The tuning of the gapless edge states and, therefore, of the the spin-current by an interfaced ferromagnet will be our main interest in the last Chapter of this thesis.
To conclude the introduction of the spin-triplet states, we can mention that many experimental evidences have shown that the chiral spin-triplet state could be realised in Sr_2RuO_4 [96, 97]. According to those results, the Fermi surface of the metallic state of Sr_2RuO_4 exhibits a three-band electronic structure made of cylindrical sheets. Its properties of conduction show that the metallic state is a strongly two-dimensional Fermi liquid, which justifies the use of the BCS theory to model the superconducting state. Moreover, in the superconducting state, the coherence length is found twenty times larger in-plane than out-of-plane. Therefore, in order to model these properties within the one-band tight-binding model, we shall consider the Cooper pairs to be formed by electrons which belong to the same planes and, in the case of three-dimensional system, we shall consider the out-of-plane hopping term to be smaller than the in-plane hopping terms. Using hopping terms only between nearest-neighbours, the energy spectrum is taken such to lead to a cylindrical Fermi surface. It is finally worth to mention that, although the chiral spin-triplet state seems to be a good candidate for Sr_2RuO_4, few experiments are still showing more complex behaviour. Recent new measurement of the Fermi surface even suggested that the spin-orbit interaction was unexpectedly large enough to induce a coupling between the different electronic band structures, which could signifies that the superconducting state is not purely spin-triplet [132].

1.2 Two-Dimensional Single-Band Extended-Tight-Binding Model

This section is devoted to the derivation of the two-dimensional extended-tight-binding model and the presentation of the lattice configuration that we shall use in the rest of the manuscript. The tight-binding model is also use to model the ferromagnet by means of an exchange field which induces a splitting of the spin up and spin down electronic structure and which can be usually use to describe itinerant ferromagnet.

Singlet-Band Extended-Tight-Binding Hamiltonian The basic ingredient of our theory is the tight-binding model which can describe the electronic band structure of a system of electrons, which are located at specific atomic sites of a lattice. In second quantization, without particle interaction, the Hamiltonian is only describe by the hopping

integral t_{ij} between two sites i and j which is associated to the energy of the electrons hopping from one site to the other. Interactions between electrons are generally added to obtain more complex models as the Hubbard model, with an additional one-site repulsion energy, and the $t-J$ model, with an additional energy associated to the spin interactions. In our model, however, an additional attractive nearest-neighbour interaction between opposite-spin electrons, V_i, and equal-spin electrons, V_i', are added to the usual tight-binding model in order to yield a spin-triplet pairing symmetry in the superconducting region. As we have mentioned previously, the pairing interactions are only use as an effective coupling to induce the existence of a condensate state and do not aim to reproduce exactly the superconducting pairing. The extended-tight-binding Hamiltonian is

$$\begin{aligned} H_0 &= -\sum_{\langle ij\rangle,\sigma} t_{i\sigma}(c_{i\sigma}^{\dagger}c_{j\sigma} + h.c.) - \mu\sum_{i\sigma} n_{i\sigma} \\ &+ \sum_{\langle ij\rangle} V_i(n_{i\uparrow}n_{j\downarrow} + n_{i\downarrow}n_{j\uparrow}) + \sum_{\langle ij\rangle} V_i'(n_{i\uparrow}n_{j\uparrow} + n_{i\downarrow}n_{j\downarrow}) \end{aligned} \tag{1.19}$$

where i and j are sites on the lattice, μ is the chemical potential, V_i is the nearest-neighbour attraction between two electrons of opposite spins on the site i and V_i' is the nearest-neighbour attraction between two electrons with same spins on the site i. We can note that the index i -and j- represents the spatial coordinates of electrons in the x- and y- directions on the two-dimensional lattice. This is implied that we have more precisely $i = (i_x, i_y)$ and $j = (j_x, j_y)$.
We use the itinerant Stoner model to induce ferromagnetism in our model. It is also based on the tight-binding model and includes additionally a local exchange field h, on each site i of the ferromagnetic region, which splits the spectrum energy of the spin up and down electrons, resulting in a local magnetic order parameter. It is used as a first approximation to describe itinerant ferromagnet. The exchange field interacts with the spin as

$$H_M = \sum_i \vec{h_i} \cdot \vec{s_i} \tag{1.20}$$

where $\vec{h_i} = (h_x(i), h_y(i), h_z(i))$ is the exchange field at the site i and where the spin density of the site i is

$$\vec{s_i} = \sum_{i\sigma\sigma'} c_{i\sigma}^{\dagger}\vec{\sigma}_{\sigma\sigma'}c_{i\sigma'} \tag{1.21}$$

with $\vec{\sigma}$ the Pauli vector

$$\vec{\sigma} = \sigma_x\vec{e_x} + \sigma_y\vec{e_y} + \sigma_z\vec{e_z}. \tag{1.22}$$

The Eq. 1.20 can therefore be assimilated to an additional shift of chemical potential μ, for which the sign depends on the direction of the spin of the electron. Finally, the final system is represented by the extended-tight-binding Hamiltonian including the Stoner mechanism for the ferromagnet

$$H = H_0 + H_M \ , \tag{1.23}$$

where the exchange field is nonvanishing only in the ferromagnetic region, for the sites $i_x \in$ FM, and where the attractive coupling are finite only when the two sites are in the superconducting region $(i_x, j_x) \ \in$ TSC. The basic two-dimensional lattice is represented

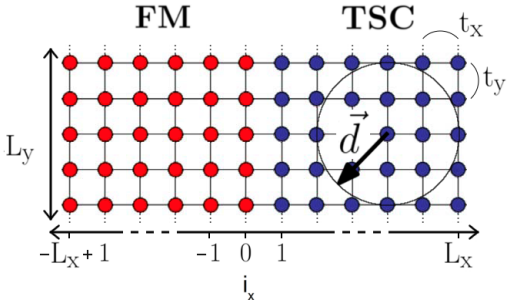

Figure 1.1: View of the $L_x \times L_y$ FM-TSC lattice with the interface perpendicular to the x-direction and infinitely long along the y-direction. t_x and t_y are the hopping terms in the x- and y-directions, respectively. In this example, the $\vec{d}$-vector is in-plane, corresponding to the helical TSC. The interface between the two regions is situated between the sites $i_x = 0$ (FM) and $i_x = 1$ (TSC).

in Fig. 1.1 where the TSC region is located at the site $i_x \geq 1$ and the ferromagnetic region is located at the sites $i_x \leq 0$. We shall use this reference for all the results presented in the following of the thesis. In this special case, the $\vec{d}$-vector is represented in the (xy)-plane, i.e. for a helical TSC, but will be perpendicular to the plane for chiral spin-triplet states.

Hartree-Fock approximation As we have seen for the BCS Hamiltonian, the quartic terms due to the attractive pairing in Eq. 1.19 must be decoupled using the Hartree-Fock approximation within the two pairing channels. We first introduce the pairing amplitudes for in-plane bond between two electrons, on sites i and j, and with spin σ and σ', as

$$F_{ij}^{\sigma\sigma'} = \langle c_{i\,\sigma} c_{j\,\sigma'} \rangle \tag{1.24}$$

where the average $\langle A \rangle$ indicates the thermal expectation value of the operator A. Within such a decoupling scheme, the four-particles interactions are approximated as

$$V_i n_{i\sigma} n_{j\sigma'} \simeq V[\, F_{ij}^{\sigma\sigma'} c_{j\sigma'}^\dagger c_{i\sigma}^\dagger + F_{ij}^{\sigma\sigma' *} c_{i\sigma} c_{j\sigma'} - |F_{ij}|^2 \,]. \tag{1.25}$$

Hence the Hartree-Fock Hamiltonian can be written as

$$\begin{aligned} H_{HF} - E_0 = & - \sum_{\langle ij \rangle, \sigma} t_{i\sigma} (c_{i\sigma}^\dagger c_{j\sigma} + h.c.) - \mu \sum_{i\sigma} n_{i\sigma} \\ & + \sum_{\langle ij \rangle} V_i [\, F_{ij}^{\uparrow\downarrow} c_{j\downarrow}^\dagger c_{i\uparrow}^\dagger + F_{ij}^{\downarrow\uparrow} c_{j\uparrow}^\dagger c_{i\downarrow}^\dagger + h.c. \,] \\ & + \sum_{\langle ij \rangle, \sigma} V_i' [\, F_{ij}^{\sigma\sigma} c_{j\sigma}^\dagger c_{i\sigma}^\dagger + h.c. \,] \end{aligned} \tag{1.26}$$

where E_0 is the energy coming from the Hartree-Fock approximation

$$E_0 = -\sum_i V_i [\, |F_{ij}^{\uparrow\downarrow}|^2 + |F_{ij}^{\downarrow\uparrow}|^2 \,] - \sum_i V_i' [\, |F_{ij}^{\uparrow\uparrow}|^2 + |F_{ij}^{\downarrow\downarrow}|^2 \,]. \tag{1.27}$$

Having derived the extended-tight-model for our lattice model, we must now numerically evaluate self-consistently the pairing amplitudes $F_{ij}^{\sigma\sigma'}$. Indeed, as we shall see in the next section, they are used to construct the superconducting order parameters on the lattice. To compute them, we first consider periodic boundary conditions in the y-direction, i.e. we

consider the system to be infinite in along the interface, we solve the BdG equations and we express the pairing amplitudes as a function of the coherent factors, in a similar way than for Eqs. 1.6 - 1.7. The complete derivation is detailed in the Appendix A. Finally, the self-consistent procedure consists in choosing an initial value for the pairing amplitudes $F_{ij}^{\sigma\sigma'}$ and, then, solving the BdG equations. The same procedure has to be repeated with the new values of the pairing amplitudes until the solutions become stable. If $F_{ij}^{\sigma\sigma'}$ does not depend on (i,j) in the superconducting bulk, we shall see that it is generally suppressed at the interface with vacuum, normal metal or ferromagnet. In the rest of the Chapter, we will focus on describing the bulk properties as well as the proximity effects for chiral spin-triplet superconductor. Therefore, the pairing amplitude between equal-spin electrons is zero in the following.

1.3 Superconducting Order Parameters and Density of States

We define in this section the spin-singlet and spin-triplet order parameters on the lattice in function of the pairing amplitudes $F_{ij}^{\sigma\sigma'}$ and we verify that they respect the symmetries with the spin and momentum. We shall introduce the spin-resolved spectral functions and electronic densities which give important information about the electronic states on each site of the lattice.

Superconducting Order parameters on the Lattice The bond pairing amplitudes are not enough to characterize the superconducting phase of the bulk system. We need to define a new quantity which also contains the symmetry, over spin and momentum, of the energy gap known for the extended s-wave, d-wave, p_x-wave and p_y-wave superconductors. For that purpose we can build the superconducting order parameters from the bond pairing amplitudes. They are generally defined as

$$\Delta_s(i) = V_i F_s(i) = V_i \left[F_i^{x+(S)} + F_i^{x-(S)} + F_i^{y+(S)} + F_i^{y-(S)} \right] /4, \tag{1.28}$$

$$\Delta_d(i) = V_i F_d(i) = V_i \left[F_i^{x+(S)} + F_i^{x-(S)} - F_i^{y+(S)} - F_i^{y-(S)} \right] /4, \tag{1.29}$$

$$\Delta_{p_x}(i) = V_i F_{p_x}(i) = V_i \left[F_i^{x+(T)} + F_i^{x-(T)} \right] /2, \tag{1.30}$$

$$\Delta_{p_y}(i) = V_i F_{p_y}(i) = V_i \left[F_i^{y+(T)} + F_i^{y-(T)} \right] /2, \tag{1.31}$$

$$\Delta_{p_x}^{\sigma\sigma}(i) = V_i' F_{p_x}^{\sigma\sigma}(i) = V_i' \left[F_{i,\sigma\sigma}^{x+} + F_{i,\sigma\sigma}^{x-} \right] /2, \tag{1.32}$$

$$\Delta_{p_y}^{\sigma\sigma}(i) = V_i' F_{p_y}^{\sigma\sigma}(i) = V_i' \left[F_{i,\sigma\sigma}^{y+} + F_{i,\sigma\sigma}^{y-} \right] /2. \tag{1.33}$$

where we used for clarity $F_{ij} \equiv F_{ij}^{\uparrow\downarrow}$ and where the spin-singlet and spin-triplet pairing amplitudes on the bond are defined by

$$F_{ij}^S = (F_{ij} + F_{ji})/2 \ ,$$
$$F_{ij}^T = (F_{ij} - F_{ji})/2 \ .$$

Moreover, we used the following notations to show the correlations from one site to its nearest-neighbour in the x- and y-directions

$$\begin{aligned} F_i^{x\pm} &= F_{i,i\pm\hat{x}}, \\ F_i^{y\pm} &= F_{i,i\pm\hat{y}}, \\ F_{i,\sigma\sigma}^{x\pm} &= F_{i,i\pm\hat{x}}^{\sigma\sigma}, \\ F_{i,\sigma\sigma}^{y\pm} &= F_{i,i\pm\hat{y}}^{\sigma\sigma}. \end{aligned}$$

It is important to keep in mind that $\Delta_\alpha(i)$ are the superconducting gap parameters while $F_\alpha(i)$ are only the pair correlations functions. The difference is that V_i being null in the ferromagnet, the SC order parameters cannot exist in this side of the junction. However, the leakage of the Cooper pairs into the metal or the ferromagnet, through the Andreev reflection, leads to a finite pairing amplitude $F_\alpha(i)$ in the ferromagnet close to the interface (infinite when T=0K).
Let us analyse the symmetries of the order parameters. The order parameters have the same symmetries that the wave functions, which are antisymmetric under particles exchanges $-k\sigma \leftrightarrow k\bar{\sigma}$. Indeed, we obtain from the general expression of the order parameter

$$\begin{aligned} \Delta_{\alpha\beta}(k) = &\quad \langle c_{-k\alpha} c_{k\beta} \rangle \\ &= -\langle c_{k\beta} c_{-k\alpha} \rangle \\ &= -\Delta_{\beta\alpha}(-k). \end{aligned}$$

By construction of the F_{ij}^S and F_{ij}^T, it is easy to verify that

$$\begin{aligned} F_{i,j} + F_{j,i} &\quad \text{is antisymmetric under spin exchange,} \\ F_{i,j} - F_{j,i} &\quad \text{is symmetric under spin exchange.} \end{aligned}$$

On the other hand, we can write the pairing amplitude after Fourier transformation as

$$F_{i,i+1} \propto \sum_k c_{k\uparrow} c_{-k\downarrow} e^{-ika} \tag{1.34}$$

and, by exchanging the sign of the momentum $k \leftrightarrow -k$ in the latter, we obtain that

$$\sum_k c_{-k\uparrow} c_{k\downarrow} e^{ika} = F_{i,i-1} \ . \tag{1.35}$$

Therefore, we obtain by construction that

$$\begin{aligned} F_{i,i+1} + F_{i,i-1} &\quad \text{is symmetric under momentum exchange,} \\ F_{i,i+1} - F_{i,i-1} &\quad \text{is antisymmetric under momentum exchange.} \end{aligned}$$

Hence, we verified that the order parameters Δ_s and Δ_d are symmetric with respect to the exchange of momentum $k \leftrightarrow -k$ while they are antisymmetric under spin exchange $\sigma \leftrightarrow \bar{\sigma}$. The difference between the two spin singlet order parameters is coming from the opposite sign in front of the orbital part in the y-direction. We also verified that Δ_{p_x} and Δ_{p_y} are antisymmetric with respect to the exchange of momentum, $(k_x, k_y) \leftrightarrow (-k_x, -k_y)$ and antisymmetric under spin exchange $\sigma \leftrightarrow \bar{\sigma}$.

Spectral Functions and Electronic Densities The spectral function is the main tool to probe the nature of the occupied and not occupied electronic states inside our system. We shall especially use it in the last Chapter in order to investigate the hybridization of the helical edge states. There are obtained by evaluating the imaginary part of the single particle Green's function through the Fourier transformation of the two-time correlator

$$A_\sigma(i_x, k_y)(\omega) = -\frac{1}{\pi}\int d\tau \mathrm{Im}[\langle c^\dagger_{i_x k_y \sigma}(\tau) c_{i_x k_y \sigma}(0)\rangle] e^{i\,\omega\tau} \tag{1.36}$$

for which we have assumed periodic boundary conditions along the y-direction and where $\langle ... \rangle$ is the average on the ground state and $c^\dagger_{ik\sigma}$ the creation operator of an electron at the site i_x with momentum k_y and spin-polarization σ. We shall use in the last Chapter the $\sigma = \uparrow$ ($\downarrow$) configurations which refer to the z-direction in the spin space. They are numerically evaluate using the coherence factors, obtain after diagonalisation of the BdG equations, and the Lehmann representation of the Green's functions.
Finally, we obtain the spin-resolved electronic densities on each site of the lattice from the spectral functions

$$N_{i\sigma} = \sum_{k_y} \int_0^{E_F} d\omega A_\sigma(i_x, k_y)(\omega)\ . \tag{1.37}$$

1.4 Properties of Two-Dimensional Bulk TSC

We show in this section the basic numerical evaluations of the superconducting order parameters of the extended-tight-binding model. More precisely, we present the convergence of the self-consistent evaluation of the order parameters by solving the gap equations and we discuss the symmetry of the $F(k_x, k_y)$ pair correlations. Finally, we present the total phase diagram of the model. This section is only devoted to chiral TSC heterostructures, with a $\vec{d}$-vector perpendicular to the plane. All the results are therefore obtained with $V' = 0$.

Convergence of the Order Parameters The stability of the converged solution can be addressed by looking at the convergence of the gap equation for different initial values of the order parameters. The left panel of the Fig. 1.2 shows an example of the variation of the computed spin-triplet order parameter F_{px} during the self-consistent procedure by starting from different initial values. The parameters are $\mu = -1.6t$, $V = 2.0t$ and T=0K. We see that, after certain amount of iterations, all the cases converge to the same final value which can be considered as stable. It is worth to mention that the initial values of the spin-singlet order parameters were also present initially but vanished with the self-consistency procedure. It insures us the convergence to a pure spin-triplet phase for this fixed values of μ and V.
The pairing interaction V influences directly the value of the order parameters as we can see on the right panel of the Fig. 1.2. It shows the variations of the spin-triplet order parameter F_{px} during the self-consistent procedure for various values of V and $\mu = -1.6t$. We can observe that the larger the pairing attraction is, the larger the order parameter is. It follows the trend of the BCS theory since, in the latter, $\Delta(0)$ is increasing when V

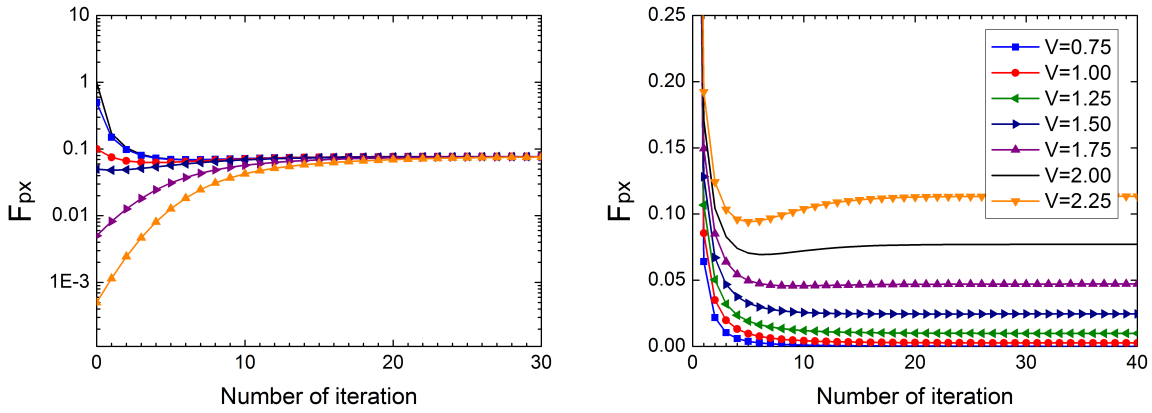

Figure 1.2: Convergence of the order parameter during the self-consistent procedure of the gap equation (A.74). The left panel shows the convergence for different initial values for a pairing coupling V$= 2.0t$ while the right panel show the convergence for different value of the pairing coupling.

increases.

We demonstrated in the previous section that the definitions of the superconducting order parameters given in Eqs. 1.28-1.33 respect the appropriate symmetries with respect to the spin and the momentum. In order to observe the symmetry of the orbital part, we plot in Fig. 1.3 the intensity of the s-wave, $d_{x^2-y^2}$-wave and p_x-wave order parameters resolved in the momentum space $F(k_x, k_y)$. The Fermi surfaces of the normal phases are denoted by the gray lines. We can observe on these figures two interesting results. First, we can see that the electrons forming the Cooper pairs have energies which are close to the Fermi surface. In BCS theory these electrons are bound into a nutshell of energy below the Debye frequency which is typically for BCS superconductors in the order of magnitude of 10^{12} - 10^{13} s^{-1}. This corresponds to a temperature of 10^2K and an energy of 3.10^{-2}eV. Adapted to our system, this will correspond approximately to 1% of the total electronic bandwidth, i.e. $0.08t$. We can see qualitatively here that electrons with lower energy than expected participate also to the pairing amplitude, although this energy is still bound. We can expect therefore that the order parameters can be over estimated compare to the BCS theory. Secondly, we can identify the symmetry of the orbital function of each superconducting phase. Indeed, the middle panel shows the $d_{x^2-y^2}$-wave superconducting phase with the $\cos(k_x)-\cos(k_y)$ symmetry while the right panel shows the p$_x$-wave phase with the $\sin(k_x)$ symmetry. The left panel is more difficult to appreciate. The extended s-wave phase has a $\cos(k_x)+\cos(k_y)$ symmetry and heigh nodes should be present, all close to the momentum $k_x = 0$ and $k_y = 0$, which are not observable here although we can see that $F(k_x, k_y)$ is not invariant by rotation. Neverthelesss, it confirms clearly for the two other cases that the symmetries of the order are the one expected. Finally, concerning the p_x-wave SC we can see that a chemical potential value chosen at $\mu = -1.8t$ gives a Fermi surface close to the γ-band observed experimentally in the case of Sr_2RuO_4 [96]. We will generally use this value for each system including the p_x+ip_y SC state.

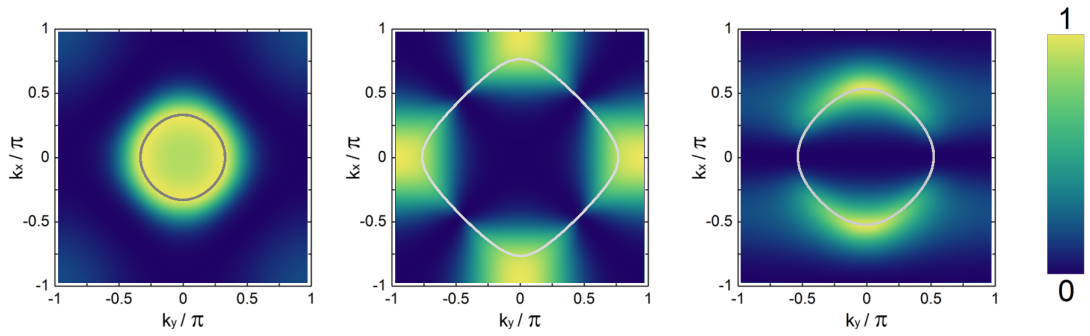

Figure 1.3: Intensity of the order parameter $\mathrm{F}_\alpha(k_x, k_y)$ for extended s-wave (left panel), $d_{x^2-y^2}$-wave (middle panel) and p_x-wave (right panel) for two-dimensional bulk superconductors. The chemical potential μ is $-3.0t$, $-0.5t$ and $-1.8t$, respectively, and the gray lines represent the Fermi surfaces in the normal state.

The results presented in the previous paragraph were obtained by computing self-consistently the gap equations Eq. A.72. Numerical convergences of physical equations are however not obvious and can demand, for some difficult problems, special expertise in numerical science and sometimes mathematics. Fortunately the convergence of the order parameters in the present case does not require many efforts. Of significance, however, is to be convince of the stability of the solution.

μ-T phase diagram and Order Parameters Symmetries Within the BCS theory, the superconducting gap parameters depend on several physical quantities. It predicts that, at zero temperature and for conventional superconductors, the gap parameter depends on the critical temperature as $\Delta(0)/kT_c = 1.764$ while T_c depends on the electronic density at the Fermi surface N_0, the pairing potential V and the Debye frequency w_c as $kT_c = 1.13 w_c \exp(-1/N_0 V_{\text{eff}})$. Moreover for $T \sim T_c$, the order parameter has a square-root dependence with respect to the temperature. Although our model is also a mean field approximation, it does not provide the exact same dependence of the critical temperature or of $\Delta(0)$ since it should depend, for instance, on the Debye frequency that is not fixed here[1]. However, the equations derived in the previous section show also a dependence of the model on parameters. More precisely it depends on the bandwidth of the electronic band structure through the hopping term $t_{i\sigma}$, on the Fermi energy through $t_{i\sigma}$ and the chemical potential μ, on the pairing potential V_i and on the temperature T.
The Fig. 1.4 shows the superconducting phases of the SC bulk with respect to the temperature T and the Fermi energy, adapted from [84], obtained after self-consistent evaluation of the lattice gap equations. At T=0K, we observe that the d-wave superconducting states is stable for $0t > \mu > -0.7t$, the p_x+ip_y-wave state for $-1.2t > \mu > -2.2t$ and the ex-

[1]It is still numerically possible to add a cutoff in energy to compute the SC order parameters but this case was not treated in the framework of this work. However we expect the results to be qualitatively close to the one found since the SC symmetries are still respected. Only the gap value, and so the density of states, should be slightly affected by an additional cutoff.

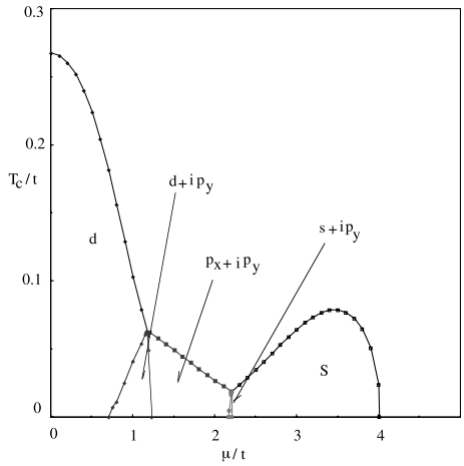

Figure 1.4: Superconducting $\mu - T$ phase diagram of the extended-tight-binding model obtained after self-consistent evaluation of the lattice gap equations (see Appendix A). The stabalised superconducting phase depends strongly on the chemical potential. At T=0K, the chiral spin-triplet state can be obtained for $\mu \in [1.3t, 2.1t]$. From Ref. [84].

tended s-wave state for $-2.2t > \mu > -4.0t$. Moreover, additional mix states can also exist in the bulk for some parameters of the system, which can be understood from a Ginzburg-Landau analysis [84]. Therefore, for fixed parameters $T < T_c$ and V, we can choose the model to exhibit one of the superconducting phase by choosing one value of the chemical potential.
It is finally worth to mention that, although T_c depends directly on the value of the pairing coupling V, the superconducting phase at T=0K are independent of V. Therefore, all the numerical analysis performed in the following are performed using a chemical potential $\mu \sim -1.8t$.

1.5 Properties at the Edges of the TSC

We investigate in this section spatial variation of the order parameters at the boundaries of the TSC. Contrary to the previous paragraph where the bulk order parameters were computed, we need to solve here the Bogoliubov-De Gennes equations self-consistently to obtain the order parameters on each point of the lattice, see Fig. 1.1, as explained in Appendix A. In the present case the ferromagnet can be replaced by either the vacuum or a normal metal. The lattice is supposed to be infinite along the y-direction and therefore the system is equivalent to a quasi one-dimensional lattice and the spatial variations are present only in the x-direction. The self-consistent procedure consists to take an initial spatial profile for all the order parameters and to repeat two following steps: (i) to solve the Bogoliubov-De Gennes equations (see Appendix A) with the new values of the order parameters and (ii) to compute the new values of the SC and magnetic order parameters using the coherence factors. These two steps are repeated until the spatial profile of the order parameters converged, or equivalently, when the total free energy of the system converged. However, it is still necessary in both cases to verify that the order parameters have the same phase in each site of the bulk. We shall now discuss the results obtained for a TSC interfaced with vacuum, normal metals or ferromagnets. As the spin-triplet states are the main interest of this thesis, we shall not present the well-known results concerning spin-singlet superconductors heterostructures although they are achievable with our model. These cases should nevertheless be discussed in the following in order to point out the

difference with the TSC cases.
The vacuum interface is modelled by taking hopping terms an $t_{ij} = 0$ in the nonsuperconducting region, while the normal state has no exchange field $\vec{h}_i = 0$ and an hopping term $t_N = t_{SC} = 1.0$. The ferromagnetic region has the same hopping term $t_{FM} = t_{SC} = 1.0$ while the exchange field is pointing along the z-direction, i.e. $\vec{h} = h_z$. The numerical results are obtained for a chemical potential $\mu = -1.8t$ and a pairing coupling $V = 2.5t$. Unless further mention, they are obtained at zero temperature.

Order Parameters and Density of States at the Vacuum-TSC and Normal Metal-TSC Interfaces We first consider the simple boundary of spin-triplet superconductor with a $\vec{d}$-vector perpendicular to the plane, or in another term, we look at the interface of the TSC with the vacuum. The left panel of the Fig. 1.5 shows the spatial variation of the spin-triplet order parameters at the interface with the vacuum for the p_x+ip_y, p_x and p_y bulk TSC. In each case, we start the self-consistent procedure with the order parameters $\Delta(i) = 1t$ constant on the lattice. After self-consistency, only spin triplet order parameters are present in the TSC side and exhibit non trivial spatial variation close to the boundary. Let us first analyse the case of pure p_x-wave and p_y-wave TSC. For the p_x-wave TSC, we can see that the order parameter decreases to zero at the interface. This effect is due to the symmetry of the order parameter compare to the direction of the interface. Indeed, we have in this case $F_{px}(k_x) = \Delta_0 \sin(k_x)$ in the bulk. At the interface, electrons are reflected along the x-direction, therefore they conserved their momentum along the y-direction but they are reflected with an opposite momentum in the x-direction. Hence, a Cooper pair experience an opposite sign of the order parameter once it gets reflected at the boundary. One says that there is a phase shift of the order parameter with, in this case, a phase shift of π. It results on the cancellation of the order parameter. This effect is also present at the surface of $d_{x^2-y^2}$ spin singlet superconductors with the interface oriented in the [110] direction. It also explains that we do not observe it in s-wave or p_y-wave superconductor since the order parameters do not undergo phase shift after reflection. The later case is plotted also in the left panel of the Fig. 1.5. We can see that the order parameter have in the bulk the same value than the p_x-wave but that it does not cancel at the boundary.
Let us inspect the p_x+ip_y case. The F_{px} and F_{py} order parameters are also plotted in the left panel of the Fig. 1.5. We first notice that the value of the order parameters in the bulk are smaller that the one in the p_x or p_y TSC. We can understand this result by looking at the energy spectrum in the gap equation Eq. A.72. Indeed, the order parameters $|\Delta_k|$ have gapless point in the momentum space in the case of single p_x-wave or p_y-wave bulk TSC while it has none in the case of a p_x+ip_y-wave TSC for which $|\Delta_k| = |\Delta_{p_x} + i\Delta_{p_y}|$. Therefore the denominator of the gap equation, i.e. E_k, is larger in the latter case and the order parameter is finally smaller.
As for the p_x-wave TSC case, F_{px} decreases at the interface. However, we can observe that, contrary to the p_y interface, F_{py} is increasing at the interface. Microscopically, this is due to the fact that, because of the presence of bound states at the interface, there are more electrons available to form a Cooper pair and therefore the order parameter increases. This effects can also be understood in the framework of the Ginzburg-Landau theory that can be use to show that it is more energetically favourable for the system to

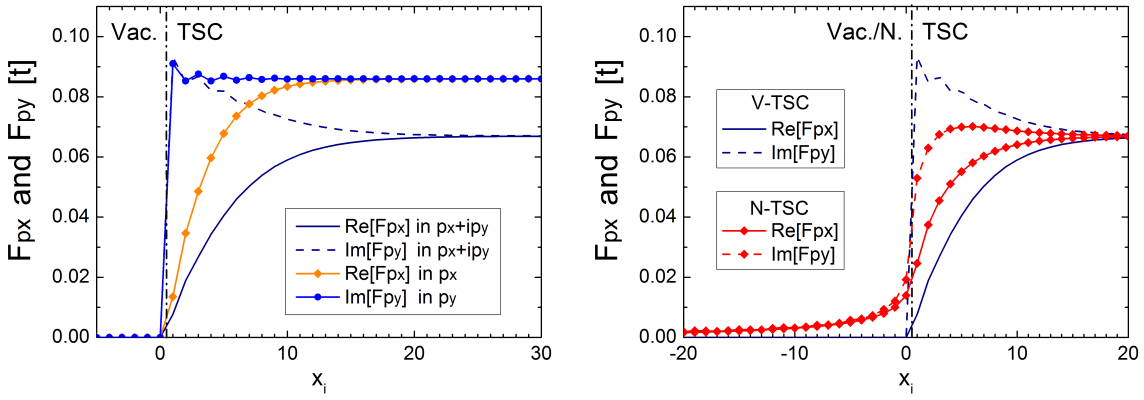

Figure 1.5: Left panel: spatial variations of the pairing amplitudes Fp_x and Fp_y for p_x (orange), p_y (blue) and p_x+ip_y (dark blue) TSC at the interface with vacuum. Right panel: spatial variations of the pairing amplitudes Fp_x and Fp_y for a p_x+ip_y TSC at the interface with vacuum (dark blue) and normal metal (red).

have F_{py} increasing while F_{px} is decreasing at the interface. Finally, the bound states at the interface are also changing of behaviour.

Let us compare these results to the normal metal-TSC interfaces. The right panel of the Fig. 1.5 shows the order parameters for both N-p_x+ip_y (red lines) and vacuum-p_x+ip_y (blue lines) interfaces. We can notice several differences between them. First, the pairing amplitudes are induced in the metal side and they decrease exponentially from the interface. This effect is due to the penetration of the Cooper pair into the metal due to the so-called Andreev reflections [5]. Indeed, an electron coming from the metallic region can not only be reflected or transmitted to the superconducting region, but also reflected as a hole. The details of this mechanism are discussed in Appendix B. It is valid for spin-triplet as well as spin-singlet superconductors and it is of great interest in superconducting heterostructure because it influences directly the properties of the conductance and the Josephson current. Secondly, we can see that the p_x order parameter is not totally suppressed at the interface any longer. This is due to the fact that a part of the Cooper pairs are not reflected at the interface but are instead transferred into the metal. Finally we can see that the p_y order parameter is also decreasing at the interface because normal electrons are also present into the gap due to the proximity effects with the metal.

Zero-Energy Edge States The cancellation of the gap at the boundary of the vacuum or, more exactly, the π shift of the order parameters after reflection of the Cooper pair, is associated to the presence of a zero-energy states (ZES) into the gap. In order to emphasize this point, we compute the spectral functions $A\sigma(i_x, k_y)(\omega)$, see Eq. 1.36, at the boundary of the p_x-wave and p_x+ip_y-wave TSC, i.e. at the interface with the vacuum. The results are shown in the left and right panels of the Fig. 1.6, respectively. We can see

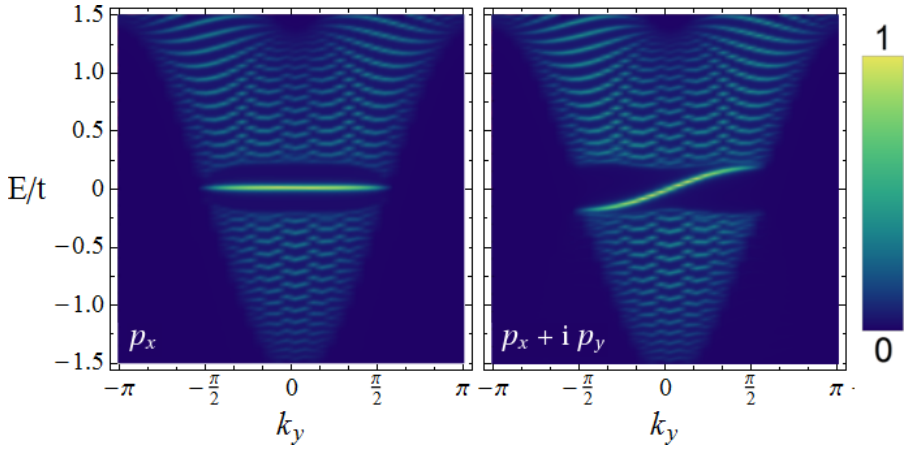

Figure 1.6: Energy Spectrum for both spin up and spin down electrons at the boundary ($i_x = 1$) of p_x-wave (left panel) and p_x+ip_y-wave (right panel) TSC, i.e. at the interface with vacuum. For the p_x-wave TSC, the states are also present in the bulk, while they are only present at the interface for the topological chiral p_x+ip_y-wave state.

can both cases exhibit zero energy states but that they are of different nature.
The p_x-wave spin-triplet superconductor exhibits a flat ZES, which is independent of the momentum in the y-direction. This state is actually also present in the bulk since, as we have seen in Fig. 1.3, the bulk gap parameter of the p_x-wave state is cancelled at $k_x = 0$. On the other hand, chiral p_x+ip_y-wave superconductor exhibits a fully gapped spectrum in the bulk while the gapless edge states are only present at the interface. As we mentioned in the first section, it is due to the time-reversal symmetry breaking of its superconducting state which induces chiral modes at the interface. The spin up and spin down electrons have the same dispersion and can carry a charge-current along the edges.

Order Parameters at the FM-TSC Interface Our main interest is the general characterization of heterostructures made of TSC and ferromagnets. It includes specially to understand the proximity effects at the FM-TSC interface. One of the main and most discussed results concern the spatial variations of the induced pairing amplitudes in the ferromagnet. In the following, we consider a FM-TSC interface with a magnetization and a $\vec{d}$-vector oriented in the z-direction, perpendicular to the plane. We reproduce in Fig. 1.7 the results of the spatial variation of the pairing amplitude at the FM-TSC interface for various values of the strength of the exchange field h [44].

Let us first consider the bottom panels of the Fig. 1.7 which show the spatial variation of the p_x and p_y components. In the TSC side, they have a very similar behaviour than the one observed in the N-TSC interface. The p_x component decreases monotonously at the interface while the p_y component exhibit a small increase few sites before the interface. The peculiar and main feature concerns the induced pairing amplitudes in the FM side of both components. Indeed, if they decrease such as the N-TSC interface, they also

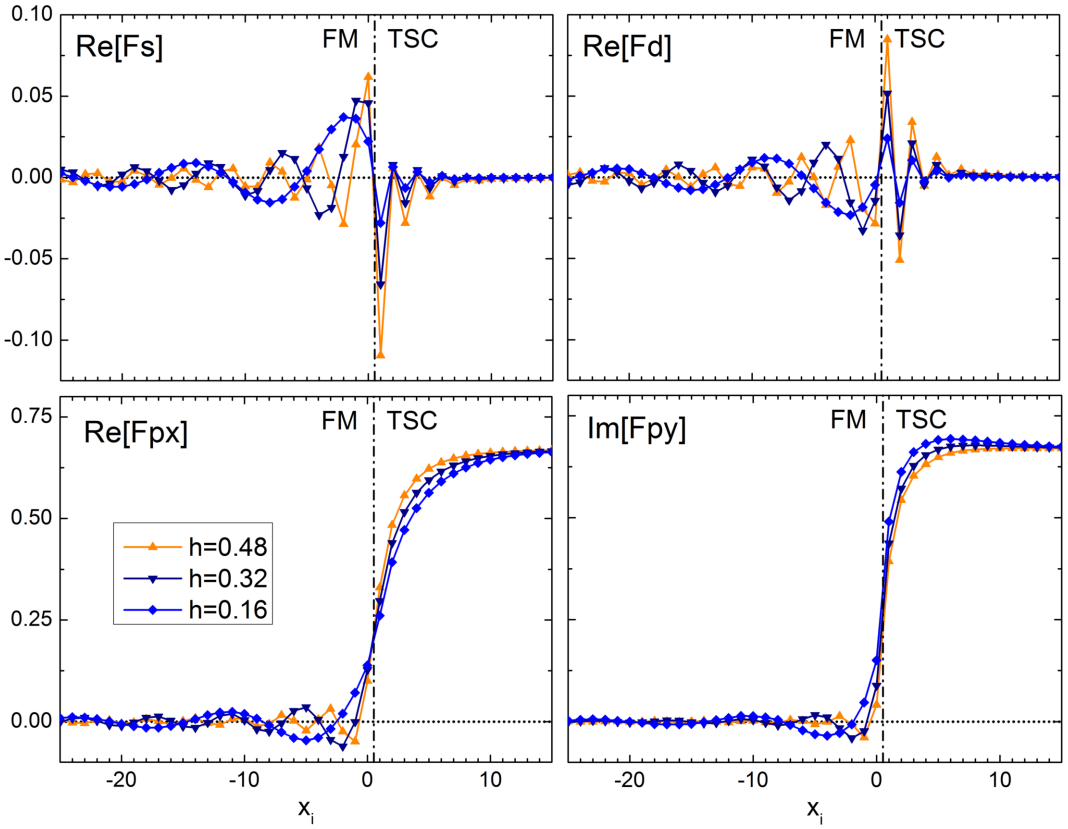

Figure 1.7: Spatial variations of the induced s-wave (top left panel), induced $d_{x^2-y^2}$-wave (top right panel), p_x-wave (bottom left panel) and p_y-wave (bottom right panel) pairing amplitudes at the two-dimensional FM - p_x+ip_y-wave interface for various values of the exchange field h aligned along the z–direction. The site $x_i = 0$ is the first FM site while the TSC starts at $x_i = 1$. The parameters are V=2.5t, T=0.005t and $\mu = -1.8t$.

oscillate in the FM side with the period of oscillations which depends on the strength of the exchange field. This general behaviour is also observed in the FM-SC interfaces and is, in both cases, similar to the so-called Fulde-Ferrel-Larkin-Ovchinnokov (FFLO) phase which determine the spatial modulation of the superconducting order parameters in superconductors with additional ferromagnetic order [58,86]. The microscopic mechanism is summarized in the Fig. 1.8. Two electrons with spin up and spin down forming a Cooper pair in the TSC (white dots) enter in the ferromagnet (black dotes). The pair is not an eigenstates in the normal metal and will decrease from the interface. Because of existence the exchange field in the FM, the spin up electron of the pair will experience a lower potential energy while the spin down electron will experience a higher potential energy. Therefore, in order to conserve their total energy, spin up and spin down electrons must increase and decrease respectively their kinetic energy. The momentum along the y-direction being conserved across the interface, the kinetic energy along the x-direction

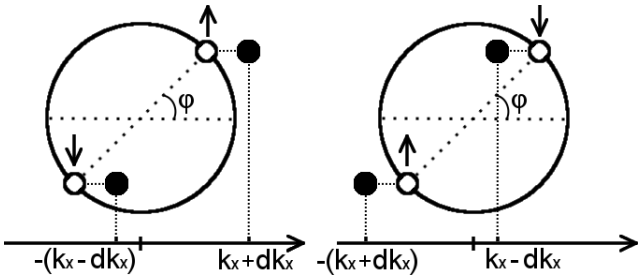

Figure 1.8: The spin up (down) electrons from Cooper pairs in the SC (electrons represented in white) increase (decrease) their kinetic energy when entering in the FM (electrons represented in black) in order to conserve their total energy. Hence the pairs of electrons entering in the FM acquire a center of mass $Q = \cos(\varphi) \cdot \mathrm{h}/\mathrm{v_f}$, φ being the angle between the momentum of the electrons and the interface.

is increased by $dk_x = h/v_F$. Hence the pair acquires a momentum in the x-direction of $Q = 2 \cdot dk_x$. The p_x+ip_y states with the $\vec{d}$-vector along the c-axis requires to form a symmetric states with the Cooper pair having opposite spin. The latter acquires therefore a momentum in the x-direction of $Q = -2 \cdot dk_x$. Finally, the oscillations of the order parameters is obtained by summing over all the incident angles φ of the Cooper pair. The spatial variations can be estimated [38, 46] as

$$F_\alpha(-x) \propto \frac{\sin(x/\xi_{FM})}{(x/\xi_{FM})} \quad \text{with} \quad \xi_{FM} = \frac{v_F}{2h}. \tag{1.38}$$

Therefore, the pairing amplitude decreases as $1/x$ in the ferromagnetic region and oscillates with a period ξ_{FM}. The period of the oscillations increases when h decreases, as observed in Fig. 1.7. It is worth pointing out that this simple approximation describes the interface at T=0K, such that long range pairing amplitudes with oscillations can be induced into the FM. However, at finite temperature the induced pairing amplitudes decrease on a shorter range and can be drastically suppressed. Moreover, the oscillations in the ferromagnetic region can also be completely cancelled if the FM is close to be half-metallic.
Another specific result to the two-dimensional FM-TSC interface is the apparition of induced spin-singlet order parameters while they are not present in the TSC bulk. Their spatial variations are shown in the top panels of the Fig. 1.7. As we can see, the singlet order parameters are oscillating and changing sign in both the FM and the TSC sides. The former effect is due to the same reason than for spin-triplet pairing amplitude, i.e. because of the momentum acquired by the Cooper pairs.

Influence of the Pairing Coupling We have seen that stabilised superconducting state obtained within the extended-tight-binding model was dependent on several parameters, as shown in the (μ,T)-phase diagram. The hopping term being taken generally as unity, it is interesting to discuss the influence of the pairing coupling on the TSC states. It is first important from a theoretical point of view to consider V such that $V \cdot \Delta_0$ is small

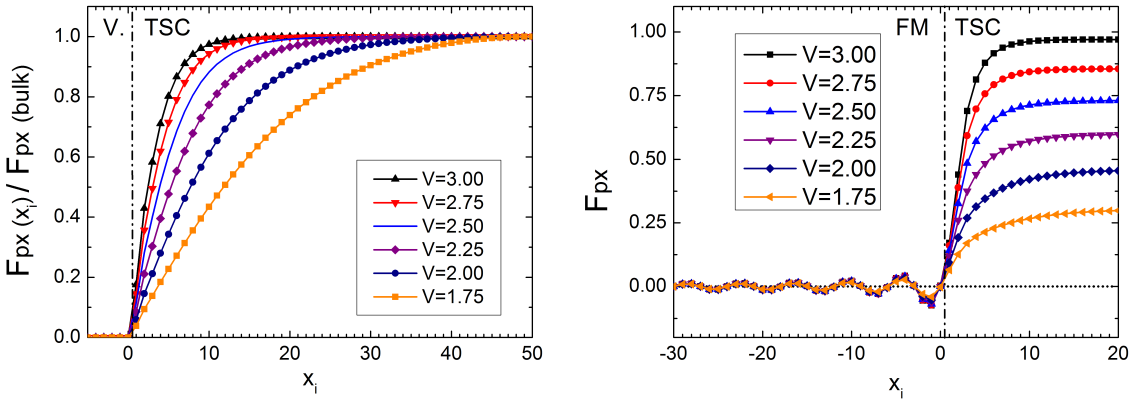

Figure 1.9: Spatial variations of the pairing amplitude F_{p_x} for various value of the pairing coupling V at the interface with vacuum (left panel) and of the ferromagnet with a magnetization along the c-axis (right panel). The pairing amplitude in the left panel are normalized by their value in the bulk.

enough in order to justify the mean field approximation. In the case of BCS theory, one condition to fulfil is that the superconducting gap should be much smaller than the energy spectrum bandwidth. So far, we have encountered examples where $0.2t \lesssim V \cdot F \lesssim 0.3t$, after self-consistency, which is much smaller than the spectrum bandwidth $4t$. Therefore, self-consistent computations with the upper limit value $V < 3.0t$ are reasonable. Moreover we already have seen in Fig. 1.2 that the order parameters in the bulk decreases when V decreases. Below one critical value $V < 0.5t$, the spin-triplet superconducting phase is not stable any longer and is suppressed during the self-consistent computations.

We are also interested in the influence of V on the spatial variations of the order parameters. The left panel of the Fig. 1.9 shows the variation of the p_x-wave state at the interface with the vacuum, the order parameters being normalized by the bulk value. We can observe that the larger V is, the larger is the region where the order parameter decreases. In other words, the coherence length of the TSC increases when V decreases. Nevertheless, it has from a qualitative point of view small influence on the observed proximity effect. We expect however the edge states and the associated current to be present deeper in the TSC bulk for smaller value of V. The results presented in the right panel of the Fig. 1.9 show also that the strength of the pairing coupling has a small influence on the oscillations of the induced pairing amplitudes in the FM. Indeed, as expected, the period of the oscillations does not depend on V, which is not present in the ferromagnetic region. However, the amplitude decreases slightly when V decreases due to the smaller amplitude of F_{px} in the superconducting region.

1.6 Conclusion

The first chapter gave us the opportunity to develop the extended-tight-binding model on the real space. Using a mean-field approach and solving the Bogoliubov-De Gennes equations self-consistently, we have shown that this model can exhibits different spin-singlet, spin-triplet or mix superconducting phases in the bulk according to the value of the parameters, in particular to the chemical potential. We have reproduced several results for two-dimensional systems with chiral spin-triplet states and we especially discussed the spatial variations of the superconducting pair correlations at the interface with vacuum and metallic regions.
The results shown a rich physics due to chiral properties of the p_x+ip_y superconductor, related to the existence of gapless edge states. We have seen, in two-dimensional system, that the F_{px} and F_{py} pairing amplitudes were cancelled and enhanced, respectively, at the interface with vacuum. The first effect is due to the translation symmetry breaking in the x-direction which induced a π-shift in the phase of the reflected Cooper pairs at the boundaries. Midgap states are then present in the electronic spectrum and tend to increase F_{py}. The same trend is observed at the interface with a metal. However, the presence of additional proximity effects, in particular the Andreev reflections at the interface, reduces the effects and both pairing amplitudes, F_{px} and F_{py}, are cancelled at the interface. On the other hand, spin-triplet pair correlations are induced in the normal metal, due to the Andreev process, and decay exponentially. Therefore, we conclude that the proximity effects directly influence the pairing amplitude in the superconducting region while the latter is induced in the metallic region.
Results for FM-TSC interfaces shown even more peculiar behaviours. Indeed, in this case the induced pairing amplitudes in the ferromagnetic region are oscillating periodically while being suppressed away from the interface. We emphasized that this behaviour is due to the pair-breaking character of the magnetization configuration, which induces a momentum to the Cooper pairs as in the FFLO states. It is worth noticing that this behaviour is similar for ferromagnetic junctions with spin-singlet superconductors. On the other hand, additional s-wave and $d_{x^2-y^2}$-wave spin-singlet states have been found to be induced in both, ferromagnetic and superconducting regions.
Due to the spin character of the spin-triplet Cooper pairs, we expect the proximity effects in FM-TSC junctions to depend directly on the relative orientation between the magnetization and the $\vec{d}$-vector. Therefore, in the next two Chapters, we aim to extend this analyse to a general investigation with respect to the magnetization angle. We do not only look at the spatial variations of the pairing amplitude, but also try to understand the effect of the spin-triplet superconductor on the magnetic profile at the interface and on the induced spin-polarisation.

Chapter 2

Proximity Effects at the Three-Dimensional FM-TSC Interfaces

The theoretical and experimental studies of the proximity effects between ferromagnets (FM) and spin-singlet superconductors (SC) during the past decades lead to a great understanding of the complex processes occurring at such interface [26, 38, 47, 50]. The first peculiar characteristics of ferromagnetic junctions compare to those made of normal metal (N) is that the induced order parameters are suppressed on smaller distance in the ferromagnetic region and are oscillating [38,46]. The latter effect started to be discussed in the early 1980s and has a great influence since it leads for instance to the existence of π Josephson junctions[1] and to the oscillations of the critical temperature [40,46]. Further analysis suggested one decade later that the spin-polarisation should also be altered at the FM-SC interfaces [53,65,83]. The spin-polarisation was found to be influenced in the ferromagnetic region by the presence of the superconductor such that its magnetization should not be constant in space and that an induced spin-polarisation should be created in short-range scale inside the superconducting region. This new inverse proximity effect have been found to be, for short and weak ferromagnet, antiparallel or parallel to the ferromagnet spin-polarisation in diffusive or ballistic limits [25, 26, 27, 129], respectively, or to be oscillating for strong ferromagnet [66, 79]. Using scanning tunneling spectroscopy, short-range [55] but also long-range [18] induced spin-polarisation have been experimentally observed and such an effect could lead to the existence of a paramagnetic Meissner effect [26, 59]. Additionally, one of the most interesting proximity effect remains the creation of spin-triplet components both at the FM-SC interface and inside the ferromagnet [24, 52] which, with the presence of spin-flip and spin-mixing processes, explains the observation of Josephson currents in junctions with half-metallic barriers [77, 78, 111].

The proximity effects between spin-triplet superconductors and ferromagnet differ from the one at the FM-SC interfaces because of the presence of an additional interaction between the magnetization and the spin of the Cooper pairs. Hence, the system is not isotropic any longer and we expect the proximity effects to be dependent on the relative orientation of the magnetization with respect to the $\vec{d}$-vector. In this regards, theoretical predictions have been made concerning the variations of the conductance and, in particular, the zero-energy peak [88, 124, 125, 126, 127]. Microscopic studies have also been performed at equilibrium

[1] See Chapter 4 for more details about the relation between the induced order parameters and the state of the Josephson junction.

using the lattice model. As we have seen in the last Chapter, the spatial variations of the the superconducting and magnetic order parameters at the interface have been studied as well as the possible variations of the charge and spin currents [44, 85].
The recent experimental achievement of three-dimensional FM-TSC junction [11] made of Sr_2RuO_4 supports the possibility to obtain experimental results concerning the proximity effects in a short term and stimulate new theoretical studies to predict the specific influence of a spin-triplet superconductor. Contrary to FM-SC interfaces, it is especially meaningful to study their dependence with respect to the magnetization orientation. In this respect, we study in this Chapter the proximity effects at the FM-TSC interface using the extended-tight-binding model on a lattice. In contrast to the previous works, we consider especially the case of three-dimensional junctions and allow the magnetization to rotate in any directions in space. As general results, we discuss the spatial variations of the superconducting order parameters and the variations of the free energy with respect to the magnetization orientation. As we shall see, the orientation of the magnetization in the ferromagnetic region not only modifies the behaviour of the induced order parameters but also the value of the order parameters in the superconducting region. Accordingly, the condensation energy is modified such way that the configuration with the magnetization lying in plane is always energetically favoured. Additionally, we study the variations of the total magnetization at the interface as a function of the orientation and the strength of the exchange field. As we mentioned, the system is not isotropic and we shall see that the magnetization contain direct information about the orientation of the $\vec{d}$-vector. Finally, we shall see that, similarly to the FM-SC interface, spin-flip mechanisms at the interface induce equal spin Cooper pairs both in the ferromagnetic and superconducting regions. Such effect has direct influence on the orientation of the $\vec{d}$-vector at the FM-TSC interface.

This Chapter is organized as follows. We first present in section 2.1 the lattice model for the three-dimensional junction. We study in section 2.2 the spatial variations of the superconducting order parameters in the FM-TSC interface for various magnetic configurations and we discuss the variations of the free energy in section 2.3. The section 2.4 is then devoted to the analysis of the variations of the magnetization at the interface for various strengths and orientations of the magnetization. We highlight in section 2.5 the existence at the interface of equal-spin pairing amplitudes induces by spin-flip mechanism and we conclude our studies in section 2.6.

2.1 Three-Dimensional Extended Tight-Binding Model

The three-dimensional FM-TSC junction upon study in this Chapter is constituted of two-dimensional planes stacked along the c-axis, i.e. the z-direction in our system, linked to each other by an additional hopping term t_i^z, see Fig. 2.1. The out-of-plane hopping term t_i^z generally differs from the in-plane one t^x and t^y, respectively in the x- and y-directions, which are taken as previously equal to unity. We consider the pairing coupling V to act only on electrons situated on two neighbouring sites, which belong to the same plane. Hence, the superconductivity is assumed to occur in-plane and the Cooper pairs to not be formed by electrons of two different planes. Such approximation is motivated by the fact that the effects of the superconductivity measured in Sr_2RuO_4 are much stronger in-plane

than out-of-plane. Moreover, this approximation still allowed the superconducting order parameters to be induced in interfaced metallic regions as we shall see. However, it is worth keeping in mind that a more complete model could also include a small pairing between electrons from two different planes. Following these approximations, the two-dimensional Hamiltonian Eq. 1.19 is modified as

$$\begin{aligned} H &= -\sum_{\langle ij\rangle,\sigma} t_{i\sigma}(c^{\dagger}_{i\sigma}c_{j\sigma} + h.c.) - \mu\sum_{i\sigma} n_{i\sigma} \\ &+ \sum_{i_z}\sum_{\langle ij\rangle\in(xy)} V_i(n_{i\uparrow}n_{j\downarrow} + n_{i\downarrow}n_{j\uparrow}) + \sum_{i_z}\sum_{\langle ij\rangle\in(xy)} V'_i(n_{i\uparrow}n_{j\uparrow} + n_{i\downarrow}n_{j\downarrow}) \end{aligned} \tag{2.1}$$

where i and j are sites on the lattice with $i = (i_x, i_y, i_z)$ and $j = (j_x, j_y, j_z)$, μ is the chemical potential, V_i is the nearest-neighbour attraction between two electrons of opposite spins on the site i and V'_i is the nearest-neighbour attraction between two electrons with same spins on the site i. The pairing terms in the Hamiltonian contain a summation over the nearest neighbours belonging to the same (xy)-plane, labelled by i_z, and these interactions apply to each layer i_z. Concerning the ferromagnet, the model is similar than in the Chapter 1. The magnetization is proportional to the exchange field $\vec{h}$ which leads to a splitting of the spin up and spin down energy spectrum and induces a spin-polarisation. We define the orientation of the magnetization by fixing the angles θ with respect to the direction of the $\vec{d}$-vector, see Fig. 2.1. Therefore, the magnetization is coplanar to the $\vec{d}$-vector for $\theta = 0$ while it is perpendicular to the $\vec{d}$-vector when $\theta = \pi/2$.

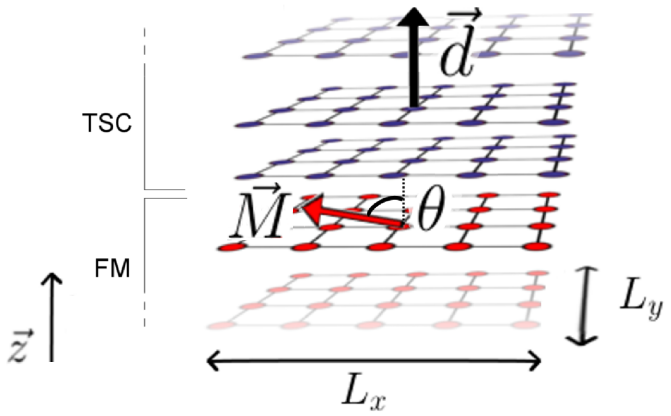

Figure 2.1: FM-TSC heterostructure with the interface perpendicular to the z-direction. The blue layers represent the spin-triplet superconductor with a $\vec{d}$-vector (thick black arrow) perpendicular to the (xy)-plane and the red layers indicate the ferromagnetic region. The red thin arrow stands for the magnetization $\vec{M}$ in the interior of the ferromagnetic region, due to the exchange field forming a relative angle θ with respect to the $\vec{d}$-vector. L_x and L_y are the in-plane lateral size of the heterostructure.

We consider the system to be infinite in the (xy)-plane, i.e. to have periodic boundary conditions in the x- and y-directions and, therefore, the Fourier transformations are applied in both directions. The rest of the derivation is similar to the two-dimensional case. The final mean field Hamiltonian, without including the magnetization, becomes

$$\begin{aligned} H &= \sum_{k,i_z,\sigma} (\epsilon_k - \mu) c^\dagger_{k\sigma}(i_z) c_{k\sigma}(i_z) + \sum_{\delta=\pm 1} \sum_{k\sigma} t_z (c^\dagger_{k\sigma}(i_z+\delta) c_{k\sigma}(i_z) + h.c.) \\ &+ \sum_{i_z} \sum_{\langle ij\rangle \in (xy)} V_{i_z} \left[F_{ij}(i_z) c^\dagger_{j\downarrow}(i_z) c^\dagger_{i\uparrow}(i_z) + F_{ji}(i_z) c^\dagger_{i\downarrow}(i_z) c^\dagger_{j\uparrow}(i_z) + h.c. \right] \\ &+ \sum_{i_z,\sigma} \sum_{\langle ij\rangle \in (xy)} V'_{i_z} \left[F^{\sigma\sigma}_{ij}(i_z) c^\dagger_{j\sigma}(i_z) c^\dagger_{i\sigma}(i_z) + F^{\sigma\sigma}_{ji}(i_z) c^\dagger_{i\sigma}(i_z) c^\dagger_{j\sigma}(i_z) + h.c. \right] \end{aligned} \tag{2.2}$$

where the two-dimensional one-band electronic structure in the normal state is

$$\epsilon_k = -2t^x \cos(k_x) - 2t^y \cos(k_y) \tag{2.3}$$

and where the in-plane bond pairing amplitudes are defined as

$$F^{\sigma\sigma'}_{ij} = \langle c_{i\,\sigma} c_{j\,\sigma'} \rangle \ , \quad (i,j) \in \text{(xy)-plane.} \tag{2.4}$$

The system being still quasi one-dimensional, the Hamiltonian can be written in a matrix form in a similar manner than Eq. A.24 as

$$H = \sum_k \sum_{i,j} D^\dagger_{i,k} \hat{h}_{ijk} D_{j,k}. \tag{2.5}$$

However, the two sites interactions matrix $\hat{h}_{ijk}$ represents here the three-dimensional Hamiltonian Eq. 2.3 and becomes

$$\hat{h}_{ijk} = \begin{bmatrix} \epsilon_{ijk\uparrow} - \mu & h^x_i + i h^y_i & \Lambda^{\uparrow\uparrow}_{ijk} & \Lambda_{ji-k} \\ h^x_i - i h^y_i & \epsilon_{ijk\downarrow} - \mu & \Lambda_{ijk} & \Lambda^{\downarrow\downarrow}_{ijk} \\ \Lambda^{\uparrow\uparrow *}_{jik} & \Lambda^*_{jik} & -\epsilon_{ijk\uparrow} + \mu & -h^x_i + i h^y_i \\ \Lambda^*_{ij-k} & \Lambda^{\downarrow\downarrow *}_{jik} & -h^x_i - i h^y_i & -\epsilon_{ijk\downarrow} + \mu \end{bmatrix} \tag{2.6}$$

$$\begin{aligned} \text{with} \quad \epsilon_{\mathrm{ijk}\sigma} &= -2t^x_{i\sigma} \cos(\mathrm{k_x}) \delta_{\mathrm{i,j}} - 2\mathrm{t^y_{i\sigma}} \cos(\mathrm{k_y}) \delta_{\mathrm{i,j}} - \mathrm{t^z_{i\sigma}} (\delta_{\mathrm{i,j+1}} + \delta_{\mathrm{i,j-1}}) \ , & (2.7) \\ \Lambda_{ijk} &= V_i [\ F^{x+}_i e^{-ik_x a} + F^{x-}_i e^{ik_x a} + F^{y+}_i e^{-ik_y a} + F^{y-}_i e^{ik_y a}\ ] \delta_{ij}, & (2.8) \\ \Lambda^{\sigma\sigma}_{ijk} &= V'_i [\ - 2i \mathrm{sin(k_x) F^{x+}_{i,\sigma\sigma}} - 2\mathrm{isin(k_y) F^{y+}_{i,\sigma\sigma}}\ ] \delta_{\mathrm{ij}}. & (2.9) \end{aligned}$$

As previously, one can derive the energy spectrum, the ground states and the excited state of the Hamiltonian by solving the Bogoliubov-De Gennes equations Eq. A.33. The bond pairing amplitudes on each (xy)-planes are computed thanks to the coherence factors as

$$F_{i_z}^{x\pm} = \frac{1}{L_y}\sum_{k_x}\langle c_{i_z k_x\uparrow} c_{i_z,-k_x\downarrow}\rangle = \frac{1}{L_y}\sum_{nk} u_{i_z n} x^*_{i_z,n}(1-f(E_n))e^{\mp ik_x a}, \quad (2.10)$$

$$F_{i_z}^{y\pm} = \frac{1}{L_y}\sum_{k_y}\langle c_{i_z k_y\uparrow} c_{i_z -k_y\downarrow}\rangle = \frac{1}{L_y}\sum_{nk} u_{i_z n} x^*_{i_z,n}(1-f(E_n))e^{\mp ik_y a}, \quad (2.11)$$

$$F_{i_z,\uparrow\uparrow}^{x\pm} = \frac{1}{L_y}\sum_{k_x}\langle c_{i_z k_x\uparrow} c_{i_z,-k_x\uparrow}\rangle = \frac{1}{L_y}\sum_{nk_x} u_{i_z n} w^*_{i_z,n}(1-f(E_n))e^{\mp ik_x a}, \quad (2.12)$$

$$F_{i_z,\uparrow\uparrow}^{y\pm} = \frac{1}{L_y}\sum_{k_y}\langle c_{i_z k_y\uparrow} c_{i_z -k_y\uparrow}\rangle = \frac{1}{L_y}\sum_{nk_y} u_{i_z n} w^*_{i_z n}(1-f(E_n))e^{\mp ik_y a}, \quad (2.13)$$

$$F_{i_z,\downarrow\downarrow}^{x\pm} = \frac{1}{L_y}\sum_{k_x}\langle c_{i_z k_x\downarrow} c_{i_z,-k_L x\downarrow}\rangle = \frac{1}{L_y}\sum_{nk_x} v_{i_z n} x^*_{i_z,n}(1-f(E_n))e^{\mp ik_x a}, \quad (2.14)$$

$$F_{i_z,\downarrow\downarrow}^{y\pm} = \frac{1}{L_y}\sum_{k_y}\langle c_{i_z k\downarrow} c_{i_z -k_y\downarrow}\rangle = \frac{1}{L_y}\sum_{nk} v_{in} x^*_{in}(1-f(E_n))e^{\mp ik_y a}. \quad (2.15)$$

Since the electrons forming the Cooper pairs are chosen to be in the same plane, their definition in Eqs. 1.28 - 1.33 remains unchanged. However, the gap equations change slightly since the energy spectrum corresponds now to the three-dimensional system. It leads to

$$\Delta_\alpha(i) = \frac{V_0}{bL^2}\sum_{\mathbf{k}}\omega_{\alpha\mathbf{k}}\frac{\Delta_{\mathbf{k}}}{E_{\mathbf{k}}} \quad \text{with} \quad E_k = \sqrt{\xi_k^2 + |\Delta_k|^2} \quad (2.16)$$

with the one-band electronic structure in the three-dimensional normal state

$$\xi_k = -2t^x\cos(k_x) - 2t^y\cos(k_y) - 2t^z\cos(k_z) - \mu. \quad (2.17)$$

In the following sections, we aim to study the spatial variations of the order parameters as well as the spin-polarisation at the FM-TSC interface. For this purpose, we solve self-consistently the Bogoliubov-De Gennes equations and evaluate the pairing amplitudes and the spin-polarisation in the complete system. All the results are obtained at zero temperature and for the in-plane hopping terms $t^x = t^y = 1$. In general, the out-of-plane hopping term t^z is taken smaller to the in-plane one. The value of the chemical potential $\mu = -1.6t$ is chosen such that the chiral spin-triplet order parameters $F_i^{x\pm}$ and $F_i^{y\pm}$ are stable in the TSC bulk after self-consistent computations. The equal-spin coupling V_i' is set to zero and therefore $F_{i,\sigma\sigma}^{x\pm}$ and $F_{i,\sigma\sigma}^{y\pm}$ are zero in the superconducting bulk.

2.2 Superconducting Spin-Triplet Pair Correlations

We know from studies on FM-SC junctions that the exchange field in the ferromagnet region breaks the Cooper pairs, effect which leads to the presence of spatial oscillations in the induced pairing amplitudes inside the ferromagnetic region. In contrast to FM-SC junctions, the magnetization is totally pair-breaking for the Cooper pairs only when it is parallel to the $\vec{d}$-vector. For the other orientations, the magnetization can be partially

or not at all pair-breaking. Therefore, as we shall analyse in this section, the magnetization orientation has a direct influence on the spatial variations of the spin-triplet order parameters since it can directly induce or cancel the oscillations. On the other hand, in a pair-breaking magnetic configuration, the period of oscillations depends only on the value of the exchange field as in FM-SC junctions. We discuss the relation between both values in the framework of our model.

Spatial Variations of the SC Order Parameters We first present in Fig. 2.2 the characteristics of the spatial evolution of the real part of pairing amplitude F_{px} for the three-dimensional FM-TSC system. The results are plotted for various magnetization orientations θ for a fixed strength of the exchange field $h \equiv |\vec{h}| = 0.5t$. The x- and y-directions being equivalent in our model, the imaginary part of $\mathrm{F_{py}}$ exhibits exactly the same behaviour than the real part of $\mathrm{F_{px}}$.
Let us first discuss the spin-triplet order parameters in the TSC region. We can first notice that the pairing amplitude is totally decreasing at the interface. It is a similar behaviour than the one observed at the interface with a normal metal or with vacuum due to the change of sign of the order parameter when the electrons of the TSC are reflected at the interface. However, in contrast to the two-dimensional model where we found that $\mathrm{F_{py}}$ could be increased close to the interface, see Fig. 1.5, both orbitals p_x and p_y have at the three-dimensional interface the same behaviour, since the x- and y-directions are equivalent.
Although the general trend hold for any relative angles between the magnetization and the $\vec{d}$-vector, we can see by closer inspection that the values of the order parameters still depend on the angle θ. The inset in Fig. 2.2 shows the variation of the order parameter on the side $\mathrm{i}_z = 2$ with respect to the magnetization angle θ, subtracted by its value at $\theta = 0°$. We can see that the spin-triplet order parameters are larger when $\vec{h}$ is in plane ($\theta = 90°$) and monotonously decrease when the magnetization gets aligned with $\vec{d}$ ($\theta = 0°$). The effect is tiny but already denotes the influence of the magnetization on the inverse proximity effects and, as we shall see in the next section, has a direction influence on the total free energy of the interface.
Finally, we should notice that, for a same value of the pairing coupling, the coherence length in the superconductor is much smaller than the one observed in the two-dimensional system. It is due to the fact that the hopping term in the z-direction t^z was chosen twice smaller than the in-plane one, i.e. t^x and t_y, and that we do not have any pairing interaction between electrons of two different two-dimensional layers. The choice of t^z influences directly the coherence length ξ_{SC} in the superconducting region by changing the possibility of the particles to move from one layer to another. For instance, in the limit in case where $t^z = 0$, the electrons are stacked on each layers and it results that the order parameters are constant in all the superconductor side. Therefore, the smaller t^z is in our model, the smaller the coherence length ξ_{SC} is. The choice of a small t_z is therefore determined in order to reproduce experimental results, which show that the coherence length of Sr_2RuO_4 in the z-direction is twenty times smaller than the one in the (xy)-plane [96,97].

Concerning the ferromagnetic region, we can see that, as expected, spin-triplet pair correlations are induced by proximity effects and decreasing as we look further from the

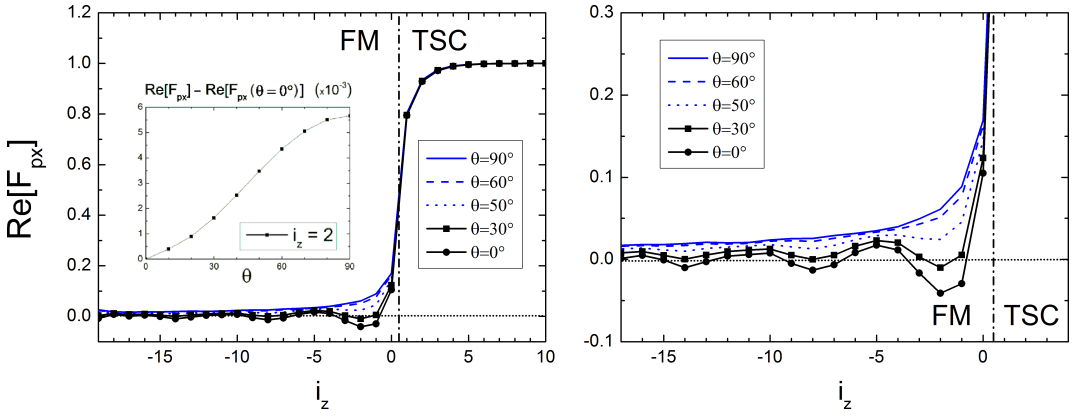

Figure 2.2: Spatial variation of the real part of the p_x-wave pairing amplitude F_{p_x} scaled to the TSC bulk value for various angles θ of the exchange field with respect to the $\vec{d}$-vector as defined in Fig. 2.1. The FM first layer ($i_z = 0$) is denoted by the dashed line. The exchange field strength $h = 0.5t$ and the pairing coupling $V = -2.0$ are fixed. The right panel provides an enlargement focused on the spatial oscillations while the inset in the left panel shows the evolution of the pairing amplitude F_{p_x} as a function of the angle θ at the layer $i_z = 2$.

interface independently of the magnetization orientation. As we have seen in the section 1.5, it is due to the leakage of Cooper pairs into the FM through the Andreev reflections and which keep a coherence over a certain distance to the interface. A close examination of $\mathrm{F_{px}}$ near the interface, i.e. for $-10 < i_z < 0$, reveals three different behaviours depending on θ.

For $\theta = 0°$, i.e. when the magnetization is parallel to the $\vec{d}$-vector, we can see that the induced pairing amplitudes is periodically oscillating in the ferromagnetic region and can be positive or negative depending on the distance to the interface. This magnetic configuration is totally pair-breaking and is equivalent to the FM-SC interface. On the other hand, when the magnetization is perpendicular to the $\vec{d}$-vector, i.e. $\theta = 90°$, $\mathrm{F_{px}}$ is monotonously decreasing the the FM side, without any oscillations. This magnetic configuration is not pair-breaking for the spin-triplet Cooper pairs and is analogue to the N-SC and N-TSC interfaces.

For the configuration with $0° < \theta < 90°$, the magnetization is partially pair-breaking and, as a consequence, induces oscillations whose amplitudes depend strongly on the magnetization angle θ. Therefore, although the induced pairing amplitudes still exhibit spatial oscillations, they do not necessary become negative. For the example upon consideration in Fig. 2.2, we can estimate that $\mathrm{F_{px}}$ and $\mathrm{F_{py}}$ do not become negative in the ferromagnetic region for all configurations with $\theta > 40°$.

Finally, it is worth mentioning that the described behaviours obtained for the specific small strength of the magnetization $h = 0.5t$ hold for any value of h. Nevertheless, the latter can still modify the angle for which the induced pairing amplitudes become strictly positive. As we shall see in the Chapter 4, it has a direct influence on the state of the

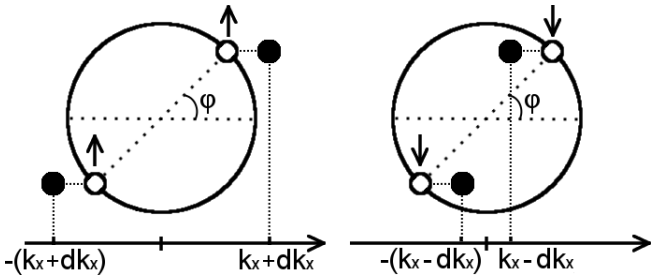

Figure 2.3: The spin up (down) electrons from Cooper pairs in the TSC (electrons represented in white) increase (decrease) their kinetic energy when entering in the FM (electrons represented in black) in order to conserve their total energy. In the case of equal spin pairing, the pairs of electrons induced in the FM do not acquire momentum.

TSC-FM-TSC Josephson junctions and should provide a key signature for the existence of spin-triplet symmetry pairing.

The modification of the oscillations of the induced pairing-amplitudes at the FM-TSC interfaces as a function of the relative angle between the magnetization and the $\vec{d}$-vector is one of the main difference in the proximity effects compare to the FM-SSC interfaces. This disparity can be understood using similar arguments than in section 1.5 about the modification of the Cooper pairs when entering the the ferromagnetic region. Indeed, we have seen that a Cooper pair entering from the SSC to the FM acquired a center of mass because, due to energy law conservation, spin up and spin down electrons increase and decrease respectively their kinetic energy. The difference with the spin-singlet superconductors arises from the spin-triplet character of the wave function.
Since the chiral TSC with a $\vec{d}$-vector perpendicular to the plane has Cooper pairs without spin projection in the z-direction, a magnetization along the z-direction is pair-breaking and induces oscillations of $\mathrm{F_{px}}$ and $\mathrm{F_{py}}$. However it is different if the magnetization is misaligned with respect to the $\vec{d}$-vector. Let us decompose the spin-singlet and spin-triplet, with the pair spin projection $\mathrm{S}_z = 0$, order parameters using a quantized axis along the x-direction. We obtain that

$$\langle c_{\uparrow k} c_{\downarrow -k}\rangle - \langle c_{\downarrow k} c_{\uparrow -k}\rangle = \langle c_{\uparrow_x k} c_{\downarrow_x -k}\rangle - \langle c_{\downarrow_x k} c_{\uparrow_x -k}\rangle \quad \text{for spin singlet,} \tag{2.18}$$

$$\langle c_{\uparrow k} c_{\downarrow -k}\rangle + \langle c_{\downarrow k} c_{\uparrow -k}\rangle = \langle c_{\uparrow_x k} c_{\uparrow_x -k}\rangle - \langle c_{\downarrow_x k} c_{\downarrow_x -k}\rangle \quad \text{for spin triplet.} \tag{2.19}$$

As we can see, the expressions of the pairing amplitudes with a singlet symmetry is the same independently of the quantized axis. Therefore the pairs of electrons acquire a center of mass and the pairing amplitudes oscillate for any magnetization orientation. However, we have an equal spin pairing for the spin-triplet symmetry when the quantized axis is in-plane. Therefore, as depicted in Fig. 2.3, although the electrons forming the Cooper

pairs change their kinetic energy, the in-plane magnetization does not induce an additional momentum to the pair and therefore does not induce any oscillations.

Characteristics of the Oscillations We have seen that a magnetization parallel to the $\vec{d}$-vector, configuration which is totally pair-breaking for the Cooper pairs, engenders periodic oscillations of the induced pairing amplitudes inside the FM. The basic understanding of the physical process at the interface, as we discussed previously [38, 46], tells us that the period of the oscillations ξ_{FM} depends on the Fermi velocity and the exchange field as

$$\xi_{FM} = \frac{v_F}{2h} \ . \tag{2.20}$$

This theoretical estimation is based on the case where only electrons with Fermi energy contribute to the pairing amplitude, where there is no electronic reconstruction in the energy spectrum at the interface and where the temperature is zero. We discuss in the following its correspondence with the results obtain within our model. The main purpose of such analysis is to be able to predict precisely the distance for which the pairing amplitudes are changing sign in realistic FM-TSC junctions.

We would like to underline the influence of the value of the out-of-plane hopping term t^z

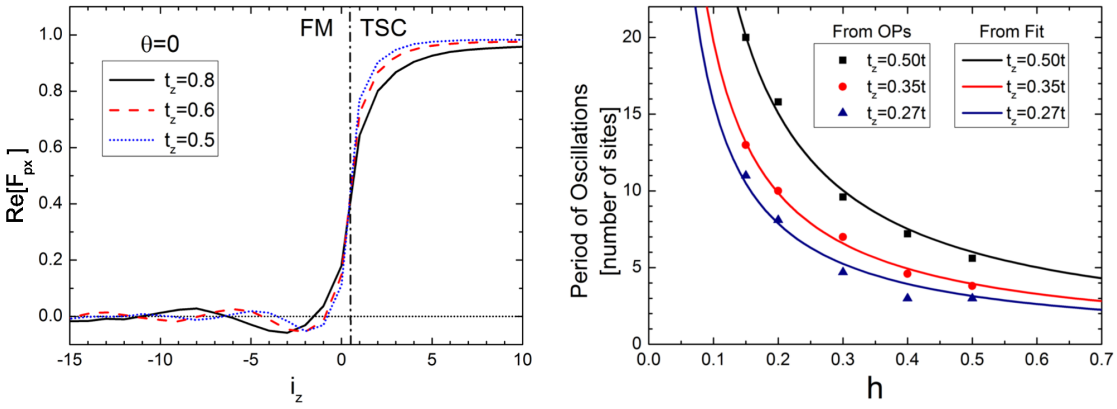

Figure 2.4: Left panel: Spatial variations of the real part of the p_x-wave pairing amplitude F_{p_x} scaled to the TSC bulk value for three values of the out-of-plane hopping term $t^z = 0.5t$ (dotted blue line), $t^z = 0.6t$ (dotted dashed line) and $t^z = 0.8t$ (solid black line). The strength and the orientation of the magnetization are $h = 0.6t$ and $\theta = 0°$, respectively. Right panel: The points depict the period of oscillations of F_{p_x} numerically inside the FM region numerically obtained for various strengths of the exchange field h and various values of the out-of-plane hopping terms t^z. The lines show qualitative estimations of $A(t^z)/h$ as a function of h where $A(t^z)$ is chosen such to fit the variations of the obtained period of oscillations.

on the spin-triplet pairing amplitudes. To do so, we plot in the left panel of the Fig. 2.4 the spatial variations of the pairing amplitudes at the FM-TSC interface for three values of the out-of-plane hopping term, $t^z = 0.5t$ (dotted blue line), $t^z = 0.6t$ (dotted dashed line) and $t^z = 0.8t$ (solid black line), for a fixed value of the exchange field $h = 0.6t$. The exchange field is oriented perpendicular to the $\vec{d}$-vector and therefore the induced pairing correlations are oscillating in the ferromagnetic region.
As we can see, the value of t^z does not change the general trend of the oscillations. However, it directly influences the period of oscillations of the induced pairing amplitudes and the later increases as t^z is increasing. The same trend is followed by the superconducting coherence length ξ_{SC} which is also increasing. The overall effects lead to a modification of the amplitude of F_{px}.
In order to have an overview of the modification of the period of oscillations, we aim to look at their value for various strength of the exchange field. Hence, we report in the right panel of the Fig. 2.4 the length of the period of oscillations as a function of h and for three values of the out-of-plane hopping terms $t^z = 0.27t$ (blue triangles), $t^z = 0.35t$ (red circles) and $t^z = 0.27t$ (black squares). As a comparison, we estimate qualitatively the function $A(t^z)/h$ as a function of h for the three values of t^z. Hence, we can see that, for all value of t^z, the period of oscillations of the induced pairing amplitudes in the ferromagnetic region follows qualitatively the quasiclassical law Eq. 2.20. As expected, $A(t^z)$ and, thus, v_F is growing as t^z is increasing.
Therefore, these results show that, in a configuration where the magnetization is perpendicular to the $\vec{d}$-vector, the oscillations of the pairing amplitudes are analogue to the one present in FM-SC junctions [38, 46]. They depend only on the characteristic of the chosen ferromagnet, i.e. the Fermi velocity and the strength of the polarisation. However, we know that the presence of magnetic impurities inside the FM region leads to a strong modification of the oscillation [102] and we expect different behaviour for FM-TSC for which the oscillations should already be modified by non-magnetic impurities.

2.3 Most Favourable Magnetic Configurations

For a simple heterostructure as described within our model, without additional bulk nor interface spin-orbit coupling in the superconducting region and without additional magnetic anisotropy in the ferromagnet, the proximity effects are totally independent of the orientation of the magnetization, be it at FM-N or FM-SC interfaces. As we have seen, it is not the case at FM-TSC interfaces due to the spin character of the Cooper pairs, which can exhibit different behaviour depending on the magnetization orientation θ. In this respect, we expect also the total free energy G of the FM-TSC junctions to depend on θ. Therefore, it is interesting to study the influence of the spin-triplet states on the energy of the system in order to predict the magnetic configuration which is the energetically the most stable.
For this purpose, we analyse the evolution of the Gibbs free energy G and of the energy associated with the TSC order parameter E_{op} for different values of the relative orientation of the ferromagnetic moment with respect to the $\vec{d}$-vector and as a function of the strength of the ferromagnetic exchange field. The Gibbs free energy can be determined from the energies which are eigenvalues of the Hartree-Fock Hamiltonian as

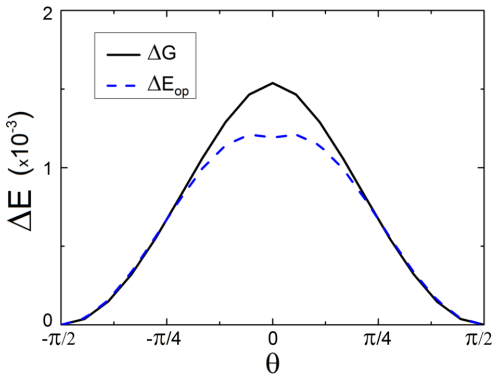

Figure 2.5: Gibbs free energy (solid black line) and the order-parameter derived energy E_{op} (blue dotted line) as functions of the angle θ at a given value of the ferromagnetic exchange $h = 1t$. Both energies are scaled with respect to their minimum amplitude ($\Delta G = G - G^{\min}$ and $\Delta E_{op} = E_{op} - E_{op}^{\min}$) and are renormalized to the $E_{\rm op}$ value of a single superconducting layer in the homogenous state.

$$G = -\frac{1}{\beta} \ln \mathrm{Tr}[\mathrm{e}^{-\beta H_{\rm HF}}] \tag{2.21}$$

where $\beta = \frac{1}{k_B T}$ is the inverse temperature, k_B being the Boltzmann constant. In order to separate the energy contributions resulting from the proximity effects and from the modification of the energy spectrum by those that enters in the superconducting condensation energy, via the change of the order parameter in the TSC side of the heterostructure, it is useful to introduce the quantity $E_{\rm op}$ defined as

$$E_{\rm op} = -\left(\frac{2}{L_z}\right) \sum_{i_z>0} \left[|F_{p_x}(i_z)|^2 + |F_{p_y}(i_z)|^2\right] . \tag{2.22}$$

Such quantity reflects the changes of the superconducting order parameter in the FM-TSC heterostructure related to the magnetization configuration of the ferromagnetic layers. In particular, a minimum in $E_{\rm op}$ implies a maximum amplitude of the superconducting order parameter.
For clarity, the results are presented by rescaling the Gibbs free energy and the order-parameter derived energy to their minimum value. Indeed, we introduce the quantities $\Delta G = G - G^{\min}$ and $\Delta E_{\rm op} = E_{\rm op} - E_{\rm op}^{\min}$ where $G^{\min}$ and $E_{\rm op}^{\min}$ are the minimum amplitude of the Gibbs energy and of the order parameter energy, respectively, in the analysed range of parameters. This rescaling allows one to directly extract the energy scale that sets the variation of the Gibbs energy landscape and to compare different energy profiles as a function of the physical parameters involved in the analysis. Still, the variation of ΔG and $\Delta E_{\rm op}$ are presented by scaling their amplitude to the value of $E_{\rm op}$ associated with a single superconducting layer in the homogeneous state.

As one can note in the Fig. 2.5 the Gibbs free energy has a non monotonous profile with two degenerate minima at $\theta = \pm\pi/2$ and a maximum for $\theta = 0$. This means that, due to the coupling with the TSC, the energetically most favourable magnetic configuration for the ferromagnet is achieved when the magnetization lies in the plane of the Cooper pairs spin. Otherwise, the maximal loss in the energy occurs when the magnetization is parallel to the $\vec{d}$-vector.

To understand the driving force in the stability of the magnetic configuration it is instructive to analyse the behaviour of the order-parameter derived energy E_{op}. The results indicate that the maximum energy gain due to the variation of the superconducting order parameter in the TSC region occurs for a magnetization that lies perpendicular to the $\vec{d}$-vector which also corresponds to a lack of spin-pair breaking in the proximity effect. Since the total energy has the same minima than the E_{op} term one can deduce that for this strength of the exchange field the changes of the spectra in the Gibbs free energy due to the proximity effect and to a possible electronic reconstruction at the interface cooperate with the gain in the condensation energy to stabilize the observed magnetic configuration. The trend observed for the pairing amplitude as a function of the angle θ can be discussed in the framework of the scattering formulation for the TSC-FM heterostructure. The pairing amplitude variation is mainly controlled by the Andreev reflections at the interface. Since Andreev scattered electron (hole) leads to hole (electron) pairs formation in the superconductor such process is expected to drive the change of the pairing order parameter close to the interface. The resulting interference of the different scattering amplitude is maximal when the Andreev reflected Cooper pair acquires a spin and/or an orbital phase shift. This observation can be justified by the fact that a sign change can lead to destructive interference. In the case upon examination in the paper, the orbital phase change for the given heterostructure is 0 at any angle of incidence of the electron that undergoes an Andreev reflection and therefore the overall phase shift is minimized when the magnetization forms an angle $\pi/2$ with the $\vec{d}$-vector.

2.4 Induced Spin-Polarisation at FM-TSC Interface

Although the penetration of the singlet superconducting order parameters into normal or ferromagnetic metals have been intensively analysed and well understood during decades, leading for instance to the existence of π-states or to the oscillations of the critical temperature, the theoretical studies about the magnetization started only relatively recently, in the beginning of the 2000s. The first hints about the existence of an induced magnetization inside the superconducting region have been seen in the analysis of the density of states at the FM-SC interface [53, 65, 83]. before to be directly analysed for various magnetic configurations [25, 26, 27, 66, 79, 129]. Since then, the existence of such induced magnetization is considered as a specific feature of superconducting heterostructures and is referred as an additional inverse proximity effect.

We report in this section new studies of the inverse proximity effects in the case of spin-triplet superconductor. In contrast to the FM-SC interfaces, they depend additionally on the relative angle between the magnetization in the ferromagnet and the $\vec{d}$-vector. We shall see that the spatial variations of the spin-polarisation are quite comparable to the one obtained for the singlet case. Our main discussion focus however on the variations of the total magnetization at the vicinity of the interface as a function of the orientation and strength of the exchange field. Indeed, we shall see that they provide distinguishable behaviour, which make possible the identification of the $\vec{d}$-vector orientation.

For clarity, we would like to specify the terms we use in the following discussion and which may be confusing. In this section, as for our complete analysis, the *magnetization* and the *exchange field* both refer to the magnetic source term h in the Hamiltonian which leads

to the splitting of the spin up and spin down energy spectrum. Such a splitting leads to a finite *spin-polarisation* in the ferromagnet, oriented in the direction of the magnetization h.

Induced Spin-Polarization in the TSC Region We begin our analysis by considering the spatial variations of the z-polarized magnetization $m_z(i_x)$ at the vicinity of the FM-TSC interface. Taken separately, the superconducting region exhibits no spin-polarisation while, inside the ferromagnetic bulk region, the exchange field h induces a constant spin-polarisation, oriented in the direction of h, due to the splitting of the spin up and spin down electronic spectrum. When both regions are interfaced, a finite spin-polarisation can be induced in the superconductor while it can be modified close to the interface in the ferromagnet.

We show the influence of the proximity effects at the FM-TSC interface in Fig. 2.6 for various magnetization orientation θ and for a small strength of the exchange field $h = 0.6t$. Firstly, we can see that the proximity effects modify the value of the magnetization in the ferromagnetic region, which is not constant any longer. Within our model, these effects are meanly located close to the interface, for the sites $-2 \leq i_x \leq 0$, but also propagate into the whole ferromagnetic bulk, as the superconducting order parameter. Indeed, we can see small oscillations of the magnetic order parameter especially when the exchange field is parallel to the z-direction. On the other hand, similarly to the superconducting order parameters, we can expect the effect to be cancelled over a distance $\xi_F \sim 1/T$ at finite temperature T. Quantitatively, we can see that the spin-polarisation increases at the interface compare to its bulk value, independently to the orientation of the exchange field h.
Secondly, we can observe that inverse proximity effects are also present at the interface and that a finite spin-polarisation is induced in the superconducting region. In our specific magnetic configuration, the orientation of the magnetization depends on the distance to the interface. Indeed, the closest site to the interface, $i_x = 1$, has a positive spin-polarisation while further in the superconducting region, for the sites $1 < i_x \lesssim 10$, the spin-polarisation is negative, opposite to the one inside the ferromagnet region. However, we can also notice

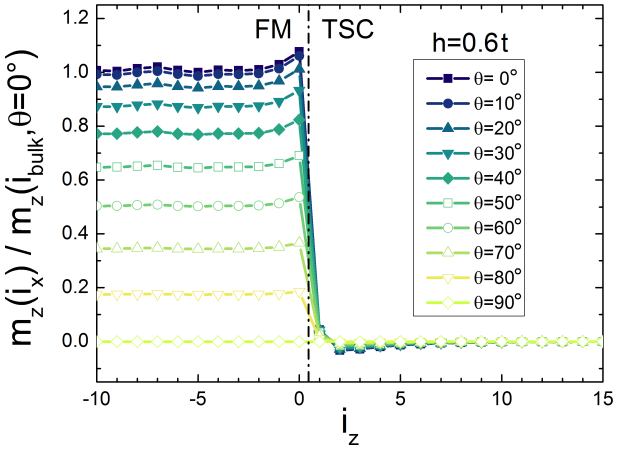

Figure 2.6: Spatial variations of the magnetization $m_z(i_x)$ along the z-direction at the three-dimensional FM-TSC interface for various magnetization angles θ and for a fixed small strength of the exchange field $h = 0.6t$. They are normalized with the FM bulk value of m_z when the exchange field is parallel to the z-direction, i.e. for $\theta = 0°$.

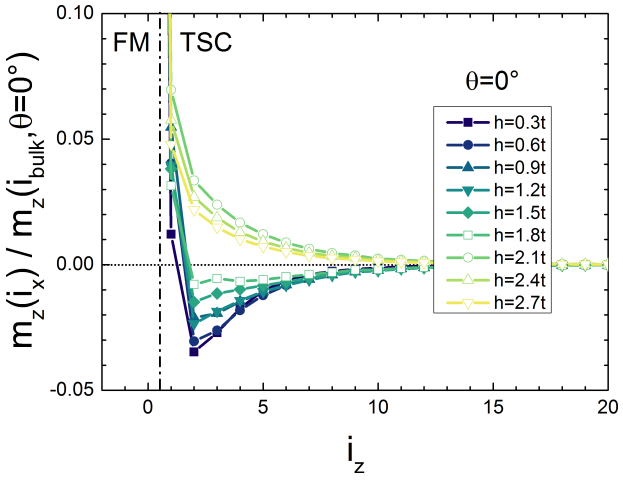

Figure 2.7: Spatial variations of the magnetization $m_z(i_x)$ along the z-direction at the three-dimensional FM-TSC interface for various magnetization angles θ and for a fixed small strength of the exchange field $h = 0.6t$. They are normalized with the FM bulk value of m_z when the exchange field is parallel to the z-direction, i.e. for $\theta = 0°$.

that no oscillations are induced in the TSC.
We can finally mention that when the magnetization of the ferromagnet is rotating in the (zy)-plane, it exists also inside the ferromagnet bulk a spin-polarisation in the y-direction, which is also induced in the superconducting region. It will also be analysed in the next paragraph.

It is worth mentioning that the spatial variations of the spin-polarisation depend qualitatively on the strength of the exchange field h. In order to emphasize this point, we plot in Fig. 2.7 the spatial variations of the induced spin-polarisation in the TSC for various strength of the exchange field. The magnetization in the ferromagnet is taken parallel to the $\vec{d}$-vector, i.e. $\theta = 0°$, and is therefore totally pair-breaking.
As we can see, the direction of the induced magnetization at the closest site to the magnetization, $i_x = 1$, does no depend on the strength of the exchange field. Indeed, in each case the induced magnetization is positive and hence parallel to the magnetization in the ferromagnetic region. Nevertheless, we can see that the induced spin-polarisation increases as the exchange field increases.
On the other hand, the direction of the induced magnetization on the sites located beyond $i_x = 1$ depends strongly on the strength of the exchange field and we can notice two different regimes. For small to intermediate values of h, the induced spin polarization is opposition to the FM magnetization, while for intermediate to strong values of h, they are in the same direction. In both case however, the reduction of the induced magnetization is monotonous and no oscillations are present.
Therefore, we can conclude that the results generally contrast with previous works on FM-SC interfaces which predicted only negative induced magnetization for small values of the exchange field or oscillating magnetization for larger value of h. Our finding is that, for FM-TSC interface, we can distinguish two different regimes depending on the strength of the exchange field, one for which the induced spin-polarisation is antiparallel to the FM magnetization and another for which they are parallel.

Variations of the total Magnetization at the FM-TSC Interface Measuring the spatial variations of the magnetization is experimentally achievable by means of several

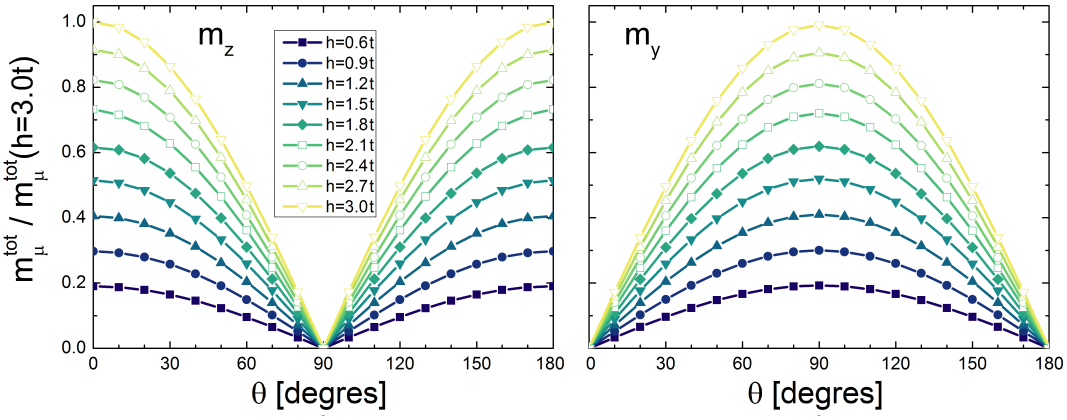

Figure 2.8: Total spin-polarisation at the three-dimensional FM-TSC interface, as defined in Eq. 2.23, along the z-direction M_z (left panel) and along the y-direction M_y (right panel) in function of the exchange field angle θ and for various strength of the exchange field h. Results on the left panel are scaled with the value of M_z for $\theta = 0°$ and $h = 3.0$ while for the right panel, the results are scaled with the value of M_y for $\theta = 90°$ and $h = 3.0t$.

methods which have also been used to probe the spin-triplet states, as the measurement of the Kerr rotation of an incident light [107, 136] or to use muon resonance experiment [80]. Therefore, variations as shown in Fig. 2.7 are experimentally reachable although not easily performed. In order to emphasize the modification of the spin-polarisation at the FM-TSC interface, we focus our discussion on more global modifications of the spin-polarisation at the interface. For this purpose, we compute the total magnetization $m_\mu^{tot}(h,\theta)$ as being the summation of the spin-polarisation over several sites

$$m_\mu^{tot}(h,\theta) = \frac{1}{(i_{max} - i_0 + 1)} \sum_{i_x=i_0}^{i_{max}} m_\mu(i_x), \tag{2.23}$$

where i_0 and i_{max} are lattice sites in the ferromagnet and superconducting bulks, respectively, and $\mu = z, y$ the direction of the spin-polarization. All the results discussed are obtained by taking the summation over 26 lattice sites, from $i_0 = -15$ to $i_{max} = 10$. Hence, all the modifications of the spin-polarisation are contained in $m_\mu^{tot}(h,\theta)$ and considering more sites do not change qualitatively the results.
For clarity of the analysis, we first consider the global variations of $m_z^{tot}(h,\theta)$ and $m_y^{tot}(h,\theta)$ as a function of the magnetization orientation θ. The results are reported in Fig. 2.8 (a) and (b), respectively, for various strengths of the exchange field, scaled by the maximal value of the spin-polarisation $m_z^{tot}(h = 3.0t, \theta = 0°)$. Since the variations of the spin-polarisation at the interface, both in the ferromagnetic and superconducting regions, are small compare to the value of the magnetization in the ferromagnetic bulk $m_\mu(i_x)$ (see Fig. 2.6), the variations of the total summation m_μ^{tot} are mainly due to variations of $m_\mu i_x$. For this reason, according to the Stoner model, the spin-polarisation $m_z(i_{bulk})$ and $m_y(i_{bulk})$ exhibit sinusoidal behaviours with respect to the magnetization angle θ. For a

fixed value of h, the maximum of $m_z(i_{bulk})$ is reached when the exchange field is oriented along the z-direction while it is suppressed when h is along the y-direction. As expected, $m_y(i_{bulk})$ show opposite variations with respect to θ.

We are now in position to analyse more carefully the total spin-polarisation at the interface and to highlight the influence of the $\vec{d}$-vector on its variations. In particular, we would like to emphasize the role of the relative angle θ between the exchange field h and the $\vec{d}$-vector, in contrast to the FM-SC interfaces where the problem is isotropic and the magnetization orientation has no influence. In this respect, we compare, for all magnetic configurations h and θ, the total magnetizations $m_z^{tot}(FM-TSC)$ and $m_y^{tot}(FM-TSC)$ obtained in Fig. 2.8 with their respective values at the FM-N interface. Indeed, we expect proximity effects to be also present at the FM-N interface and, thus, the magnetization in the ferromagnetic region to be modified as well as spin-polarisation to be induced in the metallic region. The total magnetization for this configuration depends on the strength of the exchange field h but, on the other hand, does not depend on the magnetization angle θ since the FM-N system has not magnetic anisotropy. Such comparison between the FM-TSC and FM-N interfaces can be related to experimental measurements performed above and below the critical temperature T_c. For this analysis, we consider more precisely the relative differences

$$\Delta m_z(h,\theta) = \frac{m_z^{tot}(\text{FM-TSC}) - m_z^{tot}(\text{FM-N})}{m_z^{tot}(\text{FM-N})}, \tag{2.24}$$

$$\Delta m_y(h,\theta) = \frac{m_y^{tot}(\text{FM-TSC}) - m_y^{tot}(\text{FM-N})}{m_y^{tot}(\text{FM-N})}. \tag{2.25}$$

We show in Fig. 2.9 (a) and (b) the relative differences $\Delta m_z(h,\theta)$ and $\Delta m_y(h,\theta)$, respectively, as a function of the magnetization angle θ, for various strength of the exchange field h. Obviously, the relative differences Δm_z and Δm_y are zero for $\theta = 0°$ and $\theta = 90°$, respectively, since the total magnetization m_z^{tot} and m_y^{tot} are cancelled in the ferromagnetic bulk for these magnetization orientations, see Fig. 2.8. Interestingly, the results show clear and distinct behaviours for the other values of θ.
Let us first consider the spin-polarisation in the z-direction Δm_z (a). In this case, we can clearly identify three different behaviours according the the magnetization strength. For small values of h, $\Delta m_z < 0$ for all magnetization angles, which means that the spin-polarisation along z is smaller at the FM-TSC interface compare to the one at the FM-N interface. It is the opposite for large values of the exchange field where $\Delta m_z > 0$ for all θ, which shows that the spin-polarisation is larger at the FM-TSC interface than at the FM-N one. Moreover, we can notice that in both cases $|\Delta m_z|$ is monotonously decreasing to zero. Finally, for intermediate strength of $1.5t < h < 1.8t$, the difference of the spin-polarisation Δm_z can be positive or negative, depending on the orientation of the magnetization. Hence, these characteristics directly follow the spatial variations of m_z^{tot} as we have seen in Fig. 2.7, for which we have seen that induced spin-polarisation in the TSC region is mainly negative for small exchange field while it is positive for large exchange field.

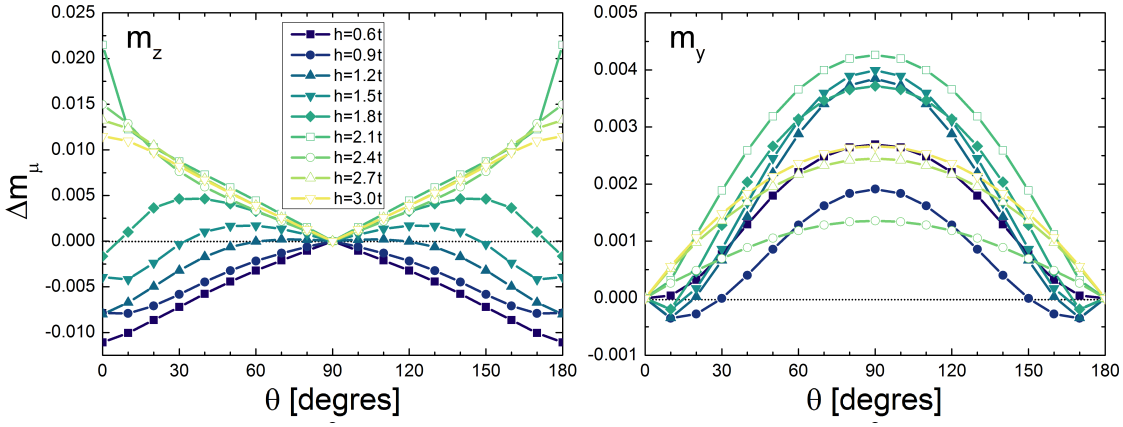

Figure 2.9: Relative differences of the total spin-polarisation between the three-dimensional FM-TSC and FM-N interfaces, as defined in Eqs. 2.24 - 2.25, M_z (left panel) and M_y (right panel), along the z- and the y-directions respectively, in function of the exchange field angle θ and for various strengths of the exchange field h.

Considering the the spin-polarisation in the y-direction Δm_y (b), we can notice that the general behaviour is qualitatively different to the previous case. Indeed, apart for few magnetic configurations when $\theta = 0°$, we find that $\Delta m_y > 0$ for all orientations of the magnetization. The maximal value is reached for $\theta = 90°$ and Δm_y is mainly decreasing monotonously to zero when the magnetization is rotating from the y-direction to the z-direction. In other words, the total spin-polarisation in the y-direction at the FM-TSC interface is generally larger than at the FM-N interface, independently of the magnetic configuration in the ferromagnetic region.

As a result, we find a remarkable difference of behaviour between Δm_z and Δm_y, which is directly related to the relative angle between the magnetization and the $\vec{d}$-vector and which can help to determine the orientation of the latter. Indeed, by increasing the exchange field in the ferromagnet, we expect to see at the FM-TSC interface the total spin-polarisation perpendicular to the $\vec{d}$-vector to be larger under T_c than above T_c. On the other hand, this is only expected for the spin-polarisation parallel to the $\vec{d}$-vector for large strengths of the bulk exchange field. However, for small values of h, we find that the spin-polarisation parallel to the $\vec{d}$-vector is smaller under T_c than above T_c.

While the norm of the total spin-polarisation $m_n(h,\theta)^2 = m_z^{tot}(h,\theta)^2 + m_y^{tot}(h,\theta)^2$ is naturally conserved at the isotropic FM-N interface when the magnetization in the bulk ferromagnet is rotating in the (zy)-plane, the results obtained in Fig. 2.9 suggest that this is not the case at the FM-TSC interface. To confirm this behaviour, we plot the variations of $m_n(h,\theta)^2$ in Fig. 2.10 as a function of the magnetization angle θ, for various strengths of the exchange field h. For each value of h, the total spin-polarisation is scaled by its value when the magnetization is aligned along the z-direction.

As for the previous results, we can notice two different behaviours depending on the

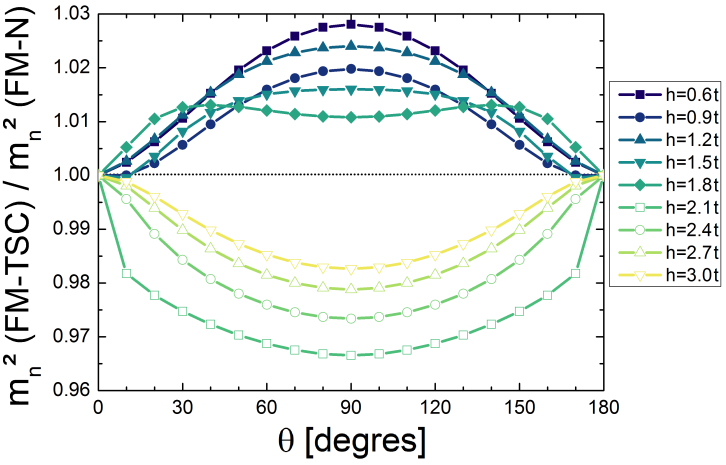

Figure 2.10: Spin-polarisation amplitudes at the three-dimensional FM-TSC interface in function of the exchange field angle θ and for various strength of the exchange field h. Each point is scaled with the value of the magnetization at the FM-N interface.

strength of the exchange field. Indeed, for $h < 1.8t$, we find that the magnitude of the total spin-polarisation at the interface is generally increasing while the magnetization is rotating and is maximal when the exchange field is lying in plane. At contrary, it is decreasing for strong exchange field $h > 1.8t$. As a consequence, the special behaviour of the spin-polarisation found in Fig. 2.10 is another indicator which can be used to probe the direction of the $\vec{d}$-vector. Indeed, let us consider an experiment which can measure, directly or indirectly, the total spin-polarisation at the interface of the FM-TSC while rotating the magnetization from a perpendicular configuration ($\theta = 0°$) to an in-plane configuration ($\theta = 90°$). If, the total spin-polarisation is increasing for weak ferromagnet and is decreasing for strong ferromagnet, it is the characteristic of a spin-triplet state with a $\vec{d}$-vector which is along the z-direction. An opposite behaviour could be however characteristic of a spin-triplet state with an in-plane $\vec{d}$-vector.

Discussion To conclude the analysis concerning the modification of the spin-polarisation at the three-dimensional FM-TSC interface, it is important to point out several limitations of the previous investigation, which could restrict the observation of such effects.
First of all, the results presented in Fig. 2.9 and Fig. 2.10 show that the maximal differences expected between the FM-N and FM-TSC interfaces is about 2% for the spin-polarisation in the z-direction while it is about 0.4% for the in-plane spin-polarisation and even smaller for the total norm. Therefore, the difference of spin-polarisation between the two interfaces are very small. Within the idea to be experimentally measured, the total spin-polarisation in the ferromagnetic region should be taken into account and, the larger the ferromagnetic region is, the smaller would be the relative difference of spin-polarisation Δm_z and Δm_y. Moreover, we know that regions where superconductivity and ferromagnetism coexist is expected to have additional Meissner currents [26]. Therefore, in order to predict quantitatively the variations of the spin-polarisation at the interface as a function of the magnetization orientation, a full analysis on the Meissner effect should also be considered to evaluate the total magnetic flux which could be measured.
It is finally worth to mention that, although the results are obtained for various relative orientation between the magnetization and the $\vec{d}$-vector, they are specifically obtained for a chiral spin-triplet state having a $\vec{d}$-vector oriented along the z-direction. Due to

the topological differences between spin-triplet superconductors having an in-plane and an out-of-plane $\vec{d}$-vector- for instance, in two-dimension, chiral p-wave TSC breaks the time-reversal symmetry and exhibit gapless edge states which carry a finite charge current along the interface while helical p-wave TSC respect the time-reversal symmetry and have gapless edge states which carry a dissipationless spin-current along the interface - we cannot predict at this point of the analysis that the results are identical in both cases. A more detailed investigation of the edge states for both cases, as partially performed in the last Chapter, could be use to have a better understanding of the alteration of the spin-polarisation at the interface. In this regards, the difference of behaviour between weak and strong ferromagnets is a great indicative of the probable important role of the energy spectrum. Indeed, the differences of behaviour observed in the spatial variations of the spin-polarisation as well as in the total spin-polarisation arise around the value $h \sim 1.8t \sim \mu$. Therefore, it suggests that the spin-polarisation should strongly depend on the filling of spin-majority and spin-minority electrons.

2.5 Induced Spin-polarised Pair Correlations

The proximity effects can induce new order parameters at the interface of a superconductor with a ferromagnet. For instance, the FM-SC systems can exhibit induced spin-triplet pair correlations at the interface [24, 50] and two-dimensional FM-TSC junction can have induced singlets extended s-wave and d-wave pair correlations [44, 85]. Within our three-dimensional model, however, the singlet pair correlations are not expected because the spin-triplet order parameters are defined such to exist only in plane.

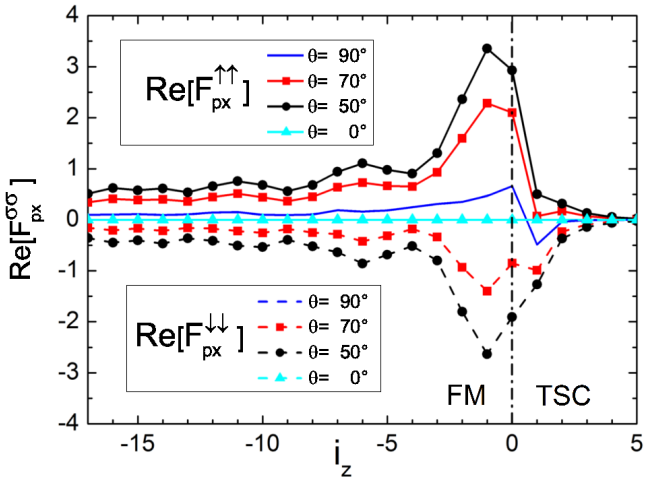

Figure 2.11: Spatial variation of the real part of $F_{p_x}^{\uparrow\uparrow}$ and $F_{p_x}^{\downarrow\downarrow}$ pair correlations associated with the $\uparrow\uparrow$ (solid lines) and $\downarrow\downarrow$ (dashed line) spin-triplet configurations for a representative case of p_x orbital symmetry as a function of the magnetization direction θ and at a given exchange field $h = 0.5t$. The amplitude of the correlator is scaled to the value of the bulk one $\mathrm{Re}[F_{p_x}]$ in the $\uparrow\downarrow$ spin configuration. The FM-TSC interface is denoted by the dashed line.

On the other hand, although there is no induced singlet pairing amplitude, the FM-TSC interface exhibits induced spin-polarized pair correlations at the interface. They are spin-triplet pair correlations, as defined in Eqs.1.32 - 1.33, with p_x and p_y orbital symmetry but having parallel $\uparrow\uparrow$ and $\downarrow\downarrow$ spin configuration along the z direction as compared to the state with zero spin projection associated with the bulk order parameter, i.e. the superposition $\uparrow\downarrow+\downarrow\uparrow$. These pair correlations are identically zero in the bulk, since the superconductor has no net spin polarization. However, it is possible to induce them close to the interface, since a magnetization that is noncollinear to the $\vec{d}$-vector can lead to spin-flip processes and, then, to a consequent spin-mixing.

We show in Fig. 2.11 the spatial profile of the $F_{p_x}^{\sigma\sigma}(i_z)$ $z-$spin polarized pair correlations for both cases $\sigma = (\uparrow, \downarrow)$ and for different orientations of the magnetization. As one can note, a magnetization parallel to the $\vec{d}$-vector ($\theta = 0$) does not induce z-spin polarized pair correlations. This can be understood by observing that to contribute in the $F_{p_x}^{\sigma\sigma}(i_z)$ amplitude, the incident electrons and the scattered holes have to be spin polarized along the same z-direction and this can occur only when the Andreev reflection involves a change in the spin orientation because of the spin symmetry of the superconducting order parameter, as depicted in Fig. 2.12 (a). Therefore, the resulting pair correlations have no contributions in the z-spin polarized pairing channel.

By changing the exchange field orientation from the direction perpendicular to the (xy)-plane (i.e. $\theta = 0$) to the in-plane ($\theta = \pi/2$), the amplitude of the z-spin polarized pair correlations exhibits a nonmonotonous behaviour. They increase upon a critical angle $\theta_{max} \sim \pi/4$ and then decrease when the exchange field tends to point within the (xy)-plane. The appearance of nonzero correlations for the z-spin polarized pairs when the exchange field is not parallel to the $\vec{d}$-vector can be addressed by analysing the process depicted in Fig. 2.12 (b). The noncollinearity between the exchange field and the spin polarization of the incident electrons (holes) allows for a spin flip of the Andreev reflected holes (electrons) and therefore generates electron (hole) pairs with parallel spin orientation along the z- direction. More specifically, we note that the amplitude of the z-spin polarized pair correlations is maximum for angles close to $\theta \sim \pi/4$. Indeed, those orientations optimize the number of incident particles with spin polarization parallel to z together with the exchange amplitude for the mechanism of spin-flip process (i.e. the h_x component of the exchange field). On the other hand, the pairing amplitude is minimum when the magnetization lies in the plane, i.e. at $\theta = \pi/2$. This is because, in this case, although the amplitude of the exchange field is maximally active as a spin flip generator, the number of incident particles with spin polarization parallel to z is minimum.

We also find that the evolution of the pair correlations in the FM side is decaying and oscillating as a function of the layer position with the same period of those associated with the bulk order parameter (see for comparison the Fig. 2.2). Since there is always an energy split between the Fermi energies of electrons with spin up and down polarization at any orientation of the magnetization, we do expect a spatial dependence with an oscillating behaviour. Indeed, the z-spin polarized pairs along the z direction get experience of the transverse component of the exchange field that is nonvanishing at any angle θ

which is different from zero. Such component acts as a pair breaking term and makes the pairs acquiring a finite momentum which results in a spatial modulation of the pairing amplitude. Moreover, it is interesting to see that in the TSC side z-spin polarized pairs are also induced by a sort of inverse proximity effect, i.e. due to the penetration of the magnetization in the superconducting layers. Therefore, in the case of the existence of a pairing potential component $V^{\sigma\sigma}$, there would be a rotation of the $\vec{d}$-vector that can have significant consequences on the electronic transport in a Josephson configuration since it could lead to the creation of spin-current inside the barrier [14,15,34]. Still, the modulation of the pair correlator does not lead to a phase change as a function of the spatial coordinate.

A change in the amplitude of the ferromagnetic exchange field does not modify the general trend obtained for the case of $h = 0.5t$. In particular, by increasing the ferromagnetic exchange one gets a reduction of the z-spin polarized triplet correlations. This is because the overall amplitude is set by the magnitude of the correlator associated with the superconducting order parameter. Taking into account the mechanisms presented in Fig. 2.12(b) one can also argue that the presence of a spin-flip process at the interface allows to generate z-spin polarized pairs even for the case of a bulk magnetization parallel to the $\vec{d}$-vector. For the other cases, we might expect that the interface-bulk misalignment tends to modify the amplitude of the z-spin polarized pair correlations close to the interface in a way that depends on the balance between the number of incident electrons and the effectiveness of

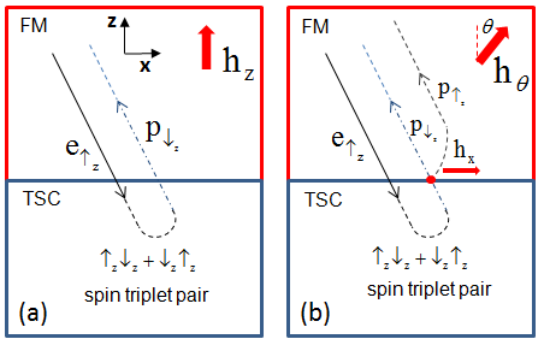

Figure 2.12: Sketch of the Andreev processes that may contribute to the build up of the $F^{\uparrow\uparrow}$ and $F^{\downarrow\downarrow}$ z-spin polarized pair correlations. An electron ($e_{\uparrow_z}$) with spin up aligned along the z direction can be scattered as a hole ($p_{\downarrow_z}$) due to the spin symmetry of the triplet order parameter. (a) For a one-component exchange field which is parallel to the z-direction, the only allowed Andreev scattering is to convert an electron $e_{\uparrow_z}$ into a hole $p_{\downarrow_z}$ with opposite spin orientation. (b) For an exchange field aligned along a given direction θ (the magnetization has component along x and z) it is possible to inject an electron $e_{\uparrow_z}$ with spin up along z and to get an Andreev reflected hole with opposite spin $p_{\downarrow_z}$ or with the same spin polarization of the incident particle $p_{\uparrow_z}$ due to the effect of the transverse h_x component to yield a spin-flip. This process allows to have z-spin polarized pair correlations along the z direction.

the spin-flip generator. It is worth pointing out that, since the maximum amplitude of the z-spin polarized triplet correlations corresponds to an angle $\theta_{max} \sim \pi/4$, they do not have a relevant role in the balance of Gibbs free energy related to the proximity effect. On the other hand, in the case of an induced pair potential in the TSC region in the spin-polarize channel, due to a modification of the pairing glue at the interface, there would be a significant change of the energy balance related to the condensation energy.

2.6 Conclusion

We have investigated in this chapter new proximity and inverse proximity effects at the three-dimensional interface between ferromagnets and chiral spin-triplet superconductors by means of the self-consistent evaluation of the superconducting correlations functions. In contrast to interfaces with spin-singlet superconductors, we have seen they depend greatly on the relative angle between the magnetization and the $\vec{d}$-vector due to the spin-triplet character of the superconducting order parameter.

We have first analysed the spatial profile of the pairing amplitudes in terms of the strength of the ferromagnetic exchange field. As expected, the penetration of the Cooper pairs in the FM leads to induced pairing amplitudes with zero-spin projection which have a damped oscillating behaviour when the magnetization is out of plane. In this configuration, we have verified that the mechanism leading to the oscillations has the same origin than at FM-SC interfaces and that the period of oscillation is inversely proportional to the strength of the exchange field. The oscillations are therefore expected to be similar than in FM-SC junctions. On the other hand, we found that the pairing amplitudes are monotonously decaying in the ferromagnet, i.e. without oscillations, when the magnetization is perpendicular to the $\vec{d}$-vector, i.e. parallel to the spin direction of the Cooper pairs. We emphasized that this behaviour is due to the spin-triplet nature of the Cooper pairs, which do not acquire finite momentum in this configuration. An important and distinctive feature of the oscillating behaviour is the existence of a phase change of the induced pair correlations when the angle between the magnetization and the $\vec{d}$-vector is in the in the range $\sim [0; \pi/4]$. As we shall see in Chapter 4, it has a direct influence on the state of the Josephson junctions and is expected to be experimentally observed in the variations of the critical current.

Additionally, we found that spin-polarized pair correlations are also induced both at the interface in the TSC and with a long-range penetration length in the FM if the magnetization is noncollinear to the $\vec{d}$-vector. We have shown that their amplitude is maximized for a magnetization angle $\theta \sim \pi/4$. We have pointed out that such correlations can play a major role in the case of the existence of a pairing coupling between electrons with same spin at the interface of the spin-triplet superconductor. This effect can lead to a reorientation of the $\vec{d}$-vector approaching the ferromagnet and drastically influences the anisotropy of the ferromagnet, as well as the charge and spin transport of the hybrid structure.

We have also analysed the spin-polarisation close to the FM-TSC interface, taking into account its modification inside the ferromagnet region as well as the spin-polarisation induced in the superconducting side. We have found the latter to be highly dependent on the amplitude and direction of the exchange field in ferromagnetic bulk. In the case of an exchange field parallel to the $\vec{d}$-vector, the induced spin-polarisation inside the TSC is

found to be parallel or antiparallel to the spin-polarisation in the FM bulk, for strong or weak exchange fields respectively. In order to highlight the influence of the spin-triplet state, particular attention has been paid to the difference of the total spin-polarisation between the FM-N and the FM-TSC interfaces with similar magnetic configurations. Accordingly to the spatial variations, we found that the presence of TSC tends to decrease (increase) the z-spin-polarisation for weak (strong) exchange field, for all orientations, compare to the spin-polarisation measured in FM-N. On the other hand, although the effect is one order of magnitude smaller, the *in*-spin-polarisation is always enhanced in the presence of the superconducting state. As we pointed out, the results can be used to determine indirectly the orientation of the $\vec{d}$-vector, although we expect the variations to be small compare to the total spin-polarisation. However, it is worth mentioning that the investigation of such effect should require more detailed analysis. Additionally to the spin-orbit coupling present in ruthenium oxide Sr_2RuO_4, which can influence the spin-polarisation, it was shown in several works [26] that the interplay between ferromagnetism and superconductivity can generally induces additional Meissner currents at the FM-SC interface, which can modify the total magnetization measured, for instance, in field-cooling experiments [59, 100]. Nevertheless, the proximity effects in FM-TSC should depend on the orientation of the exchange field in the ferromagnet bulk and, therefore, should be experimentally observed at such interface.

Finally, the have examined of the Gibbs free energy of the system revealed that, in contrast to FM-SC interface, the rotational spin invariance of the ferromagnet is generally broken due to the coupling with the superconductor. We found that, without spin-orbit coupling at the interface, the FM develops an anisotropy which favours an in-plane orientation of the magnetization. In the case of a uniform ferromagnet, we have demonstrated that the driving mechanism for the stabilization of the bulk-interface relative orientation of magnetization is based on the gain of the superconducting condensation energy, due to the modification of the pair correlations in the superconducting region, rather than on the proximity effect. In the next Chapter, we aim to extend this analysis to FM-TSC junctions with an independent magnetic layer at the interface.

Chapter 3

Three-Dimensional FM-TSC Junctions with Spin-Active Interface

Conductance measurements and Josephson effects in heterostructures made of superconducting and metallic regions are largely driven by the transfer properties of the electrons from one region to the other. In other words, the quality of the interface between superconducting and metallic regions, which can be altered by impurities and roughness, influences directly the various Andreev reflections and, hence, the transport of the electrons through the junction as well as the critical temperature for short superconducting regions [28, 38, 103]. In this regards, spin-active interfaces, characterised by additional magnetic scattering processes at the interface induced by magnetic impurities, spin-orbit coupling or lattice defaults, can modify specifically the proximity effects in Josephson junctions and change the overall behaviour of the system. As we have mentioned in the last Chapter, the study of spin-active interfaces became a great deal at the first half of the last decade when it was shown they can induce a long-range odd-frequency spin-triplet order parameters in FM-SC junctions and hence explained unexpected large conductances in corresponding experiments [24, 104]. Such effect is also believed to be responsible of the observation of Josephson currents in SC-FM-SC with half-metallic barrier [77, 78, 111]. In the meantime, in a spintronic fashion, spin-valve junctions with small superconducting region FM1-SC-FM2, where FM1 and FM2 are two ferromagnetic regions with misaligned magnetization, have be shown to exhibit specific variations of the critical temperature as a function of the magnetization misalignment [123], effect which has been soon verified experimentally [64, 112]. Following these leading results, new FM1-FM2-SC junctions have then been considered in the middle of the 2000s. Variations of the conductance and the critical temperature have been predicted as a function of the magnetization misalignment [88, 92, 134] and have been observed in experiments where the orientation of the top ferromagnetic layers FM2 could be controlled using an external magnetic field [63, 73, 141, 143].

Following the works on FM1-FM2-SC junctions, we study in this short chapter the role of spin-dependent processes at the three-dimensional interface between ferromagnets and chiral spin-triplet superconductors(TSC). Most specifically, we mainly discuss the variation of the free energy of a FM1-FM2-TSC interface, where the magnetization in the short ferromagnetic region FM2 is misaligned compare to the bulk magnetization in FM1. In the last chapter, we have seen that a magnetization perpendicular to the $\vec{d}$-vector is always

energetically favoured at the FM-TSC interface. As we shall see, we find that, in the presence of a spin-active interface, the most energetically favourable magnetic configuration is obtained when both magnetizations in the FM1 and FM2 regions are coplanar and perpendicular to the $\vec{d}$-vector. However, we show that the system energetically favours parallel or antiparallel configurations depending on the strengths of the exchange fields. This effect is partly due to the model used to describe the interface but also a direct consequence of the proximity effects induced by the spin-triplet superconductor. We shall see that, even for a fixed magnetization in FM1 parallel to the $\vec{d}$-vector, the proximity effects tend to orientate the magnetization at the interface perpendicular to the $\vec{d}$-vector. Hence, we predict that, in contrast to FM-SC interfaces, a spin-active interface can be spontaneously established at the FM-TSC interfaces without any additional magnetic scattering processes.

The Chapter is organised as follows. We describe in section 3.1 the lattice model used to model the spin-active interface. Then, the spatial variations of the pairing amplitudes are shown in section 3.2. The section 3.3 is devoted to the analysis of the free energy for various magnetic configuration. The general phase diagram of the junctions is discussed in section 3.4 and we conclude our analysis in section 3.5.

3.1 Model and Formalism

The FM-TSC interfaces analysed in the following sections are designed in a similar fashion than in the last Chapter. Indeed, we consider a three-dimensional lattice made of stacked two-dimensional planes along the z-direction and described by an extended-tight-binding model, see Eq. 2.3. The in-plane pairing amplitude V_{i_z} between electrons of different spin is taken non-zero in the upper planes of the lattice, i.e. $i_z > 0$, to yield to a chiral spin-triplet superconducting phase represented by a $\vec{d}$-vector aligned along the z-direction. Moreover, we use the Stoner mechanism to induce a spin-polarisation in the lower planes of the lattice, i.e. $i \leqslant 0$, by means of an additional exchange field h_{i_z}.
The spin-active interface is modelled in our analysis by considering the orientation of the exchange field h_{i_z} not to be constant inside the ferromagnetic region. More specifically, we consider a small ferromagnetic region close to the interface FM_{int} where the magnetization is oriented by an angle ρ compare to the $\vec{d}$-vector, while the bulk magnetisation is oriented by an angle θ as depicted in Fig. 3.1. Hence, the junction is still invariant by rotation in the (xy)-plane and the spin-polarisation is constant in each plane. However, the interfaced magnetization h_{int} can be taken misaligned compare to the bulk magnetization h. Finally, we shall consider in our analysis the possibility for strength of the magnetizations $|h_{int}|$ and $|h|$ to be different to each other.

The results presented in the following sections are obtained after solving self-consistently the Bogoliubov-De Gennes equations and computing the spin-triplet superconducting pairing amplitudes $F_{px}(i_z)$ and $F_{py}(i_z)$ for various magnetic configurations, using Eqs. 1.32-1.33. The numerics are performed at zero temperature, for in-plane hopping terms $t^x = t^y = 1$ and for a chemical potential $\mu = -1.8t$. All the results discussed are obtained with an out-of-plane hopping term $t_z = 0.5t$. As we have seen, considering an other value

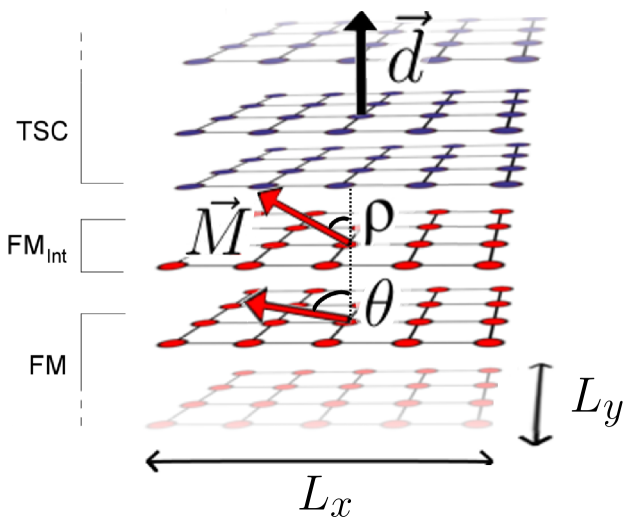

Figure 3.1: three-dimensional FM-TSC heterostructure with additional free ferromagnetic layer at the interface. The blue layers are for the spin-triplet superconductor with a $\vec{d}$-vector (black arrow) perpendicular to the (xy)-plane and the red layers indicate the ferromagnetic region. The magnetization $\vec{M}$ (red arrow) in the interior of the ferromagnetic region (at the interface) are forming a relative angle θ (ρ) with respect to the $\vec{d}$-vector. L_x and L_y are the in-plane lateral size of the heterostructure.

for t^z can modify the coherence length ξ_{SC} in the superconducting region and, thus, the amplitude of the induced correlations in the ferromagnet. Therefore, taking another value of t^z can quantitatively modify the results presented but do not change the qualitative discussion.
As in the last chapter, we shall discuss the variations of the condensation energy E_{cond} and of the total free energy G of the junctions, obtained from Eqs. 2.21 and 2.22 respectively, for various magnetic configurations.

3.2 Superconducting Spin-Triplet Pair Correlations

The presence of a spin-scattering interface modify the proximity effects at the FM-TSC interface and, therefore, the induced pairing amplitudes in the ferromagnetic regions as well as the order parameters in the superconducting one. The alterations compare to junctions without spin-active interface depend naturally on the magnetic configuration but also on the size of FM$_{int}$. In this section, we underline the main quantitative modifications in the spatial variations of the pairing amplitudes for a peculiar magnetic configurations and discuss the general effect of a misaligned magnetization at the interface.

We plot in Fig. 3.2 the spatial variations of the spin-triplet pairing amplitude $F_{px}(i_z)$ at the interface of a FM-FM$_{int}$-TSC junction for various orientations ρ of the magnetization inside the ferromagnetic interface FM$_{int}$. The magnetization in the bulk ferromagnet FM is taken parallel to $\vec{d}$-vector ($\theta = 0°$), thus totally pair-breaking for the Cooper pairs, since it is the configuration for which we can observe the most significant modifications at the interface. Indeed, without spin-active interface, we know that the induced $F_{px}(i_z)$ is decreasing and oscillating in the ferromagnetic region. It is represented by the configuration $\rho = 0°$ for which the magnetization at the interface is also parallel to the $\vec{d}$-vector. However, $F_{px}(i_z)$ is modified when $\rho \neq \theta$.
Let us first discuss the variations of $F_{px}(i_z)$ inside the interfaced barrier FM$_{int}$. As we can see, $F_{px}(i_z)$ monotonously decreases and remains positive inside FM$_{int}$ when the magne-

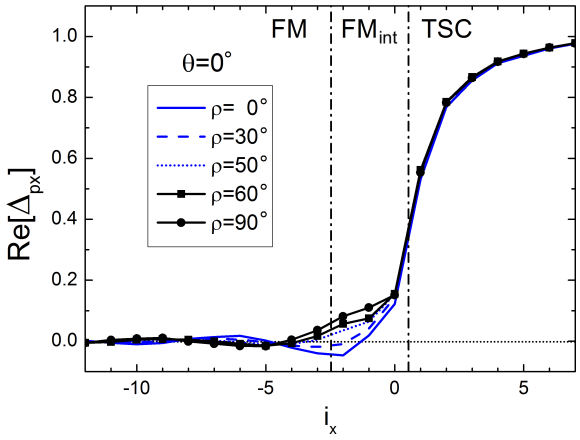

Figure 3.2: Spatial variation of the real part of the p_x-wave pairing amplitude F_{p_x} scaled to the TSC bulk value obtained for a bulk magnetization parallel to the $\vec{d}$-vector, i.e. $\theta = 0°$, and various magnetization orientations ρ in the interfaced layers FM$_{int}$. The ferromagnetic interfaced region is made of three layer $-2 \leqslant i_z \leqslant 0$ and the interfaces are denoted by the dashed lines. The exchange field strengths $h = h_{int} = 0.4t$ and the pairing coupling $V = -2.0t$ are fixed.

tization at the interface lies in plane ($\rho = 0°$). When $\vec{h}_{int}$ is rotating from an in-plane to an out-of-plane orientation, $F_{px}(i_z)$ is more and more decreasing and can also become negative when $\vec{h}_{int}$ is close to be perpendicular to the plane. This behaviour can be understand from our knowledge on the effect of pair-breaking or non-pair-breaking magnetic configurations. As we have seen in the last chapter, an exchange field $\vec{h}_{int}$ perpendicular to the $\vec{d}$-vector ($\rho = 90°$) is not pair-breaking. Instead, the interface is analogue to N-TSC junction and $F_{px}(i_z)$ is only decreasing in FM$_{int}$. For the other configurations at the interface, the magnetization tends to induce oscillations whose amplitude depends on the magnetization orientation ρ.
Then, inside the bulk ferromagnet FM, $F_{px}(i_z)$ is periodically oscillating as it is influenced only by the bulk magnetization parallel to the $\vec{d}$-vector and totally pair-breaking for the Cooper pairs. Hence, the period of oscillations is independent of the orientation of the magnetization in FM$_{int}$. On the other hand, the modifications of the spatial variations of $F_{px}(i_z)$ in FM$_{int}$ have a direct influence since they induce a shift of the oscillations in the FM region. As we shall see in Chapter four, this changes are responsible for the shift of the 0-π transitions in TSC-FM-TSC Josephson junctions.
Finally, the inverse proximity effects are also influenced by the pair-breaking or non-pair-breaking magnetization configuration at the interface. Indeed, following the results obtained in Fig. 2.2 for FM-TSC interfaces without spin active interface, we find that the order parameter $F_{px}(i_z)$ is maximized when $\vec{h}_{int}$ is perpendicular to the $\vec{d}$-vector ($\rho = 0$) and then decreases monotonously when $\vec{h}_{int}$ is rotating from an in-plane to out-of-plane orientation.

The general discussion of Fig. 3.2 is valid for any strengths of the exchange field, although some distinctive differences can emerge for larger interfaced ferromagnet or stronger magnetization. For instance, in the case of strong ferromagnets, a spin-active interface with a pair-breaking configuration induces very short oscillations in FM$_{int}$ which should also be observable with small-sized FM$_{int}$ regions and could hence modify the overall Josephson current.
Concerning the inverse proximity effects, the spin-triplet order parameter $F_{px}(i_z)$ is max-

imized in the TSC region when both the magnetization at the interface and in the bulk lies in the plane, perpendicular to the $\vec{d}$-vector. More specifically, when restricting the magnetic orientation to the (xy)-plane, we find that the pairing amplitude in the TSC region increases for θ and ρ being collinear and antiparallel. This implies a reduction of the proximity effect when the bulk-interface magnetic moments are antiparallel aligned.

3.3 Influence of the TSC on the Magnetic Profile

In the next two sections, we focus in studying the variations of the condensation energy E_{cond} and the free energy G of the junction, as defined in Eqs. 2.21 and 2.22, with respect to the strengths and the orientations of both magnetizations, in the ferromagnet bulk FM and at the interface FM_{int}. All discussed results are obtained with an interfaced ferromagnetic region FM_{int} existing only on one site $i_z = 0$ in order to observe the influence of magnetic scattering located at the interface. In this section, we are particularly interested in finding the magnetic configurations which minimized both E_{cond} and G energies in order to determine the general ground state of the interface.
The analysis of the energies variations reveals a complex scenario because the presence of spin-dependent processes at the interface tends to modify the balance in the Gibbs free energy due to the electronic spectrum and to the superconducting order parameter. In the following, we consider two possible physical situations for the search of the most favourable magnetic configuration:

> i) the magnetization in the FM bulk $\vec{h}$ and at the interface $\vec{h}_{int}$ have no preferential orientation (i.e. θ and ρ are treated as independent variational parameters)
>
> ii) the magnetization in the bulk is fixed in amplitude and orientation (for instance due to an intrinsic source of magnetic anisotropy or being pinned externally along a specific direction via an exchange-bias coupling) and we look for the optimal orientation of the magnetization at the interface which minimizes the Gibbs free energy.

For both cases the amplitude of the spin moments is chosen by fixing the value of the ferromagnetic exchange field h and h_{int} in the bulk FM layers and at the interface, respectively. The behaviour of the Gibbs free energy G and the order-parameter derived energy E_{op} with respect to the angles ρ and θ are reported in the Fig. 3.3 for which $h = h_{\mathrm{int}}$=0.3t, 1.5t, and 2.5t, respectively, are representative values for the regimes of weak, intermediate and strong ferromagnet. The amplitude of the exchange fields are scaled in such a way that $h = 1$ corresponds to the the transition into the half-metallic state with an energy gap in the minority spin band. Furthermore, in order to single out the role of the superconductivity in the energy competition, we have also analysed the ferromagnet-normal metal (FM-N) heterostructure assuming the same microscopic descriptions of the FM-TSC system with zero pairing interaction V.

Let us start by the FM-N heterostructure. The evolution of the ferromagnetic state can be monitored on the top row from Fig. 3.3. For the weak and intermediate ferromag-

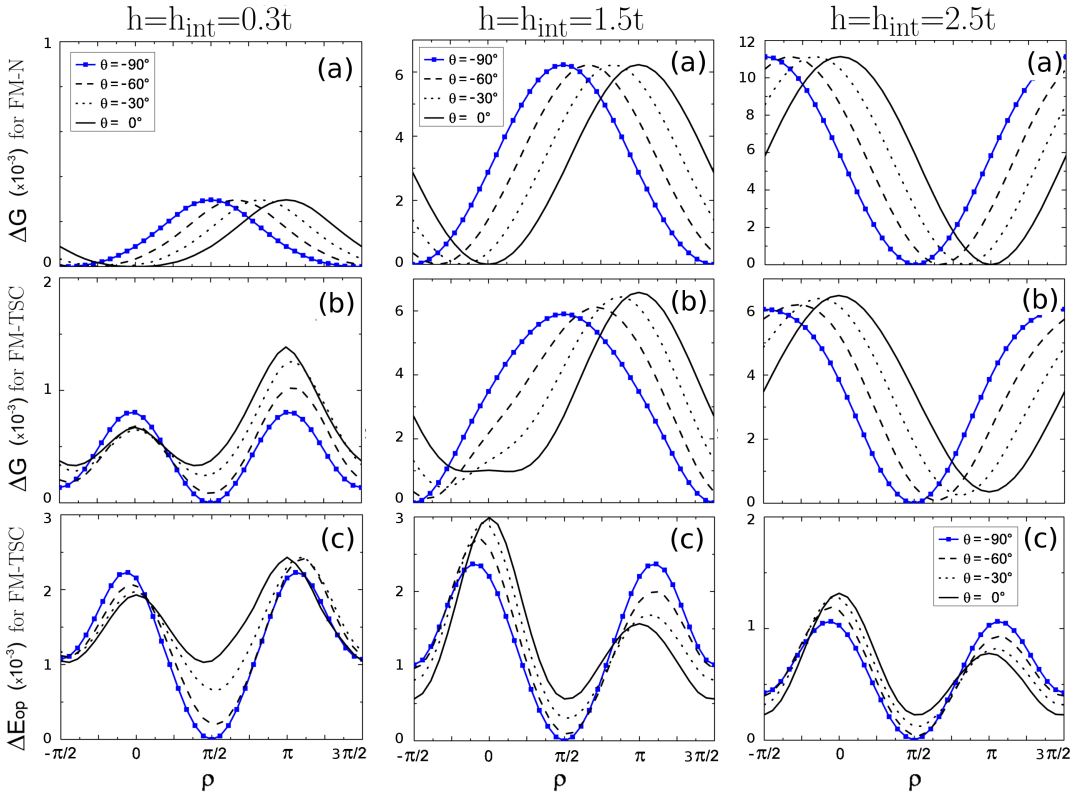

Figure 3.3: Gibbs free energy G for V=0.0t (a) and V=-2.0t (b), scaled with respect to its minimum amplitude $G^{\min}$ ($\Delta G = G - G^{\min}$) and renormalized to the energy $E_{\rm op}$ associated with a single superconducting layer in the homogenous case, as a function of the angle ρ at various angle θ and for three given values of the ferromagnetic exchange field $h = h_{\rm int} = 0.3t, 1.5t$ and $2.5t$, respectively. c) Condensation energy $E_{\rm op}$ ($\Delta E_{\rm op} = E_{\rm op} - E_{\rm op}^{\min}$) energy associated with the superconducting order parameter in the TSC region with the same renormalization and parameters as in a).

netic cases, i.e. left and middle panels, the minimum of the Gibbs potential corresponds with the configuration where the magnetization in the bulk is parallel to the one at the interface (i.e. $\rho = \theta$, Fig. 3.4 (a)). Since we are describing a ferromagnet without spin anisotropy one finds, as expected, a complete degeneracy in energy for all the possible spin orientations, i.e. the ground state, as expected, is rotational invariant in the spin space. The increase of the ferromagnetic exchange field towards the half-metallic state brings the ground state to have a transition into a different configuration. As one can note by inspection of the top right panel, the minimum of the Gibbs energy occurs at angles where the magnetization in the bulk and at the interface are antiparallel aligned (i.e. $\rho = -\theta$, Fig. 3.4 (b)). As for the previous cases the spin invariance is kept and we find that the ground state is degenerate at all the possible orientations of the ferromagnetic magnetization.

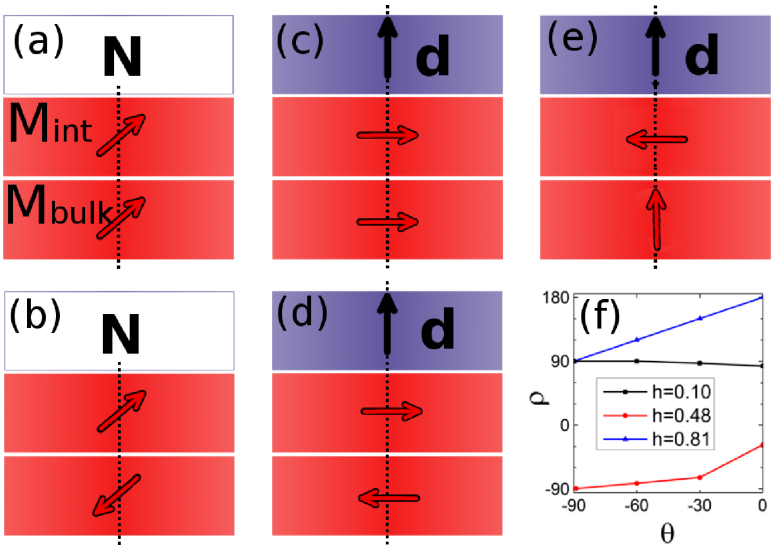

Figure 3.4: Sketches of the energetically most favourable magnetic profiles at various interfaces. Isotropic parallel (a) and antiparallel (b) configurations for a FM/N interface. Parallel (c) and antiparallel (d) configurations in the xy plane for a FM/TSC interface. (e) Configuration when the magnetization in the bulk is fixed out of plane. (f) Magnetization angle at the interface ρ_{min} which minimize the free energy for a fixed magnetization angle θ in the bulk. The ferromagnetic exchange fields are expressed in units of the exchange amplitude $h_{\mathrm{HM}} \cong 3.15t$.

When considering the physical case i) where all the magnetic orientations are assumed to be equivalent within the FM, the presence of the spin-triplet superconductor can lead to a breaking of the rotational symmetry for both the magnetic state in the bulk and at the interface. In this circumstance, since θ and ρ are taken as independent variational parameters, it is the absolute minimum of the Gibbs free energy to indicate the most favourable magnetic configuration for the FM-TSC system in the presence of spin-dependent processes at the interface. By inspection of middle row from the Fig. 3.3, left and middle panels, one can observe that for $h = h_{\mathrm{int}} = 0.3t$ and $1.5t$ the ground state corresponds to a configuration with parallel interface-bulk magnetic moments, i.e. $\theta = \pi/2$ and $\rho = \pi/2$, with the magnetization lying in the (xy)-plane perpendicular to the $\vec{d}$-vector (Fig. 3.4 (c)). However, for $h = h_{\mathrm{int}} = 2.5t$ (right panel) the Gibbs free energy is minimized by an antiparallel configuration within the (xy)-plane i.e., $\theta = \pi/2$ and $\rho = -\pi/2$ (Fig. 3.4 (d)). Finally, the behaviour of the order-parameter derived energy, presented in the bottom panels of the Fig. 3.3, shows that the maximum gain in E_{op} always occurs for an antiparallel interface-bulk configuration.

Moving to the physical case ii) where the exchange field orientation in the bulk FM is kept fixed while it can vary at the interface, all the curves of the Gibbs free energy as a function of ρ at a given angle θ have to be considered separately in order to determine the ground

state configuration. The resulting outcome is that for weak and intermediate ferromagnets the minimum of the Gibbs energy is not any longer achieved when the magnetization in the bulk and at the interface are aligned, while an antiparallel configuration remains favourable for any angle θ in the case of a strong ferromagnet. The magnetic configuration at the interface is therefore strongly related to the strength of the ferromagnetic exchange field (see Fig. 3.4 (f)).
More precisely, the most favourable configuration for a weak ferromagnet is with a magnetic orientation at the interface that lies in the plane perpendicular to the $\vec{d}$-vector almost independently of the magnetic configuration in the bulk. The Fig. 3.4 (e) represents for example the case where the magnetization in the bulk is pinned perpendicular to the plane, i.e. $\theta = 0$. This means that the superconducting correlations dominate in the scattering processes and in the energy balance. By increasing the amplitude of the ferromagnetic exchange field, the correlation between the magnetization at the interface and that in the bulk is modified in a way that the resulting ground state has a non collinear magnetic profile. The optimal magnetic orientation at the interface clearly exhibits a competition between two effects. We anticipate that this is due to the competition between scattering processes associated with the *normal* and the Andreev reflected electrons. On one side the scattering of the electrons with energies above the superconducting gap would tend to align the bulk and interface magnetization in a parallel configuration, on the other hand the Andreev reflected electrons occurring at midgap energies favour an antiparallel magnetic state with planar spin orientation. The resulting effect is to develop a magnetic interface state with components both along the bulk spin direction and in the plane perpendicular to the $\vec{d}$-vector. For the considered cases $h = 1.5t$ and $2.5t$, the deviation from having $\rho = \theta$ is due to the presence of the superconducting processes which always prefers to stabilize an in-plane magnetic orientation.
Indeed, if we look more specifically at the case $h = 1.5t$, the optimal orientation at the interface is at an angle $\rho \approx 3\pi/8$ when the bulk magnetization is parallel to the $\vec{d}$-vector (i.e. $\theta = 0$). The angle ρ corresponding to the relative minimum of the Gibbs free energy moves from about $3\pi/8$ to $\pi/2$ when θ varies from 0 to $\pi/2$ (see Fig. 3.4 (f)). Interestingly, the minimum of the order parameter energy E_{op}, corresponding to the maximal variation of the gap amplitude, occurs always at $\rho = -\pi/2$ for any value of θ if we exclude the $\theta = 0$ configuration where $\pm\pi/2$ are degenerate in energy due to symmetry reasons. The comparison between the variation of the Gibbs energy ΔG and the order parameter energy ΔE_{op} clearly indicates a competition between a contribution due to the change of the order parameter in the TSC region, and consequently of the condensation energy, and another one related to the magnetic energy close to the interface.

3.4 Energetically Most Favourable Magnetic Configurations

The analysis of the Gibbs energy profile indicates that the ground state is not unique but depends on the strength of the exchange field. Therefore it is interesting to calculate the complete phase diagram in terms of h and h_{int} by evaluating the absolute minimum of the Gibbs free energy in the $[\theta, \rho]$ landscape. Furthermore, in order to assess the role of the superconducting correlations strength in determining the most stable magnetic configuration, we have also computed the phase diagram at different values of the attractive

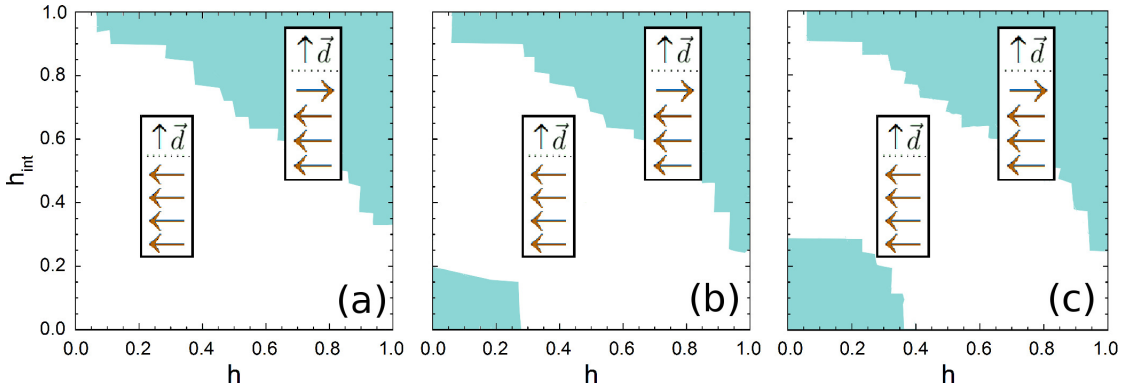

Figure 3.5: Phase diagrams for the energetically most favourable configuration in the plane $(h_{\rm int}, h)$ for V$= 0.0t$ (a), V$= -2.0t$ (b) and V$= -2.5t$ (c). The ferromagnetic exchange fields are expressed in units of the exchange amplitude $h_{\rm HM} \cong 3.15t$ corresponding to the transition value to an half-metal FM, where namely the density of the spin minority carriers goes to zero. The sketch represents the most favourable configurations with parallel (white area) and anti-parallel (blue area) interface-bulk magnetic moments alignment, respectively.

interaction for the TSC.

The results are reported in Fig. 3.5. They show that the parallel and antiparallel interface-bulk alignment of the magnetization lying on the (xy)-plane are the two most stable configurations. The antiparallel state is favoured for weak and strong ferromagnet while the parallel one is preferred at intermediate exchange values. A first order transition occurs at the boundary between the two regions of stability. Another consequence of the performed analysis is that the extension of the region for the antiparallel stability depends on the strength of the superconducting pairing coupling. This finding underlines the role of the superconducting state in modifying the magnetic configuration of the ferromagnet. Finally the boundaries of the antiparallel bulk-interface configuration for strong ferromagnet regime are only slightly affected in the direction of shrinking the region of stability for the parallel magnetic state. Indeed, in this case the antiparallel configuration is already preferred without the superconductivity and the ferromagnetic exchange field is dominant in the proximity effect.
It is worth pointing out that there is an asymmetry in the role played by the interface and the bulk exchange field which can be emphasized by scanning the phase diagram along lines with given $h_{\rm int}$ and h. Indeed at small fixed values of $h_{\rm int}/h_{\rm HM}$ ($\lesssim 0.2$) there is no re-entrant behaviour as a function of h while one does find the double transition for the antiparallel configuration in the case of small fixed values of h by tuning the amplitude of $h_{\rm int}$. Such asymmetry underlines the role of the interfacial spin-dependent scattering in driving the re-entrant behaviour from the parallel to the antiparallel configuration in the regime where the magnetization at the interface is large with a small density of spin-minority electrons.

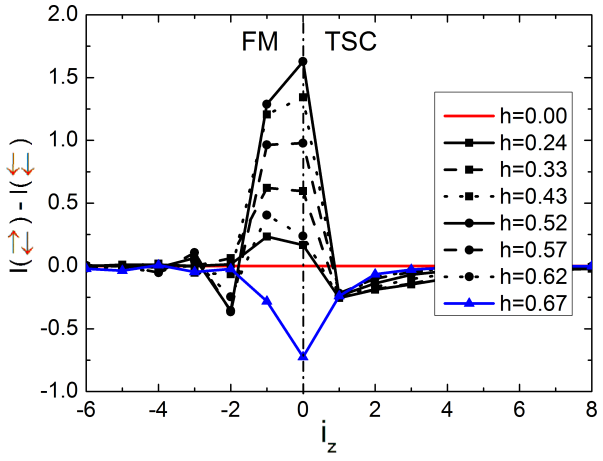

Figure 3.6: Difference of the integrated density of states for the antiparallel and the parallel configuration as a function of the layer position and of the exchange field strength for the FM-TSC interface. We consider an equal amplitude of the exchange field at the interface and in the bulk, i.e. $h = h_{\rm int}$, scaled with $h_{\rm HM}$.

Density Of States To get a deeper understanding of the modification on the energy spectrum induced by the interface-bulk misalignment we evaluate the density of states (DoS) $\rho(i_z, \omega)$ at each layer within the FM and TSC region of the heterostructure. More specifically, we analyse the integrated quantity of the latter on each layer of the lattice i_z representing the contribution to the Gibbs energy coming from the electronic spectrum. It is expressed as

$$I(i_z) = \int_{-D}^{0} \omega \rho(i_z, \omega) d\omega. \tag{3.1}$$

with $-D$ being the lowest occupied energy level and 0 the effective Fermi energy for the system after the Bogoliubov rotation.

In Fig. 3.6 we report the spatial evolution of the difference $\Delta I = I(\rightleftarrows) - I(\rightrightarrows)$ between the values of $I(i_z)$, corresponding to the antiparallel (i.e. $\rho = \pm\pi/2$ and $\theta = \mp\pi/2$) and the parallel (i.e. $\rho = \theta = \pi/2$) configurations, as a function of the ferromagnetic exchange field, assuming that $h = h_{\rm int}$. Since $I(i_z)$ is a negative quantity, a positive ΔI indicates that the electronic spectrum contribution tends to favour the parallel configuration and the opposite for negative amplitudes. The analysis of the DoS reveals a significant dependence of the contribution $I(i_z)$ on the magnetic configuration and on the strength of the ferromagnetic exchange field. As shown in Fig. 3.6, the main change in the DoS occurs at the FM layers which are close to the interface. This reflects the scale length where the energy spectrum reconstruction mainly occurs.
In the TSC region, the electronic reconstruction always favours the antiparallel state, as it is also expected from the evaluation of the order parameter energy $E_{\rm op}$. Thus, no significant renormalization of the DoS close to the Fermi energy happens that interferes with the role of the order parameter in the energy balance.
In the FM side the energy contribution due to the electronic spectrum is highly nontrivial. For small values of the ferromagnetic exchange field there is an appreciable difference between the energy related to the electronic spectrum of the two magnetic configurations.

Such difference becomes larger and larger in favour of the parallel configuration when h/h_{HM} increases from 0.32 to 0.51. Then the difference decreases until the antiparallel configuration starts to dominate. The results of the DoS confirm a scenario of electronic modification close to the interface playing a significant role in the magnetic configuration transition.

It is worth pointing out that the modifications of the DoS are substantial both in the energy range of the superconducting gap and also outside it. This is partially due to the superconducting correlations and in part to the change of the DoS due to the processes of scattering at the interface at energies which are larger than the superconducting gap in the presence of exchange field split Fermi surfaces. Interestingly, in the regime of intermediate ferromagnetic exchange field, i.e. for h/h_{HM} in the range of 0.32 to 0.57, the density of states of the ferromagnetic layers close to the interface exhibits new electronic states close to the Fermi energy when the antiparallel configuration is considered. Although such states may represent a distinctive feature of the FM-TSC heterostructure, they do not contribute significantly in determining the stability of the ferromagnetic profile.

Discussion In this section we would like to present a qualitative physical scenario related to the origin of the competing ground states in the FM-TSC heterostructure in the presence of spin-active interface processes.

We firstly consider the origin of the competition between the parallel and the antiparallel magnetic configurations within the FM-N heterostructure. To such purpose, we provide a simplified picture to justify the stability of a parallel bulk-interface state in the weak-intermediate ferromagnet and of an antiparallel one in the strong ferromagnet regime.
In the latter case, it is useful to consider the modification of the wave function in the ferromagnetic region close to the interface. We can schematically discuss this physical situation by means of a scattering formulation. Assuming that the interface plays the role of a spin-dependent barrier it is possible to determine the probability of an electron, propagating through the bulk with a given spin-direction and momentum, to be reflected or transmitted across the barrier. By solving the scattering problem, as expected the probability of reflection of a scattering electron increases as a function of the barrier potential strength Z.
Hence, an incident electron in the spin-majority band of the FM has experience of a larger (smaller) potential barrier if the magnetization at the interface is not parallel to its spin, which leads to a smaller (larger) spin-filtering effect. Still, for the antiparallel configuration, the spin-minority electrons, having a spin-polarization parallel to the magnetization at interface, have a higher probability to be transmitted. The resulting overall effect is to have more electrons reflected in the spin-majority band as well as more electrons transmitted in the spin-minority band, respectively. Thus, there is an increase of the spin polarization close to the interface because the wave-function has a larger (smaller) density probability for the spin majority electrons in the antiparallel (parallel) bulk-interface magnetic state. Such an increase of the spin-density would correspond to a higher magnetization and consequently to a larger gain in the magnetic energy. Finally, it is interesting to observe that by computing the spin-dependent reflection and transmission probabilities

for the weak ferromagnet regime, the processes become almost equivalent thus making more difficult to distinguish between the spin-polarization modification at the interface for the parallel and the antiparallel configurations. Then, the mechanism of wave-function reconstruction gets not effective in such regime.
In order to understand the origin of the antiparallel bulk-interface ground state in the phase diagram of the FM-N heterostructure for a weak ferromagnet, it is useful to analyse the problem by reducing the model to only two layers, i.e. the interface layer and its first neighbour (respectively i_z=0 and $i_z = -1$ in the notation of the heterostructure) for the two magnetic configurations. Assuming a collinear configuration, we consider the change of the energy spectrum due to the hybridization of the bands with the same spin polarization (the non collinear case does not change the results qualitatively). For the parallel configuration the spin polarized energy bands get split by the interlayer hopping and in the limit of $h = h_{\rm int}$ they are given by $E^P_\sigma = \epsilon(k) - \sigma(\, h * M + t_\perp)$. The expression for E^P_σ is obtained by assuming the same in-plane spectrum within the layer at $i_z = 0$ and -1, and the index $\sigma = 1(-1)$ labels the spin majority (minority) electrons in the bulk FM. For the antiparallel configuration the energy spectrum is split as a square root of the interlayer hopping, i.e. we have $E^{AP}_\sigma = \epsilon(k) - \sigma\sqrt{(h * M)^2 + t^2_\perp}$. By comparing the energy spectra for the two magnetic configurations for the spin-majority channels, one can deduce that for small exchange fields the energy gain is larger for the parallel configuration if compared to the antiparallel one because of the linear correction in the energy spectrum. We conclude that for weak-intermediate ferromagnets the parallel bulk-interface magnetic configuration is the most energetically favored state because of the energy spectrum reconstruction. On the other hand, in the regime of strong ferromagnetic exchange field, it is the wave function reconstruction that primarily drives the stability of the antiparallel configuration. We finally note that, for the FM-N heterostructure, the invariance of the Hamiltonian under spin rotation makes all the magnetic orientations degenerate in energy. These conclusions have been drawn for a physical situation with collinear magnetization. Similar arguments apply also for the case of a noncollinear bulk-interface configuration.

We focus now on discussing the reasons for having the spin-triplet superconductor to favour an antiparallel bulk-interface magnetic state with a planar spin orientation (i.e. perpendicular to the $\vec{d}$-vector) at any given strength of the ferromagnetic exchange field. We recall that this behaviour can be deduced by the observation of the profile for the pairing energy $E_{\rm op}$ which is always minimized when the magnetization in the bulk and at the interface lies in the plane perpendicular to the $\vec{d}$-vector and are aligned with opposite spin orientations. Since the $E_{\rm op}$ energy is directly related to the amplitude of the order parameter in the superconducting region, it is relevant to analyse the intensity and the character of the Andreev processes. Is is well known that the Andreev reflection amplitude enters plays a role in this context because it is the probability of an electron (hole) injected from the ferromagnet to be reflected as hole (electron), thus providing the intensity for the creation (annihilation) of an electrons (holes) pair in the superconductor. Then the Andreev scattering amplitude sets the strength of the pair fluctuations in the superconductor close to the interface and thus it is the main effect in driving the modification of the pair amplitude. Based on the nature of this process, we can argue that a large value of the Andreev reflection amplitude at the FM-TSC interface would then result into a significant

reduction of the pair amplitude and in turn of the superconducting order parameter in the TSC region close to the interface.
Among all the Andreev processes, those related to the creation (annihilation) of an electrons pair with a different phase are of particular relevance because they interfere destructively when they sum up in the formation of the pairing amplitude. From a general point of view, such non-trivial signs in the Andreev scattering can originate from the orbital dependence of the superconducting order parameter or they can be due to spin-dependent phase shifts for the mismatch in the magnetic configuration between the superconductor and the ferromagnet. A distinct and limiting case occurs in the presence of bound states at the interface where the Andreev probability is maximized for the correspondent energy of the incident electron (hole). The relation between the Andreev processes and the pairing amplitude variation has been shown to hold for a d-wave superconductor interfaced to the vacuum where bound states occur at specific orientations of the interface with respect to the d-wave nodal directions. There, a maximal reduction of the order parameter is observed when the orientation of the interface is such to have Andreev bound states in the density of states.
As mentioned in the Section III, for the case of a spin-triplet superconductor and for the examined layered geometry in this paper, the chiral orbital symmetry does not lead to Andreev scattering processes that involve sign changes in the pairing potential along the particle-hole trajectories. Hence, we expect that the modifications of the order parameter should be mainly ascribed to the contributions of spin-dependent scattering. Taking into account the results for the homogeneous ferromagnet, we are aware that the pair fluctuations are suppressed when the magnetization of the ferromagnet lies in the plane of the spin of the Cooper pairs, i.e. $E_{\rm op}$ is maximal for a magnetization which is perpendicular to the $\vec{d}$-vector. This is because in such a configuration there are no phase shifts in the Andreev processes. Considering now the competition between the other possible inequivalent configurations, i.e. the parallel and the antiparallel bulk-interface magnetic states, we observe that, in general and in the absence of bound states, the amplitude of the Andreev scattering decrease as a function of the barrier potential strength.
We note again that in the antiparallel configuration the incident electron in the spin-majority band gets experience of a greater barrier potential if compared to case of parallel spin-polarization. Such observation would imply that the intensity of the Andreev scattering probability is smaller for the antiparallel bulk-interface magnetic state than for the parallel one and therefore that the pairing amplitude is less affected by the scattering processes and thus less reduced. This qualitative argument would support the results of having a larger gain in the condensation energy when the bulk-interface magnetizations are antiparallel oriented. We also note that the discussed mechanism is consistent with the fact that there is a weak dependence on the strength of the ferromagnetic exchange field.

3.5 Conclusion

We have investigated in this Chapter the proximity effects of a three-dimensional FM-TSC junctions with a spin active interface, i.e. FM-FM$_{int}$-TSC junctions where the magnetizations in the FM bulk, $\vec{h}$, and interfaced region FM$_{int}$, $\vec{h}_{int}$, can be misaligned. Due to

the modification of the Andreev reflections, we have seen that the spatial variations of the spin-triplet pairing amplitude were altered compare to the FM-TSC case. However, these modifications can be totally understood by looking at the character of the magnetizations which can be pair-breaking or not for the Cooper pairs.
However, our main analysis focused on the variations of the condensation energy E_{cond} and free energy G as a function of the strengths and the orientations of both magnetizations $\vec{h}$ and $\vec{h}_{int}$. We have seen that within our model, two magnetic configurations minimized the total free energy G even for a FM-N interface depending on the strength of the exchange fields. Hence, generally for small strengths, the configuration where $\vec{h}$ and $\vec{h}_{int}$ are parallel is favoured, while for larger strengths, antiparallel configuration of $\vec{h}$ and $\vec{h}_{int}$ minimized G. In contrast to FM-N where the parallel or antiparallel configurations are isotropic, i.e. that they do not depend on the direction of $\vec{h}$ and $\vec{h}_{int}$, the TSC region favours in-plane configurations. Moreover, we found that the competition between the spectrum energy and the condensation energy lead to induce antiparallel magnetic configurations for small values of the exchange fields as well, in contrast to the FM-N interface.
Finally, the competition between both contributions have been in details analysed for equal strengths of the magnetizations, i.e. $|h| = |h_{int}|$. One interesting case to consider is when the magnetization inside the ferromagnetic bulk is fixed in one direction. Hence, we find that for strong ferromagnet, the energy of the system is always minimized for an antiparallel configuration at the interface, emphasizing the strong magnetic correlations between the two ferromagnet regions. On the other hand, we show that a weak bulk ferromagnet do not drives the behaviour of the magnetization at the interface but that the TSC does instead. Hence, the spin-triplet superconductor always favours a magnetization which is in plane. For intermediate ferromagnet, the competition lead to a misalignment of the interfaced magnetization which is neither parallel or antiparallel to the bulk magnetization.
To conclude, we have seen that the FM-TSC interfaces, in contrast to FM-SC one, can induce a spontaneous spin-active interface, i.e. an interface with a misaligned magnetization compare to the bulk one. As we shall see in the next Chapter, in clean ballistic regime, this effect can be directly observe in the variations of the critical current in TSC-FM-TSC Josephson junctions.

Chapter 4

Josephson Currents in TSC-FM-TSC Junctions

With the new experimental achievement of heterostructures made of ferromagnet (FM) and spin-triplet superconductors (TSC) [10], one of our major interest is to understand the proximity effects at the FM-TSC interface. As we have seen in the two previous chapters, they can lead to the rotation of the $\vec{d}$-vector, an induced spin-polarisation in the superconducting region and a spontaneously induced spin-active interface. One of the next promising step is the experimental realization of Josephson junctions made of spin-triplet superconductors and ferromagnets, which is of great interest for both theoretical and experimental purposes. As for the proximity effects, the Josephson effects were predicted in earlier works to be strongly depend on the magnetic configuration. It was found that, in contrast to spin-singlet superconducting (SC) junctions, the critical current as well as the state, generally denoted 0 and π, of the Josephson junctions do not only depend on the strength of the exchange field and the length of the ferromagnetic barrier, but also on the orientation of the magnetization with respect to the $\vec{d}$-vector characteristic of the spin-triplet Cooper pairs. The control of the state of the junction by the rotation of the magnetization, observable in the critical current, would be an unambiguous evidence of the spin-triplet character of the superconductors. The magnetization can also be imagined to be a key parameter to control the state of the junction in the the design of qubit made of 0 and π-junctions [54, 71, 138].

The theoretical interest in Josephson effects and conductance in junctions made of spin-triplet superconductors with metallic or insulating barriers started at the beginning of 2000s soon after the discovery of Sr_2RuO_4 [12,17,99,127,137]. The first results concerning the current-phase relation of TSC-FM-TSC (TFT) Josephson junctions were then obtained with the derivation of the Bogoliubov-DeGennes equations for quasi one-dimensional systems with infinitesimal small barriers [76], i.e. equivalent to tunnelling junctions, and was soon extended to finite potential barriers [34]. Since then, the evolution of the critical current as well the phase of the junctions have been studied for various magnetic configurations, in particular as a function of the magnetization orientation and the temperature [32, 33, 35, 76]. Moreover, the study of the phase of the junction have been also recently extended to finite ferromagnetic barrier [37]. Additionally, it has been found that spin-current across the junction could be induced due to the magnetic configuration of the barrier, which can induce spin-filtering and spin-flipping mechanisms [95], or due to the

misalignment of the $\vec{d}$-vectors on each side of the junction [14, 15, 34].

In this chapter, we aim to continue the analysis of the rich physic of the TFT Josephson junctions by solving the Bogolibov-De Gennes equations using the extended tight-binding model. The current phase relations are obtained by the computation of the Gibbs free energy of the system and the evaluation of the current density operators on the lattice. Since the probe of the current-phase relations is difficult to achieve experimentally, although possible [56, 72, 117], we mainly focus on studying the evolution of the phase of the junction with respect to the magnetization configuration. Our first results intend to reproduce the 0-π phase diagrams previously obtained for two-dimensional junctions by means the quasiclassical formalism [37]. Although quantitatively different, both methods show good agreement in the prediction of 0-π transitions and on the evaluation of the critical angles. Moreover, we demonstrate that the 0-π phase diagrams can totally be understood by looking at the oscillations of the induced spin-triplet pairing amplitudes in the ferromagnet barrier. We then extend our study in order to verify how robust are the results by using a more refined model as presented in the two previous chapters. For this purpose, we successively study two-dimensional TFT junctions with self-consistent evaluations of the order parameters and three-dimensional junctions. We show for both cases that the conditions to obtain 0-π transitions remains qualitatively similar to the previous case. On the other hand, while two-dimensional junctions with p_x, p_y and p_x+ip_y gap symmetries are different, we show that they have similar phase diagrams in three-dimension systems as expected from the consideration of the symmetries. Finally, we introduce spin active interfaces between the ferromagnetic barrier and the superconductor regions and we show that the 0-π phase diagrams is modified by the presence of misaligned magnetization at the interfaces. Finally, as a direct experimental observation, we evaluate the critical current of the TFT junction as a function of the barrier's length for various configurations. We predict anomalous oscillations in the cases of partially pair-breaking configurations of the magnetization as well as for junctions with spin-active interfaces.

This chapter is organised as follows. Section 4.1 is devoted to the presentation of the Josephson effect as well as the model use to describe the Josephson junction. The spatial variations of the current is then analysed in section 4.2 for various configurations of the junction. We discuss the 0-π phase diagrams for two-dimensional system in section 4.3 and we highlight in section 4.4 the relation between the 0-π transitions and the spatial variations of the spin-triplet order parameters. We study in section 4.5 the 0-π phase diagrams using self-consistent computations, for three-dimensional junctions and for junctions with spin active interface. Finally, the section 4.6 is devoted to the study of the critical currents and the conclusion is presented in section 4.7.

4.1 Josephson Junctions and Current Density Operators

The Josephson charge current between two superconductors separated by an insulator, a weak link or a good conductor, whether metallic or a ferromagnetic, can be obtained by several theoretical methods that we briefly review in this section. It is not only interesting to understand the microscopic physical scenario leading to finite current, but also to

introduce the main observables, which define each junctions as the state of the junction, the critical current, and the critical angle in the case of ferromagnetic barriers. It is also worth to briefly comment on possible experimental measurements since most of the results may be directly observable. Finally, we derive in the main part of this section the equations of the current densities, for the two-dimensional lattice model of the Josephson junction, from the charge and spin equations of motion.

Insight into Josephson Junctions The first derivations of the tunnelling charge current between metals and superconductors have been performed in the early sixties. Still using a BCS tunnelling model solved by perturbation theory, B.D. Josephson derived in 1962 the charge current between two superconductors. He predicted both, the oscillations of the alternating current for a finite applied voltage V with frequency $\omega = 2eV/h$ and the existence of a finite direct current even at zero difference of potential [74, 75]. The latter effect was admirably observed few months later by P.W. Anderson and M. Rowell [4] and by S. Shapiro [119]. By considering the derivative of the free energy of the Hamiltonian with respect to the vector potential, P.W. Anderson then derived [42] the well known relation between the Josephson charge current at equilibrium and the phase of the superconductors

$$J = J_c \sin(\varphi_1 - \varphi_2) \tag{4.1}$$

where φ_1 and φ_2 are the phases of the order parameters of each superconductor. Eq. 4.1 defines hence the current-phase relation of the junction and shows that, for tunnelling barrier, the DC part of the current has a sinusoidal dependence with respect to the phase difference $\phi_{SC} = \varphi_1 - \varphi_2$ and a maximal value J_c reached at $\phi_{SC} = \pi/2$, as represented in the curve (a) in Fig. 4.1. It is usual to refer to J_c as the critical current of the junction which is one of the main quantities reachable experimentally.

The sinusoidal behaviour of the current-phase relation is however obtained only in the case of perfect tunnel junctions or in point contact experiments performed close to the critical temperature. Further analysis for ballistic and diffusive point contact junctions, through the evaluation of the Green's functions within the quasiclassical approximations, shown that higher-order harmonics can additionally be present in Eq. 4.1 [61]. For instance, the critical current J_c for junctions in a diffusive regime close to T=0K or in ballistic regime is then reached for $\phi_{SC} > \pi/2$ as represented by the curve (c) in Fig. 4.1. On the other

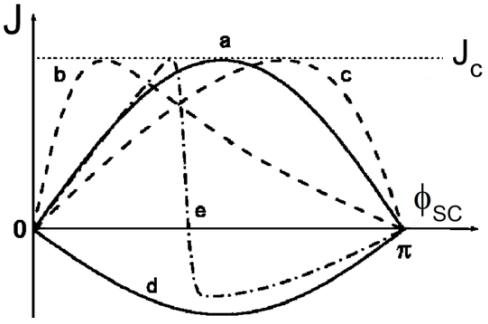

Figure 4.1: Various behaviours of current-phase relations achieved in Josephson junctions. They are generally representative of tunnelling (a), weak and metallic (b-c), and ferromagnetic (d) barriers which could exhibits a π-state. Adapted from Ref. [61].

hand, the critical current in junctions with an insulating barrier is obtained for $\phi_{SC} < \pi/2$, see curve (b). These results are also obtained for metallic barrier, where the higher-order harmonics in the phase-current relation are directly associated to the characteristic of the barrier, as the length of the metallic region, the scattering rate, the temperature as well as the quality of the interface. Moreover, second-order harmonics become a major interest in d-wave Josephson junctions for which the first order harmonic can be suppressed for specific values of the temperature. Thus, the complex variations of the current-phase relations must be analysed carefully in different regimes and we refer to the two main reviews on the subject for more details [61, 87].

The results discussed above can be obtained with various theoretical methods. In addition to the use of the full Green's functions on the lattice, the Josephson charge current can be analysed with the Ginzburg-Landau formalism for junctions near the critical temperature T$\sim$T$_c$. However, the quasiclassical methods are the most generally employed since they provide literal solutions for different limit in cases and could reproduce very accurately experiments. The so-called Eilenberger [48] and Usadel [130] equations described the spatial variations of the space and momentum integrated Green's functions between two superconductors and which are used to obtain the Josephson current in the clean and ballistic limit, respectively. The latter can be explicitly expressed for few limit in cases or be numerically evaluated [38, 39, 61]. On the other hand, Bogoliubov-De Gennes (BdG) equations can be used by approximating in each side of the junctions the wave functions of the electrons by plane waves with Fermi energy. Similarly to problem of quantum wells, the energies inside the barrier are quantified and they are contingent upon the Andreev reflections at the interface with the superconductors [140]. We refer to these localized states inside the barrier as being the Andreev Bound States (ABSs). Both quasiclassical methods depend nevertheless to the boundary conditions at the interfaces between each regions, which are directly related to the amplitudes of transmission and reflection of the electron between each region. Concerning the BdG equations, we obtain the current-phase relations by looking at the variations of the energy of the ABSs as a function of the superconducting phase difference ϕ_{SC}

$$J = \sum_n \frac{\partial E_n}{\partial \phi_{SC}} \tag{4.2}$$

where E_n are the n level of energies of the ABSs inside the barrier. Interestingly, high-order harmonics can induce a cancellation of the current for $\phi_{SC} \neq 0$ and π, see curve (e), and an additional π-phase can be present in the Eq.1.1 due to the modification of the conditions on the ABSs energies, see curve (d). Moreover, it was found that the critical current can oscillate and be cancelled as a function of the temperature, the length of the barrier and the strength of the magnetization. Therefore, Josephson junctions with metallic or ferromagnetic barrier show distinctive behaviours which can be partially captured by looking at the free energy of the system. Indeed, the energy G of the junctions is directly linked to the variations of the current as

$$G(\phi_{SC}) - G(\phi_{SC} = 0) = \int_0^{\phi_{SC}} d\phi \; J(\phi). \tag{4.3}$$

Hence, if we consider the examples of perfect normal and magnetic tunnel junctions, depicted by the curve (a) and (d) respectively in Fig. 4.1, we can see that the minimum energy of the first one is reached for $\phi_{SC} = 0$ while it is reached for $\phi_{SC} = \pi$ for the second one. The state of the junction is hence defined as the value of ϕ_{SC} for which the minimum of the free energy is obtained. As we previously mentioned, while metallic junctions only exhibit 0-state, junction with ferromagnetic barrier can exhibit 0- and π-states according to the temperature, the length of the barrier and the strength of the magnetization. We can mention that last decade has also seen growing new interest for junctions made of noncentrosymmetric superconductors or having more complex design, which have been predicted to exhibit more complex current-phase relations and could achieved $\pi/2$ or ϕ-states [20,68,81,109]. Moreover, in contrast to the sinusoidal behaviour of the current-phase relation in tunnelling Josephson junction, a behaviour in $\cos(\phi_1 - \phi_2)$ have been also predicted to appear in SC-FM-TSC junctions [36].
In the scope of this chapter, we are only interested in junctions made of chiral spin-triplet superconductors. Previous quasiclassical studies shown that, in a similar fashion than SC-FM-SC junctions, junctions made of chiral spin-triplet superconductors and ferromagnetic barriers can exhibit 0- or π-states. However, it was found that, differently from singlet junctions, additional transitions between the two states take place as a function of the relative angle between the magnetization and the $\vec{d}$-vectors. Therefore, in this chapter, we first aim to verify within the tight-binding model the various predictions about the 0-π transitions and to enlarge the study to self-consistent and three-dimensional TFT junctions. Having a finite barrier size and no impurities, our system can be identify from a quasiclassical point of view to clean junctions with small to large barriers size. In this respect, we expect the current-phase relation not to be sinusoidal but to have large higher-order harmonics.

Experimental Observations At equilibrium, the Josephson junctions are usually characterized by their current-phase relations, which contain also the information about the state of the junctions, and the energy spectrum of the Andreev bound states. Indirect techniques to observe the current-phase relations, involving the design of complex junctions, have been developed and remarkably applied for few systems with metallic and, more recently, ferromagnetic barriers [56, 117]. However, the experiments remain challenging and the difficulty to build spin-triplet junctions make such observation in the near future uncertain.

Therefore, we believe it is of main interest to experimentally obtain information, not about the current-phase relations, but about the state of the junctions. The critical current J_c is the main measurable quantity which can provide an information about the state of the junction. It is obtained by injecting a direct current J_i through a superconducting junction and to measure the induced difference of potential dV between the two sides of the junctions. As long as $J_i < J_c$, dV remains zero because of the modulation of the energies of the ABSs inside the metallic or tunnel barrier whereas dV becomes finite when $J_i \gtrsim J_c$.
However, knowing the critical current is not enough to identify the state of one precise configuration of the junctions. More exactly, it is necessary to observe the variations of $|J_c|$

as a function of the temperature, the length of the barrier or the strength of the magnetic field. For instance, it was found that $|J_c|$ should cancel, at temperature close to T_c, when there are no high-order harmonics, or oscillate, when high-order harmonics are present, as a function of these various parameters. Hence, the indirect determination of the state of the junctions is totally dependent on the theoretical predictions.
That is why the last section of this chapter is devoted to the analysis of the variations of the critical current as a function of the barrier length for various values of the exchange field and magnetization angles. We will see that the signature of the 0- and π-states can be observed in the critical current as predicted by means of the quasiclassical formalism. This behaviour is very analogue to the SC-FM-SC junctions. On the other hand, the interplay between the magnetization and the spin of the spin-triplet Cooper pairs is expected to contain additional features. We will see that, depending on the magnetization orientation and the presence of spin active interfaces, anomalies in the variations of J_c can be present. We believe these anomalies to be most likely observed in clean junctions with spin-triplet superconductors and ferromagnetic barriers.

Computation of the Current Densities on the Lattice As mentioned previously, we aim to study in this chapter spin-triplet Josephson junctions using a extended tight-binding lattice model. For this purpose, we consider a two-dimensional TSC-FM-TSC junction made of a ferromagnet metal surrounded by two spin-triplet superconductors, see Fig. 4.2. The characteristics of the system are very similar of those described in the previous chapters and all discussed results are obtained with $\vec{d}$-vectors in the TSC regions aligned along the z-direction, perpendicular to the plane. Hence, the magnetization $\vec{M}$ in the FM region is aligned in a direction having an angle θ with respect to the z-direction, and so with respect to the $\vec{d}$-vectors. The system is described by the Hamiltonian Eq. 2.3 using a mean field approach and with periodic boundary conditions in the y-direction.
The direct Josephson charge current across the junction arises usually when the order parameters of the two superconducting regions have different phases[2]. In our model, we add superconducting phases ϕ_L and ϕ_R to the spin-triplet order parameters in the left and right regions, respectively. We define the superconducting phase difference between the two superconductors as $\varphi_{SC} = \varphi_L - \varphi_R$. For clarity, we decide to fix in an equivalent manner the phase of the right TSC to zero while we choose $\varphi_L = \varphi_{SC}$. According to the definition of the gap amplitudes Eqs. 2.10-2.15, adding a phase to the order parameter is equivalent to add a phase to each of the correlation functions $F_i^{\nu\pm}$. Therefore, the coupling terms of the mean field Hamiltonian defined in Eqs. 2.8 and 2.9 become

$$\Lambda_{ijk} \longrightarrow \Lambda_{ijk}\, e^{i\varphi_{SC}\delta_{i,l}}, \tag{4.4}$$

$$\Lambda^{\sigma\sigma}_{ijk} \longrightarrow \Lambda^{\sigma\sigma}_{ijk}\, e^{i\varphi_{SC}\delta_{i,l}}, \quad \text{with } l \text{ being a site in the left TSC.} \tag{4.5}$$

The system is finally solved using the Bogoliubov- De Gennes equations Eq. A.33 as described in the first chapter. We determine hence for various values of the superconducting

[2] It is the case for spin-singlet and spin-triplet junctions. However, it was found that finite Josephson charge current can also exist without phase differences in junctions made of noncentrosymmetric superconductors. The junction can then exhibit a ϕ_{SC}-state with $\phi_{SC} \neq 0, \pi$ [81, 109].

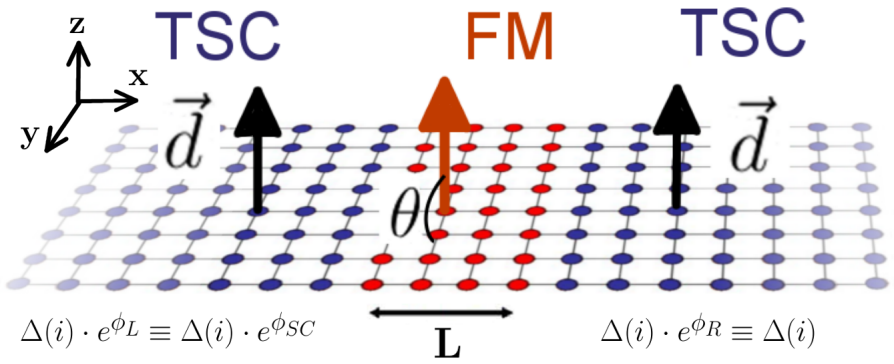

Figure 4.2: TSC-FM-TSC two-dimensional junction along the x-direction. The blue layers indicate the spin-triplet superconductors with the $\vec{d}$-vectors (black arrows) both oriented along the z-direction. The magnetization in the FM region is represented by the red arrow. Is is rotating in the (yz)-plane and is aligned in the direction having an angle θ with the z-axis. The spin-triplet order parameters have a phase ϕ_L and ϕ_R in the left and right superconducting regions, respectively.

phase difference ϕ_{SC} the energy spectrum of the Hamiltonian and so, by additionally computing the condensation energy, the total free energy G. This is our first method to obtain the current-phase relation of the junction using the relation Eq. 4.2. This method has, from a numerical point of view, the advantage to not require additional derivations and the results obtained can be directly compared to most of the quasiclassical analysis. However, this method can only give us information about the charge current across the junction but none about the spin polarized current without introducing a tunnel formalism [37].
The second method to compute the Josephson current across the junction is to derive the spin-resolved current densities on each site of the lattice from the charge and spin flow equations. Since we analyse the Josephson current in superconducting junction at equilibrium, the current operators can be computed using the usual advanced Green's functions [36, 98], without the need to develop the Keldysh formalism necessary for out-of-equilibrium problem. Let us first express the charge and spin densities defined on each point of a two-dimensional lattice with periodic conditions in the y-direction as

$$\rho(i) = e \sum_{k_y} \sum_{\sigma} c^{\dagger}_{i\sigma k_y} c_{i\sigma k_y} \ , \tag{4.6}$$

$$s^{\nu}(i) = \frac{h}{2} \sum_{k_y} \sum_{\sigma} c^{\dagger}_{i\sigma k_y} \hat{\sigma}^{\nu}_{\sigma\sigma'} c_{i\sigma' k_y} \quad \text{with} \quad \nu = \mathrm{x}, \mathrm{y}, \mathrm{z} \tag{4.7}$$

where $i \equiv i_x$ is a atomic site on the lattice, σ is the spin of the fermion, e is the elementary charge, k_y is the momentum along the y-direction and ν the direction of polarisation. In the Heisenberg picture, the equations of motion of the charge and spin densities along the x-direction are obtained by the usual commutation of the operators with the Hamiltonian

$$\partial_t \rho(i) = i\,[H, \rho(i)]\ , \tag{4.8}$$
$$\partial_t s^\nu(i) = i\,[H, s^\nu(i)]\,. \tag{4.9}$$

The derivation of the Eqs. 4.8-4.9, using the two-dimensional mean field Hamiltonian Eq. 1.26, leads to the current conservation laws for the charge and spin quantities

$$\partial_t \rho(i) = J(i-1) - J(i) - S_{charge}(i)\ , \tag{4.10}$$
$$\partial_t s^\nu(i) = J_s^\nu(i-1) - J_s^\nu(i) - S_{torque}^\nu(i) - S_{spin}^\nu(i). \tag{4.11}$$

where $J(i)$ is the charge current and $J_s^\nu(i)$ is the spin current polarized in the ν-direction at the site i. They are the usual kinetic current and are expressed as

$$J(i) = J_\uparrow(i) + J_\downarrow(i) \tag{4.12}$$
$$\text{with} \quad \mathrm{J_\sigma(i)} = it \sum_k \left[c^\dagger_{i+1,k\sigma} c_{i,k\sigma} - c^\dagger_{i,k\sigma} c_{i+1,k\sigma} \right], \tag{4.13}$$

$$\text{and} \quad \mathrm{J_s^\nu(i)} = \frac{it}{2} \sum_k \sum_{\sigma\sigma'} \left[c^\dagger_{i+1,k\sigma} \hat{\sigma}^\nu_{\sigma\sigma'} c_{i,k\sigma'} - c^\dagger_{i,k\sigma} \hat{\sigma}^\nu_{\sigma\sigma'} c_{i+1,k\sigma'} \right]. \tag{4.14}$$

using the notation $k \equiv k_y$. $J(i)$ and $J_s^\nu(i)$ represent the charge and spin kinetic currents flowing between the sites $i-1$ and i and are computed over all the bonds of the lattice. For clarity in the discussion, and without loss of generality, we define a positive value of the current as being associated to a charge flow from the left side to the right side of the junction, while a negative value is associated to an opposite charge flow. Finally we can notice that the spin current polarized in the z-direction is directly

$$J_s^z(i) = J_\uparrow(i) - J_\downarrow(i). \tag{4.15}$$

The current conservation laws show that additional source terms S_{charge} and S_{spin}^ν, coming from the TSC side, as well as S_{torque}^ν, coming from the spin torque exerted by the magnetization in the FM side, also contribute to the transfer of charge and spin over the lattice. It is worth discussing about their physical meaning and their importance in our computation. The term S_{charge} and S_{spin}^ν are non zero only in the superconducting sides [36,98]. It comes from the fact that, as already discussed for the Andreev reflections (see Appendix B), a charge coming from the FM side to the superconductors is reflected as a hole while a Cooper pair is created in the superconducting region. Indeed, the charge cannot exist in the superconductor at the Fermi energy. As detailed in Appendix B, the excited states obtained by solving the BdG equations do no conserve the number of charge when the electron is entering in the superconductor. In particular, before to be reflected as a hole, the excitation in the superconductor is an equal mixture of an electronlike and holelike

particles whose total charge is zero. The charge current in the FM is actually transferred to the superconductor as a supercurrent carried by the Cooper pairs [98, 128]. Therefore, we do not need to evaluate the source terms in order to obtain the charge current densities in the TSC since they are already obtained in the FM side before conversion into the supercurrent. It is worth keeping in mind that this process occurs on a distance of the superconducting coherence length ξ_{SC} and that, as a consequence, the normal charge current is completely suppressed at the interface but over a distance ξ_{SC}.
Differently, S^{ν}_{torque} is exerted by the fixed magnetization in the FM region. Indeed, as well known and controlled in the field of spintronic, a spin current can exert a spin torque to a magnetization, which therefore can rotate. The source term S^{ν}_{torque}, which indeed exists only when there is a spin current inside the FM region, represent the compensating spin current necessary to maintain a fixed magnetization in the ferromagnetic barrier. As a consequence, J^{ν}_{s} can be site dependent in the barrier, but it should be constant in the superconductors. On the other hand, if we do not take into account the S_{charge} and S^{ν}_{spin} in the superconductor, J^{ν}_{s} is also vanishing in the the SC. The only site where J^{ν}_{s} can be evaluated without taking in to account of any source terms, are the bonds between the ferromagnetic and superconducting regions.

Therefore, without taking into account of the additional source terms, Eqs. 4.8-4.9 show that the charge transfer is given by the divergence of the kinetical currents as expected. In order to compute the expectation values of the current density operators Eqs. 4.12-4.14, we use the solutions of the Bogoliubov- De Gennes equations as explained in Appendix A. The quantities to be evaluated are given by

$$\langle c^{\dagger}_{ik\uparrow} c_{jk\uparrow} \rangle = \sum_{n} \; u_{ink} \; u^{*}_{jnk} \; f(E_n) \; , \tag{4.16}$$

$$\langle c^{\dagger}_{ik\uparrow} c_{jk\downarrow} \rangle = \sum_{n} \; u_{ink} \; v^{*}_{jnk} \; f(E_n) \; , \tag{4.17}$$

$$\langle c^{\dagger}_{ik\downarrow} c_{jk\downarrow} \rangle = \sum_{n} \; v_{ink} \; v^{*}_{jnk} \; f(E_n) \; , \tag{4.18}$$

$$\langle c^{\dagger}_{ik\downarrow} c_{jk\uparrow} \rangle = \sum_{n} \; v_{ink} \; u^{*}_{jnk} \; f(E_n) \; , \tag{4.19}$$

with $i - j = \pm 1$. We point out that these derivations are sufficient for out current analysis since they describe our system at equilibrium. Junctions in a regime out of equilibrium, for instance systems with spatial variations of the chemical potential or with a precessing magnetization, should be treated according to the Keldysh formalism which involves non-equilibrium Green's functions. Such a studies have been for instance performed for the computation of conductance [49, 93].
The generalization of the current conservation laws to the three-dimensional junctions is straightforward. In this case, the FM region is made of L two-dimensional layers stacked along the z-direction and surrounded on the top and the bottom by TSC regions. Periodic boundary conditions are used along the x- and y-direction in the two-dimensional planes. The kinetic currents give the spin and charge flow along the z-direction and Eqs. 4.12-4.14 become

$$J(i_z) = J_\uparrow(i_z) + J_\downarrow(i_z) \tag{4.20}$$

$$\text{with} \quad \mathrm{J}_\sigma(\mathrm{i_z}) = it \sum_k \left[c^\dagger_{i_z+1,k\sigma} c_{i_z,k\sigma} - c^\dagger_{i_z,k\sigma} c_{i_z+1,k\sigma} \right] \tag{4.21}$$

$$\text{and} \quad \mathrm{J}^\nu_\mathrm{s}(\mathrm{i_z}) = \frac{it}{2} \sum_k \sum_{\sigma\sigma'} \left[c^\dagger_{i_z+1,k\sigma} \hat{\sigma}^\nu_{\sigma\sigma'} c_{i_z,k\sigma'} - c^\dagger_{i_z,k\sigma} \hat{\sigma}^\nu_{\sigma\sigma'} c_{i_z+1,k\sigma'} \right]. \tag{4.22}$$

where the summation over the momentum become $\sum_k \sim \sum_{k_x,k_y}$ and where the site i_z refers to a two-dimensional layer in the z-direction.

In the following sections, we discuss in details the properties of the TFT junction for various configurations of the system. Although not exhaustive, it will include results about the two- and three-dimensional systems as well as systems with spin active interfaces between the ferromagnet and superconducting regions. Most of the results are obtained without using self-consistent computations for the superconducting order parameters, but the latter will still be discussed in one of the section.

4.2 Analysis of the Josephson Charge Current

In order to discuss the general results concerning the TFT junctions, i.e. the 0-π transitions as well as the associated critical angle and the critical current, we first need to analyse the spatial variations of the current densities obtained from Eqs. 4.12 - 4.14. Indeed, as we shall see they provide us primitive results that we use to define which quantity represents the charge current crossing the interface as well as the critical current J_c. We also discuss the variations of the free energy and of the current densities as a function of the superconducting phase difference ϕ_{SC} and see that both quantities contain evidence of 0-π transitions. All results are obtained at T=0K as previously.

Spatial Variations of the Current Densities When the superconducting phases in both sides of the junction represented in Fig. 4.2 are not equal, i.e. $\phi_{SC} \neq 0$, we expect a finite charge flow to be present in the system. As we have seen, we can evaluate the charge current densities associated to spin up and spin down electrons $J_\uparrow(i)$ and $J_\downarrow(i)$, computed between each site i and $i+1$ along the x-direction of the lattice, using Eqs. 4.13 while the charge current $J_c(i)$ is obtained by taking the summation of both contributions, see Eq. 4.12. We expect the latter to be conserved over the complete system due to usual charge conservation law. However, due to the presence of a magnetic barrier in the system, we expect the electrons to encounter spin flip and, therefore, $J_\uparrow(i)$ and $J_\downarrow(i)$ not to be necessarily conserved along the junction.
In order to illustrate the charge conservation inside the system, we plot in Fig. 4.3 (a) the spatial variations of the spin-resolved current densities $J_\uparrow(i)$ and $J_\downarrow(i)$ (purple lines) as well as the charge current $J_c(i)/2$ (red line) in a p_x+ip_y junction for a fixed value of

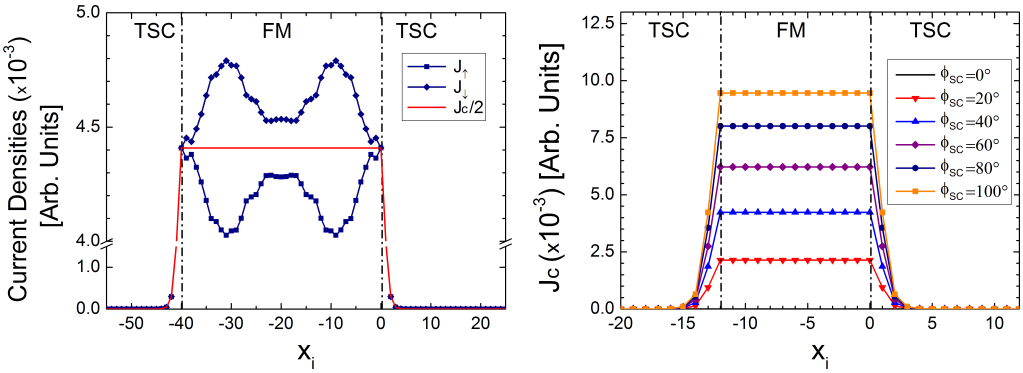

Figure 4.3: Spatial variations of the current densities $J_{\uparrow}(i)$, $J_{\downarrow}(i)$ and $J_c(i)$ in two-dimensional p_x+ip_y junctions for various configurations. Left panel: spatial variations of $J_{\uparrow}(i)$, $J_{\downarrow}(i)$ and $J_c(i)$ for a fixed SC phase $\phi_{SC} = 120°$, with $L = 40$, $h = 0.3t$ and $\theta = 40°$. Right panel: spatial variations of $J_c(i)$ for various SC phase ϕ_{SC} with a fixed magnetization orientation $\theta = 90°$, with $L = 9$ and $h = 0.3t$.

the superconducting phase $\phi_{SC} = 120°$. In this example, the magnetization is oriented in (OXZ) plane in the direction $\theta = 40°$. The ferromagnetic region is taken large enough, $L = 40$, and the magnetization small enough, $|h| = 0.3t$, in order to better observe the spatial variations of $J_{\uparrow}(i)$ and $J_{\downarrow}(i)$. It is worth keeping in mind that the spatial variations of the current densities are plotted such that the all current densities $J(i)$ evaluated at the site i represent the current flow between the site i and $i + 1$. Hence, the quantities $J(i = -40)$ and $J(i = 0)$ give the values of the current flow between two neighbours sites, one in the FM side and the other in the TSC side, on each sides of interfaces.

We first discuss the spatial variations of the current densities inside the ferromagnet region between the sites $i = -40$ and $i = 0$. As expected from the charge conservation law, the charge current $J_c(i)$ inside the ferromagnet is constant. However, the current associated to the spin up and spin down electrons, $J_{\uparrow}(i)$ and $J_{\downarrow}(i)$, are oscillating. First of all, we can observe that the oscillations are totally symmetric with respect to the value of the charge current $J(i)/2$, such that $J_{\downarrow}(i) < J(i)/2$ and $J_{\uparrow}(i) > J(i)/2$ for all sites i inside the ferromagnetic barrier. The amplitude of the oscillations, not shown here, is maximal for $\theta \sim 45°$ while it goes to zero when the magnetization is parallel or perpendicular to the $\vec{d}$-vector, i.e. with $\theta = 0°$ and $\theta = 90°$ respectively. In this case, we obtain in the ferromagnet barrier $J_{\uparrow}(i) = J_{\downarrow}(i) = J(i)/2$. It follows the behaviour of the spin-polarized pair correlations $\Delta^{\sigma\sigma}$ as we have seen in the previous chapter in Fig. 2.2. Finally, the period of the oscillations is identical to the period of oscillations of the superconducting order parameters inside the ferromagnet and has the same dependence with respect to the magnetization strength $|h|$, i.e. it increases as the exchange field decreases.
The described particularities of the spatial variations of $J_{\uparrow}(i)$ and $J_{\downarrow}(i)$ are intrinsically related to the existence of $\Delta^{\sigma\sigma}$ at the FM-TSC interfaces. Indeed, a spin up (down) electron can be reflected at the interface not only as a spin down (up) hole, but also as a spin up (down) because of additional spin flip induced by the magnetization and the

correlation functions, as we have seen for $\Delta^{\sigma\sigma}$, are still oscillating in space because of the finite momentum of the Cooper pairs. As a consequence, spin up and spin down electrons with different energies are mixing and induce a modulation of the spatial variations of $J_\uparrow(i)$ and $J_\downarrow(i)$. The effects are symmetric in the two cases but they have different directions. While the spin-flips of the spin down electrons are creating an additional positive current (from the left region to the right region) of spin up electrons, the spin-flips of spin up electrons are creating an additional negative current (from the right region to the left region) of spin down electrons.

Let us now examine the spatial variations of the charge current densities $J_c(i)$ in the superconducting regions, i.e. for the site $i < -40$ and $i > 0$, plotted in the left panel of the Fig. 4.3. As we can notice, the charge current is not conserved and instead decreases rapidly to zero in the range of few sites. This effect is due to the nature of the charge transfer across the interface. Indeed, we have seen that the charge current flow coming from a metallic region is transferred as a supercurrent carried by the Cooper pairs into superconductors, see Appendix B. Therefore, the expectation values $\langle c^\dagger_{i\pm1,\sigma} c_{i,\sigma}\rangle$ computed in Eqs. 4.12-4.14, and which represent the charge transfer across two neighbours sites, must be zero in the SC side, where only quasiparticles exist. Nevertheless, $J_c(i)$ is not exactly zero for few sites close to the interface because the proximity effects modify the energy spectrum in both FM and TSC sides and that the values of the SC order parameters are reduced at the FM-TSC interface. The wave function associated to the electrons can penetrate into the superconductor as an evanescent wave on a distance of the superconducting coherence length ξ_0. The results of the Fig. 4.3 being obtained without self-consistent evaluation of the order parameters, the penetration depth of the current density in the superconducting side is small because the SC order parameters are constant. On the other hand, after self-consistent computations we can verify that the charge current is decreasing more slowly in the superconducting region. In a similar way, the arguments apply to the spin-resolved currents $J_\uparrow(i)$ and $J_\downarrow(i)$. Additionally, we can notice that $J_\uparrow(i) = J_\downarrow(i) = J_c(i)/2$ in the superconducting region. Indeed, in this region both spin up and spin down electrons have the same energy spectrum and do not undergo spin flip.

Hence, we have seen that within the lattice model the Josephson charge current across the TFT junction J_c is obtained by evaluating the kinetic current operator Eq. 4.12 inside the ferromagnetic barrier, $J_c = J_c(i \in FM)$.

The first characteristic of Josephson effect is that the value of the charge current across the junction depends directly on the superconducting phase difference between the two superconductors. We plot in the right panel of the Fig. 4.3 the spatial variations of the charge current densities for various values of the SC phase ϕ_{SC}. The ferromagnetic barrier has a length of $L = 9$ sites while the magnetization is oriented along the y-direction ($\theta = 90°$) and has a strength $h = 0.3t$.

As expected, there is no current in the junction when the two superconductors have the same superconducting phase, i.e. $\phi_{SC} = 0$ and then current is generated for finite values of ϕ_{SC}. In this example, we see that the value of the charge current is only positive and increasing when the superconducting phase is increasing. However, we will see that the variations of J_c with respect to ϕ_{SC} depend greatly on the configuration of the system.

Our last remark concerns the variations of the spin currents densities J_s^ν, which are not yet investigate experimentally and which must be directly compared to the results obtained within the quasiclassical framework. In our case, the spin-current are obtained on the bounds between the FM and the TSCs, i.e. at sites $i = 0$ and $i = -40$ in the left panel of the Fig. 4.3. Therefore, we can see that, although $J_s^Z(i) \neq 0$ in the ferromagnet region, it is cancelled in the left and right TSC regions since $J_\uparrow(i) = J_\downarrow(i)$ at sites $i = 0$ and $i = -40$. The variations of the spin currents can be complex and depend on the orientation of the magnetization, which can induce spin filtering and spin slipping in the barrier [95]. Moreover, the presence of spin currents is also expected when the $\vec{d}$-vectors of the two superconducting regions are misaligned. Nevertheless, although directly accessible with our model using Eq. 4.22, they will not be discussed in this manuscript.

Current-Phase Relation and Evidences of the 0-π Transitions The current-phase relation of a Josephson junction is indirectly reachable by experimental measurements and is one of the main relation which characterize the Josephson junctions. It is particularly instructive to identify for which values of the phase ϕ_{SC} the Josephson current is cancelling. Although it did not have much importance for conventional singlet SC-N-SC junctions for which $J_c(\phi_{SC})$ is expected to cancel in $\phi_{SC} = 0$ and $\phi_{SC} = \pi$, it appears to be more important in the case of unconventional superconductors or noncentrosymmetric superconductors [81, 109]. Indeed, in such junctions, the shape of the current-phase relation is highly depending on the ratio between singlet and triplet order parameters and influences the phase of the junction. Ferromagnetic barriers inside the junctions influence also substantially the response of the current to the superconducting phase, which depends on the strength and the orientation of the magnetization in the FM region.
Quasiclassical studies showed that the current-phase relation of spin-triplet superconductors junctions exhibit various non trivial behaviours when the $\vec{d}$-vector on each side of the junction are misaligned [34]. However, for junctions made of two chiral TSC, i.e. with $\vec{d}$-vector along the c-axis, the current-phase relation remains quasi-sinusoidal with the variations of the magetization strength and orientation or of the length of the barrier [16,34,95]. Indeed, the relation is 2π-periodic and the current is cancelling for $\phi_{SC} = n\pi$, but can nevertheless contains higher harmonics. These results have also been found in the case of SC-FM-TSC junctions made of d_{yz}-wave superconductor [36]. Although it is not in the scope of this chapter to investigate the current-phase relation of the junction for all configurations of the system, it is interesting to discuss the current-phase relation for few examples in order to observe the main features expected for TSC-FM-TSC junctions as well as to identify the 0-π transitions. Hence, we discuss in the following, for few representative configurations, results concerning the current-phase relations and the variations of the free energy in TFT junctions where 0-π phase transitions occur.

We plot in Fig. 4.4 the current-phase relations in a TFT junction for various magnetization angles θ. The system being invariant by phase translation $\phi_{SC} = \phi_{SC} + 2\pi$, the variations of the current is 2π-periodic and therefore the results are plotted for $\phi_{SC} \in [0, 2\pi]$. In this peculiar example, the length of the barrier is $L = 12$ sites and the exchange field is fixed $h = 0.45t$. This configuration is particularly interesting since it exhibits a 0-π transition

with respect to the magnetization angle.
For $\theta = 90°$, when the magnetization is in plane, we can see that the current-phase relation shows a quasi-sinusoidal behaviour, the current being cancelled for $\phi_{SC} = n\pi$ with n integer. $J_c(\phi_{SC})$ is positive for $\phi_{SC} \in [0, \pi]$, while it is negative for $\phi_{SC} \in [\pi, 2\pi]$. The variation of the charge current with respect to the superconducting phase difference is in each point similar to a singlet SC-N-SC junction with weak metallic barrier, exhibiting higher harmonics [61]. It is closely related to the behaviour of the induced order parameters in the ferromagnet. As we have seen in Fig. 2.2, the spatial variations of the OPs at the FM-TSC interface when the magnetization is in plane are similar to the one at the N-TSC interfaces due to the breaking of the Cooper pairs entering the the metallic region.
On the other hand, when the magnetization is parallel to the $\vec{d}$-vector, the current-phase relation exhibits an opposite quasi-sinusoidal behaviour, $J_c(\phi_{SC})$ being negative for $\phi_{SC} \in [0, \pi]$ and positive for $\phi_{SC} \in [\pi, 2\pi]$.
When the magnetization rotates from an orientation $\theta = 0°$ to $\theta = 90°$, the shape of the current-phase relation is highly modified due to the subtle modifications of sinusoidal harmonics. Thus, the charge current is still cancelled at $\phi_{SC} = n\pi$, but also at $\phi_{SC} \neq 0$ or π for a magnetizations angle in the range $30° \lesssim \theta \lesssim 60°$.

We have seen that the phase of the junction ϕ_0 is defined as the value of ϕ_{SC} minimizing the free energy of the system and that the Josephson current is directly related to the variations of the energy with respect to ϕ_{SC}. Using Eq. 4.3, we can easily determine in our example Fig. 4.4 that the energy $G(\phi_{SC})$ is minimum at $\phi_{SC} = 0$ for a junction with a magnetization orientation $\theta = 0°$ whereas, for $\theta = 90°$, the minimum energy is reached at $\phi_{SC} = \pi$. They correspond to the 0- and π-states of the Josephson junction, respectively. The junction also exhibits either a 0- or π-state for the other orientations of the magnetization in the ferromagnetic barrier. Indeed, we can see that $G(\phi_{SC})$ is minimized at $\phi_{SC} = 0$ when $\theta \lesssim 50°$ and at $\phi_{SC} = \pi$ for $\theta \gtrsim 50°$. More generally, TFT junctions with both chiral spin-triplet superconductors having parallel $\vec{d}$-vector can only exhibit 0- or π-states contrary, for instance, to junctions made of non-centrosymmetric superconductors [81,109].

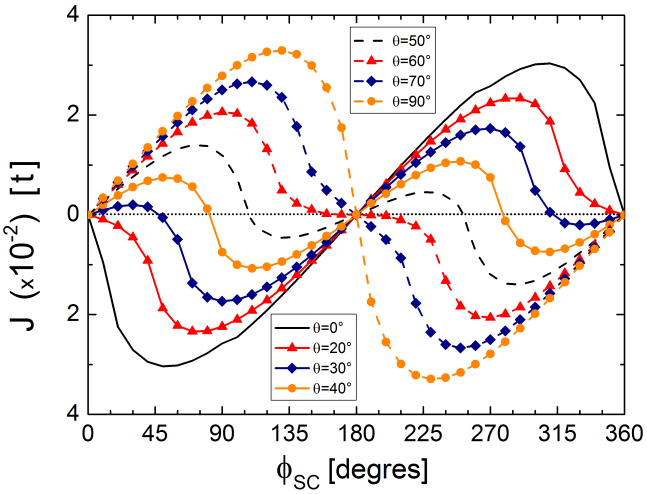

Figure 4.4: Charge current J_c across the two-dimensional p_x+ip_y junction as a function of the superconducting phase difference ϕ_{SC} for various magnetization angles θ, obtained at T=0K. J_c is 2π periodic and cancels for $\phi_{SC} = n\pi$, n being integer. The length of the barrier is $L = 12$ and strength of the exchange field is $h = 0.45t$. For this configuration, 0-π transition occurs at the critical angle $\theta_c \sim 45°$.

In a similar manner that for the study of the magnetic stability at the FM-TSC interface, we can compute the free energy for various configurations of the TFT junction using Eqs. 2.21. We plot in the left panel of the Fig. 4.5 the value of G in function of the superconducting phase difference ϕ_{SC} for various lengths of the ferromagnetic barrier L. In this example the magnetization is taken parallel to the $\vec{d}$-vectors and the strength of the exchange field is $|h| = 0.9t$.
We can see that for the configurations with $L = 6$, $L = 7$ and $L = 8$ sites, the minimum energy is obtained for $\phi_{SC} = 0$ and hence the junction is in a 0-phase. Then, a 0-π transition occurs with the length of the barrier increasing and the energy for the configurations with $L = 9$ and $L = 10$ sites is minimized for $\phi_{SC} = \pi$. Hence, for Josephson TFT junction with a magnetization parallel to the $\vec{d}$-vector, $0 - \pi$ transitions with respect to the ferromagnetic barrier length occurs in a similar way that for the SC-FM-SC Josephson junctions. This results were recently confirmed by solving the Bogoliubov-De Gennes equations with quasiclassical approximation [37].

The derivation of the free energy with respect to the superconducting phase difference ϕ_{SC} gives the variations of the charge current in the junction. We can verify that it gives for our system similar results than the calculation of the kinetic current operators and that therefore both methods are equivalent to obtain information about the critical current, the critical angle and the existence of 0-π transitions. We plot on the right panel of the Fig. 4.6 the variations of the Josephson current across the junction in function of ϕ_{SC} for various magnetization angles. It is computed using both methods, the current densities operators (solid lines) and the derivation of the free energy (points). The barrier has a length of $L = 9$ sites and the magnetization is taken $|h| = 0.3t$. The current is computed following the two methods. The results obtained from the kinetic current operators are hence in very good agreement with behaviour than the Fig. 4.4. The junction undergoes a 0-π transition with respect to the magnetization angle, being in a π-phase when $\theta = 0°$ and in a 0-phase when $\theta = 90°$. We can see that the results obtained by the derivation of the free energy are very close to the one computed with the current operators. Nevertheless, we can still observe small deviations to the latter one especially when for the cases with $\theta = 30°$ and $\theta = 60°$. They arise from the finite size of the system since the boundaries of the TSC regions also influence the total energy spectrum of the system.

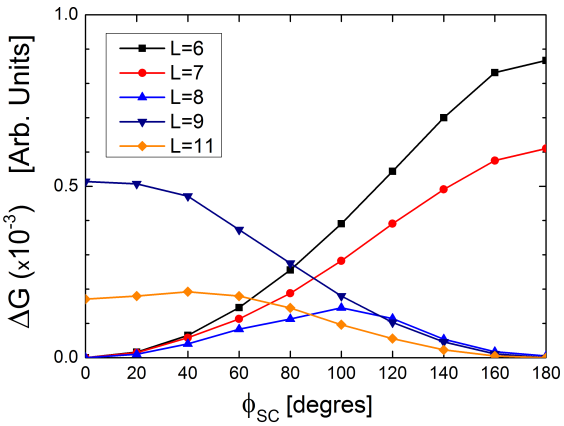

Figure 4.5: Free energy G of the two-dimensional p_x+ip_y junction as a function of ϕ_{SC} for various barrier length L. The magnetization is perpendicular to the plane ($\theta = 0$) and $|h| = 0.9t$.

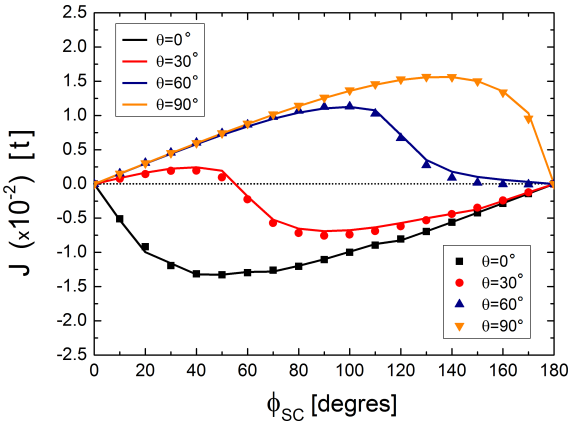

Figure 4.6: Comparison between the charge current densities computed using the kinetic current operators (solid lines) and obtained from the derivation of the free energy G (points). The length of the barrier is $L = 9$ and $|h| = 0.3t$.

Although it exists small deviations between the two methods, both methods provide very similar results concerning the characteristic of the junctions.

To conclude, let us introduce two of the main quantities related to the 0-π transitions and that we shall consider in the following to characterize the TFT junctions. There are highly relevant in the studies of the the Josephson effects since they can be directly reached by experiments [38, 61].
Firstly, the critical current is defined for a given configuration of the junction as the maximal value of the charge current with respect to the superconducting phase difference, i.e. $J_c^{max} = \mathrm{Max}\left[\mathrm{Abs}(Jc(\phi_{SC}))\right]$. We can see in Fig. 4.4 that the critical current $J^{max} \simeq 0.03t$ for both configurations, when the magnetization is in-plane ($\theta = 90°$) or perpendicular to the plane ($\theta = 0°$). Moreover, we can observe that J^{max} is decreasing when the magnetization is rotating from a direction $\theta = 0°$ to $\theta = 40°$ before to increase from $\theta = 40°$ to $\theta = 90°$, without never cancelling.
Then, for a fixed length of the ferromagnetic barrier L and a fixed strength of the magnetization $|h|$, the critical angle θ_c is defined as the angle for which the transition from the 0- to the π-phase occurs. As we have seen in Fig. 4.4, the 0-π transitions occurs when the angle of the magnetization is $40 < \theta_c < 50°$.

4.3 Phase Diagrams of Two-Dimensional TFT Junctions

We have seen in the previous section that TFT junctions, in the similar manner that the SFS one, can be partially characterized by the phase difference between the two superconductors which minimized the energy of the system, what we defined as the state of the junction. In this section, we examine the transitions between different states as a function of the length of the ferromagnetic barrier as well as the strength and the orientation of the magnetization. For this propose, we evaluate the free energy of the system for various configurations.

In a first place, we discuss the phase diagram of TFT junctions having a magnetization oriented along the z-direction, parallel to the $\vec{d}$-vectors. Then, for junctions with fixed barrier length and magnetization strength, we determine the critical angles by looking at

the transitions of states which occur when the magnetization rotates in the (xz)-plane. Finally, in order to understand the establishment of the different states for the various junctions, we highlight the relation between the spatial variations of the spin-triplet order parameters and the minimum energy of the system.

Magnetization parallel to the $\vec{d}$-vectors We are first interested to determine the state of two-dimensional TFT junction with a magnetization parallel to the $\vec{d}$-vectors. Indeed, for such configuration, we already have seen in Fig. 4.6 that, for a fixed value of the exchange field h, the junction can exhibit either a 0-phase or a π-phase according to the length of the barrier L.
We plot in the Fig. 4.7 the general phase diagram of the TFT junction with respect to the length of the ferromagnetic barrier L and the strength of the exchange field h. The results are obtained without self-consistent evaluations of the SC order parameters which are taken constant $\Delta_{ini} = 0.35t$ in the TSC sides. Moreover, the hopping terms between the FM and TSC layers are all equal to unity inside the three regions, i.e. $t_{perp} = t_{FM} = t_{TSC} = 1.0$. The results show, as for quasiclassical analysis, that more generally the junction can only exhibit a 0-state (blue areas) or a π-state (green areas) according to the configuration of the barrier.

Let us analyse the main particularities of the phase transitions between the 0- and π-state domains that we can observe in Fig. 4.7 and focus firstly on configurations with small values of the exchange field, $h < 1.5t$.
At $h = 0t$, i.e. for metallic barrier, the junction is in 0-state. Then, as we have seen in Fig. 4.6, the junction exhibits 0-π transitions with respect to the length of the ferromagnetic barrier for fixed values of the exchange field. For clarity in the discussion, we define the distance $L_p \sim L_p(h)$ as the distance between two 0-π transitions for a fixed value of the exchange field h and for the magnetization oriented parallel to the $\vec{d}$-vectors. Hence, we can observe with the phase diagram that the transitions are $2L_p$-periodic and that L_p depends on the strength of the magnetization. Indeed, the domains of 0- and π-states,

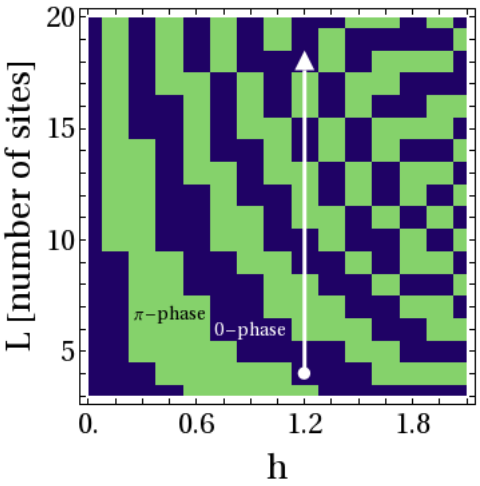

Figure 4.7: Phase diagram representing the 0- and π-state domains of two-dimensional TFT junction as a function of the strength of the exchange field h and the length of the FM barrier L. The 0-phase is represented by the green area while the π-phase by the blue area. The white arrow denotes the periodic 0-π transitions with respect to the FM barrier length for a fixed value of the exchange field $h = 1.20t$. This configuration is described in more details in Fig. 4.8 to discuss the critical angles.

and thus L_p, decrease when then strength of the exchange field is increasing.
Moreover, 0-π transitions also exist with respect to the exchange field for fixed values of the barrier's length L. In a similar way that for the exchange field, we can see that, for a fixed value of L, the 0- and π-state domains decrease when the exchange field increases. However, although the discrete character of the phase diagram makes difficult the precise analysis of the different domains in most of the cases, we can see that the 0-π transitions do occur periodically for small value of L.
Hence, both effects make the phase diagram to exhibit a special pattern where we can distinguish a regular succession of 0 and π-states domains when both the length of the barrier and the exchange field are increasing. This pattern is characteristic of ferromagnetic Josephson junctions and confirm qualitatively the recent results obtained for TFT junctions by means of the quasiclassical formalism [37].

It is worth discussing about the discrete aspect of the phase diagram, especially concerning the transitions of states with respect to the length of the barrier for large magnetization. Indeed, as it is explained in more details in the next section, the oscillations between the two states of the junctions are related to the spatial oscillations of the superconductor order parameters induced in the ferromagnetic barrier. Hence, the period L_p characteristic of the 0-π transitions becomes smaller than two atomic sites for large values of h. Therefore, for $h > 1.5t$, the transitions of states appearing on the length $L < 1$ cannot be correctly pictured in the phase diagram. Within our model, we should consider bigger atomic cells to be able to obtain a clear oscillation behaviour of the phase transitions at large values of the exchange field. Nevertheless, Fig. 4.7 confirms qualitatively the general results about the TFT junctions for small values of the exchange field and then the possibility for the model to describe the Josephson junctions.

Finally, we can note that the phase diagram does not depend qualitatively on the value of the order parameter Δ_{ini}, which should in any case remains small enough compare to the spectrum width $8t$, nor on the value of the hopping term t_{perp}. However, in both cases the values of the critical current J_c are modified and, accordingly to the previous paragraph, the state domains are quantitatively modified especially at large values of the exchange field because of the discrete character of the model. Additionally, although we find that the phase diagram depends quantitatively on the symmetry of the order parameters in the superconductors, i.e. p_x+ip_y , p_x or p_y , we can still observe (not shown here) a very similar behaviour for the three cases [37].

Critical Angle in TFT Josephson Junctions For Josephson junctions made of spin-singlet superconductors, the 0-π phase diagram does not depend on the magnetization orientation. However, as we have seen in the last chapter, the $\vec{d}$-vector plays an important role in the FM-TSC interface since it interacts, through the spin of the electrons and so the angular momentum of the spin-triplet Cooper pairs, with the magnetization of the ferromagnetic barrier. Such interactions are also occurring in the TFT junctions and are responsible for changing the conditions to obtain the phase transitions. One of the main predictions ensued from this effect is that TFT junctions can exhibit 0-π transitions with respect to the magnetization orientation, as we have shown in Fig. 4.4. As we shall

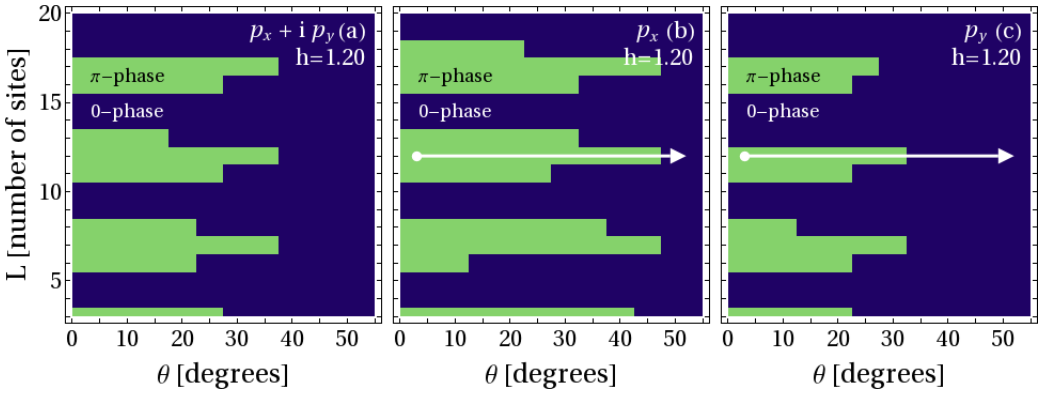

Figure 4.8: Phase diagrams representing the 0- and π- states domains of two-dimensional TFT junction as a function of the barrier length L and the magnetization angle θ. There are obtained for p_x junction (a), p_y junction (b) and p_x+ip_y junction (c) with a fixed magnetization strength $h = 1.20t$. The 0-phase is represented by the green area while the π-phase by the blue area. The white arrow denotes the 0-π transitions with respect to the magnetization angle for a fixed value of the barrier length $L = 12$.

see, the critical angles for which the transitions of states occur depends on the configuration of the junction as well as the nature of the spin triplet pairing in the superconductors.

In order to picture the 0-π transitions when the magnetization is rotating, we plot in Fig. 4.8 the phase diagrams of the p_x+ip_y (a), p_x (b) and p_y (c) junctions with respect to the length of the barrier L and the magnetization angle θ. The configuration of the junction is similar to the Fig. 4.7 and the results are obtained for a fixed value of the magnetization $h = 1.2t$.

We first consider the phase diagram obtained for the p_x+ip_y junction (a). Firstly, when the magnetization is parallel to the $\vec{d}$-vectors ($\theta = 0°$), we can notice that phase transitions occur periodically with respect to the length of the barrier. The state domains are similar to the one observed for $h = 1.2t$ in Fig. 4.7, depicted by the white arrow. Then, all configurations with π-state undergo a phase transitions while the magnetization is rotating in the (xz)-plane and, at larger values of θ, all configurations exhibit a 0-state. As we can see, the phase transitions depends highly on the length of the ferromagnetic barrier and, in our analysis, the critical angles vary between $\theta_c = 15°$ and $\theta_c = 40°$. Except for very small value of L, the maximal critical angle obtained for the π-state domains is $\theta_c^{max} \sim 37°$.

Similar qualitative behaviours are also obtained for the p_x (b) and p_y (c) junctions. Nevertheless, we can notice that the maximal value of the critical angle θ_c^{max} is larger for the p_x junctions while it is smaller for the p_y junctions. Once again, as we shall see in the last paragraph, this difference can be understood by looking at the superconductors order parameters.

The critical angles of the junction depends also on the value of the magnetization inside the

ferromagnetic barrier. To emphasize this point, we consider now the phase diagrams of the p_x+ip_y junction with respect to L and h, similarly to the Fig. 4.7, for three magnetization angles $\theta = 20°$, $\theta = 30°$ and $\theta = 40°$. The three phase diagrams are respectively plotted in the left (a), center (b) and right (d) panels of the Fig. 4.9.

It is then interesting to discuss the maximal value of the critical angle θ_c^{max} for fixed values of the exchange field h independently to the length of the barrier. The general trend shows that the larger is the magnetization, the smaller is the maximal critical angle. Indeed, we can estimate that for $h > 1.8t$, the maximal critical angle is inferior to 20° while for $0.9t < h < 1.8t$, it is ranged from 20° to 30°. Finally, we can see that $\theta_c^{max} > 40°$ in the cases where $h < 0.8t$. Nevertheless, we found in any case that the TFT junctions only exhibit a 0-state when $\theta > 50°$ (not shown here).

It is then interesting to compare our results to the results obtained with the quasiclassical formalism [37]. Concerning the qualitative aspect, the results obtained for the 0-π phase diagram as a function of the length of the ferromagnetic barrier L and the exchange field h are very similar. The same variations can be observed between the 0- and π-state domains. Moreover, the 0-π transitions with respect to L for a fixed value of h are periodic in both cases and the period L_p is decreasing when the strength of the magnetization is enhanced. Concerning the critical angles, the results are still in good agreement with the quasiclassical analysis. It is found in both cases that $\theta_c^{max}(p_x) > \theta_c^{max}(p_y)$ and that $\theta_c^{max}(p_x + ip_y)$, at small and intermediate values of h, ranges from 30° to 40°.

On the other hand, our results show strong deviation from the tunnelling formalism with infinitely thin barrier [32, 35]. Indeed, at T=0K, it was found that the TFT junctions made of chiral spin-triplet superconductor do not exhibit π-state for small magnetization. On the other hand, the π-state has been found to exist at larger value of the magnetization and that the critical angle θ_c was increasing while the magnetization is increasing. This behaviour is therefore different from our analysis since we find that the junctions with small exchange field show the largest critical angles.

Finally, it is worth mentioning that the results obtained for the tunnelling junctions are strongly dependent on the temperature. The highest values of the critical current are obtained at $T \ll T_c$. Moreover, the maximal critical angle possible in this model is $\theta_c = 45°$, which does not disagree with our results.

To conclude, we mention that all the results concerning the 0-π transitions and the critical angles discussed in this section were obtained for a magnetization lying in the (xz)-plane, i.e. for a magnetization always parallel to the interface. However, in the case of two-dimensional junction, the x- and y-directions are not equivalent. Indeed, in TFT junctions, differences are expected to be found especially in the variations of the spin current where the x-direction acts as a spin-flip barrier while the y-direction acts as a spin-filter [95]. However, it is worth mentioning that we find within our model (not shown here) that the 0-π phase diagrams do not depend on the direction of the magnetization in plane. Thus, the results presented in Figs. 4.8 and 4.9 are identical for a magnetization lying in the (xy)-plane.

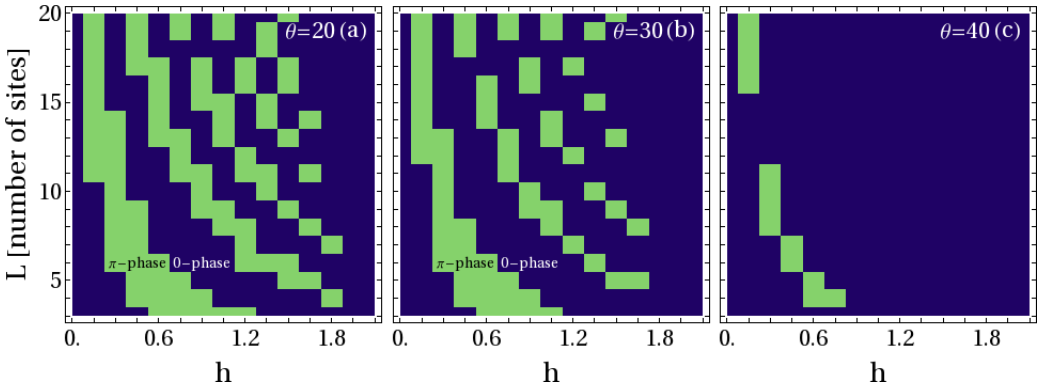

Figure 4.9: Phase diagrams representing the 0- and π- states domains of two-dimensional p_x+ip_y junctions as a function of the barrier length L and the magnetization strength h. There are obtained for three magnetization orientations, $\theta = 20°$ (a), $\theta = 30°$ (b) and $\theta = 40°$ (c), respectively, with a fixed magnetization strength $h = 1.20t$. The 0-phase is represented in blue area while the π-phase is the green area.

4.4 Understanding of the Phase Transitions

In order to get a better understanding on the phase transitions in TFT junctions, it is necessary to look in more details at the processes leading to the transfer of charges in the Josephson junctions. Using results from the BTK formalism [28, 103], we first discuss the instructive case of a well known one-dimensional junction made of singlet superconductors and a metallic barrier. Obviously, the behaviour of the Josephson current in the case of a ferromagnetic barrier is more complex and has to be numerically computed as it was done within the quasiclassical formalism. Nevertheless, we will see in some extend that the phase transitions can be simply related to the spatial variations of the superconductors order parameters and therefore to the configuration of the ferromagnetic barrier.

Phase Transitions and Spin Triplet Order Parameters As already mentioned in section 1.5, Andreev reflections occur at the interface between a metal and a superconductor. During this processes, an incoming electron (hole) from the normal region is reflected as a hole (electrons) at the interface while a Cooper pair is created in the superconductor, see Appendix A. Due to the momentum conservation during the Andreev reflection, the momentum of the reflected particle is slightly different than the momentum of the incoming particle. For the reflection of an electron at the one-dimensional N-SC interface, the difference is

$$k_e - k_h = \frac{2v_F\hbar}{\epsilon} \tag{4.23}$$

where v_F is the Fermi velocity and $\epsilon = E - \mu$ with E being the energy of the incoming particle [140]. Therefore, the phase difference between the electrons and holes forming

the induced Cooper pair in the normal metal, given by the correlation function $\langle c^{\dagger}_{k_e} c^{\dagger}_{k_h} \rangle$, is increasing with the distance to the interface. Then, we already mentioned that the electrons in the metallic barrier have quantified energies, in a similar manner than in a quantum well, associated to the ABSs. Solving the BTK equations in one-dimensional junction with conventional spin-singlet superconductor, it can be shown [140] that the energy of n quantized level of the ABSs must satisfy

$$-2\mathrm{arcos}\left[\frac{\epsilon_{\mathrm{n}}^{\pm}}{\Delta_0}\right] \pm (\phi_{\mathrm{L}} - \phi_{\mathrm{R}}) + (\mathrm{k_e}(\epsilon_{\mathrm{n}}^{\pm}) - \mathrm{k_h}(\epsilon_{\mathrm{n}}^{\pm}))\mathrm{L} = 0, \tag{4.24}$$

where $k_{e(h)}$ is the wave vector of the electron (hole), $\epsilon^{\pm}$ are the energies of the ABS, Δ is the superconducting gap, ϕ_A is the phase of the order parameters in the superconductor A and L is the size of the barrier. The + and − energies denote two different ABSs which carry current in opposite directions and which cannot be larger than the superconducting gap Δ. Therefore, we can see that the possible energy levels inside the metallic barrier depends on both, the phase difference between the two superconductors $\phi_{SC} = \phi_L - \phi_R$ and the phase difference between the electrons and the holes which depends on the length of the barrier L. The analytical solutions of Eq. 4.24 for an infinite small barrier $L = 0$, representing the tunnel junction, are then

$$\epsilon^{+} = \epsilon^{-} = \pm\Delta\mathrm{cos}(\frac{\phi_{\mathrm{SC}}}{2}). \tag{4.25}$$

Thus, the derivative of the energy with respect to the phase difference gives rise to a sinusoidal behaviour of the current-phase relation, as we have seen in Eq. 4.1. Moreover, we can see that minimum energy is obtained for $\phi_{SC} = 0$ and therefore that the SNS junction exhibit a 0-state in a tunnel limit. This can also be numerically verified for any value of the barrier's length L.

We now consider the case of a Josephson junctions with a finite magnetic barrier. In this configuration, although the Andreev reflections are still occurring at the FM-SC interfaces, Eq. 4.24 is not valid any longer. Complex conditions on the ABS energies can be found using the Bogoliubov-De Gennes equations, as for the TFT junctions [76], which then depend on the orientation and the strength of the magnetization. However, we can already appreciate the mechanism leading to the 0-π transitions by looking at the induced pairing amplitudes inside the barrier. We attempt in the following to explain with a basic picture why π-states occur in ferromagnetic Josephson junction, although the complete picture need much refined model. We have seen that, due to the finite momentum of the Cooper pairs, the pairing amplitudes are oscillating in the ferromagnetic region. In the region where they are negative, the wave functions of electrons and holes have, in average[1], an additional π phase. In the case of SFS junctions and TFT junctions with a magnetization parallel to the $\vec{d}$-vectors, the conditions on the ABS energies are hence modified since the Cooper pairs can acquire an additional phase and the Eq. 4.24 can be written, as first approximation, as

[1]The oscillations of the induced pairing amplitudes are indeed obtained after integrations over all momenta, see Chapter 1.

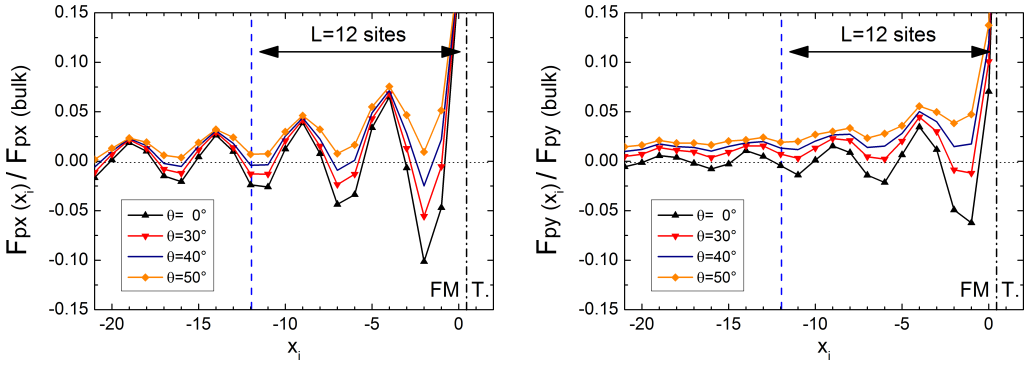

Figure 4.10: Spatial variations of the superconducting order parameters Δ_{px} (left panel) and Δ_{py} (right panel) in the FM side of a two-dimensional FM-TSC interface for various magnetization orientations. They are scaled to their respective bulk values. The black dashed line denotes the FM-TSC interface while the blue dashed line is drawn only for the discussion of the TFT junction and depict a second TSC such that the ferromagnetic barrier has a size $L = 12$ sites. The results are obtained for $h = 1.2t$. Oscillations with change of sign occur for configurations with $\theta \leq 40°$ for Δ_{px}, but only for $\theta < 30°$ for Δ_{py}.

$$-2\arccos\left[\frac{\epsilon_{\mathrm{n}}^{\pm}}{\Delta}\right] \pm (\phi_{\mathrm{L}} - \phi_{\mathrm{R}} + \phi'(\xi_{\mathrm{F}})) + (\mathrm{k_e}(\epsilon_{\mathrm{n}}^{\pm}) - \mathrm{k_h}(\epsilon_{\mathrm{n}}^{\pm}))\mathrm{L} = 0, \tag{4.26}$$

where $\phi'(\xi_F)$ is the additional phase representing the induced order parameters oscillations and which can only take 0 and π values. It depends on the strength of the magnetization h and is periodic, as the oscillations of the pairing amplitude, with respect to the length of the barrier. Hence, by analogy with the Eq. 4.24, the phase of the junction is given by $\phi_{SC} = \phi_L - \phi_R$ with the new condition $\phi_{SC} + \phi' = 0$. Therefore, if the two superconducting regions are separated by a distance L such that the induced pairing amplitudes are negative, i.e. $\Delta_s(L) < 0$ in the case of SFS junctions, the additional phase is none zero, $\phi' = \pi$, and thus the junction exhibits a $\phi_{SC} = \pi$ state.

The above discussion is valid for chiral TFT Josephson junctions. When the magnetization is oriented parallel to the $\vec{d}$-vectors, the physical pictures is similar to the SFS junctions. In this case, the induced spin triplet order parameters are periodically oscillating in the ferromagnetic barrier and hence lead to 0-π transitions with respect to the barrier length. On the other hand, we have seen in the previous chapters that the oscillations were cancelling when the magnetization is rotating from a perpendicular to a in-plane direction, leading the induced correlations functions to be only positive once the magnetization is in plane. The Eq. 4.26 still explains basically the presence of 0- and π-states for all magnetization orientations but then, the induced pairing amplitudes being not periodically negative, the complete 0-π phase diagram is modified.
The relation between the phase transitions and the spatial variations of the order parameters can be observed in the results obtained with the lattice model. We plot in Fig. 4.10 the spatial variations of the spin-triplet order parameters for FM-TSC interfaces with p_x (left

panel) and p_y (right panel) symmetries. The results are shown for various magnetization orientations while the strength of the exchange field is fixed $h = 1.20t$. The 0-π transitions related to this configuration are shown in Fig. 4.8 for both p_x and p_y junctions. Before to comment on the correspondence between the induced pairing amplitudes and the phase diagram, it is worth mentioning one again that the analysis can only be approximative since more complex proximity effects can also alter the value of the order parameters, especially close to the FM-TSC interfaces. Moreover, the presence of a second superconductor, in order to achieve the TSC-FM-TSC junction, modify the induced correlations inside the barrier. Nevertheless, such analysis remains relevant to understand the 0-π transitions as a function of the magnetization orientation.

We first consider the spatial variations of the induced order parameters for $\theta = 0°$, i.e. when the magnetization is parallel to the $\vec{d}$-vectors. In this configuration, we can see that the spin triplet correlation functions are oscillating in the ferromagnet due to the action of the pair breaking magnetic field. This situation is very similar to what we already have seen for the SFS junctions or for three-dimensional TFT junctions, see Chapter 2. Nonetheless, in contrast to the latter case, both components F_{p_x} and F_{p_y} are not exactly similar due to the translation symmetry which is broken only in the x-direction [44]. Still, for both junctions the period of the oscillations ξ_F is 5 and 6 sites long and hence the induced order parameters alternate between positive and negative values every 2 or 3 sites. According to the above discussion, these oscillations are associated to 0-π transitions as a function of the barrier's length. This can be indeed seen in Fig. 4.8 where, for $\theta = 0°$, the phase transitions occur every 2 or 3 lattice sites.

When the magnetization is rotating, the amplitude of the oscillations decreases because the magnetic configuration is only partially pair-breaking. Then, we can observe in Fig. 4.10 that it exists for both interfaces limit angles, $\theta^0_{p_x}$ and $\theta^0_{p_y}$, for which the order parameters do not change sign any longer and remain positive for every site, although they are still oscillating.

A precise comparison between the results obtained with the phase diagrams and the induced pairing amplitudes shows that they quantitatively differ since, as mentioned previously, the presence of a second superconductors modify the overall order parameters. As an example, we can analyse the case of a ferromagnetic barrier long of $L = 12$ sites. For clarity, the configuration is depicted in Fig. 4.10 by the dashed blue lines and by the white arrows in Fig. 4.8 (b) and (c). In this configuration, we expect from the results of the phase diagrams the junction to exhibit critical angles $\theta_c \sim 45°$ and $\theta_c \sim 32°$ for p_x and p_y junctions, respectively. By analysis the oscillations of the pairing amplitudes, we can see that we expect $\theta^0_{p_x} \sim 40°$, in good agreement with the results of the phase diagram while, on the other hand, $\theta^0_{p_y}$ would be expected close to 0°.

Nevertheless, a qualitative analysis shows good agreement between both kind of results. Indeed, according to the oscillations of the pairing amplitudes of the p_x junction, the limit angle $\theta^0_{p_x}$ ranges from $\theta = 40°$ to $\theta = 50°$ while $\theta^0_{p_y}$ is mainly situated between $\theta = 0°$ and $\theta = 30°$ for the p_y junction. Thus, we expect as a general trend that the angles $\theta^0_{p_x}$ and $\theta^0_{p_y}$ for which the 0-π transitions occur to be different and, moreover, that $\theta^0_{p_x} > \theta^0_{p_y}$. It corresponds indeed with good agreement to the behaviours obtained for θ_c^{max} in Fig. 4.8, also numerically observed using the quasiclassical BdG equations [37]. Therefore, we can

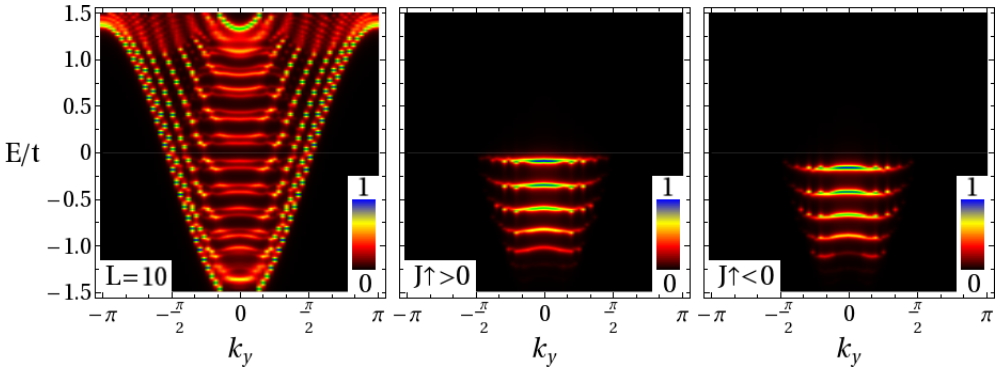

Figure 4.11: Momentum- and energy-resolved spectral functions A(i,k$_y$)(ω)(left panel) and current density J$_\uparrow$(i,k$_y$)(ω)(middle right panels) computed on a site i_x in the metallic barrier of a two-dimensional TSC-N-TSC junction. The length of the metallic barrier is $L = 10$.

see that the oscillations of the induced pairing amplitudes in the ferromagnet capture the essential of the effects leading to the 0-π transitions.

Andreev Bound States It is interesting, although not necessary for our current analysis, to look at the energy spectrum inside the junction in order to understand what are the mechanisms responsible for the charge transport inside the metallic barrier. We shall focus to describe such mechanisms in the case of a spin-triplet junctions with metallic barrier, but the main discussion still hold for a ferromagnetic barrier.

As we have mentioned, electrons and holes from a normal metal can undergo Andreev reflections at the interface of a superconductor. More precisely, the SC can be seen as a peculiar potential wall for which exists certain probabilities for an incident electron (hole), depending on its energy and the potential barrier at the interface, to be normally reflected as an electron (hole), to be Andreev reflected as a hole (electron) or to be transmitted, over a certain distance, in the superconductor, see Appendix B. When the metal is surrounded by two superconductors, that means by two effective walls, the system is analogue to a quantum well. Following basic laws from quantum mechanics, the energies of electrons and holes are hence quantized inside the metallic well of the junction, see Eq. 4.24, and the standing waves associated to these quantized energies are the so-called Andreev Bound States. Hence, the energies generally depend on the parameters of the barrier and the number of energy inside the barrier on the length of the barrier.

We plot in the left panel of the Fig. 4.11 the energy spectrum at one site inside the barrier of a TSC-N-TSC junction. As expected, we can clearly distinguish the different levels of energy of the ABSs inside the barrier which, naturally, can only exist for a certain range of the momentum k_y. Then, we plot in the middle and right panels of the Fig. 4.11 the absolute value of the momentum- and energy-resolved current density $|J_\uparrow(\omega, k_y)|$, on the site corresponding to the energy spectrum, and are similar for spin down electrons. The

general current density is made of two contributions, a charge flow going from the left side to the right side of the junction, represented by $J_\uparrow > 0$, and a charge flow going in opposite direction, with $J_\uparrow < 0$. Both contributions are shown respectively in the middle and the right panels.
It is interesting to notice that the positive and negative charge flows are not carried by the same ABSs. Indeed, as we have mentioned for the Eq. 4.24, they correspond to the two solutions ϵ^+ and ϵ^-.
Positive and negative charge flows are cancelling when the difference of phase between the two superconductors ϕ_{SC} is zero, although $\epsilon^+ \neq \epsilon^-$, but it is not the case for junction with $\phi_{SC} \neq 0$. Indeed, as we know from the quasiclassical studies of the Bogoliubov-De Gennes equations, the energies of the ABSs vary as a function of ϕ_{SC} and leads to a non zero Josephson charge current across the junction. It is worth mentioning that this picture, thermodynamically correct, holds only for zero or very small applied difference of potential dV between the two electrons. Otherwise, non equilibrium processes is modifying the energies and the overall response of the charge current.
In the case of ferromagnetic barriers, the energies of the ABSs are additionally shifted according to the strength of the exchange field. These subtle modifications, as a function of the value of the magnetization as well as the length of the barrier, lead to the 0-π transitions that we observe in the phase diagram. Being very small and present all over the energy spectrum, they cannot be directly analysed in our model as it is done in the quasiclassical studies. However, they modify to total free energy that we can directly analyse.
To conclude, the results in Fig. 4.11 show that the Josephson charge current is still directly associated to the energies of the ABSs and that they are, therefore, also directly linked to the state of the junction. We can also see that, within this model, the energies of the ABSs are highly dependent on the momenta and the energies of the quasiparticles as well as the parameters of the system.

4.5 Refinements of the TFT Lattice Model

So far, the results concerning the 0-π transitions were obtained for two-dimensional TFT junctions without self-consistent computation of the spin-triplet order parameters in the TSC regions. Using constant bulk values for the superconducting order parameters in both TSC regions, we found the existence of 0-π-transitions with respect to the length of the ferromagnetic barrier as well as the orientation of the magnetization and we have seen that there were depending on the strength of the exchange field.
The lattice model allows us to go beyond this initial analysis by evaluating the spin-triplet order parameters self-consistently in the junction. Moreover, as discussed in the previous chapter, we expect the TFT Josephson junctions to be first experimentally built layers by layers along the c-axis and therefore it is necessary to obtain results for a three-dimensional configurations of the system. In this section, we addressed both cases separately and found that the general results concerning the phase diagrams are preserved.
More interestingly, we finally study the case of a two-dimensional TFT junctions with a spin active interface. Indeed, as we have seen in the previous chapter, we found various stable magnetization configuration at the FM-TSC interface depending to the strength of

the magnetization. Hence, we discuss here the 0-π phase digram for configurations with misaligned magnetization at the interface.

Self-Consistent Evaluation of the Order Parameters In a first place, we discuss the results concerning the variations of the phase of the two-dimensional spin-triplet Josephson junctions by computing self-consistently the order parameters in the system. More precisely, using the same configuration than previously, the procedure consists in solving first the Bogoliubov-De Gennes equations for a TFT junction without additional superconducting phase. Then, once the convergence of the pairing amplitudes achieved, we solve once again the BdG equations after adding a superconducting phase ϕ_{SC} on the left side of the junction. Finally, as previously, we determine the value of the superconducting phase difference ϕ_{SC} which minimizes the free energy of the system. It is worth noticing that using this method, although the order parameters are not constant in the superconducting regions, the free energy is only given by the spectrum energy since the condensation energy E_{cond} is independent to a complex phase added to the superconducting order parameters, see Eq. 2.22.
Not surprisingly, we found that the Josephson junction can only exhibits one the of two 0- and π- states, depending on the barrier length L and the exchange field h. The right panel of the Fig. 4.12 shows the complete 0-π phase diagram as a function of L and h for a magnetization parallel to the $\vec{d}$-vector, i.e. $\theta = 0°$. We reproduce in the left panel the phase diagram previously obtained with constant order parameters in the superconducting regions.

We can mainly observe in Fig. 4.12 that the self-consistent computations do not qualitatively modify the general trend of the 0-π transitions and that, in this case as well, the transitions of states are not well defined for larger values of the exchange field $h > 1.5t$. Quantitatively, the junction undergoes, for fixed values of h, quasi-periodic 0-π transitions

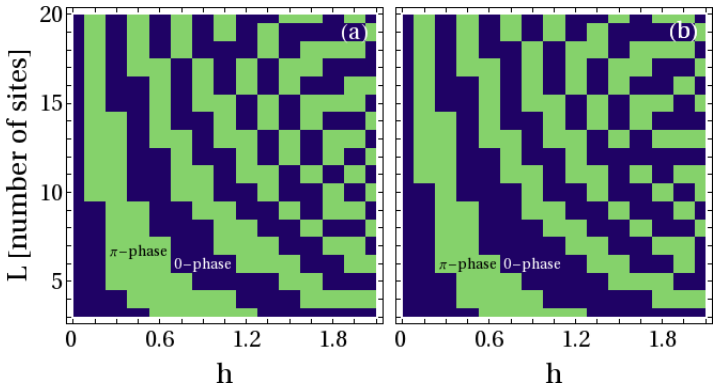

Figure 4.12: Comparison of the 0-π phase diagrams computed with (right panel) and without (left panel, see Fig. 4.7) self-consistent evaluation of the spin-triplet order parameters. The 0-phase is represented by the blue area while the π-phase by the green area.

with respect to the barrier's length. For each values of h, the periods L_p are comparable to the one obtained without self-consistency, although the transitions do generally take place for different values of the parameters. It seems legitimate to refer to the 0-π transitions as being quasi-periodic as a function of L since we can observe, especially for smaller values of h, that the 0- and π-state domains can have small difference in size. A detailed analysis show that, compare to the previous results, the 0-state domains tend to expend while the π-state domains are slightly decreasing. The importance of this effect can be minimized by the fact that the discrete character of the system cannot provide an accurate value of L, for which the transitions occur. However, this effect is still directly linked to the induced pairing amplitude in the ferromagnetic barrier. Indeed, the periods of the oscillations of the correlations functions are not modified by the self-consistent computations since they only depend, in analogy with the FFLO states [58, 86], on the values of the exchange field and on the Fermi velocity inside the barrier, see Eq. 2.20, which are unmodified. On the other hand, the amplitudes of the bulk order parameters inside the superconductors are modified as well as the overlap of the induced pairing amplitudes coming from the left and right superconducting regions.

0-π Transitions in three-dimensional TFT Junctions The results discussed in this paragraph are obtained by evaluating the free energy of three-dimensional junctions using the model defined in Chapter 2. As in the previous cases, it is equivalent to the study of the current-phase relation by evaluating the charge current densities. Except further mention, the chemical potential is fixed at $\mu = -1.6t$ and the in-plane hopping term are equal in both directions $t_x = t_y = 1.0t$. Moreover, the pairing coupling between nearest neighbours is fixed $V^{\sigma\sigma'} = -2.0t$ and is non zero only between electrons belonging to the same superconducting plane.
In our framework, the three-dimensional TFT junctions differ from the two-dimensional one by the fact that the system is now invariant by rotation of the (xy)-plane and, thus, both components of the spin-triplet order parameter, Δ_{p_x} and Δ_{p_y}, are equivalent. We have emphasized this point in the last chapter while looking at the spatial variations of the pairing amplitudes, see Fig. 2.2. Despite this difference, both components of the induced correlation functions in the ferromagnetic barrier obey to a similar behaviour for the two- and three-dimensional interfaces in the sense that, depending on the orientation of the magnetization, they can oscillate in the ferromagnet and that the period of oscillation depends only on the strength of the magnetization and on the Fermi velocity. As previously, the order parameters can hence become periodically negative in the ferromagnetic barrier and we therefore expect the three-dimensional Josephson junction to still exhibit transitions of states.

We are first interested to analyse the phase diagram of the three-dimensional p_x+ip_y junction with respect to the strength of the magnetization and the length of the ferromagnetic barrier, for a complete pair-breaking magnetic configuration, i.e. with the magnetization being orientated parallel to the $\vec{d}$-vectors ($\theta = 0°$).
Our first results are obtained for a junction having the out-of-plane hopping term equal to the in plane one, i.e. $t_z = t_x = t_y = 1.0t$. The phase diagram is shown in the left panel of the Fig. 4.13. In this case, we can see that the junctions exhibits only 0- and π-phases

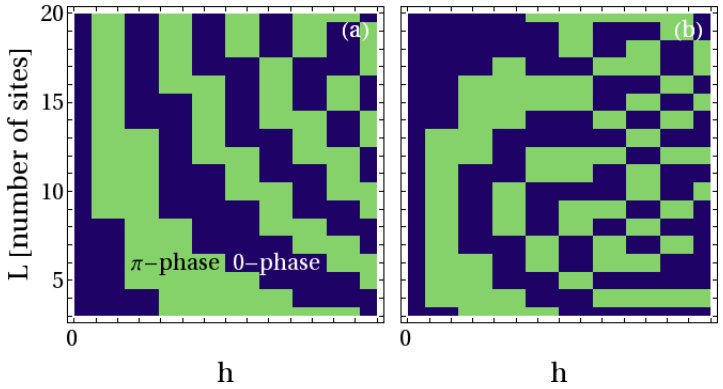

Figure 4.13: Comparison of the 0-π phase diagrams, as a function of the magnetization strength h and the ferromagnetic barrier length L, obtained for a three-dimensional p_x+ip_y junction with an out-of-plane hopping term $t_z = 1.0t$ (left panel) and $t_z = 0.5t$ (right panel). The 0-phase is represented by the blue area while the π-phase by the green area.

and that the 0-π transitions occur with respect to the barrier's length L as well as the exchange field h. As for the two-dimensional case, the transitions of states are periodic with respect of L and the period L_p are similar in both cases.
On the other hand, we are also interested of the phase diagrams for junction with smaller values of the out-of-plane hopping term t_z. Indeed, as we argued in the previous chapters, in the case where we consider experimental interfaces or junctions to be build with the spin-triplet superconductors Sr_2RuO_4 [11], we expect the value of t_z to be smaller between each plane compare to the in-plane values. Theoretically, we have seen that, for fixed values of the exchange field and the barrier's length, the period of the oscillations of the correlation functions in the ferromagnetic region is decreasing as the hopping term between layers is decreasing, see Fig. 2.4. Hence, it results for the TFT Josephson junction that the distance L_p between each transitions of states with respect to the L should be smaller than in the case $t_z = 1.0t$. This is verified in the right panel of the Fig. 4.13, where the phase diagram is obtained for an out-of-plane hopping term $t_z = 0.5t$. The phase diagram still exhibits a succession of 0 and π phases with respect to the barrier's length and the magnetization strength. For fixed values of h, the 0-π transitions are still periodic with respect to L but we can see, for small values of $h < 0.6t$, that the 0- and π-state domains are smaller compare to the system with $t_z = 1.0t$, as expected from the period of oscillations of induced pairing amplitudes in the ferromagnetic barrier. And since the period of oscillations L_p is getting smaller, the domains of states obtained for $h > 0.6t$ become too small to be completely relevant.

The second important point to consider concerns the values of the critical angle for various configurations of the three-dimensional TFT junctions. For this purpose, we aim to study the phase diagrams of the junction with respect to the length of the barrier L and the magnetization angle θ, for an out-of-plane hopping term $t_z = 1.0t$. The results are shown

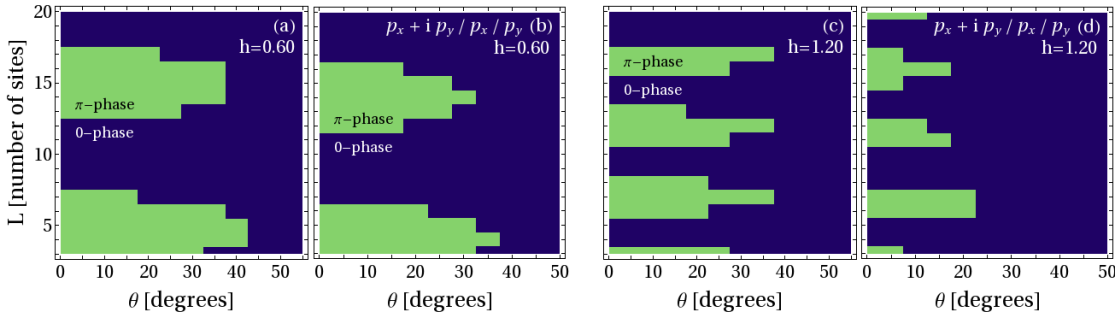

Figure 4.14: Comparison of phase diagrams representing the 0- and π-state domains obtained for two- (a-c) and three-dimensional (b-d) TFT junctions as a function of the the barrier length L and the magnetization angle θ. They are obtained for small, (a) and (b) panels, and intermediate, (c) and (d), strength of the exchange field, $h = 0.6t$ and $h = 1.2t$, respectively. The 0-phase is represented by the blue area while the π-phase by the green area.

in Fig. 4.14 for two fixed and representative exchange fields $h = 0.6t$ (b) and $h = 1.2t$ (d). For comparison, we additionally plot the results obtained for the two-dimensional p_x+ip_y junctions for the two same values of the exchange field, in Fig. 4.14 (a) and (b) respectively. As first comment, it is worth mentioning that the phase diagrams obtained for the three-dimensional junctions are identical for the three different symmetries of the superconducting order parameters, i.e. p_x, p_y and p_x+ip_y , which is explained as we have mentioned by the symmetry of the system. It contrasts therefore with the two-dimensional case where the three symmetries give different critical angles for a same configuration of the junction, see our previous results in Fig. 4.8 or the quasiclassical one [37].
As a general trend, we can observe that, as for the two-dimensional TFT junctions, the value of the maximal critical angles θ_c^{max} of each π-state domains are decreasing as the exchange field is increasing. Indeed, while there are found between $\theta_c = 30°$ and $\theta_c = 40°$ for $h = 0.6t$, there are for $h = 1.2t$ generally situated between $\theta_c = 15°$ and $\theta_c = 25°$.
However, we found that, for fixed value of the exchange field h, the maximal critical angles are generally smaller for three-dimensional junction than for the two-dimensional one. It is particularly noticeable for higher values of h where the difference can reach 20° between both cases, for a fixed value of L. This behaviour can be understood by looking at the 0-π phase diagrams of the three different junctions p_x, p_y and p_x+ip_y in Fig. 4.8. Indeed, we can see in the latter that θ_c^{max} was found to be smaller for p_y junctions than for p_x junction and that the p_x+ip_y junction had critical angles between both cases. Yet, the spatial variations of the p_x and p_y order parameters at the three-dimensional FM-TSC interface, which are both similar, are very similar to the one obtained for the p_y junction in two-dimension since, in each case, the translation symmetry is respected. Therefore, we expect θ_c^{max} to be smaller in three-dimensional junction than in two-dimensional one.

We conclude that, qualitatively, the main results concerning the phase diagrams in TFT junctions hold in the case of three-dimensional junctions and that the 0-π phase transitions

are still driven by the spatial variations of the superconducting order parameters. Hence, for a fixed value of the exchange field and for a magnetization parallel to the $\vec{d}$-vector, the 0- and π-state domains become smaller as the hopping term between layers is decreasing. Finally, we expect the p_x, p_y and p_x+ip_y junctions to exhibit similar phase diagrams, in contrast with the two-dimensional junctions, and to have smaller maximal critical angles.

Influence of a Spin Active Interface In this paragraph we study the phase diagram of TFT junctions including a more complex magnetic configuration at the FM-TSC interfaces. More precisely, we focus on the analysis of two-dimensional p_x+ip_y ferromagnetic Josephson junctions without self-consistent evaluation of the order parameters. As for the model used in Chapter 3, the spin active interfaces are represented by two sites, one at each FM-TSC interfaces, for which the orientation of the magnetization is independent to the bulk magnetization in the ferromagnetic barrier. We denote, as in Chapter 3, ρ as being the relative angle between the exchange field of the spin-active interfaces and the $\vec{d}$-vector.

We have seen in the last two chapters that the spin-triplet superconductor has a direct influence on the magnetic profile at the FM-TSC interface and that the most favourable magnetic configuration was obtained for a magnetization lying in plane, see Fig. 2.5. On the other hand, the results are more complex when the magnetization at the interface is independent to the orientation of the magnetization in the bulk. Indeed, we found that depending on the strength of the exchange field, the proximity effects due to the spin-triplet superconductor lead to a magnetic profile having parallel or antiparallel configuration at the FM-TSC interface, see phase diagrams of the Fig. 3.5. However, in the frame of our current analysis, the possibility to have in-plane antiparallel magnetic configurations in experimental junctions has no influence on our results concerning the TFT junctions. Indeed, both in-plane parallel or antiparallel configurations are not pair-breaking and lead

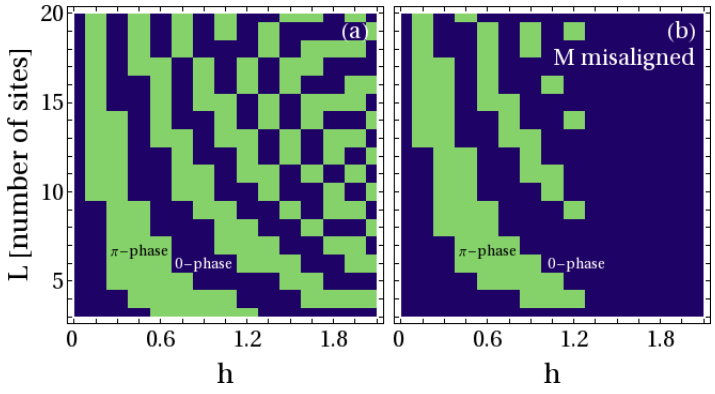

Figure 4.15: Compairosn of the 0-π phase diagrams obtained for a two-dimensional TFT junctions with (b) and without (a) spin-active interface. The magnetization located at the interface is oriented along the y-direction, i.e. $\theta = 90°$. The 0-phase is represented by the blue area while the π-phase by the green area.

only to a 0-state, independently to the length of the barrier or the strength of the exchange field, in a very similar way to a SNS junction.
On the other hand, we have seen that, by fixing the direction of the magnetization in the ferromagnetic bulk, the spin-triplet superconductor can favours various orientations of the magnetization at the FM-TSC interface, depending for instance on the strength of the magnetization, see Fig. 3.4(f). The most interesting magnetic configuration inside the ferromagnetic barrier to study is when the bulk magnetization is parallel to the $\vec{d}$-vectors, fully pair breaking, and for which we obtained the 0-π phase diagrams, see Fig. 4.7. Then, we analysis in the following the state of the TFT junctions in the special case when the magnetizations at both FM-TSC interfaces are lying plane, i.e. $\theta = 0°$. Although this configuration have been found to minimize the energy at the interface only for small values of the exchange field, we also study both small and intermediate strength of h.

Using the magnetic configuration described above, we plot on the right panel (b) of the Fig. 4.15 the phase diagram of the junction with respect to the strength of the exchange field and the length of the barrier plotted. For comparison, we reproduce on the left panel (a) the phase diagram found for TFT junction without spin active interface.
The results show that, as previously, the Josephson junction exhibits only 0- and π-states. At intermediate values of h, the spin active interfaces modify the phase diagram and the junction can only be in a 0-state. For smaller strength of the exchange field, the 0-π phase diagram shows however the same trend in both cases with periodic alternation of 0- and π-state domains.
By looking more in details, we can observe that for small fixed values of h, $h < 0.6t$, the size of the 0- and π-state domains are identical with or without spin active interface. On the other hand, when h is increasing, the spin active interfaces modify the phase diagram and we can see that for fixed value $h > 0.6t$, the 0-state domains are mostly present while the π-state domains are suppressed. Once again this proximity effect is related to the

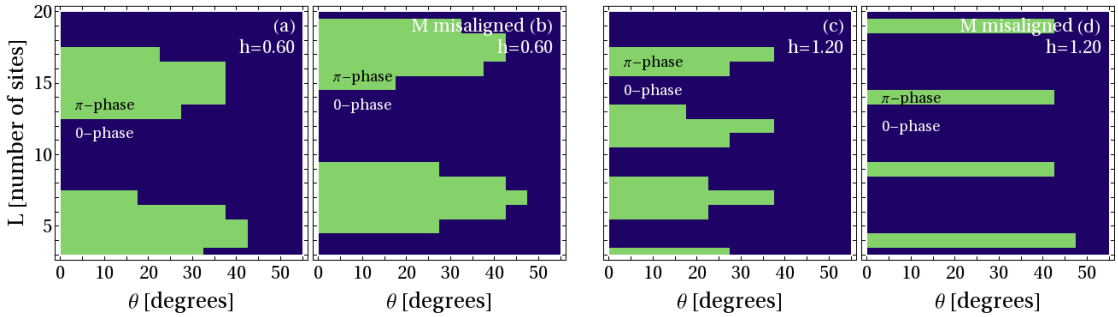

Figure 4.16: Comparison of the 0-π phase diagrams, as a function of the the barrier length L and the magnetization angle θ, of two-dimensional TFT junctions with (b-d) and without (a-b) spin active interfaces. They are obtained for small (a-b) and intermediate (c-d) strength of the exchange field, $h = 0.6t$ and $h = 1.2t$, respectively. The 0-phase is represented by the blue area while the π-phase by the green area.

induced pairing amplitudes in the ferromagnetic barrier which are shifted because of the spin active interfaces and which then do not become periodically negative, in a similar way to the junctions with partially pair-breaking configuration, see Fig. 4.9. They also lead to a general shift of all 0- and π-state domains of the phase diagram as we can see in our results.
Although the spin active interfaces modify the π-state domains, especially for intermediate values of the exchange field, they have only a limited influence on the critical angle. We show, in the (b) and (d) panels of the Fig. 4.16, the phase diagram of two-dimensional p_x+ip_y junctions as a function of the bulk magnetization angle θ and the ferromagnetic barrier length L. The magnetization at the interface is still lying in plane, i.e. $\theta = 0°$. For comparison, we reproduce in (a) and (c) panels the phase diagram for junction without spin active interface. For small values of the exchange field, we observe a shift of the π-states domains, as explained previously due to the two additional non pair-breaking layers at each FM-TSC interfaces. For larger values of h, the π-states domains are shrink and exist only for specific values of L. Nevertheless, the maximal critical currents θ_c^{max} for each π-state domains remain unaffected.

4.6 The Critical Current as an Experimental Evidence

As we emphasized at the beginning of this chapter, the two main methods that we can use to experimentally probe the Josephson junctions at equilibrium are the measurement, through an additional electronic device, of the current-phase relations and the measurement of the critical current by injection of a current across the junction. The latter, experimentally more accessible, has been successfully employed on Josephson junctions with singlet superconductors and made possible the observation of 0-π phase transitions in ferromagnetic junctions with respect to the temperature as well as the barrier length [32,35,37]. In order to predict the observation of the 0-π phase transitions in the case of TFT junctions, we analyse in the following the variations of the critical current J_c as a function of the ferromagnetic barrier length for various values of the exchange field and orientations of the magnetization. We focus particularly on Josephson junctions with spin active interface which show significant differences compare to junctions with homogeneous magnetic barrier.

To understand how the phase transitions can be deduced from the critical current, let us discuss the current-phase relations that we have described in the two first sections.
In the simple case of tunnelling junctions, the relation between the Josephson charge current and the phase of the junction is sinusoidal. Therefore, having a junction in a 0- or π-state, by considering the free energy, is equivalent to have a critical current J_c, defined in Eq. 4.1, which is positive or negative, respectively. In the case where the junction is inclined to undergo phase transitions as a function of an external parameter, for instance the temperature or the magnetization strength, the critical current is expected to vary from positive to negative values. Although positive and negative critical currents cannot be dissociated, it is possible to observe experimentally the cancellation, or the minima in the configurations with higher-harmonics, of the current by tuning external parameters. The the observation of such a feature is associated to a phase transition of the junction.

On the other hand, the current-phase relation in the case of junctions made of weak links or good conductors contain higher harmonics due to the multiple Andreev reflections. In these cases, we can see from Fig. 4.4 that the critical current does not necessary cancelled during the 0-π transitions. However, the phase transition is still associated to a non-zero minimum of the critical current, what has been observed in several SC-FM-SC experiments [29, 38, 102].

Finally, it is worth mentioning that, in a general context, the observation of minima of the critical current does no insure the existence of a phase transitions. Indeed, in the case of junctions showing a complex current-phase relations including high harmonics, the critical current can vary non monotonously even without the presence of phase transitions. This has been especially predicted in junctions made of NCS which can exhibit a more general φ -state [81, 109]. Therefore, in this kind of measurements, the theoretical prediction of the evolution of the phase of the junction is absolutely determinant in the interpretation of the results.
In our system made of pure chiral spin-triplet superconductors, we already have found that the junctions can only exhibit a 0-state or a π-state, depending on the configuration of the magnetic barrier. Moreover, we know for which values of the barrier length or the exchange field we expect 0-π phase transitions to occur, see Fig. 4.7. According to these results, we are then in position to determine how the variations of the critical charge current are associated to the phase transitions.

Critical Current in TFT Junctions We are first interested to study the critical current in the two-dimensional p_x+ip_y Josephson junction as presented in section 4.3 and for which we obtained the 0-π phase diagrams with respect to the length of the ferromagnetic barrier as well as the strength and orientation of the magnetization. The parameters of the model are similar to the one used in the previous sections. To obtain the critical current for each configuration, we first compute in each case the Josephson charge current for a finite number of superconducting phase difference ϕ_{SC} in order to obtain the current-phase relation. The difference between two superconducting phases is taken to be 10°, similarly to the Fig. 4.4, which allow us to have a good estimation of the maximal value of $|J(\phi_{SC})|$.
We plot the variations of the critical current as a function of the barrier length in Fig. 4.17 for three different magnetization angles. The results are shown for various strengths of the exchange field, which are taken small enough in order to have 0- and π-states domains large enough and well defined.

One of the main results of the Fig. 4.17 is that, for all strengths of the exchange field, the variations of the critical current as a function of the length of the barrier depend on the angle between the magnetization and the $\vec{d}$-vectors. Indeed, we can see that J_c monotonously decreases when the magnetization is perpendicular to the $\vec{d}$-vectors, i.e. for the case $\theta = 90°$, while it oscillates for the $\theta = 0°$ and $\theta = 60°$ orientations. In the former case, the magnetization is not pair-breaking while it is partially and totally pair-breaking for $\theta = 60°$ and $\theta = 0°$, respectively. In this respect, the TFT junctions differ notably from singlet Josephson junctions. Indeed, in SC-N-SC junctions, correlated pairs are induced

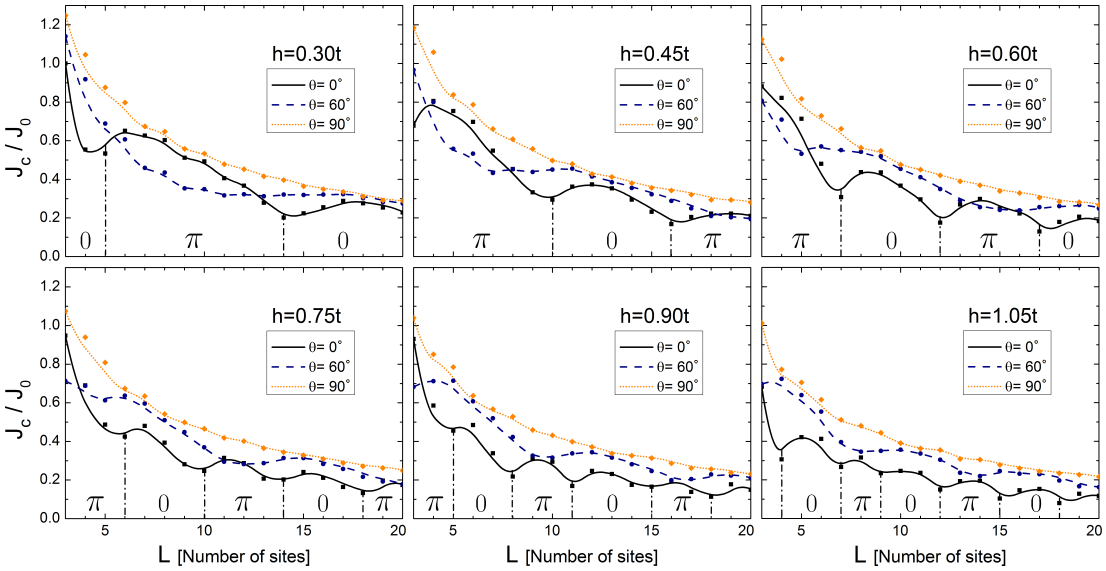

Figure 4.17: Critical charge current J_c^{max} in a two-dimensional p_x+ip_y TFT junction as a function of the length of the FM barrier L. We plot for each case an additional spline function as a visual guide in order to highlight minimum and maximum values of the critical current[1]. The results are plotted for three magnetization angles $\theta = 0°$ (solid lines), $\theta = 60°$ (dashed lines) and $\theta = 90$ (dotted lines), for various strength of the exchange field h. All the results are scaled with the value of the critical current J_0 obtained for the configuration with $h = 0.30t$, $\theta = 0°$ and $L = 3$. The vertical dashed-dotted lines depict the local minima of J_c corresponding to phase transitions.

in the metallic barrier without any spin mixing and the critical current is monotonously decreasing when L is increasing. On the other hand, in SC-FM-SC junctions the ferromagnetic barrier is totally pair-breaking independently of the magnetization orientation and, thus, the critical current is oscillating. This particular aspect of TFT junctions was first analysed in a recent work using quasiclassical formalism [37] which is qualitatively recover within our lattice model. Finally, we can notice that, for a fixed value of L, the critical current is always maximized in the configuration where the magnetization is perpendicular to the $\vec{d}$-vectors, $\theta = 90°$.

Let us now inspect in more details the oscillations of the critical current. By comparing the variations of J_c when the magnetization is perpendicular to the $\vec{d}$-vectors, i.e. $\theta = 0°$, with the phase diagram of the junction in Fig. 4.7, we find that the minima of the current are all associated to 0-π phase transitions. The latter are depicted by vertical dashed-dotted

[1] It is important to keep in mind that the lattice being discrete, the continuous approximated functions have no physical meaning. They only give us the possibility to make simpler the comparison with results obtained within continuous models [37] and, in this respect, only the presence of oscillations in the critical current are meaningful.

lines in Fig. 4.17. Then, as expected from the phase diagram of the junction, we find the distance between two minima of the critical current is decreasing as the magnetization is increasing. For $h \geqslant 0.60t$, we confirm that the phase transitions appear periodically as a function of the barrier's length and that the period of oscillations decreases when L increases. Therefore, although not sharp because of the presence of higher harmonics in the current-phase relations, the minima are in this particular case a signature of the phases transitions between 0-states and π-states and can be tuned accordingly to the strength of the exchange field as in SC-FM-SC junctions.

On the other hand, we know that, for all values of the exchange field, the TFT junctions only exhibit a 0-state behaviour when the angle of the magnetization is superior to $\theta_{limit} = 55°$. Therefore, it appears that the oscillations of the critical current for the configuration $\theta = 60°$ do not correspond to any phase transition. As general features, we can still observe for this orientation of the magnetization that the broad minima appear periodically, see especially the case $h = 1.05t$, that the period of oscillations is smaller than the orientation $\theta = 0°$ and that it also decreases as the length of the barrier increases. These behaviours are qualitatively in good agreement with the quasiclassical results.

Finally, we can observe that the critical current tends to decrease as the length of the barrier is increasing. This feature, common to all magnetization configurations, is due to the fact that the variations of the energies of the ABSs depend directly on L. This can be seen for instance by considering the solutions of the Eqs. 4.24 and 4.26 for large size of the barrier. It can be shown that these variations are inversely proportional to L [94,140].

Finally, it is interesting to have a more quantitative discussion on the experimental results that we can expect for clean TFT interfaces. In a total pair-breaking configuration, with a constant magnetization parallel to the $\vec{d}$-vector, we predict exactly the same behaviour than for SSC-FM-SSC Josephson junctions. Indeed, in both cases the oscillating behaviour of $J_c(L)$ in function of the barrier length L is only due to the exchange field in the ferromagnet. Therefore, in both cases the oscillations are present and the distance between two minima depends only at T=0K on the strength of the magnetization as well as the Fermi velocity. The characteristic lengths for the oscillations are $\xi_{FM} \sim v_F/h$ in clean limit and $\xi_{FM} \sim \sqrt{D/h}$ in the diffusive limit [38], where D is the diffusion coefficient which becomes smaller as the density of impurities is increasing. Few experimental realisations of SC-FM-SC junctions have been achieved last decade using weak, such as Cu_xNi1_x or Pd_xNi_{1-x}, or stronger ferromagnets, such as Ni and Co [38,110]. According to the reported parameters for all ferromagnets, ξ_{FM} is generally found to be in the range of 0.5-3nm while the oscillations of the critical current measured in various experiments as a function of the barrier length, which depends also on the temperature and on the density of magnetic impurities, are on the order of 1-10nm. The ferromagnetic $SrRuO_3$ is generally admitted to be a strong itinerant ferromagnet with a magnetization induced by Stoner mechanism, similar to nickel or cobalt ferromagnets and with a Fermi velocity $v_F \sim 1 \cdot 10^5$ m.s^{-1} of the same order of magnitude [82], although recent measurements have been showing deviation from this model (see for instance Ref. [118]). Therefore, the period of oscillations of $J_c(L)$ should be expected to have the same order of magnitude, although it is still dependent on the density of impurities or of the misalignment of the magnetization in the ferromagnetic bulk or at the interface. On the other hand, if the magnetization is perpendicular to the

$\vec{d}$-vector, no oscillations should be observed in the variations of $J_c(L)$, as in SSC-N-SSC or TSC-N-TSC junctions.

Spin Active Interfaces : Anomaly in the Critical Current We demonstrated that considering a three-dimensional junctions or a self-consistent computation of the spin-triplet order parameters do not modify the general phase diagram of the TFT junctions. This is mainly due to the stability of the oscillations of the induced superconducting order parameters inside the ferromagnetic barrier. On the other hand, TFT junctions with spin active interface showed a modification of the phase diagram, in particular for intermediate values of the exchange field. It is therefore interesting to observe how the presence of spin active interfaces, i.e. misaligned magnetization at the FM-TSC interfaces, influence the behaviour of the critical current.

Similarly to the Fig. 4.17, we plot in Fig. 4.18 the variations of the critical current as a function of the ferromagnetic barrier length L. We use the same parameters to describe the junction but additional spin active interfaces, represented by a misalignment of the magnetization, are present at the FM-TSC interfaces. Hence, the results for the cases $\theta = 90°$ are exactly the same than the one obtained in the Fig. 4.17 since in both cases the magnetization lies in plane for all the sites inside the ferromagnetic barrier.
Moreover, the general trend is conserved for all configurations. The critical current is decreasing as the length of the barrier is increasing and oscillations appear when the configuration is partially ($\theta = 60°$) or totally ($\theta = 0°$) pair-breaking.

By comparing the results of the critical current for the maximal pair-breaking configuration, i.e. when the magnetization is parallel to the $\vec{d}$-vectors, with the phase diagram Fig. 4.15, we are able to confirm that all minima of J_c correspond to 0-π phase transitions. We can see that the variations of the critical current differ distinctly from the results obtain without spin active interfaces. We can distinguish two different regimes depending on the strength of the exchange field.
For magetization strength $h < 0.60t$, the oscillations do not show clear deviation from the results obtained without spin-active interface. The minima of J_c correspond to the phases transitions whereas maxima decreases monotonously with L. Moreover, following the phase diagrams, the phase transitions are shift of two or three sites as a function of the barrier's length.
On the other hand, the variations of the critical current for intermediate values of the exchange field show a strong divergence compare to the previous results. Indeed, as expected from the phase diagram, the critical current is oscillating as a function of the barrier's length but the oscillations are not periodic any longer since the 0-state domains become larger that the π-state domains. Additionally, we can notice that the maximum values of J_c, located between two minima, are not decreasing monotonously, feature which was not predictable from the analysis of the phase diagrams. The variations of the critical current is thus made of a succession of small and high maxima which make it particularly distinguishable of the previous case.

Let us now discuss the case where the magnetization in the ferromagnetic barrier has

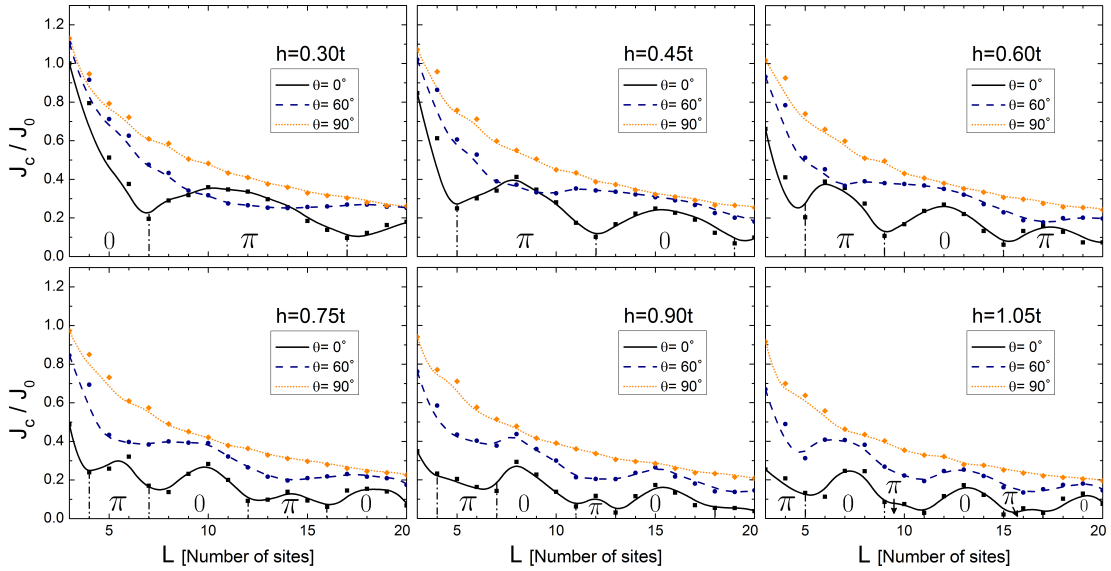

Figure 4.18: Critical charge current J_c^{max} as a function of the length of the FM barrier L in a two-dimensional p_x+ip_y TFT junctions with an additional spin active interfaces. The magnetization at both spin-active interfaces is aligned along the y-direction, i.e. $\theta = 90°$. The results are scaled similarly than Fig. 4.17.

a configuration which is not totally pair-breaking but which still allows the junction to exhibit a π-state depending on the length of the barrier and the strength of the exchange field. Indeed, by referring to the results in Fig. 4.9 (b), we have seen that for intermediate orientations of the magnetization, for instance with $\theta = 30°$, the 0-π phase diagram were similar to the phase diagram for junction with spin active interface. Especially for intermediate values of the exchange field, we observed in both cases that for a fixed value h the 0-state domains were becoming broader while the π-state domains were smaller as a function of the barrier's length. It is then necessary to see how the critical current is evolving for such configuration.

We plot in Fig. 4.19 the variations of the critical current as a function of the barrier length for three intermediate values of the exchange field and for three different orientation of the magnetization. Two of them, $\theta = 0°$ and $\theta = 60°$ are similar to the previous cases and we plot additionally the case $\theta = 30°$. The results are shown for junction with and without spin active interface at the bottom and top row, respectively.

The main observation concerns the variations of J_c for junctions without spin active interface (top row) and with a magnetization oriented with $\theta = 30°$ (red dotted lines). Indeed, in this configuration we can observe that the critical currents show very similar features than the junction with spin active interface in the configuration $\theta = 90°$ (black solid lines in the bottom row). The variations of J_c exhibit broad minima and small maxima.

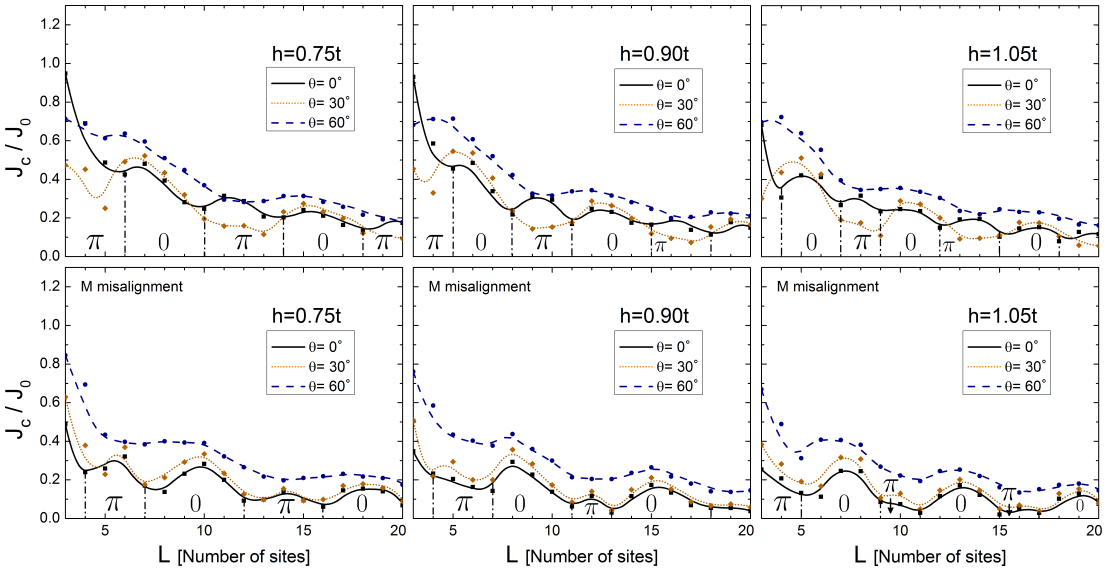

Figure 4.19: Comparison of the critical charge current J_c^{max} as a function of the length of the FM barrier L in two-dimensional p_x+ip_y TFT junctions with (bottom row) and without (top row) spin active interfaces. They are obtained for for intermediate values of the exchange field $h \in [0.75t, 1.05t]$. The results are scaled similarly than Fig. 4.17.

We can conclude from the results that it becomes experimentally very likely to observe in p_x+ip_y junctions anomalies in the variations of the critical current for intermediate values of the exchange field. There, the critical current does not exhibit perfect oscillations as a function of the barrier's length as it is the case normally for SC-FM-SC junctions. These anomalies can be observed for perfect TFT junctions, i.e. without spin active interface, when the magnetization configuration is not totally pair-breaking but still allows the existence of π-states ($0° < \theta < 40°$) and for junctions with spin active interfaces with a partial or total pair-breaking configuration ($\theta < 30°$).

Finally, it is interesting to address the question on whether it is experimentally possible, through the analysis of the critical current, to determine whether a spin-triplet Josephson junction undergoes spin active interfaces or not. In a more general way, it is equivalent to determine, by the observation of the critical current, whether there is a misalignment of the magnetization inside the ferromagnetic barrier. The differences between both cases are tiny and the answer to the former question can be found by analysing the Fig. 4.19.

First of all, we predict with our model that there are no experimentally distinguishable differences between the two cases at very small values of the exchange field. We found for both cases regular oscillations of the critical current when the magnetization has a pair-breaking component and no oscillation when it has none.

On the other hand, two main differences arise for intermediate values of h. Indeed, when

the magnetization is parallel to the $\vec{d}$-vectors for $h > 0.60t$, the critical current across the junction with spin active interface does not oscillate periodically as a function of the barrier's length. Therefore, the non observation of periodic oscillations for any orientation of the magnetization in an experiment would correspond to the existence of a magnetization misalignment inside the p_x+ip_y junction.

Moreover, we can observe a clear difference between both cases when the magnetization is rotating from an orientation corresponding to $\theta = 0°$ to $\theta = 60°$. Junctions with spin active interfaces show a very constant modification of the overall variations of the critical current. For a fixed value of L, J_c increases mostly monotonously as the magnetization is rotating and the maxima as well as the minima are still preserved. Oppositely, the variations of J_c for junctions without spin active interface are highly modified. We can observe that some maxima are preserved while some other become minima. Therefore, we expect that the preservation of maxima and minima in the overall variations of the critical current when the magnetization is rotating to be the sign of the existence of a misalignment of the magnetization inside the barrier.

It is worth mentioning that our analysis can only partially answer this problematic since we only consider one misaligned layer, at both FM-TSC interfaces, for which the magnetizations lie only in plane. However, according the our analysis on the energy, we know that this magnetic configuration is the most favourable at the vicinity of the chiral spin-triplet superconductor and, therefore, our results provide already a good evaluation of misalignment effects inside TFT junctions.

It is finally important to comment on the general decrease of J_c as a function of the barrier's length L. We know from the studies of the Eilenberger and Usadel equations that the suppression of J_c as the size of the barrier increases depends directly on the temperature of the junctions. Hence, it is expected to be exponentially reduced to zero for finite temperature close to T_c, while it decreases as a power low in the case of very low temperature [38]. Moreover, additional scattering events in the barrier are also expected to cause a faster reduction of J_c, what was observed in SC-FM-SC junctions and very well described by the Usadel equations [102].

In the limit of a clean metallic barrier at T=0K, as in our current analysis, the critical current decreases slowly and is not substantially suppressed as long as the length of the barrier is of the order of magnitude of the coherence length. Hence, the study of the junctions at finite temperature should show a much stronger reduction of J_c as a function of L. Although the previous quasiclassical study does not show such a reduction, it nevertheless predicts a 0-π transition to occur as a function of the temperature. Therefore, it is not clear whether the anomalies in the variations of J_c, due to the spin active interface, can survive at finite temperature. Moreover, we can mention that the case of TFT junctions in dirty limit with magnetic scattering inside the barrier would be interesting to consider since it was shown in SC-FM-SC junctions that the characteristic lengths of the oscillations can be greatly modified by such a disorder [102].

4.7 Conclusion

We have studied in this Chapter the Josephson charge current in clean TSC-FM-TSC junction at equilibrium and at T=0K, by using a mean field tight-binding model and solving the Bogoliubov-De Gennes equations on the lattice. Compare to the previous Chapters, an additional phase ϕ_{SC} was added to the spin-triplet order parameters in one superconducting region to induce a direct Josephson current across the ferromagnetic barrier. The latter was numerically evaluated from the kinetical current operators on each bond of the lattice, obtained from the charge continuity equations, and by derivation of the free energy G. We shown that both methods give very similar results for the current-phase relation. We were especially interested to examine the state of the p_x+ip_y TFT junction for various barrier's length and magnetic configurations. Indeed, the later is believed to exhibit, in a similar fashion than SC-FM-SC junctions made of spin-singlet superconductors, 0- and π-states which correspond to the difference of superconducting phase ϕ_{SC} which minimizes the energy of the junction.

Our first results were obtained for a two-dimensional TFT junctions without self-consistent evaluation of the order parameters. We first computed the phase diagram of the junction for a magnetization parallel to the $\vec{d}$-vectors as a function of the strength of the exchange field and the length of the barrier. We observed that the junctions exhibits 0- and π-state domains and that transitions of state is periodic, for a fixed strength of the magnetization, with respect to the barrier's length. Hence, it exhibits in this configuration a similar behaviour than for junctions made of spin-singlet superconductors.

On the other hand, we found that the junctions can only be in a 0-state when the magnetization is perpendicular to the plane. We have seen that this feature was explained by the spatial variations of the spin-triplet order parameters in the ferromagnetic region. Indeed, the junction can only exhibit a π-state if the induced pairing amplitudes, not only oscillate, but also become negative in the ferromagnet. Therefore, in good agreement with the spatial variations of the order parameters observed in Chapter 1, we found that the maximal critical angle for which a transition occurs between the 0-state to the π-state is about $\theta_c = 40°$. We emphasized that these results are in very good agreement with the recent quasiclassical computations of the phase diagram [37] but differ substantially from the tunnelling junctions [32, 35] .

We have then extended our results using a more sophisticated numerical analysis by, first, computing the phase diagram with self-consistent solution of the Bogoliubov-De Gennes equations and, then, for three-dimensional junction. In both cases, we showed that the phase diagram is also made of 0- and π-domains and exhibit qualitatively the same behaviour than for simple two-dimensional TFT junction. On the other hand, we found that the θ_c is smaller in the three-dimensional case, especially for intermediate and strong ferromagnets, similarly than for the two-dimensional p_y junction. Indeed, for three-dimensional FM-TSC interface, both Δ_{px} and Δ_{py} order parameters are analogue to Δ_{py} in two-dimensional case since they do not undergo any breaking of the translation symmetry, in contrast to Δ_{px} in two-dimensional junctions.

A drastic modification of the phase diagram has been observed for junction with spin-active interfaces. This effect is especially interesting since we have shown in Chapter 3 that the TSC tends to orientate spontaneously the magnetization perpendicular to the $\vec{d}$-vector,

i.e. in the plane. Since an in-plane magnetization is pair-breaking for the Cooper pairs, we found that the spin-active interfaces tend generally to suppress the π-state domains. This effect has been found particularly distinctive for intermediate and strong ferromagnets. Surprisingly, we also found that the critical angle can be increased in such configuration, showing a more subtle relation between the spatial variations of the order parameters and the state of the junctions.
In the last part of this Chapter, the critical current $J_c(L)$ was computed as a function of the ferromagnetic barrier length L for various magnetic configurations. It is of first interest since it is one of the easiest way to experimentally probe the state of Josephson junctions. If the magnetization is totally pair-breaking, i.e. parallel to the $\vec{d}$-vector, $J_c(L)$ is oscillating and decreasing when the length of the barrier increases. The local minima of the $J_c(L)$ appear periodically, as the oscillations of the order parameters, and denote the 0-π phase transitions which occur with respect to the barrier length. Therefore, the oscillations of $J_c(L)$ is an indirect proof of the different states of the junction. When the magnetization is perpendicular to the $\vec{d}$-vector, $J_c(L)$ is only monotonously decreasing as in SC-N-SC of TSC-N-TSC junctions. This behaviour is qualitatively similar to the quasiclassical results although, due to the presence of high-order harmonics in the current-phase relation, $J_c(L)$ is never cancelled. Finally, we predict the variations of $J_c(L)$ to be drastically modified in presence of spin-active interfaces, especially for intermediate strengths of the ferromagnet. In these cases, the 0-π phase transitions do not appear periodically any longer and, therefore, the minima of $J_c(L)$ can be shifted such that nonmonotonic oscillations are induced.

Chapter 5

Edge Currents at the Two-Dimensional Ferromagnet - Helical Spin-Triplet Superconductor Interfaces

Helical spin triplet superconductors, in contrast to the chiral one, exhibit at their boundaries one or more pairs of spin up and spin down gapless edge states having opposite dispersion [67, 105, 106]. This behaviour is analogue to the Quantum Spin Hall Effect (QSHE) although realised without external magnetic field and, in contrast to Integer Quantum Hall Effect (IQHE), spin up and spin down electrons are counter-propagating at the edges of the superconducting metal leading to the existence of a dissipationless spin current. Hence, due to the rich physical properties of the edge states, the study of helical TSC interfaced to itinerant ferromagnet has relevant implications for getting deeper insight into the nature of topological states and on the appealing possibility to achieve new spintronic devices based on the coupling between magnetism and superconductivity.
Most of the recent theoretical investigation on heterostructures focused on chiral TSC, due to its possible realisation in Sr_2RuO_4 [96, 97], and noncentrosymmetric superconductors (NCS), triggered by the discovery in the beginning of the 2000s of superconducting materials with a lack of inversion symmetry such as the heavy fermion CePtSi [22, 23]. In these systems, the lack of inversion center induces a spin-orbit coupling which can lead to superconducting states made of a mixture of spin-singlet and spin-triplet order parameters [62]. Hence, it has be shown that the conductance or the density of states in metallic [70, 89, 90, 133] or ferromagnetic [8, 9, 135] junctions could be used to identify more precisely the superconducting states, i.e. the symmetry of the order parameters as well as the degree of mixture between singlet and triplet Cooper pairs. The analysis have also been extended to Josephson junctions made of one or two NCS [19, 81, 109]. The studies of NCS are worth to mentioned because the possible spin-triplet state achieved in these systems is an helical state with a in-plane $\vec{d}$-vector and, thus, they contain generally results for pure helical TSC. On the other hand, the realisation of such state in materials is still uncertain and, therefore, exhausting studies of proximity effects in heterostructures including pure helical TSC are still limited. Recently, however, new theoretical predictions for promising candidate materials have been made. Hence, this peculiar superconducting state is believed to be possibly achieved especially in Cu-doped Bi_2 [57, 69, 113] but also in p-type $TlBiTe_2$ [139], at the interface of Sr_2RuO_4 [122] and in BC_3 [43].
In this chapter, we aim to investigate the proximity effects at the interface between an

itinerant ferromagnet and a pure helical TSC. More specifically, we are interested in the influence of the magnetization on the spin-current at the interface of the topological superconductors. In this regards, it follows the works done on ferromagnetic heterostructures made on chiral superconductors [85] and, more recently, on NCS [36, 116], although our analysis differs substantially. Indeed, we are especially interesting to understand how the behaviour of both, spin and charge currents, depends on the number of gapless edge states in the presence of ferromagnetism. Using the tight-binding lattice model, we obtain the spatial profile of the superconducting and magnetic order parameters via a self-consistent solution of the Bogoliubov-De Gennes equations for a two-dimensional planar heterostructure and, then, the spin- and charge-currents at the interface. We find that the intensity for the spin and charge currents rescaled to the vacuum interface generally increases with the number of helical modes. An important element in the control of the interface current is represented by the degree of mixing between the ferromagnetic states and the helical modes. This effective hybridization is linked to the amplitude and orientation of the spin polarization in the ferromagnet with respect to the superconducting $\vec{d}$-vector as well as to the topology of the ferromagnet Fermi surface. Hence, we show that the tuning of the currents with respect to the magnetization is mainly understandable by analysing the hybridization of the edge states through the spectral functions. It results that the presence of a finite amount of electronic hybridization with the double pairs of Majorana helical modes leads to nonvanishing charge current independently on the strength of the ferromagnetic exchange while it gets much suppressed for strong ferromagnet in presence of only one gapless edge state. Moreover, we shall see that the presence of a second gapless edge states also modifies quantitatively the tuning of the spin-current for weak ferromagnet.

The chapter is organized as follows. We present in section 5.1 the model for the ferromagnet - spin triplet superconductor interface and we discuss the existence of the helical edge states at the boundaries of the TSC as well as the spin-current associated. Then, we discuss briefly the spatial variations of the spin-triplet order parameters in section 5.2. Section 5.3 is devoted to the analysis of the spectral functions close to the interface as a function of the strength and the orientation of the magnetization. The tuning of the charge and spin current with respect to the magnetization strength is discussed in section 5.4 for the case where the magnetization is perpendicular to the plane, i.e. perpendicular to the $\vec{d}$-vector. Then, the same analysis is done in section 5.5 for a magnetization coplanar to the $\vec{d}$-vector. Finally, the section 5.6 is devoted to the concluding remarks.

5.1 Helical TSC and Lattice Model

We first present in this section the tight-binding Hamiltonian used to model the helical spin-triplet superconductor. Contrary to the chiral TSC, the helical state is induced by the existence of a equal-spin pairing between electrons as introduced in the Chapter 1, Eq. 1.26. Using this model, we shall then discuss the electronic properties at its boundaries, in particular to highlight the existence of the edge states by means of the spectral functions and by computing the spatial variations of the spin-resolved current along the edges.

Model and Formalism We consider as previously a single-band extended tight-banding model Hamiltonian to describe a two-dimensional FM-TTSC junction on a lattice, see Fig. 5.1. An attractive nearest-neighbour interaction is added to yield a spin-triplet pairing with helical symmetry in the superconducting side and, following the Stoner model for itinerant magnets, an exchange field h is introduced to yield a nonzero spin polarization in the ferromagnetic region. The interface is chosen perpendicular to the x-direction and the lattice size is $L_x \times L_y$ with periodic boundary conditions imposed along the y-direction parallel to the interface. Indicating each site by a vector $\mathbf{i} \equiv (i_x, i_y)$, with i_x and i_y representing the sites in the x and y-directions, the general Hamiltonian, as introduced in Chapter 1, is expressed as

$$\begin{aligned} H &= -\sum_{\langle \mathbf{i},\mathbf{j}\rangle,\,\sigma} t_{\mathbf{ij}}(c^{\dagger}_{\mathbf{i}\,\sigma}c_{\mathbf{j}\,\sigma} + H.c.) - \mu\sum_{\mathbf{i},\sigma} n_{\mathbf{i}\sigma} \\ &\quad - \sum_{\langle \mathbf{i},\mathbf{j}\rangle \in \mathrm{TTSC}} V^{\sigma\sigma'} n_{\mathbf{i}\sigma} n_{\mathbf{j}\sigma'} - \sum_{\mathbf{i}\in \mathrm{FM}} \vec{h}\cdot\vec{s}(\mathbf{i}), \end{aligned} \tag{5.1}$$

where $c_{\mathbf{i}\,\sigma}$ is the annihilation operator of an electron with spin σ at the site $\mathbf{i}$, $n_{\mathbf{i}\,\sigma} = c^{\dagger}_{\mathbf{i}\,\sigma}c_{\mathbf{i}\,\sigma}$ is the spin-σ number operator and $t_{\mathbf{ij}}$ is the hopping amplitude that is nonvanishing only between the nearest neighboring sites $\mathbf{i}$ and $\mathbf{j}$. Moreover, $\vec{s}(\mathbf{i}) = \sum_{s,s'} c^{\dagger}_{\mathbf{i}\,s}\vec{\sigma}_{s,s'}c_{\mathbf{i}\,s'}$ is the local spin density polarization and $V^{\sigma\sigma'}$ is the pairing coupling between electrons of spin σ and σ' on two nearest-neighbours sites. The lattice is divided in two regions, the ferromagnetic side is located at $i_x \leq 0$ while the superconducting is at $i_x > 0$.
Concerning the ferromagnet, the model is similar than in the previous Chapters. Indeed, the magnetization is proportional to the exchange field $\vec{h}$ which leads to a splitting of the spin up and spin down energy spectrum and induces a spin-polarisation. In contrast to the previous chapter where the three-dimensional system was invariant by rotation with respect to the c-axis and where the all in-plane magnetization orientations were equivalent, it is necessary here to distinguish between the x- and the y-directions. Hence, we define here the orientation of the magnetization by fixing the angles θ and ϕ with respect to the direction of the $\vec{d}$-vector (see Fig. 5.1). Therefore, the magnetization is coplanar to the $\vec{d}$-vector for $\theta = 0°$ while it is perpendicular to the $\vec{d}$-vector when $\theta = 90°$. Moreover, in the case $\theta = 0°$, the spin-polarization is collinear to the x-component (y-component) of the $\vec{d}$-vector for $\phi = 0°(90°)$, respectively. The ϕ angular dependence is nontrivial because it couples to zero spin projections having an inequivalent orbital symmetry. Although the topology of the Fermi surface in the ferromagnet can have a role in modifying the character of the interface states, we consider in the present analysis the hopping terms $t_x = t_y = t = 1.0$ to be uniform along the x- and y-directions in the FM side.

Following the BCS theory for spin-triplet superconductors, we consider the spin-triplet states to be obtained within the mean field approximation, i.e. with a weak pairing coupling. Hence, the Hamiltonian in Eq. 5.1 is decoupled within the Hartree-Fock approximation as

$$V^{\sigma\sigma'} n_{\mathbf{i}\sigma} n_{\mathbf{j}\sigma'} \simeq V^{\sigma\sigma'}(\Delta^{\sigma\sigma'}_{\mathbf{ij}} c^{\dagger}_{\mathbf{j}\sigma}c^{\dagger}_{\mathbf{i}\sigma'} + \bar{\Delta}^{\sigma\sigma'}_{\mathbf{ij}} c_{\mathbf{i}\,\sigma'}c_{\mathbf{j}\,\sigma} - |\Delta^{\sigma\sigma'}_{\mathbf{ij}}|^2), \tag{5.2}$$

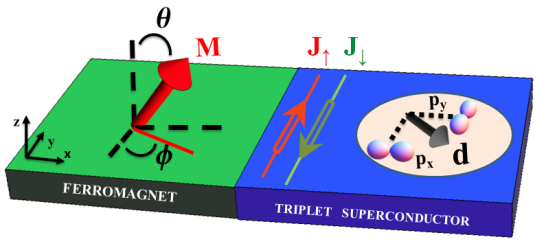

Figure 5.1: Schematic view of the FM-TTSC heterostructure with the interface perpendicular to the x-direction. The right side (blue) shows the spin-triplet superconductor region, having a $\vec{d}$-vector (thick black arrow) that lies within the (xy)-plane with orbital components $(d_x, d_y) = (p_y, p_x)$. $J_{\uparrow/\downarrow}$ are the spin-polarized currents flowing along the interface due to the presence of helical edge states in the superconductor. The left side (green) indicates the ferromagnetic region. The red thick arrow stands for the magnetization $\vec{M}$ in the interior of the ferromagnet due to an exchange field forming relative angles θ (out-of-plane) and ϕ (in-plane) with respect to the $\vec{d}$-vector.

where the general pairing amplitude on a bond between spin σ and σ' electrons at the sites $\mathbf{i}$ and $\mathbf{j}$ is given by $\Delta_{\mathbf{ij}}^{\sigma\sigma'} = \langle c_{\mathbf{i}\,\sigma} c_{\mathbf{j}\,\sigma'} \rangle$. As detailed in Chapter 1, the spin-triplet order parameters can be expressed in a matrix form as

$$\Delta(k) = \begin{pmatrix} \Delta_{\uparrow\uparrow}(k) & \Delta_{\uparrow\downarrow}(k) \\ \Delta_{\downarrow\uparrow}(k) & \Delta_{\downarrow\downarrow}(k) \end{pmatrix} = \begin{pmatrix} -d_x + id_y & d_z \\ d_z & d_x + id_y \end{pmatrix},$$

where the $\vec{d}$-vector components are related to the pair correlations for the various spin-triplet configurations having zero spin projection along the corresponding symmetry axis. The three components $d_x = \frac{1}{2}(-\Delta_{\uparrow\uparrow}(k) + \Delta_{\downarrow\downarrow}(k))$, $d_y = \frac{1}{2i}(\Delta_{\uparrow\uparrow}(k) + \Delta_{\downarrow\downarrow}(k))$ and $d_z = \Delta_{\uparrow\downarrow}(k)$ are expressed in terms of the equal spin $\Delta_{\uparrow\uparrow}(k)$ and $\Delta_{\downarrow\downarrow}(k)$, and the anti-aligned spin $\Delta_{\uparrow\downarrow}(k)$ pair potentials. In order to model an helical superconducting state, we assume the pairing interaction V to be non zero only in the $\uparrow\uparrow$ and $\downarrow\downarrow$ channels and, hence, $\Delta_{\sigma\sigma}(k)$ to be the only non-vanishing order parameters. In this case, the $\vec{d}$-vector lies in the (xy)-plane, which is chosen to be coincident with the (xy)-plane of the heterostructure as indicated in Fig. 5.1. As discussed in section 1.1, the orbital symmetry of the components of the $\vec{d}$-vector should also exhibit an odd symmetry with respect to a change of sign of the momentum, be it in the x- and the y-directions. These are achieved by the p_x- and p_y-wave orbital symmetries of the spin-triplet order parameters, having a sinusoidal dependence in momentum. As we have seen in Chapter 1, we can construct the order parameters on the lattice with the appropriate symmetries using the pair correlations defined on each site of the lattice

$$\Delta_{p_{x(y)}}^{\sigma\sigma}(\mathbf{i}) = \Delta_{\mathbf{i},\mathbf{i}+\hat{\mathrm{x}}(\hat{y})}^{\sigma\sigma} \tag{5.3}$$

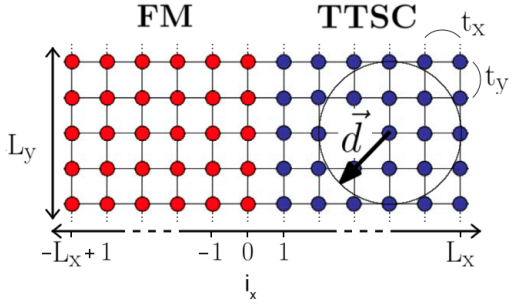

Figure 5.2: View of the $L_x \times L_y$ FM-TTSC lattice with an in-plane $\vec{d}$-vector and where t_x and t_y are the hopping terms in the x- and y-directions, respectively. The interface between the two regions is situated between the sites $i_x = 0$ (FM) $i_x = 1$ (TTSC).

such that

$$\Delta^{\sigma\sigma}_{p_{x(y)}}(\mathbf{i}) = \Delta^{\sigma\sigma}_{\mathbf{i},\mathbf{i}+\hat{\mathrm{x}}(\hat{\mathrm{y}})} \tag{5.4}$$

$$\Delta^{\sigma\sigma}_{p_{x(y)}}(\mathbf{i}) = \Delta^{\sigma\sigma}_{\mathbf{i},\mathbf{i}+\hat{\mathrm{x}}(\hat{\mathrm{y}})}. \tag{5.5}$$

In this particular configuration, the superconducting region exhibits hence a spin-triplet state with helical $\vec{d} = (p_y, p_x, 0)$ symmetry. The numerical analysis of the FM-TTSC interface consists then in evaluating self-consistently, by solving the Bogoliubov-De Gennes equations using the Hamiltonian defined in Eq. 5.1. All the results discussed in the following are obtained at zero temperature, for a lattice size $L_x = L_y = 80$ sites and by choosing a pairing interaction $V = -2.0t$ such that the bulk gap $V \cdot \Delta$ is still small compare to the spectrum bandwidth. As we shall see, the results depend essentially on the modification of the helical edge states at the interface and, thus, do not depend substantially on V.

Finally, the key feature of our analysis resides in the number of pair of gapless edge states which can be formed at the boundaries of the two-dimensional helical TSC. For this purpose, we exploit the fact that this number is intimately linked to the topological invariants of the Fermi surface in the normal state [114] which depends, within the tight-binding model, directly on the value of the in-plane hopping terms t_x and t_y. Hence, by suitably choosing the topology of the Fermi surface for the considered single-band model, it is possible to obtain a superconducting state with $N_0 = 0, 1, 2$ edge states as depicted in the top panels of Fig. 5.3 and for which the hopping parameters for the x and y directions are (a) $t_x = 0.4\,t$, $t_y = 1.0\,t$, $\mu = -0.7\,t$ ($N_0 = 0$), (b) $t_x = 1.0\,t$, $t_y = 1.0\,t$, $\mu = -1.1\,t$ ($N_0 = 1$) and (c) $t_x = 0.4\,t$, $t_y = 1.0\,t$, $\mu = -1.1\,t$ ($N_0 = 2$), respectively.
In our analysis of the edge currents at the superconducting interface, we will only focused on the two last cases since the helical edge states are clearly identifiable and related to the current along the interface.

Electronic Properties of the TTSC Before considering the proximity with the ferromagnet, it is instructive to investigate the edge states of the spin-triplet superconductor interfaced with the vacuum by solving the Hamiltonian in Eq. 5.1 without interfaced ferromagnet and for open boundary conditions along the x-direction. The site- and spin-dependent spectral function $A_\sigma(i_x, k_y)(\omega)$, defined in Eq. 1.36, are obtained from the

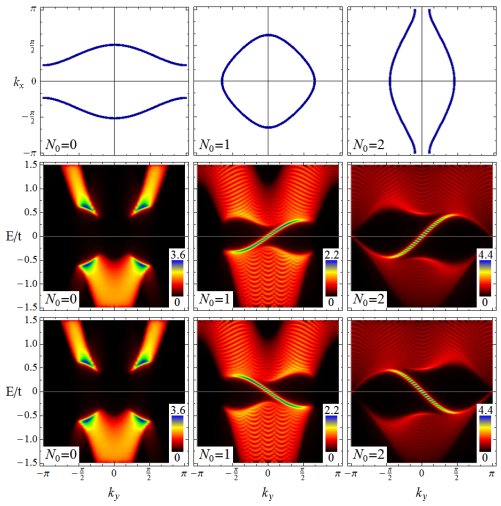

Figure 5.3: Energy spectra (bottom panels) at the edge of vacuum-TTSC interfaces for different values of the hopping terms in Hamiltonian Eq. 5.1. The number of zero-energy helical edge states $N_0 = 0$ (left panels), $N_0 = 1$ (middle panels) and $N_0 = 2$ (right panels) depends on the Fermi Surface of the metallic state (top panels). The parameters are $t_x = 0.4$, $t_y = 1.0$ and $\mu = -0.7\,t$ for $N_0 = 0$, $t_x = 1.0$, $t_y = 1.0$ and $\mu = -1.1\,t$ for $N_0 = 1$, and $t_x = 0.4$, $t_y = 1.0$ and $\mu = -1.1\,t$ for $N_0 = 2$.

self-consistent evaluation of the TTSC order parameter at any given distance from the interface with the vacuum.

In Fig. 5.3 we report the density plot of the spin-up (middle panels) and spin-down (bottom panels) spectral functions evaluated at the boundary of the TTSC, i.e. at the site $i_x = 1$, where the weight of the helical modes in the energy spectrum is maximal. Nevertheless, the edge states are located inside a region of about one superconducting coherence length ξ_{sc} close to the interface, which is of the order of 20 atomic distances for the given value of the superconducting pairing coupling V. Let us first analyse the spectral functions in the configuration with $N_0 = 1$ gapless mode obtained for isotropic hopping amplitudes within the lattice. For both, the spin-up and spin-down channels, we can clearly identify the superconducting gap in the spectrum in the energy range $-0.25\,t < E < 0.25t$ as well as midgap states. The latter are gapless at $k_y = 0$ and almost linearly dispersing. Furthermore, the helical modes connect the edges of the continuum band above and below the Fermi level at about $k_y = -\pi/2$ and $k_y = \pi/2$. We note that the dominant spectral weight resides in the helical modes which are fully spin polarized and that, due to the time reversal constraint, are symmetrically linked by inverting the direction of the momentum, i.e. $A_\uparrow(i_x, k_y)(\omega) = A_\downarrow(i_x, -k_y)(\omega)$. When considering an open Fermi surface along the k_y direction, see (a2), the midgap helical modes have a different structure and exhibit two gapless branches crossing at the momenta $k_y = 0$ and π of the Brillouin zone. The spectral weight distribution is however not symmetric with a larger amplitude close to $k_y = 0$. The case of a Fermi surface that is open along the x-direction, see (a), yields midgap states which are fully gapped and confined close to the gap edge of the spectrum in the momentum window around $k_y = \pm\pi/2$.

The center and bottom rows of the Fig. 5.3 represent the spectral functions for spin up and spin down electrons, respectively. They are obtained for three different topology of the Fermi Surface represented in the top row of the Fig. 5.3.

Let us first analyse the spectral functions in the configuration (b) for which the hopping terms are equal in both direction of the lattice. For both cases, spin up and spin down electrons, we can identify a gap in the metallic spectrum between $-0.25t < E < 0.25t$ as well as electronic states with a quasi linear dispersion situated inside the gap and

with momentum $k_y = -\pi/2$ to $k_y = \pi/2$, which includes gapless states at $k_y = 0$. The states inside the gap are called edge states by definition since they are localized at the boundary of the TTSC region but not in the bulk where the energy spectrum is fully gapped. Moreover, the edge states are polarized since they differ between spin up and spin down electrons and the symmetry $A_\uparrow(i_x, k_y)(\omega) = A_\downarrow(i_x, -k_y)(\omega)$ is respected.
The configuration (c) exhibits very similar properties than the configuration (b), where midgap edge states are present in the energy spectrum. In this case, however, the edge states can be found at any momentum $-\pi < k_y < \pi$ and two gapless edge states with momentum $k_y = 0$ and $k_y = \pm\pi$ are present.
Finally, we can see that there are no gapless states in the spectrum in the configuration (a). Nevertheless, edge states can be identify at lower energies for momenta around $k_y = \pi/2$ and the symmetry $A_\uparrow(i_x, k_y)(\omega) = A_\downarrow(i_x, -k_y)(\omega)$ is again respected.
We define N_0 as the number of gapless edge states present at the boundaries and we will use it to refer to the three different cases (a) $\mathrm{N}_0 = 0$, (b) $\mathrm{N}_0 = 1$ and (c) $\mathrm{N}_0 = 2$.

Spin Currents at the Vacuum-TTSC Interface The Fig. 5.3 shows that for a given spin polarization the dispersion $\omega(k_y)$ of the midgap states is odd in momentum. Therefore, the spin-polarized configurations can sustain a flowing current along the boundaries of the TTSC. This is an important and the main physical quantity for the present study which we aim to investigate in the proximity of the ferromagnetic interface. The σ spin-polarised kinetic currents flowing along the TTSC interface at the site i_x, having a spin polarization along the α direction ($\alpha = x, y, z$), is expressed as

$$J^\alpha_\sigma(i_x) = \frac{2\,t}{L_y} \sum_{k_y} \sin(k_y) \langle c^\dagger_{i_x, k_y \sigma} c_{i_x k_y \sigma} \rangle. \tag{5.6}$$

The charge current is hence obtained by summing the contribution of the $\uparrow$ and $\downarrow$ spin-polarized electrons as $J_c(i_x) = J^z_\uparrow(i_x) + J^z_\downarrow(i_x)$ while the z-polarised spin current is obtained from their subtraction as $J^z_s(i_x) = J^z_\uparrow(i_x) - J^z_\downarrow(i_x)$. As we have seen in Fig. 5.3, the time reversal symmetry insures the dispersion of the spin-up and spin-down gapless modes, for both $\mathrm{N}_0 = 1$ and $\mathrm{N}_0 = 2$ cases, to be opposite. Hence, spin-up and spin-down electron are counter-propagating, i.e. $J^z_\uparrow(i_x) = -J^z_\downarrow(i_x)$, which leads to the existence of a finite z-polarised spin current along the TTSC interface while the charge current is perfectly cancelled, i.e. $J_c(i_x) = 0$.
The spatial variations of the spin-polarised currents $J^z_\uparrow(i_x)$ and $J^z_\uparrow(i_x)$ as well as the spin current $J^z_s(i_x)$ at the edge of the helical superconductors, i.e. at the vacuum-TTSC interface, are plotted in Fig. 5.4. As we can observe, the edge currents along the y-direction at both $\mathrm{N}_0 = 1$ and $\mathrm{N}_0 = 2$ interfaces exhibit a qualitative similar behaviour and differ only by their amplitude. Their are scaled by the total current $J^0_s = \sum_{i_x=1}^{bulk} J^z_s(i_x)$ evaluated for the $\mathrm{N}_0 = 2$ TTSC.
Hence, we observe that the spin current is maximal at the interface of the TTSC, and then decays moving into the FM and further into the superconducting region. The characteristic length for which the spin current is suppressed is set by the coherence length of the superconductor that for the chosen value of the pairing amplitude is $\xi_{sc} \sim 20$ in unit of the atomic sites distance. This spatial domain in the TTSC corresponds to that where

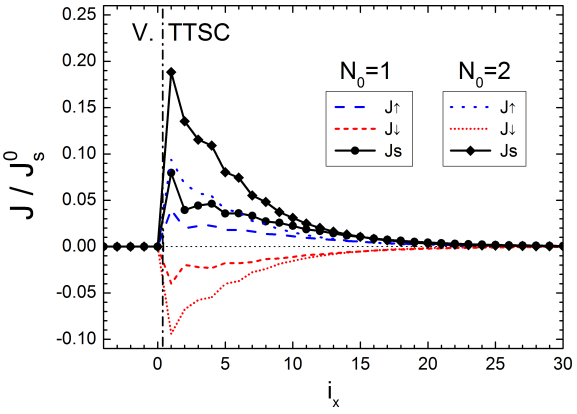

Figure 5.4: Spatial variations of the spin currents $J_\uparrow(i_x)$ (dashed lines), $J_\downarrow(i_x)$ (dotted lines) and $J_s(i_x)$ (solid lines) along the Vacuum-TTSC interface for both configurations with one and two zero-energy edge states, i.e. $N_0 = 1$ and $N_0 = 2$. They are scaled by the spatially integrated spin current in the $N_0 = 2$ configuration. The dashed-dotted line represents the interface between the Vacuum and TTSC regions.

the edge states in the spectrum have a nonvanishing spectral weight. At larger distances from the interface, i.e. $i_x > \xi_{sc}$, the spectrum turns out to be fully gapped and the spin currents is suppressed to zero.
Moreover, a close view to the spin-polarised $J^z_\uparrow(i_x)$ and $J^z_\uparrow(i_x)$ current shows that, in both cases, their are exactly opposite. Hence, a finite spin-current is flowing along the edge while there is no charge current.

5.2 Spatial Variations of the Superconducting Order Parameters

In connection with our previous results for heterostructures made of chiral TSC, we discuss briefly in this section the spatial profile of the spin-triplet order parameters at the ferromagnet-helical TSC for various magnetization orientations. As we know from our previous analysis, we expect the magnetization to act as non, partially or totally pair breaking for the triplet Cooper pairs induced in the ferromagnet region depending on its orientation. However, we shall see that, in contrast to the chiral interface, the p_x- and p_y-wave order parameters are not equivalent with respect to the pair breaking effect. The results are qualitatively equivalent for both helical TSC with one ($N_0 = 1$) or two ($N_0 = 2$) pairs of gapless edge states and, therefore, only the first case is discussed in the following, represented in Fig. 5.3(a1,b1,c1).

The spatial variations of the spin-triplet order parameters $\Delta^{\uparrow\uparrow}_{px}$ and $\Delta^{\uparrow\uparrow}_{py}$ at the FM-TTSC interface for various magnetization orientations are plotted in the left and right panel of the Fig. 5.5, respectively, and have been obtained by solving self-consistently the BdG equations for an exchange field strength $h = 0.60t$. In both cases, the results are obtained for a magnetization rotating in the (yz)-plane ($\rho = 0°$) and in the (xz)-plane ($\rho = 90°$).
First of all, let us comment about the modification of the OPs inside the superconducting region. There, independently of the magnetization orientation, we observe two different behaviours depending on the momentum symmetry of the order parameters. Indeed, we can see that $\Delta^{\uparrow\uparrow}_{px}$, respecting a $\sin(k_x)$ symmetry, is decreasing at the interface compare to its bulk value while $\Delta^{\uparrow\uparrow}_{py}$, with a $\sin(k_y)$ symmetry, is increasing. These features are equivalent to what have been found in the two-dimensional FM-chiral TSC interface,

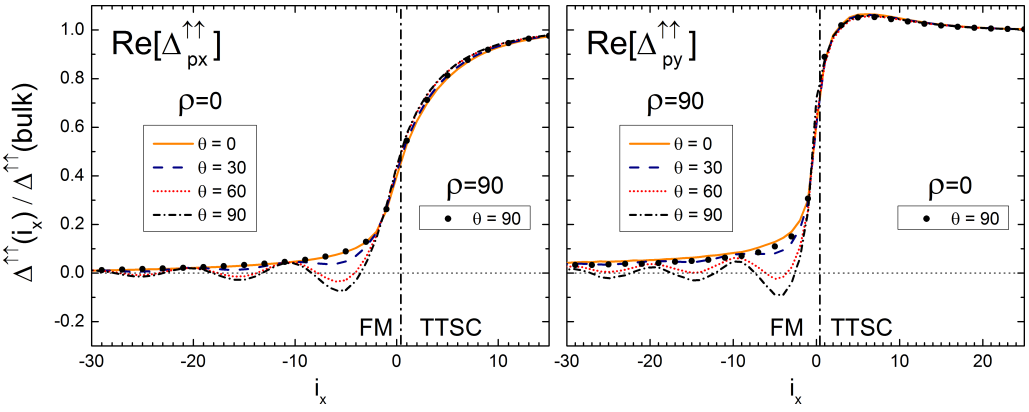

Figure 5.5: Spatial variations of the real part of the p_x-wave pairing amplitude Δ_{p_x} (left panel) and the p_y-wave pairing amplitude Δ_{p_y} (right panel) at the two-dimensional FM-TTSC interface for a $N_0 = 1$ configuration. They are obtained for various angles θ and ρ and scaled to the TSC bulk values. They are obtained for an exchange field $h = 0.60t$.

shown in Fig. 2.2, since they are directly related to the nature of the Andreev reflections at the interface, depending on the momentum symmetry of the order parameters. Hence, the breaking of the translation symmetry in the x-direction induces the cancellation of the OP with $\sin(k_x)$ symmetry.

Let us now focus on the induced pairing amplitudes in the ferromagnetic side. Concerning $\Delta_{px}^{\uparrow\uparrow}$, we can observe that the magnetization is non pair-breaking when it is orientated in the z-direction ($\theta = 0°$) since the spin-triplet OP is induced in the ferromagnetic region without oscillations and is decreasing while getting further from the interface. It is due to the fact that, in this configuration, the magnetization is perpendicular to the (xy)-plane where lies the $\vec{d}$-vector. By rotating the magnetization in the (yz)-plane ($\rho = 0°$), periodic oscillations in the ferromagnetic regions are induced. Their amplitude are maximal when the magnetization is coplanar to the $\vec{d}$-vector ($\rho = 0°$ and $\theta = 90°$) while the period of the oscillations is independent of the orientation of the exchange field. On the other hand, a magnetization rotating in the (xz)-plane ($\rho = 90°$) induced no oscillations, as it is highlighted by the configuration where the magnetization is along the x-direction ($\rho = 90°$ and $\theta = 90°$). Once again, the presence or not of the oscillations when the magnetization is in plane is related to its relative orientation compare to the $\vec{d}$-vector. Indeed, we have seen in the previous section that the order parameter of our spin-triplet superconducting state is such that $d = (\Delta_{py}, \Delta_{px}, 0)$. Hence, by construction, the chosen pair correlations $\Delta_{px}^{\sigma\sigma}$ is related to the d_y component of the $\vec{d}$-vector. Hence, the magnetization is pair-breaking and induces oscillations in the ferromagnetic side when it is oriented parallel to the d_y component, i.e. in the y-direction ($\rho = 0°$ and $\theta = 90°$).

These behaviours are also verified for the $\Delta_{py}^{\uparrow\uparrow}$ pair correlations. Indeed, in this case, the magnetization is pair breaking when it is oriented parallel to the d_x component, i.e. in the x-direction ($\rho = 90°$ and $\theta = 0°$). Nonetheless, a closer look to the results shows that, in contrast to $\Delta_{px}^{\uparrow\uparrow}$, the two non-pair-breaking magnetization orientations are non equivalent.

As we shall see in the next section by analysing the spectral functions, this is due to a more complex modification of the edge states at the interface due to the time-reversal breaking symmetry of the configuration.
We can finally add that, as for the chiral TSC, changing the strength of the magnetization increases or decreases the period of oscillations but does not qualitatively modify the discussion. Moreover, the $\uparrow\uparrow$ and $\downarrow\downarrow$ components of the OPs are equal in absolute value.

From our understanding of the proximity effects at the FM-TSC interfaces, it is interesting to discuss shortly the possible consequences of such spatial variations of the spin-triplet order parameters at the interface of helical TSC although we shall not in this chapter make further investigations in these directions.
By looking carefully of the variations of the order parameters in the TSC region, we can see that their amplitudes depend on the orientation of the magnetization. Hence, as in the Chapter 3, we can expect the condensation energy to depend on the magnetization orientation and, therefore, to energetically favour a non trivial magnetic profile at the interface. Additionally, such modification should lead to modify the orientation of the $\vec{d}$-vector although this effect should be rather small. Moreover, the computation of the $\Delta_{\uparrow\downarrow}$ component possibly induced at the interface should also be considered for such study. Interestingly, the competition between the behaviour of the two induced pair correlations in the ferromagnetic can especially have important consequences on the Josephson junctions. Indeed, since the magnetic configuration cannot be in the same time pair-breaking for the two different symmetries of the OPs, a subtle competition should arise and lead to significant modifications of the current-phase relations compare to the Junctions with a metallic barrier, which has been been recently predicted [9]. Although it seems indeed to be altered, the study does not show the possibility to achieve φ-state in such junctions.

5.3 Edge States Hybridization at the FM-TTSC interface

In this section we discuss the evolution of the electronic states at the interface between the FM and the TTSC, both inside and above the superconducting energy gap, for the cases with one and two pairs of Majorana helical modes. Such analysis is particularly relevant to understand how the degree of mixing between the midgap edge modes and the magnetic states of the FM close to the Fermi level is interrelated to the variation of the spin and charge currents. We shall consider an orientation of the magnetic exchange both perpendicular and coplanar to the $\vec{d}$-vector. We expect the effects on the helical modes to be significantly distinct because a magnetization parallel to the $\vec{d}$-vector is generally pair breaking for the spin-triplet superconducting state.

Magnetization perpendicular to the $\vec{d}$-vector The first analysis concerns the case with an exchange field parallel to the z-direction, thus perpendicular to the $\vec{d}$-vector. We report in Figs. 5.6 and 5.7 the spectral functions for the spin majority (spin-up) and minority (spin-down) components for three values of the ferromagnetic exchange h. They are chosen to be representative of the regimes of weak ($h = 0.6\,t$), intermediate ($h = 1.5\,t$) and strong ferromagnet ($h = 2.7\,t$), respectively, in order to single out the role of the magnetization strength in controlling the modification of the helical modes in the TTSC.

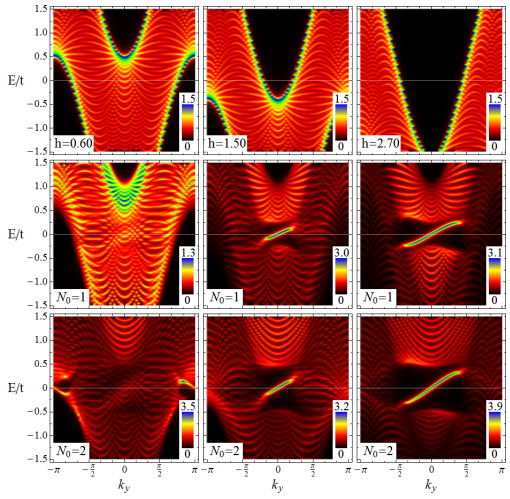

Figure 5.6: Energy Spectrum for spin up electrons for three values of the exchange field along the z-direction $h = 0.6t$ (left column panels), $1.50t$ (middle column panels) and $2.70t$ (right column panels). They are computed for in the bulk FM (top row panel) and at the edge of the TTSC for two the two configurations $N_0 = 1$ (middle row panels) and $N_0 = 2$ (bottom row panels).

The upper row panels in Fig. 5.6 and 5.7 depict the ferromagnetic single particle spectral functions obtained inside the ferromagnetic bulk while the middle and lower rows show the spectral functions obtained at the FM-TSC interface, i.e. at the site $i_x = 1$, for the $N_0 = 1$ and $N_0 = 2$ superconductors, respectively.

One can note that, as expected from the variation of the occupation number for each spin in the Brillouin zone along the direction of the exchange field, the distribution of the electronic states around the Fermi level, as a function of the transverse momentum k_y, manifests an energy splitting between the spin-up and spin-down channels. The features of the electronic structure in the FM are tied to the considered two-dimensional tight-binding model, for which the spectrum is $\xi(k_x, k_y) = -2t[\cos(k_x) + 2t\cos(k_y)] - \mu$, thus having a topology of the Fermi surface that is closed (electron-like) around the center of the Brillouin zone. Then, projected on the conserved momentum along the y-direction, the increase of the spin density leads to a reduction of the electronic states around the point at $k_y = 0$ at low energy and an increase of the electronic states close to the zone boundary ($k_y = \pi$) both at low and high energies exhibiting a continuum of excitations that extends up to about half of the bandwidth. Such a variation of the electronic distribution reflects the change of the electronic structure for the majority and the minority spin electrons. For a given total electron density the effective Fermi level $k^F_{y\uparrow}$ depends on h for each projected spectrum and separates two different regions of the Brillouin zone. In the range $[-k^F_{y\uparrow}, k^F_{y\uparrow}]$ there are no states available for the spin majority electrons close to the zero energy because the bottom of the band is at $k_y = 0$ and it gets lowered in energy by the exchange field (see Fig. 5.6) to allow the increment of the spin-majority electron density. Outside this range of moments, the electronic states are accessible in a continuum of energies with a bandwidth that grows with the amplitude of h. The evolution is opposite for the spin minority electrons. As one can see in top panels of Fig. 5.7 already at $h = 0.6t$ the effective $k^F_{y\downarrow}$ is close to $k_y = 0$ with a distribution of electronic states close to the Fermi level that tends to be vanishing at all k points in the Brillouin zone. The further increase of h in the FM leads to a shrinking of the window in the Brillouin zone where there are allowed occupied states and they become more and more concentrated uniquely around the $k_y = 0$ point.

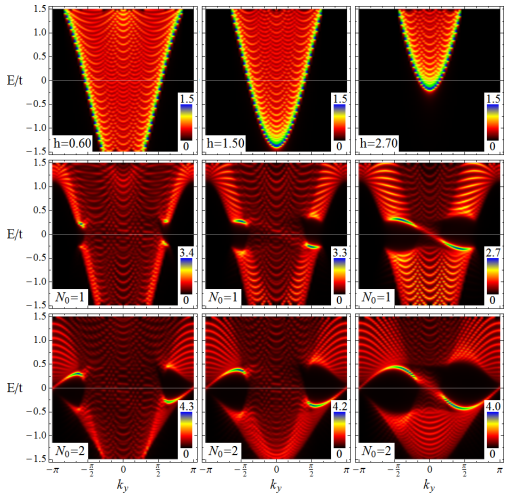

Figure 5.7: Energy Spectrum for spin down electrons for three values of the exchange field along the z-direction $h = 0.6t$ (left column panels), $1.50t$ (middle column panels) and $2.70t$ (right column panels). They are computed for in the bulk FM (top row panel) and at the edge of the TTSC for two the two configurations $N_0 = 1$ (middle row panels) and $N_0 = 2$ (bottom row panels).

The energy bandwidth is also reduced as one is approaching the half-metallic regime where the spin-minority electron density tends to zero. Hence, the spectral-function evolution clearly shows that the electronic states close to zero energy accumulate around the zone boundary (center) of the Brillouin zone for the spin majority (minority) electrons as the exchange field is varied from zero to the half-metallic amplitude. Moreover, the bandwidth of the low energy states grows (decreases) as a function of the exchange field for the majority (minority) spin electrons. Such interrelation holds for an electron-like Fermi surface and it is reversed if one considers a different dispersion in the FM with a hole-like type of Fermi surface.

Taking into account these features, one can closely analyse how the edge states in the TTSC region get modified by the presence of the FM. Let us start by the $N_0 = 1$ case for which two spin-polarized helical modes with opposite velocity crossing zero energy at $k_y = 0$ are present inside the gap. Then, according to the distribution of the electronic spectrum in the FM, we expect the spin-minority channel to be more affected than the spin-majority one, at least at large values of the exchange field. This result is confirmed by inspection of the Figs. 5.6 and 5.7 showing the dependence of the spectral functions in the superconducting region of the heterostructure.

For $h = 0.6t$, we can observe for both spin-up and spin-down spectral functions that the gap is suppressed and that the hybridization with the magnetic states in the FM destroys the midgap states, see (a1).

The evolution of the electronic structure inside the superconducting gap follows directly that of the spectra in the ferromagnetic region. For the majority spin electrons, the edge modes around the centre $k_y = 0$ of the Brillouin zone gets more robust as the magnetization grows up to the half-metallic limit, Fig. 5.6(b1) and (c1). Moreover, the large distribution of spectral weight at the zone boundary persists in such a way that the gap is suppressed there and the spectral weight of the edge states is also renormalized down to zero. On the other hand, for the minority spin electrons there is a substantial renormalization of the spectral weight for the edge modes even when the superconducting gap is clearly visible. Due to the distribution of the electronic structure in the FM it is the part of the edge states which joins the continuum above the superconducting gap that acquires spectral weight in

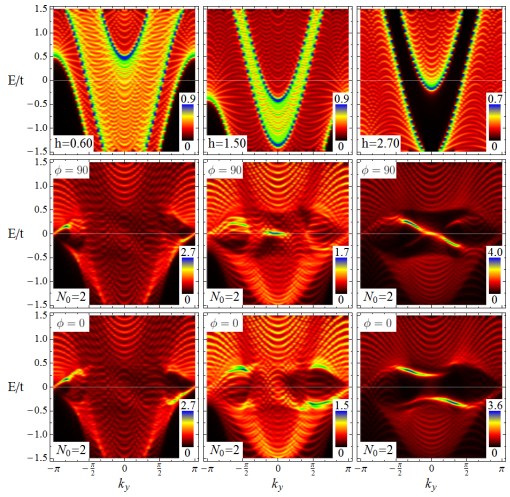

Figure 5.8: Energy Spectrum for spin down electrons for three values of the exchange field along the x-direction ($\phi = 90°$) and the y-direction ($\phi = 0°$), $h = 0.6t$ (left panels), $1.50t$ (middle panels) and $2.70t$ (right panels). They are obtained in the FM bulk (top row panels) and at the site $i_x = 1$ of the FM-TTSC interface (bottom row panels) for the configuration $N_0 = 2$.

the strong ferromagnet regime while the spectrum close to $k_y \sim 0$ becomes more coherent though with a reduced occupation probability, Fig. 5.7(b1) and (c1). When comparing the edge modes in Figs. 5.6 and 5.7 with that of the interface to the vacuum, one can observe that the coupling with the FM results into a significant renormalization of the helical-modes spectral weight, with a minor change of the dispersion mainly related to the increase of the effective velocity at large momenta close the gap edge.
Concerning the case $N_0 = 2$, the hybridization of the electronic states with momentum $-\pi/2 < k_y < \pi/2$ is similar to the case $N_0 = 1$. However, differences arise at momentum $k_y = \pm\pi$ since, in this case, additional gapless edge states are present. For spin up electrons, we can observe in Fig. 5.6(a2) that the states are unmodified around $k_y = \pm\pi$ at small values of h. Then, they hybridize completely with the ferromagnet states for intermediate and large values of the exchange field, Fig. 5.6(b2) and (c2). Finally, as a distinct feature of the helical modes variation at the interface, the spectrum for the minority spin electrons in Fig. 5.7(a2-c2)is completely unaffected around $k_y = \pm\pi$ at any value of the exchange field.

Magnetization coplanar to the $\vec{d}$-vector The behaviour of the spectral function is more complex when the exchange field is coplanar to the $\vec{d}$-vector because such an orientation can be pair breaking and transverse to the spin configuration of the superconducting state. Furthermore, due to the structure of the $\vec{d}$-vector with orbital inequivalent x and y components, i.e. $\vec{d} = (p_y, p_x, 0)$, the orientation of the magnetic exchange can lead to significant in-plane anisotropy in the edge electronic spectrum. Since for a magnetic exchange that lies in the (xy)-plane of the spin-space the up and down orientations are equivalent, i.e. $A_\uparrow(i_x, k_y)(w) = A_\downarrow(i_x, k_y)(w)$ for $i_x \in$ FM, and due to the existence of the time reversal symmetry which insures $A_\uparrow(i_x, k_y)(w) = A_\downarrow(i_x, -k_y)(w)$ for $i_x \in$ TTSC, we limit the study of the energy spectrum to one spin polarization. Moreover, we discuss the spectral function corresponding to $N_0 = 2$ helical modes as it presents all the relevant features arising from a coplanar magnetic exchange field, the case with $N_0 = 1$ modes can be deduced by direct inspection of the structures close to $k_y \sim 0$.
In Fig. 5.8 we compare the spin-down spectral functions for two magnetic exchange

orientations along the x- and y-direction moving from weak to half-metallic ferromagnet. The electronic spectra in the ferromagnet (top row) presents a two-band structure that reflects the nonzero spectral weight of both the up and down split bands when the exchange is coplanar to the $\vec{d}$-vector. This implies that, already at small values of the exchange h, there is a distribution of spectral weight close to the Fermi level at any value of k_y which makes possible a mixing with all the midgap helical modes. For the weak ferromagnet regime, i.e. $h = 0.6t$, the degree of magnetic quasiparticle poisoning makes the gap undetectable and one cannot identify significant differences when switching the exchange from x- to y-direction, see Fig 5.8(a1) and (a2). In this regime the helical modes close to $k_y \sim \pi$ do not hybridize much with the magnetic states and a slight xy asymmetry in the spectral weight can be observed with more coherent intensity along the y-direction associated with the $\sin(k_x)$ orbital pairing symmetry.
More evident anisotropies emerge by analysing the behaviour at larger values of the exchange ($h = 2.7t$) when, as a consequence of an inverse proximity effect, the edge states acquire a spin polarization that is more robust, Fig 5.8(a1) and (a2). Then, due to the up-down mixing induced by leaking of the magnetization in the superconductor, the spectral function for a given spin polarization exhibits shadows of the helical modes with opposite spin configuration as well. The role of mixing is considerably relevant when comparing the case of a ferromagnet with x or y orientations. For the exchange parallel to the x-direction, the up-down mixing strengthens the intensity of the helical modes close to $k_y = 0$ leading to a flattening of the dispersion (Fig. 5.8(c1)). On the other hand, a spin-polarization parallel to the y-component of the $\vec{d}$-vector couples to the orbital component of the superconducting state that leads to the zero energy states. This implies a splitting helical modes with a gap opening at $k_y = 0$ and a dramatic modification of the dispersion (Fig. 5.8(c2)).

5.4 Tuning of the Edge Currents: Magnetization perpendicular to the $\vec{d}$-vector

From the modification of the spectral functions with respect to the exchange field, through the modification of the Fermi surface, we expect the spin-resolved currents $J_\uparrow$ and $J_\downarrow$ to be altered independently to each other. Hence, the spin current J_s is modified and charge currents J_c can be created along the interface. We discuss in this section the variations of the currents along the interface with respect to the strength of the exchange field for the two cases $\mathrm{N}_0 = 1$ and $\mathrm{N}_0 = 2$. In this section, we focus only on results obtained with magnetization oriented along the z-direction, perpendicular to the $\vec{d}$-vector, which is not pair-breaking for both order parameters.

Spatial Variations of the Spin Current We start the discussion by considering the case of a magnetization in the FM that is perpendicular to the $\vec{d}$-vector. For such configuration, the spatial variation of the $\mathrm{N}_0 = 1$ and $\mathrm{N}_0 = 2$ spin current flowing along the FM-TTSC interface is presented in Fig. 5.9 at different values of the exchange field, moving from the unpolarized normal state, i.e. $h = 0t$, until the half-metallic regime at $h = 3.0t$.
As one can note, the general trend is similar for both cases, $\mathrm{N}_0 = 1$ (Fig. 5.9(a)) and

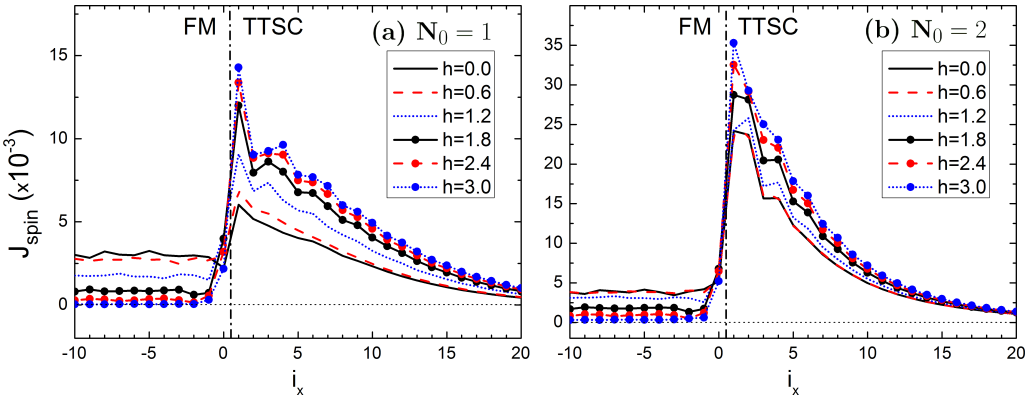

Figure 5.9: Spatial variations of the spin current $J_s(i)$ along the FM-TTSC interface for various strengths of the exchange field $|h|$. They are plotted for the TTSC configurations with one (a) and two(b) zero-energy edge states. The magnetization is perpendicular to the d-vector, i.e. $\theta = 0°$. The dashed-dotted line represents the interface between the FM and TTSC regions.

$N_0 = 2$ (Fig. 5.9(b)) and follow qualitatively, in the superconducting region, the trend observed at the vacuum-TTSC interface in Fig. 5.4.

Nevertheless, by close inspection of the profile of the spin-current, we can observe distinct features between the two cases. We find that the spin-current grows faster for the case $N_0 = 1$ than for $N_0 = 2$ when moving from the bulk TTSC to the interface because the presence of additional helical modes in the latter allows for a larger penetration in the inner side of the superconductor. We point out that the characteristic length of the spatial variation of the spin current does not seem to be significantly modified if compared to the case obtained at the vacuum-TTSC interface. On the other hand, the penetration of the spin currents in the FM region goes through an abrupt jump at the interface and it can stay into the ferromagnet almost unchanged on the scale of the proximity coherence length. It is worth mentioning that, for a magnetization perpendicular to the $\vec{d}$-vector, the exchange is not pair breaking and the proximity scale is basically set in the clean limit by the proximity coherence length as given by the ratio between the Fermi velocity and the temperature, i.e. $\sim v_F/T$. Hence, since we are dealing with a ballistic ferromagnet, the spin current can be sustained on long distances from the interface at low temperature. Approaching the half-metallic regime, due to the large suppression of the Andreev processes close to the interface, the spin current gets strongly reduced and confined close by the interface.

Tuning of the Total Spin Current In order to further analyse the evolution of the spin current in the TTSC region and to extract possible differences in the capacity of carrying currents in terms of the number of helical modes, we compute the integrated current densities for spin-up and spin-down electrons evaluated within the TTSC region. Following Eq. 5.6, the expressions for the total spin and charge currents are

$$J_\sigma^{tot} = \sum_{i_x \in TTSC} J_\sigma(i_x), \tag{5.7}$$

$$J_s^{tot} = J_\uparrow^{tot} - J_\downarrow^{tot}, \tag{5.8}$$

$$J_c^{tot} = J_\uparrow^{tot} + J_\downarrow^{tot}. \tag{5.9}$$

Hence, J_s^{tot} and J_c^{tot} represent the total spin and charge currents in the TTSC, respectively, flowing along the interface, i.e. in the y-direction. All the results concerning the total currents shown in the following, for both cases $\mathrm{N}_0 = 1$ and $\mathrm{N}_0 = 2$, are scaled to the value of the total spin current J_s^0 at the $\mathrm{N}_0 = 1$ and $\mathrm{N}_0 = 2$ superconductors, respectively, interfaced with the vacuum. They verify the relation $J_s^0(\ \mathrm{N}_0 = 2\ ) \simeq 2 \cdot J_s^0(\ \mathrm{N}_0 = 1\ )$.
The variations of $J_\uparrow^{tot}$(solid blue), -$J_\downarrow^{tot}$(dashed red) and J_s^{tot}(dotted black) as a function of the exchange h are shown in Fig. 5.10. As we can see, the presence of the FM breaks the up-down symmetry in the current, and the majority spin electrons in general exhibit a smaller capacity to carry current when a magnetization is put in proximity of the helical superconductor. This asymmetry tends to reduce down to zero as the ferromagnetism becomes stronger although the asymptotic behaviour turns out to be different for the case of $\mathrm{N}_0 = 1$ and $\mathrm{N}_0 = 2$ helical modes. Such behaviour can be understood by taking into account how the mixing of the helical and magnetic states occur in the Brillouin zone according to the analysis of the spectral function presented in Sec. III. For $\mathrm{N}_0 = 1$ at larger values of the exchange field, i.e. above $h \sim 1.5\,t$, the low energy helical modes around $k_y \sim 0$, for both spin polarizations, are not any longer hybridized with the magnetic states (see Figs. 5.6 and 5.7) and thus the up-down symmetry is about to be recovered, with a small residual difference mainly arising from the contributions at energies above the superconducting gap. On the other hand, the $\mathrm{N}_0 = 2$ helical superconductor has spin-current contributing modes at $k_y \sim 0$ and at momenta close to the zone boundary $\pm\pi$. The increase of the exchange field can avoid the magnetic-midgap states mixing nearby $k_y \sim 0$ in both spin channels, nevertheless it is not possible to get rid of the hybridization at the zone boundary between the helical modes and the majority spin channel. This residual single-particle poisoning of the helical modes will keep a nonvanishing asymmetry between the majority and minority spin currents even in the half-metallic ferromagnet regime.
Let us discuss in more details on the evolution of the integrated spin-current for the case of $\mathrm{N}_0 = 1$ helical modes. The evolution of the spin current identifies two different regimes in terms of the strength of the ferromagnet. Starting from the unpolarized configuration, i.e. $h = 0t$, we find that the spin current is more than half suppressed if compared with the amplitude at the vacuum-TTSC interface. Then, in the range from weak to intermediate ferromagnet, i.e. moving from $h = 0t$ to about $h = 1.0t$, we can observe that $J_\downarrow^{tot}$ grows linearly while $J_\uparrow^{tot}$ remains almost constant. These variations can be understood by inspection of the spectral functions in Figs. 5.6 and 5.7. Indeed, for small values of h, we have found that the edge states are ubiquitously hybridizing with the spin-split electronic states in the FM. As a direct consequence, the spectral weight of the midgap states is reduced and the spin-current along the interface is highly suppressed. More specifically, spin-up edge states keeps the same degree of hybridization for about $h < 1.0t$ and thus

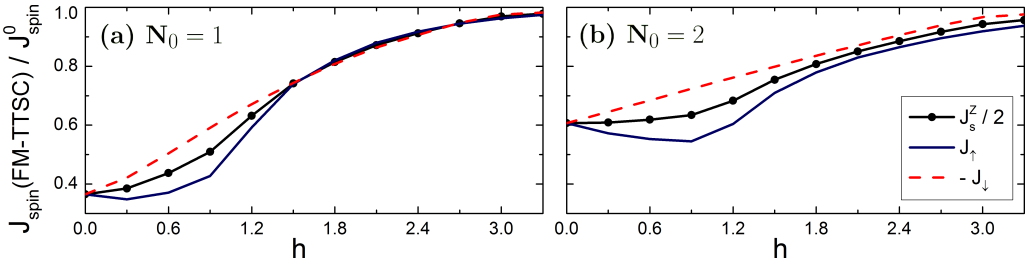

Figure 5.10: Summation of all contributions of the spin current $J_s(i)$ inside the TTSC region for various strengths of the exchange field $|h|$ and normalized by its value for the vaccum-TTSC interface. The results are showed for configurations with one (left panel) and two (right panel) zero-energy edge states, i.e. $N_0 = 1$ and $N_0 = 2$ respectively. The magnetization is perpendicular to the d-vector, i.e. $\theta = 0°$.

the spin up current $J_{\uparrow}^{tot}$ stays essentially unchanged. On the contrary, for the spin-down channel, one can observe that the states with momenta around $k_y = \pm\pi/2$ are less and less modified when h is increasing and, therefore, $J_{\downarrow}^{tot}$ gets more electronic contributions and tends to grow.

Differently from the regime of weak-intermediate FM, above an exchange threshold of the order of $h = 1.0t$, both $J_{\uparrow}^{tot}$ and $J_{\downarrow}^{tot}$ exhibit a monotonous upturn with an almost linear trend. This dependence on the exchange field in the regime of a large FM magnetization can be justified by noticing that the spin-up polarized states with momentum around $k_y = 0$ and those with spin-down configuration close to $k_y = \pm\pi/2$ become less hybridized with the ferromagnet spectrum. Therefore, the spin currents carried by the unmodified part of the edge states are increasing for both spin polarization.

Taking into account the different regimes of the integrated spin-current for the case of $N_0 = 1$, it is useful to consider how the capacity of carrying spin-currents is modified by the presence of additional helical modes. The first difference to point out is that J_s^{tot} is more suppressed, with respect to the vacuum-TTSC interface amplitude, for the case $N_0 = 1$ than for $N_0 = 2$. This quantitative disparity arises from the fact that the $N_0 = 2$ edge states remain not hybridized close to the zone boundary at $k_y = \pm\pi$ and, thus, still have a net capacity to carry spin-current without the effect of the mixing with the metallic electronic states close to the Fermi level. The second relevant difference between the $N_0 = 1$ and $N_0 = 2$ helical superconductor is observed in the regime of weak-to-intermediate ferromagnet. In this range, while $J_{\uparrow}^{tot}$ remains constant when h is growing from $h = 0t$ to $1.0t$ for the case $N_0 = 1$, the $N_0 = 2$ current response exhibits a monotonous decrease. As we can observe in the spectral functions of Fig. 5.6, this is directly related to the evolution of the majority spin-polarized edge states with momentum close to $k_y = \pm\pi$ where the degree of hybridization with the ferromagnetic states is more pronounced and increases with the exchange field. Hence, the capacity of carrying current along the interface results into a net suppression and the total spin current J_s^{tot} remains constant in this range of values for the exchange field. It is worth pointing out that the

amplitude of the spin-polarized currents is not only due to the midgap helical edge states at the boundary of the TTSC but there is also a tiny contribution arising from the states above the superconducting gap. Since this part is negligible with respect to that of the midgap states the current variations with respect to the exchange field can be addressed by focusing only on the part of edge states spectral functions as in Figs. 5.6 and 5.7.

Analysis of the Induced Charge Current As discussed previously, the FM breaks the up-down spin symmetry and, thus, leads to a net integrated charge currents due to the difference between the majority and minority spin electrons currents. While within the TTSC there is a definite relation between the integrated spin-up and spin-down currents with a general tendency to provide a negative total charge current being $-J_{\uparrow}^{tot} < J_{\downarrow}^{tot}$, the spatial dependence of the charge current is non-monotonous and exhibits a decaying behaviour moving towards the inner side of the TTSC and the FM with an oscillatory component whose amplitude scales with the exchange field. This is shown in Fig. 5.11 where we present the site dependent evolution of the charge current $J_c(i_x) = J_{\uparrow}(i_x) + J_{\downarrow}(i_x)$ in the proximity of the FM-TTSC interface, for both $\mathrm{N}_0 = 1$ (a) and $\mathrm{N}_0 = 2$ (b) superconductors, for small to large values of the exchange field h.
The spatial behaviour of the charge current reveals a subtle dependence on the hybridization between the ferromagnetic and the helical states that leads to a distinct response at the two sides of the heterostructure and is qualitatively sensitive to the strength of the FM exchange. As a general trend, we can note that the charge current is maximal at the interface and then decreases when one moves away from the interface.
A peculiar aspect is represented by the flow direction of the charge current in the TTSC and FM domains. For weak-to-intermediate FM, the charge current has a one-way flow within the TTSC and the FM side of the heterostructure with opposite relative direction. Moreover, for such a range of exchange fields the size of the charge current grows (decreases) in the TTSC (FM) regions, respectively. When the exchange in the FM overcomes a critical threshold of about $h \sim 1.0t$ with a magnetization that is larger than half of its maximal value, the behaviour of the charge currents is completely modified as it becomes oscillatory with a change in the flow direction that depends on the distance from the interface. An important feature is that the oscillatory length scale does not depend on the strength of the exchange h, being hence uncorrelated to the spin split of the magnetic

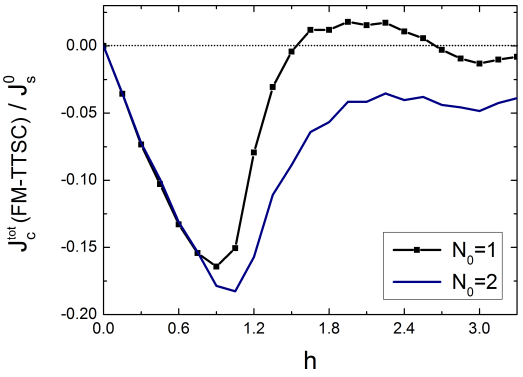

Figure 5.11: Summation of all contributions of the charge current $J_c(i)$ inside the TTSC region for various strengths of the exchange field $|h|$ and normalized by its value for the vaccum-TTSC interface. The results are obtained from the spin-polarised current $J_{\uparrow}$ and $J_{\downarrow}$ shown in the Fig. 5.10 for configurations with one and two gapless edge states, i.e. $N_0 = 1$ and $N_0 = 2$ respectively, the exchange field being perpendicular to the d-vector ($\theta = 0°$).

states in the FM but connected to the spatial dependence of the spectral weight renormalization of the helical states. These characteristics are fundamentally common to the $N_0 = 1$ and $N_0 = 2$ TTSC.

Among the $N_0 = 1$ and $N_0 = 2$ differences we point out that they emerge mainly in the strong FM regime where the charge currents oscillates with a sign change in the ferromagnetic region for $N_0 = 1$ while it keeps the same sign (flow) for the case of $N_0 = 2$ TTSC. Another distinct aspect is that the amplitude of the charge current at the interface within the TTSC domain is more sensitive to the exchange for the $N_0 = 1$ than the $N_0 = 2$ helical superconductor.

For further pinpointing the differences between the charge currents response for the $N_0 = 1$ and $N_0 = 2$ helical superconductors, it is useful to investigate the integrated amplitude within the TTSC region of the heterostructure. As we have done previously for the spin currents, we evaluate the total charge current $J_c^{tot} = J_\uparrow^{tot} + J_\downarrow^{tot}$ flowing in the TTSC region and compare its evolution as a function of the exchange field in the FM for the $N_0 = 1$ and $N_0 = 2$ cases (Fig. 5.11). The spin-polarized currents have been already shown in Fig. 5.10.

Here, due to the presence of the spatial oscillatory behaviour, the results of J_c^{tot} cannot be easily inferred from the variation of $J_c(i_x)$. Indeed, for small values of the exchange field, i.e. in the range $h = 0t$ to $h = 1.0t$, it is interesting to see that the charge current is insensitive to the number of helical modes. J_c^{tot} reaches its maximum at about $h = 1.0t$ where the ferromagnet magnetization approaches about the half of the fully polarized configuration. Then, due to the reduction of the mixing between the ferromagnetic and the helical modes, J_c^{tot} decreases when the exchange field moves towards the strong ferromagnet limit.

In this range we can observe the main difference between the two helical cases, i.e. for $h > 1.5t$. While the charge current remains non zero and almost constant for $N_0 = 2$ when the magnetization gets to the half-metallic limit, for the $N_0 = 1$ case it gets smaller with a sign change accompanied by an oscillatory behaviour for large exchanges $h > 1.5t$. This qualitative difference can be understood by looking at the spectral functions for spin-up and spin-down electrons, Figs. 5.6 and 5.7. Indeed, by approaching the half-metallic regime for $N_0 = 1$, the Fermi surfaces of the spin-up and spin-down electrons are such that the edge states, with momentum $-\pi/2 < k_y < \pi/2$, are mostly not hybridizing with the ferromagnetic spectra. Hence, $J_\uparrow^{tot}$ and $J_\downarrow^{tot}$ are close to the expected values for the the vacuum-TTSC interface configuration. However, such a decoupling does not occur for $N_0 = 2$. The majority spin edge states close to $k_y = \pm\pi$ are mixed with the ferromagnetic electronic states close to the Fermi level. Therefore, $J_\uparrow^{tot}$ tends to diminished and there is no compensation in amplitude between the opposite spin-polarized currents with a resulting net charge current flowing at the interface.

These results for FM magnetization that is perpendicular to the plane indicates that the evolution of the integrated charge current at the interface with respect to the strength of the exchange field can give important hints to discern between superconductors having different number of helical modes at the edge.

5.5 Tuning of the Edge Currents: Magnetization coplanar to the $\vec{d}$-vector

The spin and charge currents at the FM-TTSC interface exhibit a behaviour that includes new effects when the magnetization is coplanar to the spin-triplet $\vec{d}$-vector order parameter. Since the components of the $\vec{d}$-vector have different orbital character with respect to the interface orientation, the spin content of the helical states depends on the transverse momentum along the interface. Hence, the coupling of the ferromagnetic spin-exchange to the helical states with x and y zero spin projections naturally leads to an anisotropic response and to a momentum-dependent modification of the electronic spectrum. We remind that the physical configuration of the FM-TTSC heterostructure analysed here has an interface orientation that is perpendicular to the x component of the $\vec{d}$-vector with a p_x orbital symmetry.

The first distinctive feature of a ferromagnetic exchange that is coplanar to the $\vec{d}$-vector is provided by the up-down symmetry of the electronic spectrum. Hence, the relation $A_\uparrow(i_x, k_y)(\omega) = A_\downarrow(i_x, -k_y)(\omega)$ hold at any site of the system and for all strength of the exchange field h. It leads to a spin resolved current $J_\uparrow(i_x) = -J_\downarrow(i_x)$ and, therefore, a vanishing charge current at the interface, $J_c(i_x) = 0$. We present in Fig. 5.12 the comparison between the spatial variation of the z-polarized spin current for two orientations of the exchange and a representative value of $h = 0.6t$ for $\mathrm{N}_0 = 1$ and $\mathrm{N}_0 = 2$ TTSC. We can observe that, due to the proximity effect, the spin current is oscillating in the ferromagnetic region. Indeed, an in-plane magnetization acts as a pair-breaking of the Cooper pairs that penetrate into the FM and in turn induces oscillations in the spin current. Due to the xy symmetry of the pair-breaking mechanism, the period of the oscillations does not depend on the orientation of the in-plane magnetization and it is weakly linked to the number of helical modes. When h is increasing, the period of the oscillations shrinks and the amplitude is suppressed, such that there is no induced spin current in the ferromagnetic region for the regimes of intermediate-strong FM.

On the other hand, the spatial variation of J_s^z in the TTSC is very similar to the case at $\theta = 0$ with a magnetization that is perpendicular to the $\vec{d}$-vector. Indeed, J_s^z reaches its maximal value at the the boundary of the TTSC while it decreases over a distance $\xi_{sc} = 20$ sites in the TTSC side. Additionally, for both cases $\mathrm{N}_0 = 1$ and $\mathrm{N}_0 = 2$, we can see that the spin current along the interface is slightly larger when the magnetization is

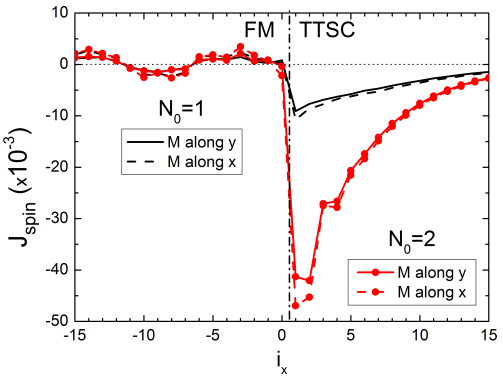

Figure 5.12: Spatial variations of the y-polarized spin current $J_s^y(i)$ along the FM-TTSC interface for various strengths of the exchange field $|h|$, plotted for the TTSC configurations $\mathrm{N}_0 = 1$. The magnetization is oriented along the y-direction, i.e. $\theta = 0°$ and $\phi = 0°$. The dashed-dotted line represents the interface between the FM and TTSC regions.

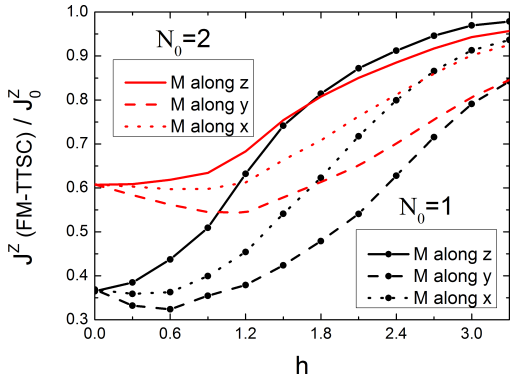

Figure 5.13: Summation of all contributions of the z-polarized spin current $J_s^Z(i)$ inside the TTSC region for various strengths of the exchange field $|h|$ and normalized by its value for the vaccum-TTSC interface. The results are showed for configurations $N_0 = 1$ (solid line) and $N_0 = 2$ (dashed line). The magnetization is oriented in-plane, i.e. $\theta = 90°$.

parallel to d_x than to d_y. This effect is due to the gap opening at zero momentum for the Majorana states associated with the p_x orbital symmetry of the d_y component of the spin-triplet order parameter (Fig. 5.8). The anisotropy is small for the weak FM regime because the edge states are completely mixed close to $k_y = 0$ and hence the tendency to split of the Majorana modes cannot fully contribute to the decrease of the spin current.

The in-plane orientation's dependence of the spin current for coplanar magnetization is significantly linked to the intensity of the FM and to the number of helical modes in the TTSC. In order to emphasize this point, we present in Fig. 5.13 the evolution of the z-polarized spin current J_Z^{tot} integrated within the TTSC region as a function of the exchange field h, for several orientation of the magnetization in the ferromagnet. As a general observation, we can distinguish three different regimes for the spin-current response when the magnetic exchange is tuned from weak to strong FM.
For the case of weak FM and a magnetization that is longitudinal to the d_x component is basically flat independently of the number of helical modes. On the other hand, an orientation that is parallel to d_y generally leads to a decrease of the spin-current. The

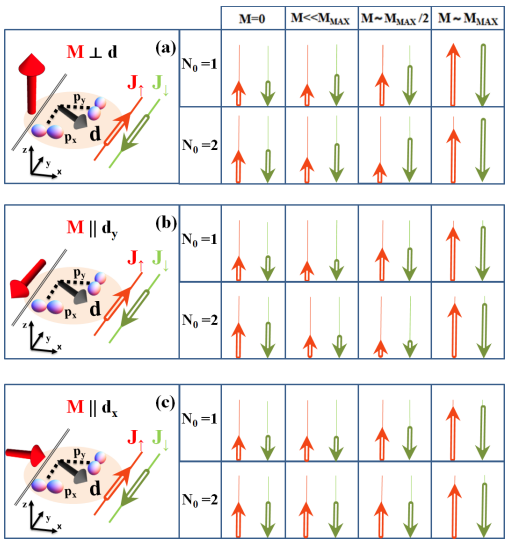

Figure 5.14: Conclusive sketch illustrating the strengths of the spin-up (red arrows) and spin-down (green arrows) currents at the N-TTSC ($M = 0$) and FM-TTSC interfaces, for weak ($M \ll M_{max}$), intermediate ($M \sim M_{max}/2$) and strong ($M \sim M_{max}$) regimes. They are shown for different orientations of the ferromagnetic magnetization and number N_0 of helical modes. The thin lines depict the maximal strength of the spin-polarized currents at the vacuum-TSC interfaces. Finite spin currents are present for each configurations and charge currents are induced only in the configuration (a) when $J_\uparrow \neq -J_\downarrow$.

increase in the exchange amplitude leads to an upturn of the spin-current at lower values of the magnetization for the case $N_0 = 1$ than for $N_0 = 2$ TTSC.
The particularity of the $N_0 = 2$ TTSC is that, to achieve a spin-current that is larger than the value of the normal-TTSC interface, one needs to approach the regime of intermediate-strong FM at any orientation of the magnetization coplanar to the $\vec{d}$-vector. On the contrary, while approaching the half-metallic FM configuration, the spin-current response of the FM-TTSC does not exhibit significant differences between the two case, both qualitatively and quantitatively.

5.6 Conclusion

We have studied in this chapter the proximity effects at the interface of ferromagnet - helical spin-triplet superconductors heterostructures by means of the tight-binding lattice model and the self-consistent evaluation of the spin-triplet order parameters. We briefly discussed the spatial variations of the order parameters at the interface for various magnetization orientations. We have seen that, similarly to the chiral TSC, the magnetic configuration can be or not pair breaking for the spin-triplet Cooper pairs, producing in the first case oscillations of the induced pair correlations. However, in contrast to the chiral TSC, the components of the in-plane $\vec{d}$-vector have different orbital symmetries. It leads thus to different behaviours for the p_x- and p_y-wave order parameters.
Our main results concern the capacity of tuning the spin and charge currents as well as the individual spin polarized component J_σ by means of the number of helical modes in the spin-triplet superconductor and the amplitude-orientation of the ferromagnetic exchange with respect to the $\vec{d}$ vector. The presence of two helical channels allows to have opposite trends in the current response of the majority and minority spin channels that are quantitatively and qualitatively different with respect to the single pairs of helical modes, as sketched in Fig. 5.14, in all regimes from weak-to-strong ferromagnet. The anisotropic hybridization of the FM states with the helical modes is shown to be the key dynamical parameter that controls the current behaviour. While our study has been performed for a specific shape of the FM Fermi surface, the unveiled mechanisms allow to immediately generalize the current response to a suitably designed FM material with single or multiple bands hybridizing with the helical modes.
Due to the symmetry of the superconductor, we find that the current polarization is mainly perpendicular to the $\vec{d}$-vector, and two main behaviours can be achieved with flat and monotonous trend depending on the strength of the FM magnetization. The presence of multiple helical modes at the edge makes generally more difficult to recover the capacity of carrying spin current with an amplitude that is comparable to that observed at the edge of the TTSC with the vacuum. The two-mode helical TTSC can exhibit an almost flat behaviour with a magnetization being not longitudinal to the $\vec{d}$-vector component and an orbital symmetry that is perpendicular to the interface (i.e. d_y for the analysed configuration). For a magnetization that is transversal to the $\vec{d}$-vector, the flatness is generated by a peculiar compensation of the opposite spin-polarized currents. On the contrary, an exchange that is able to split the time-reversal Kramers pairs tends to open a gap in the helical electronic spectra and results into a suppression of the spin-current. The $N_0 = 2$ TTSC tends to amplify this effect and the spin-current keeps decreasing for

a large range of exchange fields.
The orientation dependence underlines a strong difference when the FM-TTSC heterostructure has an FM magnetization that is perpendicular to the $\vec{d}$-vector exhibiting a nonvanishing total charge current that can flow together with the spin current. We find that the charge current amplitude is maximal for intermediate strength of the FM and exhibits the same response at weak FM independently of the number of helical modes. While the integrated current has a net flow within the TTSC region close to the interface, the spatial dependence of the charge current shows a complex sign changing profile that changes with the distance from the interface. The spatial dependence of the current reveals the subtle interplay behind the mixing of the magnetic and helical states at the interface. Finally, the capacity of carrying spin current in the FM depends on the orientation of the magnetization and can be even counterpropagating with respect to that flowing in the TTSC.

General Conclusion

We have presented in this thesis various novel aspects of proximity effects in heterostructures made of itinerant ferromagnets (FM) and chiral (TSC) or helical (TTSC) spin-triplet superconductors. The numerical studies were exclusively performed using an extended-tight-binding lattice model together with a non-local coupling between fermionic particles leading to the existence of a condensate state in the mean field approximation. The superconducting order parameters were constructed by means of the usual pair correlation functions and computed self-consistently by solving the Bogoliubov-De Gennes equations, giving us information about the spatial variations of the magnetic and superconducting order parameters on the atomic scale. Due to spin-triplet character of the Cooper pairs formed in such materials, the physical mechanisms at the interface is much richer than in junctions involving spin-singlet superconductors (SC). Differently from the latter, we have shown that all the proximity effects, and therefore physical observables, are depending directly on the orientation of the magnetization in the ferromagnet.

In this regards, the magnetization is found to be totally, partially or not at all pair-breaking for the spin-triplet Cooper pairs depending on its orientation with respect to the $\vec{d}$-vector, which characterised the superconducting state. When the exchange field is aligned parallel to the $\vec{d}$-vector, the configuration is pair-breaking as for spin-singlet junctions. It leads to a perfect oscillating behaviour of the induced pairing amplitudes in the ferromagnetic region, which are periodically changing sign. On the other hand, a magnetization perpendicular to the $\vec{d}$-vector is not pair-breaking and, therefore, the pairing amplitudes decay monotonously in the ferromagnet, similarly than at the N-SC and N-TSC interfaces. Between both configurations, the magnetization is partially pair-breaking. The pairing amplitudes still exhibit oscillations but become negative only if the relative angle with the $\vec{d}$-vector is inferior to about $\theta < 45°$.
Furthermore, we have shown that the magnetization orientation not only alters the behaviour of the induced pairing amplitudes in the ferromagnet, but also modifies slightly the cancellation of the order parameters in the superconducting region. Focusing on three-dimensional chiral interfaces, we found by computing the free energy of the interface that this modification, together with an electronic reconstruction of the energy spectrum at the interface, energetically favours a configuration where the magnetization is perpendicular to the $\vec{d}$-vector regardless of its strength. We extended next this results by considering a spin-active interface between the ferromagnetic and the superconducting regions, i.e. by considering the magnetization orientation of one layer between both regions to be independent to the ferromagnet bulk magnetization. We found that the spin-triplet superconductor always tends to favour a magnetic configuration such that both magnetizations

in the bulk and at the interface are perpendicular to the $\vec{d}$-vector, but with opposite directions. The subtitle reconstruction of the electronic density at the interface showed that this antiparallel configuration is finally favoured at the FM-TSC interface especially for weak to intermediate ferromagnets. On the other hand, if the magnetization in the bulk ferromagnet is fixed along one out-of-plane direction, the chiral superconductor, which tends to favour the magnetization to lie in-plane, induces a misalignment between two magnetizations. In other words, we predicted that a spin-active interface, i.e. a misalignment between the magnetization at the interface compare to its bulk orientation, can spontaneously be induced at the FM-TSC interface due to the spin-triplet character of the Cooper pairs.

The spin-polarisation at the three-dimensional chiral FM-TSC interface, taking into account its modification inside the ferromagnet region as well as the spin-polarisation induced in the superconducting side, has been also investigated. We have found the latter to be highly dependent on the amplitude and direction of the magnetization in ferromagnetic bulk. In the case of an exchange field parallel to the $\vec{d}$-vector, the induced spin-polarisation inside the TSC is found to be parallel or antiparallel to the spin-polarisation in the FM bulk for strong or weak exchange fields, respectively. In order to highlight the influence of the spin-triplet state, particular attention has been paid to the difference of the total spin-polarisation between the FM-N and the FM-TSC interfaces with similar magnetic configurations. Accordingly to the spatial variations, we found that the presence of TSC tends to decrease (increase) the z-spin-polarisation for weak (strong) exchange field, for all orientations, compare to the spin-polarisation measured at FM-N interface. On the other hand, although the effect is one order of magnitude smaller, the in-plane spin-polarisation is always enhanced in the presence of the superconducting state. As we pointed out, the results can be used to determine indirectly the orientation of the $\vec{d}$-vector, although we expect the variations to be small compare to the total spin-polarisation. Nevertheless, the proximity effects in FM-TSC should depend on the orientation of the exchange field in the ferromagnet bulk and, therefore, should be experimentally observed at such interface.

The consequences of the pair-breaking effect on the spin-triplet Cooper pairs have been in details analysed in the charge Josephson current in two-dimensional chiral TSC-FM-TSC junctions. In particular, we focused on the determination of the state of the junction for various configurations of the ferromagnetic barrier. The latter is defined as being the superconducting phase difference ϕ_{SC} between the two TSC regions which minimized the free energy and is directly linked to the sign, i.e. the flow direction, of the critical Josephson current.

By first considering the magnetization to be parallel to the $\vec{d}$-vector, i.e. for a pair-breaking configuration, the junctions has been found to exhibit a phase diagram made of 0- and π-state domains appearing periodically as a function of the magnetization strength and the length of the ferromagnetic barrier. This behaviour is therefore identical to what can be observed in SC-FM-SC junctions. On the other hand, the junctions can only exhibits a 0-state if the magnetization is not at all pair-breaking, i.e. when it is perpendicular to the $\vec{d}$-vector. Between both configurations, the magnetization is partially pair-breaking and it has been found that the TSC-FM-TSC junction can exhibit 0-π transitions according to the relative angle between the magnetization and the $\vec{d}$-vector. We have shown that the

critical angle for which such transitions occur depend on the length of the barrier and the strength of the magnetization and ranges in $20^\circ \lesssim \theta_c \lesssim 45^\circ$. We emphasized in particular that the existence of the phase transitions could be directly related to the change of sign of the induced pairing amplitudes when the latter is oscillating. As we have mentioned, these behaviours appeared to be in good agreement with the recent quasiclassical studies but differ from the tunnelling junctions, in particular for the determination of the critical angle. The extension of our analysis to three-dimensional TSC-FM-TSC junctions has shown that the general behaviour concerning the 0-π transitions remains qualitatively unchanged although the critical angle is found to be smaller in the latter case due to the slightly modifications of the induced pairing amplitudes.

A drastic modification of the phase diagram has been observed for junction with spin-active interfaces. This effect is especially interesting since we have seen that the TSC tends to orientate spontaneously the magnetization perpendicular to the $\vec{d}$-vector, i.e. in the plane. By considering the bulk and interface magnetizations to be parallel and perpendicular to the $\vec{d}$-vector , respectively, we found that the spin-active interfaces generally tend to suppress the π-state domains. This effect has been found particularly distinctive for intermediate and strong ferromagnets. Surprisingly, we also found that the critical angle can be increased in such configuration, showing a more subtle relation between the spatial variations of the order parameters and the state of the junctions.

The variations of the critical current, which is the most common way to experimentally probe the state of the junctions, were finally discussed as a function of the barrier length. In clean junctions with a magnetization parallel to the $\vec{d}$-vector, without spin-active interface, it has been shown that the 0-π transitions could be identified thanks to the minima of the critical current, which oscillates periodically as a function of the barrier length. Therefore, such observations make indirectly possible the identification of the state of the junctions. On the other hand, no oscillations have been found when the magnetization is perpendicular to the $\vec{d}$-vector, as for usual SC-N-SC. This modification of the behaviour in the critical current is characteristic to the spin-triplet ferromagnetic junctions. Nevertheless, we have highlighted the fact that oscillations can also be present in the critical current without being associated to 0- and π-states. For this reason, the experimental identification of the state of the junctions need to be closely related to the prediction made by the theoretical models. Furthermore, the oscillations of the critical current as a function of the barrier length are found to be greatly altered by the presence of spin-active interfaces between the ferromagnetic and superconducting regions. Indeed, although the 0- and π-states can be still identified, we have shown that they induce a strong modification of the oscillations which are not periodic any longer. Additionally, we found the critical current to have a non monotonic suppression as the length of the barrier increases.

Finally, we inspected the influence of the magnetization on the edge states of an helical superconductors, characterised by an in-plane $\vec{d}$-vector and exhibiting dissipationless spin current at the interface. We have shown that the presence of an exchange field coplanar to the $\vec{d}$-vector not only modifies the spin current but can also induces a charge current. Remarkably, we predicted that the tuning of the charge current with respect to the strength of the magnetization depends strongly on the number of helical mode present at the interface for strong ferromagnet. In this case, the charge current is usually suppressed

when one pair of gapless edge states are present while it remains finite when two pairs are present. Moreover, orienting the magnetization perpendicular to the $\vec{d}$-vector modifies the overall behaviour. Hence, such magnetic configuration tends to decrease the spin current while, as expected, no charge current are induced at the interface. We have shown that the alterations of the spin-polarised currents are closely connected to the electronic reconstruction of the energy spectrum at the interface. In particular, the hybridization of the gapless edge states with the Fermi surfaces for spin up and spin down electrons in the ferromagnet directly tunes the currents along the edge of the helical spin-triplet superconductor.

As a final conclusion, we showed that the interplay between the magnetization and the spin-triplet superconducting states is highly nontrivial. The magnetization can be used to induce and to tune charge current at the edge of helical superconductor, to probe the orientation of the $\vec{d}$-vector and to switch the state of the Josephson junction by changing its orientation. Therefore, our analysis gave not only a deeper understanding of the mechanisms at such interface, but also predicted novel proximity effects which are present only in the case of spin-triplet superconductors. It is important to emphasize that the experimental observations of these specific proximity effects due to the spin-triplet nature of the Cooper pairs can be seen not only as key evidences of the spin-triplet pairing in the superconducting materials but also has a direct probe to determine the orientation of the $\vec{d}$-vector, i.e. to determine the topological nature of the superconducting state.

The experimental achievement of junctions made of Sr_2RuO_4 thin films, which are believed to exhibit a chiral spin-triplet pairing, make very interesting the theoretical investigation of novel proximity effects at the interface of ferromagnet and spin-triplet superconductors. New short term perspectives would include a more refined study of the magnetic profile at the interface, taking especially into account the spin-orbit coupling since it has been recently shown that the influence of such interaction could be more important in Sr_2RuO_4 than previously expected. Moreover, a more complete investigation should include an analysis of the spin-polarisation also at the interface with the helical superconductor. Still, in both cases, additional dipolar field effects and Meissner currents should be taken into account to obtain a more accurate estimation of the measurable spin-polarisation.
In the case of the proximity effects at the interface of the helical spin-triplet superconductors, one of the major issue is to estimate how robust they are with respect of disorder. Indeed, gapless edge states appearing at the boundaries of the topological superconductor can be either preserved or destroy in presence of roughness, which is the case in our system when a even number of edge states are present. Hence, following our results, the tuning of the charge and spin current with the magnetization should be confirmed in a system having a rough interface, which could be concretely done with our model by adding an additional scattering term.

Appendix A

Bogoliubov-De Gennes Equations and Correlation Functions

In the following, we present in detail the derivation of the two-dimensional mean field extended-tight-binding model that we use to describe the superconductor in Chapter 1. Periodic boundary conditions are applied in the direction parallel to the interface. The study of the interface is then done by solving self-consistently the quasi one-dimensional Bogoliubov-De Gennes (BdG) equations to obtain the eigenvectors and the excitation spectrum of the system. The procedure consists in diagonalized the Hamiltonian to compute the correlations functions $F_{ij}^{\sigma\sigma'}$ thanks to the coherence factors, as defined in Eq. B.2. We finally derive the gap equations on the lattice verified by the superconducting gaps defined in Eqs.1.28 - 1.33.

Mean Field Hamiltonian Let us first recall the form of the mean field Hamiltonian of the extended-tight-binding model that we obtain in Chapter 1, Eq. 1.26. We obtained, without the energy constant E_0, that

$$\begin{aligned} H_{HF} = & - \sum_{\langle ij\rangle,\sigma} t_{i\sigma}(c_{i\sigma}^{\dagger}c_{j\sigma} + h.c.) - \mu \sum_{i\sigma} n_{i\sigma} \\ & + \sum_{\langle ij\rangle} V_i[\ F_{ij}^{\uparrow\downarrow} c_{j\downarrow}^{\dagger} c_{i\uparrow}^{\dagger} + F_{ij}^{\downarrow\uparrow} c_{j\uparrow}^{\dagger} c_{i\downarrow}^{\dagger} + h.c.\ ] \\ & + \sum_{\langle ij\rangle,\sigma} V_i'[\ F_{ij}^{\sigma\sigma} c_{j\sigma}^{\dagger} c_{i\sigma}^{\dagger} + h.c.\ ] \end{aligned} \tag{A.1}$$

where the correlation functions are defined such that

$$F_{ij}^{\sigma\sigma'} \ = \ \langle c_{i\,\sigma} c_{j\,\sigma'} \rangle \tag{A.2}$$

and where i and j are sites on the lattice, μ is the chemical potential, V_i is the nearest-neighbour attraction between two electrons of opposite spins on the site i and V_i' is the nearest-neighbour attraction between two electrons with same spins on the site i. We can note that the index i -and j- represents the spatial coordinates of electrons in the x- and y- directions on the two-dimensional lattice. Within our notation, $i = (i_x, i_y)$ and $j = (j_x, j_y)$.
Before to derive the BdG equations, we can simplify the expression by noticing that the terms including the correlation functions $F_{ij}^{\downarrow\uparrow}$ and $F_{ij}^{\uparrow\downarrow}$ in the Eq. A.1 are equivalent. Indeed, we obtain for the first term in V_i that

$$\begin{aligned}\sum_{\langle ij\rangle} V_i F_{ij}^{\downarrow\uparrow} c_{j\uparrow}^\dagger c_{i\downarrow}^\dagger = & \sum_{\langle ij\rangle} V_j F_{ji}^{\downarrow\uparrow} c_{i\uparrow}^\dagger c_{j\downarrow}^\dagger \\ = & -\sum_{\langle ij\rangle} V_j F_{ji}^{\downarrow\uparrow} c_{j\downarrow}^\dagger c_{i\uparrow}^\dagger \\ = & \sum_{\langle ij\rangle} V_j F_{ij}^{\uparrow\downarrow} c_{j\downarrow}^\dagger c_{i\uparrow}^\dagger. \end{aligned} \tag{A.3}$$

Moreover, the pairing amplitude being constant in the whole superconducting region, i.e. $V_i = V$ for i, we find that

$$\sum_{\langle ij\rangle} V F_{ij}^{\downarrow\uparrow} c_{j\uparrow}^\dagger c_{i\downarrow}^\dagger = \sum_{\langle ij\rangle} V F_{ij}^{\uparrow\downarrow} c_{j\downarrow}^\dagger c_{i\uparrow}^\dagger. \tag{A.4}$$

The two terms being equal, we only keep the second one in order to simplify the following derivations although, obviously, both terms must be present in the final BdG equations. Moreover, for clarity, it is convenient to define a new notation for the opposite-spin bond pairing as

$$F_{ij} \equiv F_{ij}^{\uparrow\downarrow}. \tag{A.5}$$

Finally, since the two-electrons pairing occurs only between the first nearest neighbours, it is useful to introduce the notation as

$$F_i^{x\pm} = F_{i,i\pm\hat{x}}, \tag{A.6}$$
$$F_i^{y\pm} = F_{i,i\pm\hat{y}}, \tag{A.7}$$
$$F_{i,\sigma\sigma}^{x\pm} = F_{i,i\pm\hat{x}}^{\sigma\sigma}, \tag{A.8}$$
$$F_{i,\sigma\sigma}^{y\pm} = F_{i,i\pm\hat{y}}^{\sigma\sigma}, \tag{A.9}$$

where $\hat{x}$ and $\hat{y}$ denote the distance between two sites in the x- and y-directions, respectively. In the following, we write explicitly the summation over the nearest neighbours $\langle ij\rangle$ using this notation. For clarity of exposition, we will dissociate three parts of the Hartree-Fock Hamiltonian which include a first nearest neighbours pairing. The hopping term H_t, the opposite spin pairing H_V and the equal spin pairing $H_{V'}$ are respectively

$$H_t = -\sum_{i\sigma} t_{i\sigma}[\ c_{i\sigma}^\dagger c_{i+a_x,\sigma} + c_{i\sigma}^\dagger c_{i-a_x,\sigma} + c_{i\sigma}^\dagger c_{i+a_y,\sigma} + c_{i\sigma}^\dagger c_{i-a_y,\sigma} + h.c.\ ], \tag{A.10}$$

$$\begin{aligned} H_V = \sum_i V_i[\ & F_i^{x+} c_{i+a_x,\downarrow}^\dagger c_{i\uparrow}^\dagger + F_i^{x-} c_{i-a_x,\downarrow}^\dagger c_{i\uparrow}^\dagger \\ & + F_i^{y+} c_{i+a_y,\downarrow}^\dagger c_{i\uparrow}^\dagger + F_i^{y-} c_{i-a_y,\downarrow}^\dagger c_{i\uparrow}^\dagger + h.c.\ ], \end{aligned} \tag{A.11}$$

$$H_{V'} = \frac{1}{2}\sum_{i\sigma} V'_i[\ F^{x+}_{i,\sigma\sigma}c^\dagger_{i+a_x,\sigma}c^\dagger_{i\sigma} + F^{x-}_{i,\sigma\sigma}c^\dagger_{i-a_x,\sigma}c^\dagger_{i\sigma} + F^{y+}_{i,\sigma\sigma}c^\dagger_{i+a_y,\sigma}c^\dagger_{i\sigma} + F^{y-}_{i,\sigma\sigma}c^\dagger_{i-a_y,\sigma}c^\dagger_{i\sigma} + h.c.\ ]. \tag{A.12}$$

Fourier Transformations We adopt periodic boundary conditions in the direction parallel to the interface, i.e. the y-direction for the two-dimensional system, and we perform the Fourier transformations along this direction. In this formalism, the fermionic creation and annihilation operators become

$$c_{i\sigma} = \frac{1}{\sqrt{L_y}}\sum_{k_y} c_{i_x k_y\sigma}e^{ik_yL_y}, \tag{A.13}$$

$$c^\dagger_{i\sigma} = \frac{1}{\sqrt{L_y}}\sum_{k_y} c^\dagger_{i_x k_y\sigma}e^{-ik_yL_y}, \tag{A.14}$$

where L_y is the number of sites in the y-direction and the index i_x denotes the site position on the lattice along the x-direction. Once again for clarity, we avoid in the following to write the labels x and y, unless it is necessary. Instead, we shall consider the simplified notation

$$c_{ik\sigma} \equiv c_{i_x k_y\sigma}\ .$$

We follow now the usual procedure for the derivation of the Fourier transformations of the Hamiltonians Eqs. A.10 - A.12. Let us first derive the Fourier transformations for the hopping term Hamiltonian. Inserting Eqs. A.13 - A.14 in Eq. A.10, we find that

$$\begin{aligned} H_t &= \sum_\sigma\sum_{x_iy_i}\sum_{kk'}\frac{t_{i\sigma}}{L_y}[\ c^\dagger_{x_ik\sigma}c_{x_i+a_x,k'\sigma}e^{-i(k-k')y_i} + c^\dagger_{x_ik\sigma}c_{x_i-a_x,k'\sigma}e^{-i(k-k')y_i} \\ &+ c^\dagger_{x_ik\sigma}c_{x_i,k'\sigma}e^{-i(k-k')y_i}e^{ik'a} + c^\dagger_{x_ik\sigma}c_{x_i,k'\sigma}e^{-i(k-k')y_i}e^{-ik'a}\ ] + h.c. \end{aligned} \tag{A.15}$$

By noticing that for a function $f(k,k')$ independent of y_i we have

$$\frac{1}{\sqrt{L_y}}\sum_{kk'}\sum_{y_i} f(k,k')e^{-i(k-k')y_i} = \sum_k f(k,k')\delta_{k,k'} \tag{A.16}$$

we obtain

$$H_t = -\sum_{ijk\sigma} c^\dagger_{ik\sigma}c_{jk\sigma}[\ 2t^y_{i\sigma}cos(ka)\delta_{ij} + t^x_{i\sigma}(\delta_{i,j+1} + \delta_{i,j-1})\ ], \tag{A.17}$$

where we make the distinction between the hopping terms t^x and t^y in the x- and y-direction, respectively. For the two other terms in the Hamiltonian, Eqs. A.11 and A.12, we obtain however that the Fourier transformation is non equal to zero only for $k' = -k$, which is related to a non vanishing pairing amplitude between two electrons with opposite

wavevector as expected for the Cooper pairs. The two terms become after the Fourier transformations

$$\begin{aligned} H_V &= \sum_{ijk} V_i[\ c_{i-k\uparrow}c_{jk\downarrow}(F_i^{x+*}\delta_{j,i+1} + F_i^{x-*}\delta_{j,i-1} + (F_i^{y+*}e^{ika} + F_i^{y-*}e^{-ika})\delta_{ij}) \\ &+ c^\dagger_{ik\downarrow}c^\dagger_{j-k\uparrow}(F_j^{x+}\delta_{i,j+1} + F_j^{x-}\delta_{i,j-1} + (F_i^{y+}e^{-ika} + F_i^{y-}e^{ika})\delta_{ij})\ ] \end{aligned} \tag{A.18}$$

and

$$\begin{aligned} H_{V'} &= \frac{1}{2}\sum_{ijk} V_i'[\ c_{i-k\sigma}c_{jk\sigma}(F_{i,\sigma\sigma}^{x+*}\delta_{j,i+1} + F_{i,\sigma\sigma}^{x-*}\delta_{j,i-1} - 2isin(-ka)F_{i,\sigma\sigma}^{y+*}\delta_{ij}) \\ &+ c^\dagger_{ik\sigma}c^\dagger_{j-k\sigma}(F_{j,\sigma\sigma}^{x+}\delta_{i,j+1} + F_{j,\sigma\sigma}^{x-}\delta_{i,j-1} - 2isin(ka)F_{i,\sigma\sigma}^{y+}\delta_{ij})\ ]. \end{aligned} \tag{A.19}$$

In order to have compact and clear expressions, it is useful to notice that $F_{i,\sigma\sigma}^{y+} = -F_{i,\sigma\sigma}^{y-}$. Indeed, we can develop the expression as

$$\begin{aligned} F_{i,\sigma\sigma}^{y+} &= \langle c_{i\sigma}c_{i+1,\sigma}\rangle \\ &= -\langle c_{i+1,\sigma}c_{i,\sigma}\rangle \\ &= -\langle c_{j\sigma}c_{j-1,\sigma}\rangle \quad \text{with j = i + 1} \\ &= -F_{j,\sigma\sigma}^{y-}\ . \end{aligned} \tag{A.20}$$

The statement is demonstrated by having in mind that, in the y-direction, the bond pairing is constant, i.e. that $F_{i_y,\sigma\sigma}^{y\pm} = F_{j_y,\sigma\sigma}^{y\pm}$. It is obviously not the case in the x-direction.

Bogoliubov-De Gennes Equations We follow the method developed by Bogoliubov and Valentin in order to diagonalise the total Hamiltonian and which provides information about the energy spectrum of the system as well as the the excited states. The method consist in finding the operators α_k such that

$$H = E_0 + \sum_k \epsilon_k\ \alpha_k^\dagger\alpha_k, \tag{A.21}$$

ϵ_k being the energy excitations of the system and α_k being a linear combination of the operators c_k and $c^\dagger_{-k}$

$$\alpha_k = \sum_k (A_k c_k + B_k c^\dagger_{-k}). \tag{A.22}$$

For exact solvable systems, ϵ_k, A_k and B_k can be expressed analytically. However, they have to be numerically computed in more complex problem like at the interface with a normal or ferromagnetic metal without additional quasiclassical approximation. An elegant way to perform the diagonalisation is to write the Hamiltonian in a matrix form, also called Nambu form. By considering the operator basis

$$D^\dagger_{i,k} = [\ c^\dagger_{ik\uparrow}, c^\dagger_{ik\downarrow}, c_{ik\uparrow}, c_{ik\downarrow}\ ], \tag{A.23}$$

we can rewrite the Hamiltonian as a summation of matrices

$$H = \sum_k \sum_{i,j} D^\dagger_{i,k} \hat{h}_{ijk} D_{j,k}. \tag{A.24}$$

The matrix $\hat{h}_{ijk}$, with dimension of $\dim(\mathrm{D_i}) \cdot \dim(\mathrm{D_j}) = 4 \cdot 4$, represents the interaction between the sites i and j. According to Eqs A.10 - A.12, and taking into account the exchange field Hamiltonian Eq. 1.20, we find that the matrix is expressed as

$$\hat{h}_{ijk} = \begin{bmatrix} \epsilon_{ijk\uparrow} - \mu & h^x_i + ih^y_i & \Lambda^{\uparrow\uparrow}_{ijk} & \Lambda_{ji-k} \\ h^x_i - ih^y_i & \epsilon_{ijk\downarrow} - \mu & \Lambda_{ijk} & \Lambda^{\downarrow\downarrow}_{ijk} \\ \Lambda^{\uparrow\uparrow *}_{jik} & \Lambda^*_{jik} & -\epsilon_{ijk\uparrow} + \mu & -h^x_i + ih^y_i \\ \Lambda^*_{ij-k} & \Lambda^{\downarrow\downarrow *}_{jik} & -h^x_i - ih^y_i & -\epsilon_{ijk\downarrow} + \mu \end{bmatrix} \tag{A.25}$$

$$\begin{aligned} \text{with} \quad \epsilon_{\mathrm{ijk}\sigma} &= -2t^y_{i\sigma}\cos(\mathrm{k_y})\delta_{\mathrm{i,j}} - \mathrm{t^x_{i\sigma}}(\delta_{\mathrm{i,j+1}} + \delta_{\mathrm{i,j-1}}) \ , & \text{(A.26)} \\ \Lambda_{ijk} &= V_i[\ F^{x+}_j \delta_{i,j+1} + F^{x-}_j \delta_{i,j-1} + (F^{y+}_i e^{-ika} + F^{y-}_i e^{ika})\delta_{ij}\ ], & \text{(A.27)} \\ \Lambda^{\sigma\sigma}_{ijk} &= V'_i[\ F^{x+}_{j,\sigma\sigma}\delta_{i,j+1} + F^{x-}_{j,\sigma\sigma}\delta_{i,j-1} - 2i\mathrm{sin(k)F^{y+}_{i,\sigma\sigma}}\delta_{\mathrm{ij}}\ ], & \text{(A.28)} \end{aligned}$$

where we write explicitly the three components of the exchange field $\vec{h}_i = (h^x_i, h^y_i, h^z_i)$ on the site i. The total Hamiltonian can now be written has the concatenation of the interaction between all sites as

$$H = \sum_k W^\dagger_k \hat{H}_k W_k \tag{A.29}$$

where the complete matrix is

$$\hat{H}_k = \begin{bmatrix} h_{1,1} & h_{1,2} & \cdots & h_{1,L_x} \\ h_{2,1} & h_{2,2} & \cdots & h_{2,L_x} \\ \vdots & \vdots & \ddots & \vdots \\ h_{L_x,1} & h_{L_x,2} & \cdots & h_{L_x,L_x} \end{bmatrix} \tag{A.30}$$

and the total operator basis is

$$W^\dagger_k = [\ D^\dagger_{1,k}, \cdots, D^\dagger_{i,k}, \cdots, D^\dagger_{L_x,k}\ ]. \tag{A.31}$$

It is worth noticing that the hermitian character of the matrix $\hat{H}_k$ is easily verified by the fact that

$$h_{ijk} = h^\dagger_{jik}. \tag{A.32}$$

Solutions of the Bogoliubov-De Gennes Equations The matrix is hermitian and, therefore, is diagonalized with real eigenvalues. Hence, we are looking for the solution of the BdG equations such that

$$\forall k \ , \quad \hat{H}_k \Phi_{nk} = E_{nk} \Phi_{nk} \tag{A.33}$$

where E_{nk} are the eigenvalues corresponding to the energy of the quasiparticles created by the operator $\alpha_k^\dagger$ and Φ_{nk} are the associated eigenvectors, which can be written as

$$\Phi_{nk} = \begin{bmatrix} \varphi_{1nk} \\ \vdots \\ \varphi_{ink} \\ \vdots \\ \varphi_{L_x nk} \end{bmatrix} \quad \text{with} \quad \varphi_{\text{ink}} = \begin{bmatrix} u_{ink} \\ v_{ink} \\ w_{ink} \\ x_{ink} \end{bmatrix}. \tag{A.34}$$

Here, the coefficients $u_{ink}, v_{ink}, w_{ink}$ and x_{ink} are the coherence factors equivalent to u_k and v_k found in Eqs. 1.6 - 1.7. The main difference with the latter arises from the fact that they are obtained in our model for each site of the lattice independently. While they are equal in a bulk configurations, in our case they are modified at the boundaries of the superconductor or at the interface with a metal or ferromagnet. We obtain from the diagonalisation of the Hermitian matrix $\hat{H}_k$ that

$$\hat{H}_{d,k} = P_k^{-1} \hat{H}_k P_k \tag{A.35}$$

where $\hat{H}_{d,k}$ is a diagonal matrix and P_k is the unitary matrix for the change of basis. The latter is the concatenation of the eigenvectors of $\hat{H}_k$ as

$$\begin{aligned} P_k &= [\Phi_{1k} \ \dots \ \Phi_{nk} \ \dots \ \Phi_{L_x k}] \\ &= \begin{bmatrix} u_{1,1,k} & \cdots & u_{1,n,k} & \cdots & u_{1,L_x,k} \\ v_{1,1,k} & \cdots & v_{1,n,k} & \cdots & v_{1,L_x,k} \\ \vdots & \vdots & \vdots & \ddots & \vdots \\ x_{L_x,1,k} & \cdots & x_{L_x,n,k} & \cdots & x_{L_x,L_x,k} \end{bmatrix} \end{aligned} \tag{A.36}$$

Therefore, the basis of operators α_{nk} from Eq. A.21, for which $\hat{H}_k$ is diagonal, is a linear combination of the creation and annihilation operators such that

$$\alpha_{nk} = \sum_i \left[u_{ink} c_{ik\uparrow} + v_{ink} c_{ik\downarrow} + w_{ink} c^\dagger_{i-k\uparrow} + x_{ink} c^\dagger_{i-k\downarrow} \right]. \tag{A.37}$$

The basis α_{nk} has an important meaning in such a correlated system as it is discussed in Appendix B about the Andreev reflections. Indeed, it tells us that excited states, created by the operators $\alpha^\dagger_{nk}$, are not only made of an electron or a hole, but of a linear combination of electronlike and holelike particles. The coherence factors u_{ink} (v_{ink}) and w_{ink} (x_{ink}) are associated to the probability that an electronlike and holelike states with spin up (spin down) are occupied or not. While they can be expressed analytically for a bulk BCS superconductor, they are obtained numerically after the diagonalisation in our quasi

one-dimensional model.

The inverse transformation can be used to express the usual electron and hole operators in function of the qusiparticle of the superconductor. Using the inverse matrix P_k^{-1}, we obtain that

$$c_{ik\uparrow} = \sum_n u_{ink}\alpha_{nk} \ , \tag{A.38}$$

$$c_{ik\downarrow} = \sum_n v_{ink}\alpha_{nk} \ , \tag{A.39}$$

$$c^\dagger_{i-k\uparrow} = \sum_n w_{ink}\alpha_{nk} \ , \tag{A.40}$$

$$c^\dagger_{i-k\downarrow} = \sum_n x_{ink}\alpha_{nk} \ . \tag{A.41}$$

These expressions are the main ingredient to evaluate the order parameters of the superconducting state. Indeed, using the expressions of the creation and annihilation operators with the eigenvectors of the system, we can express the bond pairing amplitudes with the coherence factors and the eigenvalues as

$$F_i^{x\pm} = \frac{1}{L_y}\sum_k \langle c_{ik\uparrow}c_{i\pm a,-k\downarrow}\rangle = \frac{1}{L_y}\sum_{nk} u_{in}x^*_{i\pm a,n}(1-f_D(E_{nk})) \ , \tag{A.42}$$

$$F_i^{y\pm} = \frac{1}{L_y}\sum_k \langle c_{ik\uparrow}c_{i-k\downarrow}\rangle = \frac{1}{L_y}\sum_{nk} u_{in}x^*_{i,n}(1-f_D(E_{nk}))e^{\mp ika} \ , \tag{A.43}$$

$$F_{i,\uparrow\uparrow}^{x\pm} = \frac{1}{L_y}\sum_k \langle c_{ik\uparrow}c_{i\pm a,-k\uparrow}\rangle = \frac{1}{L_y}\sum_{nk} u_{in}w^*_{i\pm a,n}(1-f_D(E_{nk})) \ , \tag{A.44}$$

$$F_{i,\uparrow\uparrow}^{y\pm} = \frac{1}{L_y}\sum_k \langle c_{ik\uparrow}c_{i-k\uparrow}\rangle = \frac{1}{L_y}\sum_{nk} u_{in}w^*_{in}(1-f_D(E_{nk}))e^{\mp ika} \ , \tag{A.45}$$

$$F_{i,\downarrow\downarrow}^{x\pm} = \frac{1}{L_y}\sum_k \langle c_{ik\downarrow}c_{i\pm a,-k\downarrow}\rangle = \frac{1}{L_y}\sum_{nk} v_{in}x^*_{i\pm a,n}(1-f_D(E_{nk})) \ , \tag{A.46}$$

$$F_{i,\downarrow\downarrow}^{y\pm} = \frac{1}{L_y}\sum_k \langle c_{ik\downarrow}c_{i-k\downarrow}\rangle = \frac{1}{L_y}\sum_{nk} v_{in}x^*_{in}(1-f_D(E_{nk}))e^{\mp ika} \ . \tag{A.47}$$

$$\tag{A.48}$$

using the fact that $\langle \alpha^\dagger_{nk}\alpha_{nk}\rangle = f_D(E_{nk})$, $f_D(E_{nk})$ being the Fermi-Dirac distribution. Hence, the procedure to compute the proximity effect at the interface consist in the diagonalisation of the mean field extended-tight-binding model in order to evaluate the superconducting order parameters, i.e. the pairing amplitudes which are used to construct the superconducting gap on each site of the lattice, thanks to the numeral computation of the coherence factors.

Gap Equations on the Lattice In the BCS theory, the superconducting order parameter Δ_k verifies the self-consistent gap equation which takes into account the pairing $V_{k,k'}$ between pairs of electrons, the temperature T of the system and the energy spectrum of the normal state ξ_k. It is the one of the most important equation of the model since it predicts the critical temperature T_c of the superconductor and the evolution of the gap $\Delta(T)$ with respect to the temperature. In this paragraph, we would like to develop the equivalence of the gap equations for the pair correlations functions made of electrons with opposite spin within the lattice model, equations which are used in particular to establish the phase diagram of the model, see Fig. 1.4.
Let us first recall the gap equations in momentum space derived from the BCS theory at T=0K. They are generally written in the form

$$\Delta_{k'} = \sum_{k''} V_{k'k''} F_{k''} \quad \text{with} \quad F_{k''} = \langle c_{k''\sigma} c_{-k''\bar{\sigma}} \rangle, \tag{A.49}$$

$$\Delta_k = \sum_{k'} \frac{V_{kk'} \Delta_{k'}}{2E_{k'}} \quad \text{with} \quad E_{k'} = \sqrt{\xi_{k'}^2 + |\Delta_{k'}|^2} \tag{A.50}$$

where $\xi_{\mathbf{k}}$ is the energy spectrum in the two-dimensional one-band system of the normal state

$$\xi_{\mathbf{k}} = -2t \left[\cos(k_x a) + \cos(k_y a)\right] - \mu. \tag{A.51}$$

(i) The order parameters defined in Eqs. 1.28-1.33 can be written explicitly using the Eq.A.2. In the case of the s^+-wave order parameter, we obtain

$$\Delta_s(i) = V_i \left[F_i^{x+(S)} + F_i^{x-(S)} + F_i^{y+(S)} + F_i^{y-(S)}\right] \tag{A.52}$$

$$= \frac{V_i}{4L^2} \sum_{\mathbf{k}} \langle c_{\mathbf{k}\uparrow} c_{-\mathbf{k}\downarrow} \rangle \left[e^{-ik_x a} + e^{ik_x a} + e^{-ik_y a} + e^{ik_y a}\right] \tag{A.53}$$

$$= \frac{V_i}{2L^2} \sum_{\mathbf{k}} \langle c_{\mathbf{k}\uparrow} c_{-\mathbf{k}\downarrow} \rangle \left[\cos(k_x a) + \cos(k_y a)\right] \ . \tag{A.54}$$

It is worth noticing that the order parameter Δ_s has the correct symmetry with respect to spin and momentum parities. Using the same development for the other order parameters, we find the general equality

$$\Delta_\alpha \equiv \Delta_\alpha(i) = \frac{V_i}{2L^2} \sum_{\mathbf{k}} \omega_{\alpha,\mathbf{k}} F_{\mathbf{k}} \tag{A.55}$$

where $F_{\mathbf{k}}$ is defined in Eq. A.49 and with

$$\omega_{s,\mathbf{k}} = \cos(k_x) + \cos(k_y) \ , \tag{A.56}$$

$$\omega_{d,\mathbf{k}} = \cos(k_x) - \cos(k_y) \ , \tag{A.57}$$

$$\omega_{p_x,\mathbf{k}} = i\sin(k_x) \ , \tag{A.58}$$

$$\omega_{p_y,\mathbf{k}} = i\sin(k_y) \ . \tag{A.59}$$

(ii) Combining the BCS gap equations defined in Eqs. A.49 and A.50, we obtain

$$F_{\mathbf{k}'} = \sum_{\mathbf{k}} \frac{V_{\mathbf{k}'\mathbf{k}} F_{\mathbf{k}}}{2E_{\mathbf{k}'}} \tag{A.60}$$

which, inserting in Eq. A.55, leads to

$$\Delta_\alpha = \frac{V_i}{2L^2} \sum_{\mathbf{k}} \left[\frac{\omega_{\alpha,\mathbf{k}}}{2E_{\mathbf{k}}} \cdot \sum_{\mathbf{k}'} V_{\mathbf{k}\mathbf{k}'} F_{\mathbf{k}'} \right]. \tag{A.61}$$

(iii) Let us now express the pairing coupling V_i used in our lattice model in momentum space. First of all, we have seen that V_i is a constant coupling between a lattice site $i = (i_x, i_y)$ and its first nearest neighbours. Therefore, it can be explicitly written as a function acting on the pair particle using the Kronecker delta notation

$$V_i c_{i\sigma} c_{j\sigma'} \equiv V_{ij} c_{i\sigma} c_{j\sigma'} = \frac{V_0}{4} \left[\delta_{i_x,j_x+1} + \delta_{i_x,j_x-1} + \delta_{i_y,j_y+1} + \delta_{i_y,j_y-1} \right] c_{i\sigma} c_{j\sigma'} \tag{A.62}$$

and, after Fourier transformation, we find that the pairing coupling in the momentum space is

$$V_{\mathbf{k}\mathbf{k}'} = \frac{V_0}{2L^2} \left[\cos(k_x - k'_x) + \cos(k_y - k_y) \right]. \tag{A.63}$$

It reads that

$$\sum_{\mathbf{k}'} V_{\mathbf{k}\mathbf{k}'} F_{\mathbf{k}'} = \frac{V_0}{2L^2} \sum_{\mathbf{k}'} \left[\cos(k_x - k'_x) + \cos(k_y - k'_y) \right] F_{\mathbf{k}'} \tag{A.64}$$

$$= \frac{V_0}{2L^2} F_{\mathbf{k}}. \tag{A.65}$$

(iv) Finally, we need to derive the Fourier Transformation of the pair correlations $F_{\mathbf{k}}$. We obtain that

$$F_{\mathbf{k}} = \sum_{R_i R_j} F_{ij}\ e^{i\mathbf{k}\cdot(R_i - R_j)} \tag{A.66}$$

$$= \left[F_{i_x,i_x+1}\ e^{-i_x k_x a} + F_{i_x,i_x-1}\ e^{i_x k_x a} + F_{i_y,i_y+1}\ e^{-i_y,k_y a} + F_{i_y,i_y-1}\ e^{i_y k_y a} \right] \tag{A.67}$$

$$= e^{-ik_x a} \left[F_s(i) + F_d(i) + iF_{p_x} \right] + e^{ik_x a} \left[F_s(i) + F_d(i) - iF_{p_x} \right] \tag{A.68}$$

$$+ e^{-ik_y a} \left[F_s(i) - F_d(i) + iF_{p_y} \right] + e^{ik_x a} \left[F_s(i) - F_d(i) - iF_{p_y} \right] \tag{A.69}$$

$$= 2F_s(i) \left[\cos(k_x) + \cos(k_y) \right] + 2F_d(i) \left[\cos(k_x) - \cos(k_y) \right] \tag{A.70}$$

$$+ 2iF_{p_x}(i)\sin(k_x) + 2iF_{p_y}(i)\sin(k_y). \tag{A.71}$$

The gap equations on the lattice are obtained by inserting this last result in Eq. A.61 and using the result in Eq. A.65. It leads to

$$\Delta_\alpha = \frac{V_0}{bL^2} \sum_{\mathbf{k}} \omega_{\alpha\mathbf{k}} \frac{\Delta_{\mathbf{k}}}{E_{\mathbf{k}}} \tag{A.72}$$

where $b = 4$ for the s-wave and d-wave order parameters while $b = 2$ for spin-triplet one and with

$$\Delta_{\mathbf{k}} = 2 \sum_{\alpha} \omega_{\alpha\mathbf{k}} \Delta_\alpha. \tag{A.73}$$

It is straightforward to generalise this result for a system with finite temperature from the BCS gap equations. The Eq. A.72 becomes

$$\Delta_\alpha = \frac{V_0}{bL^2} \sum_{\mathbf{k}} \omega_{\alpha\mathbf{k}} \frac{\Delta_{\mathbf{k}}}{E_{\mathbf{k}}} \tanh\left(\frac{E_{\mathbf{k}}}{2T}\right). \tag{A.74}$$

As a final remark, we can notice that all the order parameters have to be self-consistently evaluated at each steps of the procedure. Hence, they can compete inside the bulk superconductors and it becomes possible for the system to exhibit mix states as shown in Fig. 1.4. This feature can be understood especially by looking at the free energy using the Ginzburg-Landau theory [84]. Nevertheless, using no on-site repulsion pairing between electrons in our model, the mean field Hamiltonian exhibits pure single states for a certain range of parameters that we use in the current analysis.

Appendix B

Andreev Reflections

We discuss in the following the mechanisms of charges transfer between a metal and a spin-singlet superconductor with isotropic gap parameter, i.e. $\Delta_k = \Delta_0$. One particularity of such interface is that an electron in the metallic region can be reflected as a hole at the superconducting interface. The so-called Andreev reflection is crucial to understand the proximity effects in heterostructures made of superconductor. It is for instance responsible for the induced pairing amplitudes in the metallic or ferromagnetic region but also for a special dependence of the conductance as we shall see.
Although it may seem straightforward to understand intuitively the appearance of a pairing amplitude in the normal metal, as shown in Fig. 1.5, by saying that the Cooper pairs *leak* from the TSC into the metal, the microscopic concept behind this effect is however more complex. Indeed, let us take the problem in the other way and wonder what happens to an electron with an energy E coming from the metal and entering into the SC. Our first intuition by looking at the energy spectra tells us that the electron can be transferred as an excited state in the SC if $E > E_F + \Delta_0$, see electron (ii) in Fig. B.1, while it should be reflected if it has an energy in the range $E_F \leq E < E + \Delta_0$ since no excited state exist in the SC, see electron (i) in Fig. B.1. However, due to the nature of the excitations in the superconducting region, this later statement is incorrect and we owe to Andreev the first idea that the electron can be reflected as a hole (white circles in Fig. B.1) through the mechanism referred nowadays as the Andreev reflection. The charge conservation is respected by the fact that an additional Cooper pair is induced in the superconducting region.
In order to understand this mechanism, let us first recall the expression of the diagonalised

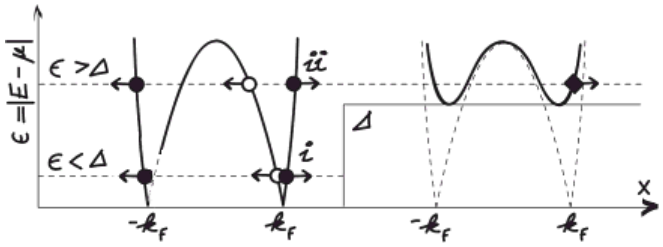

Figure B.1: Schematic representation of the Andreev reflection at the metal-SC interface. An incident electron (black dot in position i) with an energy in the superconducting gap can only be reflected as a hole (white dot in position i) with almost the same energy but in opposite direction. An electron with an energy above the gap (black dot in position ii) has a probability to be transferred in the superconductor, reflected has an electron or reflected as hole if the transparency of the barrier is not perfect. Adapted from Ref. [140].

BCS Hamiltonian

$$H_{BCS}^{MF} = \sum E_k(\gamma_{k\uparrow}^\dagger \gamma_{k\uparrow} + \gamma_{k\downarrow}^\dagger \gamma_{k\downarrow}) \tag{B.1}$$

$$\text{with} \quad E_k = \sqrt{\xi_k^2 + |\Delta_0|^2}, \tag{B.2}$$

where the eigenvectors, i.e. the excited states of the BCS superconductor, are quasiparticles made of linear combinations of the both electrons and holes operators such that

$$\gamma_{k\uparrow} = u_k^* c_{k\uparrow} - v_k^* c_{-k\downarrow}^\dagger, \tag{B.3}$$

$$\gamma_{-k\downarrow}^\dagger = v_k c_{k\uparrow} + u_k c_{-k\downarrow}^\dagger, \tag{B.4}$$

where the coefficient u_k and v_k satisfy $|u_k|^2 = 1 - |v_k|^2 = (1 - \epsilon_k/E_k)/2$. It is convenient for the following discussion to rewrite these conditions as

$$u_k(E_k)^2 = \frac{1}{2}\left(1 + \sqrt{1 - \Delta_0/E_k}\right), \tag{B.5}$$

$$v_k(E_k)^2 = \frac{1}{2}\left(1 - \sqrt{1 - \Delta_0/E_k}\right). \tag{B.6}$$

However, these operators are not suitable since they do not conserved the exact number of charge, which is crucial point in tunnelling problem. Instead, it is convenient to introduce the operators $S_k^\dagger$ and S_k which create an annihilate, respectively, a Cooper pair with electron momentum (k,-k), see Refs. [75, 128]. The excited states of the BCS Hamiltonian with well defined charge are then

$$\gamma_{ek\uparrow}^\dagger = u_k^* c_{k\uparrow}^\dagger - v_k^* S_k^\dagger c_{-k\downarrow} \tag{B.7}$$

$$\gamma_{hk\uparrow}^\dagger = u_k^* S_k c_{k\uparrow}^\dagger - v_k^* c_{-k\downarrow} \tag{B.8}$$

$$\gamma_{ek\downarrow}^\dagger = u_k^* c_{-k\downarrow}^\dagger - v_k^* S_k^\dagger c_{k\uparrow} \tag{B.9}$$

$$\gamma_{hk\downarrow}^\dagger = u_k^* S_k c_{-k\downarrow}^\dagger - v_k^* c_{k\uparrow}, \tag{B.10}$$

where the operators for define number of electron and hole are related by

$$\gamma_{ek\sigma}^\dagger = S_k^\dagger \gamma_{hk\sigma}^\dagger. \tag{B.11}$$

Hence, we see that it is strictly equivalent to add an electron in the superconductor than a hole with an additional Cooper pair. Let us now analyse in details the tunnelling of a charge with energy E_k entering from the normal region to the superconducting region [94, 128, 140]. The process is depicted in Fig. B.2, adapted from Ref. [94], where we can see that the value of the superconducting gap $\Delta_0(x)$ depends on the position x at the interface. It is suppressed in the metallic region at x_0 while it reach the bulk value in the superconducting bulk at x_1. Following the second quantification formalism, a charge in the metallic region, in position x_0, can be represented by the creation operator of an

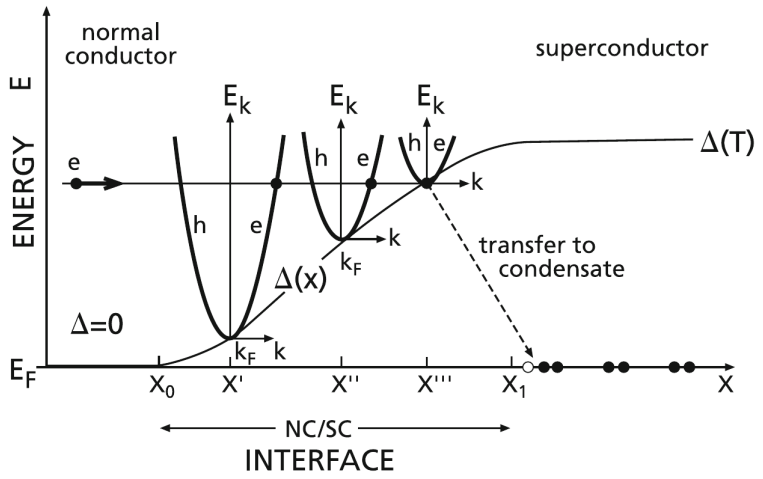

Figure B.2: Detailed representation of the Andreev reflection at the metal-SC interface. An incident electron e in the metal (at x_0) is transferred as a electronlike charge in the superconducting region (at x' and x''). When the gap parameter Δ_0 is large enough (at x'''), the negative charge is transformed in Cooper pair existing in the superconductor and a positive charge with an opposite group velocity. Adapted from Ref. [94].

excited state $\gamma^{\dagger}_{ek\sigma} \sim c^{\dagger}_{ek\sigma}$ since there is no gap in this region. Indeed, in this case $\Delta_0(x) = 0$ such that $u_k = 1$ while $v_k = 0$. Therefore, the charge is an electron. When the charge penetrates into the superconducting region, the superconducting gap increases. Hence, moving to the position x' and x'', the coherence factor u_k decreases while v_k increases. According to Eqs. B.7 and B.8, the charge is not an electron any longer but a mixture of electronlike and holelike, with opposite spin, excitations together with an additional Cooper pair. When it reaches the position x''', the negative charge creates a Cooper pair in the superconducting region together with a positive charge having the same energy and almost the same momentum than the incoming negative charge. The holelike excitation has an opposite group velocity and therefore is propagating to the metallic region. Once in the metallic region, the positive charge is equivalent to the hole.
Hence, the Andreev reflection denotes the reflection of an electron as a hole with the, almost, same momentum and the creation of a Cooper pair into the superconducting region. The incoming electron and the reflected hole form a coherent pair inside the metallic region over a distance of few superconducting coherent length ξ_{SC}. This is the pairing amplitude that we obtained in our computations.

To conclude, it is worth to mention few important remarks although we do not provide detailed and clear argumentations which require a more refined analysis of the tunnelling processes.
The probabilities for an electron to be reflected as an electron, as a hole or transmitted into the superconductor depend directly on the energy of the electrons and the quality of the barrier as we show in Fig. B.3. They are obtained using the Blonder-Tinkham-

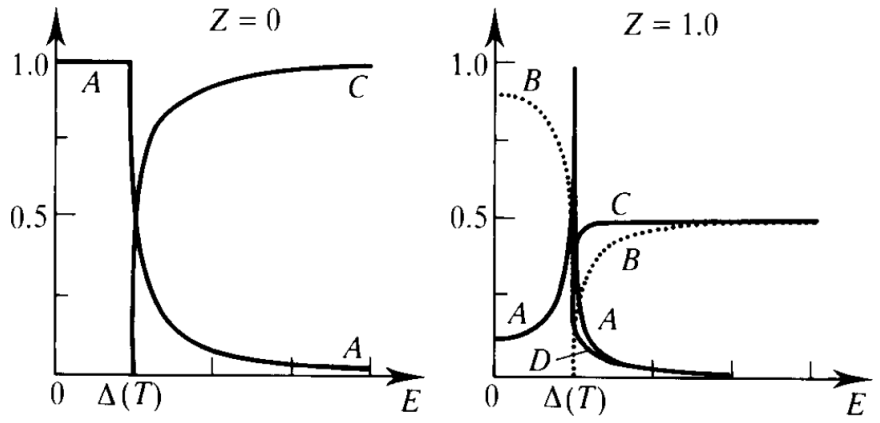

Figure B.3: Probabilities of transmission and reflection of an electron at the interface between a metal and a superconductor. A gives the probability of Andreev reflection, B of normal reflection, C and D of transmissions without and with branch crossing, respectively. The parameter Z is the barrier strength at the interface and $Z = 0$ denotes the clean limit. Adapted from Ref. [28,128].

Klapwijk (BTK) formalism which consists in solving the Bogoliubov-de Gennes equations for plane-wave electrons and modelling the quality of the interface with an additional potential Z. As we can see for a clean interface ($Z = 0$), it was found that all electrons with energy $E_F \leq E \leq E_F + \Delta_0$ inferior to the superconducting gap was reflected as holes (probability A) while electrons with higher energy $E > E_F + \Delta_0$ can be reflected as a hole or transmitted as an electrons in the superconductor (probability C). On the other hand, for a bad interface, the normal reflection of the electron become more and more probable in the tunnelling process and the Andreev reflections are cancelled. This model have been successfully applied to predict the conductance in tunnelling experiments [28, 103].
Finally, we can mention that similar processes are present in ferromagnetic junctions but that the probabilities can be modified due to the the difference of energy between spin up and spin down electrons [45], which can change the conductance. Moreover, as we discuss in Chapters 1 and 2, the electron and hole forming the coherent pair induced inside the ferromagnet acquire an additional momentum and therefore the induced pairing amplitude is oscillating. The magnetization can also induced a spin-flip to the reflected hole at the interface which can induce, in the case of spin-triplet superconducting junctions, spin-singlet or equal-spin pairing components as discussed in sections 1.5 and 2.5, respectively.

Bibliography

[1] Alexandrov, A. S. *Theory of Superconductivity: From Weak to Strong Coupling.* CRC Press, Oct. 2003.

[2] Andersen, B. M., Bobkova, I. V., Hirschfeld, P. J., and Barash, Y. S. Bound states at the interface between antiferromagnets and superconductors. *Physical Review B 72*, 18 (Nov. 2005), 184510.

[3] Andersen, B. M., Bobkova, I. V., Hirschfeld, P. J., and Barash, Y. S. 0-pi transitions in josephson junctions with antiferromagnetic interlayers. *Physical Review Letters 96*, 11 (Mar. 2006), 117005.

[4] Anderson, P., and Rowell, J. Probable observation of the josephson superconducting tunneling effect. *Physical Review Letters 10*, 6 (Mar. 1963), 230–232.

[5] Andreev, A. F. The thermal conductivity of the intermediate state in superconductors. *Soviet Physics-JETP 19*, 5 (1964), 1228.

[6] Annett, J. F. *Superconductivity, Superfluids and Condensates.* OUP Oxford, Mar. 2004.

[7] Annunziata, G., Cuoco, M., Gentile, P., Romano, A., and Noce, C. Does a ferromagnet with spin-dependent masses produce a spin-filtering effect in a ferromagnetic/insulator/superconductor junction? *Superconductor Science and Technology 24*, 2 (Feb. 2011), 024021.

[8] Annunziata, G., Cuoco, M., Noce, C., Sudbø, A., and Linder, J. Spin-sensitive long-range proximity effect in ferromagnet/spin-triplet-superconductor bilayers. *Physical Review B 83*, 6 (Feb. 2011), 060508.

[9] Annunziata, G., Manske, D., and Linder, J. Proximity effect with noncentrosymmetric superconductors. *Physical Review B 86*, 17 (Nov. 2012), 174514.

[10] Anwar, M. S., Shin, Y. J., Lee, S. R., Kang, S. J., Sugimoto, Y., Yonezawa, S., Noh, T. W., and Maeno, Y. Ferromagnetic SrRuO3 thin-film deposition on a spin-triplet superconductor sr2ruo4 with a highly conducting interface. *Applied Physics Express 8*, 1 (Jan. 2015), 015502.

[11] Anwar, M. S., Shin, Y. J., Lee, S. R., Yonezawa, S., and Noh, T. W.and Maeno, Y. Prototype hybrid of a ferromagnet and a spin triplet superconductor.

[12] Asano, Y. Direct-current josephson effect in SNS junctions of anisotropic superconductors. *Physical Review B 64*, 22 (Nov. 2001), 224515.

[13] Asano, Y. Numerical method for dc josephson current between d-wave superconductors. *Physical Review B 63*, 5 (Jan. 2001), 052512.

[14] Asano, Y. Spin current in p-wave superconducting rings. *Physical Review B 72*, 9 (Sept. 2005), 092508.

[15] Asano, Y. Josephson spin current in triplet superconductor junctions. *Physical Review B 74*, 22 (2006), 220501.

[16] Asano, Y., Tanaka, Y., and Kashiwaya, S. Anomalous josephson effect in p-wave dirty junctions. *Physical Review Letters 96*, 9 (Mar. 2006), 097007.

[17] Asano, Y., Tanaka, Y., Sigrist, M., and Kashiwaya, S. Josephson current in s-wave-superconductor/sr2ruo4 junctions. *Physical Review B 67*, 18 (2003), 184505.

[18] Asulin, I., Yuli, O., Koren, G., and Millo, O. Evidence for induced magnetization in superconductor-ferromagnet heterostructures: A scanning tunneling spectroscopy study. *Physical Review B 79*, 17 (2009), 174524.

[19] Badiane, D. M., Houzet, M., and Meyer, J. S. Nonequilibrium josephson effect through helical edge states. *Physical Review Letters 107*, 17 (Oct. 2011), 177002.

[20] Bakurskiy, S. V., Klenov, N. V., Karminskaya, T. Y., Kupriyanov, M. Y., and Golubov, A. A. Josephson phi-junctions based on structures with complex normal/ferromagnet bilayer. *Superconductor Science and Technology 26*, 1 (Jan. 2013), 015005.

[21] Bardeen, J., Cooper, L. N., and Schrieffer, J. R. Theory of superconductivity. *Physical Review 108*, 5 (Dec. 1957), 1175–1204.

[22] Bauer, E., Hilscher, G., Michor, H., Paul, C., Scheidt, E. W., Gribanov, A., Seropegin, Y., Noël, H., Sigrist, M., and Rogl, P. Heavy fermion superconductivity and magnetic order in noncentrosymmetric CePt3si. *Physical Review Letters 92*, 2 (Jan. 2004), 027003.

[23] Bauer, E., and Sigrist, M. *Non-Centrosymmetric Superconductors: Introduction and Overview*. Springer Science & Business Media, Jan. 2012.

[24] Bergeret, F., Volkov, A., and Efetov, K. Long-range proximity effects in superconductor-ferromagnet structures. *Physical Review Letters 86*, 18 (2001), 4096–4099.

[25] Bergeret, F., Volkov, A., and Efetov, K. Induced ferromagnetism due to superconductivity in superconductor-ferromagnet structures. *Physical Review B 69*, 17 (2004), 174504.

[26] Bergeret, F., Volkov, A., and Efetov, K. Odd triplet superconductivity and related phenomena in superconductor-ferromagnet structures. *Reviews of Modern Physics 77*, 4 (Nov. 2005), 1321–1373.

[27] Bergeret, F., Yeyati, A., and Martín-Rodero, A. Inverse proximity effect in superconductor-ferromagnet structures: From the ballistic to the diffusive limit. *Physical Review B 72*, 6 (2005), 064524.

[28] Blonder, G., Tinkham, M., and Klapwijk, T. Transition from metallic to tunneling regimes in superconducting microconstrictions: Excess current, charge imbalance, and supercurrent conversion. *Physical Review B 25*, 7 (Apr. 1982), 4515–4532.

[29] Blum, Y., Tsukernik, A., Karpovski, M., and Palevski, A. Oscillations of the superconducting critical current in nb-cu-ni-cu-nb junctions. *Physical Review Letters 89*, 18 (Oct. 2002), 187004.

[30] Bruder, C. Andreev scattering in anisotropic superconductors. *Physical Review B 41*, 7 (Mar. 1990), 4017–4032.

[31] Brydon, P. M. R., Chen, W., Asano, Y., and Manske, D. Charge and spin supercurrents in triplet superconductor-ferromagnet-singlet superconductor josephson junctions. *Physical Review B 88*, 5 (Aug. 2013), 054509.

[32] Brydon, P. M. R., Iniotakis, C., and Manske, D. The chiral superconductor–ferromagnet–chiral superconductor josephson junction. *New Journal of Physics 11*, 5 (May 2009), 055055.

[33] Brydon, P. M. R., Iniotakis, C., Manske, D., and Sigrist, M. Functional superconductor interfaces from broken time-reversal symmetry. *Physical Review Letters 104*, 19 (May 2010), 197001.

[34] Brydon, P. M. R., Kastening, B., Morr, D. K., and Manske, D. Interplay of ferromagnetism and triplet superconductivity in a josephson junction. *Physical Review B 77*, 10 (Mar. 2008), 104504.

[35] Brydon, P. M. R., and Manske, D. 0-pi transition in magnetic triplet superconductor josephson junctions. *Physical Review Letters 103*, 14 (Sept. 2009), 147001.

[36] Brydon, P. M. R., Timm, C., and Schnyder, A. P. Interface currents in topological superconductor–ferromagnet heterostructures. *New Journal of Physics 15*, 4 (Apr. 2013), 045019.

[37] Bujnowski, B., Timm, C., and Brydon, P. M. R. The josephson effect between triplet superconductors through a finite ferromagnetic barrier. *Journal of Physics: Condensed Matter 24*, 4 (Feb. 2012), 045701.

[38] Buzdin, A. Proximity effects in superconductor-ferromagnet heterostructures. *Reviews of Modern Physics 77*, 3 (Sept. 2005), 935–976.

[39] Buzdin, A., and Baladié, I. Theoretical description of ferromagnetic pi junctions near the critical temperature. *Physical Review B 67*, 18 (May 2003), 184519.

[40] Buzdin, A. I., Bulaevskii, L. N., and Panyukov, S. V. Critical-current oscillations as a function of the exchange field ans thickness of the ferromagnetic (f) in an s-f-s josephson junction. *Soviet Physics-JETP 35* (1982), 179.

[41] Buzdin, A. I., and Kupriyanov, M. Y. Josephson junction with a ferromagnetic layer. *Soviet Physics-JETP 53* (1991), 322.

[42] Caianiello, E. R. *Lectures on The Many-Body Problems*. Elsevier, Dec. 2012.

[43] Chen, X., Yao, Y., Yao, H., Yang, F., and Ni, J. 2d topological p+ip superconductivity in doped graphenelike BC3. *arXiv:1404.3346 [cond-mat]* (Apr. 2014). arXiv: 1404.3346.

[44] Cuoco, M., Romano, A., Noce, C., and Gentile, P. Proximity effect between an unconventional superconductor and a ferromagnet with spin bandwidth asymmetry. *Physical Review B 78*, 5 (2008), 054503.

[45] de Jong, M., and Beenakker, C. Andreev reflection in ferromagnet-superconductor junctions. *Physical Review Letters 74*, 9 (Feb. 1995), 1657–1660.

[46] Demler, E. A., Arnold, G. B., and Beasley, M. R. Superconducting proximity effects in magnetic metals. *Physical Review B 55*, 22 (1997), 15174–15182.

[47] Efetov, K. B., Garifullin, I. A., Volkov, A. F., and Westerholt, K. Proximity effects in ferromagnet/superconductor heterostructures. In *Magnetic Heterostructures*, H. Zabel and S. D. Bader, Eds., no. 227 in Springer Tracts in Modern Physics. Springer Berlin Heidelberg, Jan. 2008, pp. 251–290.

[48] Eilenberger, G. Transformation of gorkov's equation for type II superconductors into transport-like equations. *Zeitschrift für Physik 214*, 2 (Apr. 1968), 195–213.

[49] Eschrig, M. Scattering problem in nonequilibrium quasiclassical theory of metals and superconductors: General boundary conditions and applications. *Physical Review B 80*, 13 (Oct. 2009), 134511.

[50] Eschrig, M. Spin-polarized supercurrents for spintronics. *Physics Today 64*, 1 (Dec. 2010), 43–49.

[51] Eschrig, M., Kopu, J., Cuevas, J., and Schön, G. Theory of half-metal/superconductor heterostructures. *Physical Review Letters 90*, 13 (2003), 137003.

[52] Eschrig, M., and Löfwander, T. Triplet supercurrents in clean and disordered half-metallic ferromagnets. *Nature Physics 4*, 2 (2008), 138–143.

[53] Fazio, R., and Lucheroni, C. Local density of states in superconductor-ferromagnetic hybrid systems. *EPL (Europhysics Letters) 45*, 6 (Mar. 1999), 707.

[54] Feofanov, A. K., Oboznov, V. A., Bol'ginov, V. V., Lisenfeld, J., Poletto, S., Ryazanov, V. V., Rossolenko, A. N., Khabipov, M., Balashov, D., Zorin, A. B., Dmitriev, P. N., Koshelets, V. P., and Ustinov, A. V. Implementation of superconductor/ferromagnet/ superconductor pi-shifters in superconducting digital and quantum circuits. *Nature Physics 6*, 8 (Aug. 2010), 593–597.

[55] Fridman, I., Gunawan, L., Botton, G., and Wei, J. Scanning tunneling spectroscopy study of c-axis proximity effect in epitaxial bilayer manganite/cuprate thin films. *Physical Review B 84*, 10 (Sept. 2011), 104522.

[56] Frolov, S. M., Van Harlingen, D. J., Oboznov, V. A., Bolginov, V. V., and Ryazanov, V. V. Measurement of the current-phase relation of superconductor/ferromagnet/superconductor pi josephson junctions. *Physical Review B 70*, 14 (Oct. 2004), 144505.

[57] Fu, L., and Berg, E. Odd-parity topological superconductors: Theory and application to CuBi2se3. *Physical Review Letters 105*, 9 (Aug. 2010), 097001.

[58] Fulde, P., and Ferrell, R. A. Superconductivity in a strong spin-exchange field. *Physical Review 135*, 3A (Aug. 1964), A550–A563.

[59] Garifullin, I. A., Tikhonov, D. A., Garif'yanov, N. N., Fattakhov, M. Z., Theis-Bröhl, K., Westerholt, K., and Zabel, H. Possible reconstruction of the ferromagnetic state under the influence of superconductivity in epitaxial v/PdFe bilayers. *Applied Magnetic Resonance 22*, 3 (Sept. 2002), 439–452.

[60] Gentile, P., Cuoco, M., Romano, A., Noce, C., Manske, D., and Brydon, P. Spin-orbital coupling in a triplet superconductor-ferromagnet junction. *Physical Review Letters 111*, 9 (2013), 097003.

[61] Golubov, A. A., Kupriyanov, M. Y., and Il'ichev, E. The current-phase relation in josephson junctions. *Reviews of Modern Physics 76*, 2 (Apr. 2004), 411–469.

[62] Gor'kov, L. P., and Rashba, E. I. Superconducting 2d system with lifted spin degeneracy: Mixed singlet-triplet state. *Physical Review Letters 87*, 3 (July 2001), 037004.

[63] Gu, J., Kusnadi, J., and You, C.-Y. Proximity effect in a superconductor/exchange-spring-magnet hybrid system. *Physical Review B 81*, 21 (June 2010), 214435.

[64] Gu, J., You, C.-Y., Jiang, J., Pearson, J., Bazaliy, Y., and Bader, S. Magnetization-orientation dependence of the superconducting transition temperature in the ferromagnet-superconductor-ferromagnet system: CuNi/nb/CuNi. *Physical Review Letters 89*, 26 (Dec. 2002), 267001.

[65] Halterman, K., and Valls, O. Proximity effects at ferromagnet-superconductor interfaces. *Physical Review B 65*, 1 (Nov. 2001), 014509.

[66] Halterman, K., and Valls, O. Layered ferromagnet-superconductor structures: The pi state and proximity effects. *Physical Review B 69*, 1 (Jan. 2004), 014517.

[67] Hasan, M. Z., and Kane, C. L. Colloquium on topological insulators. *Reviews of Modern Physics 82*, 4 (Nov. 2010), 3045–3067.

[68] Heim, D. M., Pugach, N. G., Kupriyanov, M. Y., Goldobin, E., Koelle, D., and Kleiner, R. Ferromagnetic planar josephson junction with transparent interfaces: a phi junction proposal. *Journal of Physics: Condensed Matter 25*, 21 (May 2013), 215701.

[69] Hsieh, T. H., and Fu, L. Majorana fermions and exotic surface andreev bound states in topological superconductors: Application to CuxB2se3. *Physical Review Letters 108*, 10 (Mar. 2012), 107005.

[70] Iniotakis, C., Hayashi, N., Sawa, Y., Yokoyama, T., May, U., Tanaka, Y., and Sigrist, M. Andreev bound states and tunneling characteristics of a noncentrosymmetric superconductor. *Physical Review B 76*, 1 (July 2007), 012501.

[71] Ioffe, L. B., Geshkenbein, V. B., Feigel'man, M. V., Fauchère, A. L., and Blatter, G. Environmentally decoupled sds -wave josephson junctions for quantum computing. *Nature 398*, 6729 (Apr. 1999), 679–681.

[72] Jackel, L. D., Buhrman, R. A., and Webb, W. W. Direct measurement of current-phase relations in superconducting weak links. *Physical Review B 10*, 7 (Oct. 1974), 2782–2785.

[73] Jara, A. A., Safranski, C., Krivorotov, I. N., Wu, C.-T., Malmi-Kakkada, A. N., Valls, O. T., and Halterman, K. Angular dependence of superconductivity in superconductor/spin-valve heterostructures. *Physical Review B 89*, 18 (May 2014), 184502.

[74] Josephson, B. Coupled superconductors. *Reviews of Modern Physics 36*, 1 (Jan. 1964), 216–220.

[75] Josephson, B. D. Possible new effects in superconductive tunneling. *Physic Letters 1*, 7 (1962), 251.

[76] Kastening, B., Morr, D., Manske, D., and Bennemann, K. Novel josephson effect in triplet-superconductor–ferromagnet–triplet-superconductor junctions. *Physical Review Letters 96*, 4 (2006), 047009.

[77] Keizer, R. S., Goennenwein, S. T. B., Klapwijk, T. M., Miao, G., Xiao, G., and Gupta, A. A spin triplet supercurrent through the half-metallic ferromagnet CrO2. *Nature 439*, 7078 (2006), 825–827.

[78] Khaire, T., Khasawneh, M., Pratt, W., and Birge, N. Observation of spin-triplet superconductivity in co-based josephson junctions. *Physical Review Letters 104*, 13 (Mar. 2010), 137002.

[79] Kharitonov, M., Volkov, A., and Efetov, K. Oscillations of induced magnetization in superconductor-ferromagnet heterostructures. *Physical Review B 73*, 5 (Feb. 2006), 054511.

[80] Kidwingira, F., Strand, J. D., Harlingen, D. J. V., and Maeno, Y. Dynamical superconducting order parameter domains in sr2ruo4. *Science 314*, 5803 (Nov. 2006), 1267–1271.

[81] Klam, L., Epp, A., Chen, W., Sigrist, M., and Manske, D. Josephson effect and triplet-singlet ratio of noncentrosymmetric superconductors. *Physical Review B 89*, 17 (May 2014), 174505.

[82] Koster, G., Klein, L., Siemons, W., Rijnders, G., Dodge, J. S., Eom, C.-B., Blank, D. H. A., and Beasley, M. R. Structure, physical properties, and applications of SrRuO3 thin films. *Reviews of Modern Physics 84*, 1 (Mar. 2012), 253–298.

[83] Kuboki, K. Proximity effects near the interface between d-wave superconductors and ferro/antiferromagnets. *Journal of the Physical Society of Japan 68*, 10 (Oct. 1999), 3150–3153.

[84] Kuboki, K. Effect of band structure on the symmetry of superconducting states. *Journal of the Physical Society of Japan 70*, 9 (Sept. 2001), 2698–2702.

[85] Kuboki, K., and Takahashi, H. Spontaneous spin current near the interface between unconventional superconductors and ferromagnets. *Physical Review B 70*, 21 (Dec. 2004), 214524.

[86] Larkin, A. I., and Ovchinnikov, I. U. N. Inhomogeneous state of superconductors(production of superconducting state in ferromagnet with fermi surfaces, examining green function). *Soviet Physics-JETP 20* (1965), 762.

[87] Likharev, K. Superconducting weak links. *Reviews of Modern Physics 51*, 1 (Jan. 1979), 101–159.

[88] Linder, J., Cuoco, M., and Sudbø, A. Spin-active interfaces and unconventional pairing in half-metal/superconductor junctions. *Physical Review B 81*, 17 (2010), 174526.

[89] Linder, J., Grønsleth, M. S., and Sudbø, A. Conductance spectra of ferromagnetic superconductors: Quantum transport in a ferromagnetic metal/non-unitary ferromagnetic superconductor junction. *Physical Review B 75*, 5 (Feb. 2007), 054518.

[90] Linder, J., and Sudbø, A. Quantum transport in noncentrosymmetric superconductors and thermodynamics of ferromagnetic superconductors. *Physical Review B 76*, 5 (Aug. 2007), 054511.

[91] Linder, J., Yokoyama, T., and Sudbø, A. Theory of superconducting and magnetic proximity effect in s/f structures with inhomogeneous magnetization textures and spin-active interfaces. *Physical Review B 79*, 5 (Feb. 2009), 054523.

[92] Linder, J., Yokoyama, T., Sudbø, A., and Eschrig, M. Pairing symmetry conversion by spin-active interfaces in magnetic normal-metal–superconductor junctions. *Physical Review Letters 102*, 10 (Mar. 2009), 107008.

[93] Linder, J., Yokoyama, T., Tanaka, Y., Asano, Y., and Sudbø, A. Quantum transport in a normal metal/odd-frequency superconductor junction. *Physical Review B 77*, 17 (May 2008), 174505.

[94] Lüth, H. *Solid Surfaces, Interfaces and Thin Films*. Springer, Nov. 2014.

[95] M. R. Brydon, P., Manske, D., and Sigrist, M. Origin and control of spin currents in a magnetic triplet josephson junction. *Journal of the Physical Society of Japan 77*, 10 (Oct. 2008), 103714.

[96] Mackenzie, A., and Maeno, Y. The superconductivity of sr2ruo4 and the physics of spin-triplet pairing. *Reviews of Modern Physics 75*, 2 (May 2003), 657–712.

[97] Maeno, Y., Kittaka, S., Nomura, T., Yonezawa, S., and Ishida, K. Evaluation of spin-triplet superconductivity in sr2ruo4. *Journal of the Physical Society of Japan 81*, 1 (Jan. 2012), 011009.

[98] Mathews, W. N. Quasiparticle, charge, and energy conservation in weak-coupling superconductors. *physica status solidi (b) 90*, 1 (1978), 327–338.

[99] Matsumoto, M., and Sigrist, M. Quasiparticle states near the surface and the domain wall in a px+ipy-wave superconductor. *Journal of the Physical Society of Japan 68*, 3 (Mar. 1999), 994–1007.

[100] Mühge, T., Garif'yanov, N. N., Goryunov, Y. V., Theis-Bröhl, K., Westerholt, K., Garifullin, I. A., and Zabel, H. Influence of superconductivity on magnetic properties of superconductor/ferromagnet epitaxial bilayers. *Physica C: Superconductivity 296*, 3–4 (Feb. 1998), 325–336.

[101] Mineev, V. P., Samokhin, K., Landau, L. D., and Landau, L. D. *Introduction to Unconventional Superconductivity*. CRC Press, Sept. 1999.

[102] Oboznov, V. A., Bol'ginov, V. V., Feofanov, A. K., Ryazanov, V. V., and Buzdin, A. I. Thickness dependence of the josephson ground states of superconductor-ferromagnet-superconductor junctions. *Physical Review Letters 96*, 19 (May 2006), 197003.

[103] Octavio, M., Tinkham, M., Blonder, G., and Klapwijk, T. Subharmonic energy-gap structure in superconducting constrictions. *Physical Review B 27*, 11 (June 1983), 6739–6746.

[104] Petrashov, V., Sosnin, I., Cox, I., Parsons, A., and Troadec, C. Giant mutual proximity effects in ferromagnetic/superconducting nanostructures. *Physical Review Letters 83*, 16 (Oct. 1999), 3281–3284.

[105] Qi, X.-L., Hughes, T. L., Raghu, S., and Zhang, S.-C. Time-reversal-invariant topological superconductors and superfluids in two and three dimensions. *Physical Review Letters 102*, 18 (May 2009), 187001.

[106] Qi, X.-L., and Zhang, S.-C. Topological insulators and superconductors. *Reviews of Modern Physics 83*, 4 (Oct. 2011), 1057–1110.

[107] Qiu, Z. Q., and Bader, S. D. Surface magneto-optic kerr effect. *Review of Scientific Instruments 71*, 3 (Mar. 2000), 1243–1255.

[108] Radović, Z., Ledvij, M., Dobrosavljević-Grujić, L., Buzdin, A., and Clem, J. Transition temperatures of superconductor-ferromagnet superlattices. *Physical Review B 44*, 2 (July 1991), 759–764.

[109] Rahnavard, Y., Manske, D., and Annunziata, G. Magnetic josephson junctions with noncentrosymmetric superconductors. *Physical Review B 89*, 21 (June 2014), 214501.

[110] Robinson, J. W. A., Piano, S., Burnell, G., Bell, C., and Blamire, M. G. Critical current oscillations in strong ferromagnetic pi junctions. *Physical Review Letters 97*, 17 (Oct. 2006), 177003.

[111] Robinson, J. W. A., Witt, J. D. S., and Blamire, M. G. Controlled injection of spin-triplet supercurrents into a strong ferromagnet. *Science 329*, 5987 (July 2010), 59–61.

[112] Rusanov, A., Habraken, S., and Aarts, J. Inverse spin switch effects in ferromagnet-superconductor-ferromagnet trilayers with strong ferromagnets. *Physical Review B 73*, 6 (Feb. 2006), 060505.

[113] Sasaki, S., Kriener, M., Segawa, K., Yada, K., Tanaka, Y., Sato, M., and Ando, Y. Topological superconductivity in CuBi2se3. *Physical Review Letters 107*, 21 (Nov. 2011), 217001.

[114] Sato, M., and Fujimoto, S. Topological phases of noncentrosymmetric superconductors: Edge states, majorana fermions, and non-abelian statistics. *Physical Review B 79*, 9 (Mar. 2009), 094504.

[115] Schnyder, A. P., Ryu, S., Furusaki, A., and Ludwig, A. W. W. Classification of topological insulators and superconductors in three spatial dimensions. *Physical Review B 78*, 19 (Nov. 2008), 195125.

[116] Schnyder, A. P., Timm, C., and Brydon, P. M. R. Edge currents as a signature of flatbands in topological superconductors. *Physical Review Letters 111*, 7 (Aug. 2013), 077001.

[117] Sellier, H., Baraduc, C., Lefloch, F., and Calemczuk, R. Half-integer shapiro steps at the 0-pi crossover of a ferromagnetic josephson junction. *Physical Review Letters 92*, 25 (2004), 257005.

[118] Shai, D. E., Adamo, C., Shen, D. W., Brooks, C. M., Harter, J. W., Monkman, E. J., Burganov, B., Schlom, D. G., and Shen, K. M. Quasiparticle Mass Enhancement and Temperature Dependence of the Electronic Structure of Ferromagnetic SrRuO3thin Films. *Physical Review Letters 110*, 8 (Feb. 2013), 087004.

[119] Shapiro, S. Josephson currents in superconducting tunneling: The effect of microwaves and other observations. *Physical Review Letters 11*, 2 (July 1963), 80–82.

[120] Shirai, S., Tsuchiura, H., Asano, Y., Tanaka, Y., Inoue, J.-i., Tanuma, Y., and Kashiwaya, S. Josephson effect in d-wave superconductor junctions in a lattice model. *Journal of the Physical Society of Japan 72*, 9 (Sept. 2003), 2299–2307.

[121] Sigrist, M., and Ueda, K. Phenomenological theory of unconventional superconductivity. *Reviews of Modern Physics 63*, 2 (Apr. 1991), 239–311.

[122] Tada, Y., Kawakami, N., and Fujimoto, S. Pairing state at an interface of sr2ruo4: parity-mixing, restored time-reversal symmetry and topological superconductivity. *New Journal of Physics 11*, 5 (May 2009), 055070.

[123] Tagirov, L. Low-field superconducting spin switch based on a superconductor/ferromagnet multilayer. *Physical Review Letters 83*, 10 (Sept. 1999), 2058–2061.

[124] Tanaka, Y., Asano, Y., Golubov, A., and Kashiwaya, S. Anomalous features of the proximity effect in triplet superconductors. *Physical Review B 72*, 14 (Oct. 2005), 140503.

[125] Tanaka, Y., and Kashiwaya, S. Anomalous charge transport in triplet superconductor junctions. *Physical Review B 70*, 1 (2004), 012507.

[126] Tanaka, Y., Kashiwaya, S., and Yokoyama, T. Theory of enhanced proximity effect by midgap andreev resonant state in diffusive normal-metal/triplet superconductor junctions. *Physical Review B 71*, 9 (Mar. 2005), 094513.

[127] Tanaka, Y., Tanuma, Y., Kuroki, K., and Kashiwaya, S. Theory of magnetotunneling spectroscopy in spin triplet p-wave superconductors. *Journal of the Physical Society of Japan 71*, 9 (Sept. 2002), 2102–2105.

[128] Tinkham, M. *Introduction to Superconductivity*. Courier Corporation, Apr. 2012.

[129] Tollis, S., Daumens, M., and Buzdin, A. Inversion of the proximity effect in atomic-scale ferromagnet/superconductor/ferromagnet trilayers. *Physical Review B 71*, 2 (Jan. 2005), 024510.

[130] Usadel, K. D. Generalized diffusion equation for superconducting alloys. *Physical Review Letters 25*, 8 (Aug. 1970), 507–509.

[131] Vaccarella, C. D., Duncan, R. D., and Sá de Melo, C. A. R. Triplet superconductors: Josephson effect in quasi-one-dimensional systems. *Physica C: Superconductivity 391*, 1 (2003), 89–97.

[132] Veenstra, C., Zhu, Z.-H., Raichle, M., Ludbrook, B., Nicolaou, A., Slomski, B., Landolt, G., Kittaka, S., Maeno, Y., Dil, J., Elfimov, I., Haverkort, M., and Damascelli, A. Spin-orbital entanglement and the breakdown of singlets and triplets in sr2ruo4 revealed by spin- and angle-resolved photoemission spectroscopy. *Physical Review Letters 112*, 12 (Mar. 2014), 127002.

[133] Vorontsov, A. B., Vekhter, I., and Eschrig, M. Surface bound states and spin currents in noncentrosymmetric superconductors. *Physical Review Letters 101*, 12 (Sept. 2008), 127003.

[134] Wu, C.-T., Valls, O. T., and Halterman, K. Tunneling conductance and spin transport in clean ferromagnet/ferromagnet/superconductor heterostructures. *Physical Review B 90*, 5 (2014), 054523.

[135] Wu, S., and Samokhin, K. V. Tunneling conductance of ferromagnet/noncentrosymmetric superconductor junctions. *Physical Review B 80*, 1 (July 2009), 014516.

[136] Xia, J., Maeno, Y., Beyersdorf, P. T., Fejer, M. M., and Kapitulnik, A. High resolution polar kerr effect measurements of sr2ruo4: Evidence for broken time-reversal symmetry in the superconducting state. *Physical Review Letters 97*, 16 (Oct. 2006), 167002.

[137] Yamashiro, M., Tanaka, Y., and Kashiwaya, S. Theory of the d.c. josephson effect in s-wave/ p-wave/ s-wave superconductor junction. *Journal of the Physical Society of Japan 67*, 10 (Oct. 1998), 3364–3367.

[138] Yamashita, T., Tanikawa, K., Takahashi, S., and Maekawa, S. Superconducting pi qubit with a ferromagnetic josephson junction. *Physical Review Letters 95*, 9 (Aug. 2005), 097001.

[139] Yan, B., Liu, C.-X., Zhang, H.-J., Yam, C.-Y., Qi, X.-L., Frauenheim, T., and Zhang, S.-C. Theoretical prediction of topological insulators in thallium-based III-v-VI2 ternary chalcogenides. *EPL (Europhysics Letters) 90*, 3 (May 2010), 37002.

[140] Zagoskin, A. *Quantum Theory of Many-Body Systems: Techniques and Applications*. Springer, 2014.

[141] Zdravkov, V., Kehrle, J., Obermeier, G., Lenk, D., Krug von Nidda, H.-A., Müller, C., Kupriyanov, M., Sidorenko, A., Horn, S., Tidecks, R., and Tagirov, L. Experimental observation of the triplet spin-valve effect in a superconductor-ferromagnet heterostructure. *Physical Review B 87*, 14 (Apr. 2013), 144507.

[142] Zhang, Y., Cheng, Q., and Jin, B. Tunneling conductance in ferromagnet/sr2ruo4 junction: Detection of the d-vector direction. *Physica C: Superconductivity 470*, 11–12 (2010), 502–507.

[143] Zhu, L., Liu, Y., Bergeret, F., Pearson, J., te Velthuis, S., Bader, S., and Jiang, J. Unanticipated proximity behavior in ferromagnet-superconductor heterostructures with controlled magnetic noncollinearity. *Physical Review Letters 110*, 17 (2013), 177001.